NASA CR-167955
R81AEG284

National Aeronautics and
Space Administration

ENERGY EFFICIENT ENGINE

High Pressure Turbine Test Hardware Detailed Design Report

by

E.E. Halila
D.T. Lenahan
T.T. Thomas

GENERAL ELECTRIC COMPANY

June 1982

Prepared For

National Aeronautics and Space Administration

NASA Lewis Research Center

NAS3-20643

1. Report No.	2. Government Accession No.	3. Recipient's Catalog No.
NASA CR-167955		

4. Title and Subtitle	5. Report Date
ENERGY EFFICIENT ENGINE HIGH PRESSURE TURBINE TEST HARDWARE DETAILED DESIGN REPORT	June 1982
	6. Performing Organization Code
7. Author(s)	8. Performing Organization Report No.
E.E. Halila, D.T. Lenahan, and T.T. Thomas	R81AEG284
	10. Work Unit No.
9. Performing Organization Name and Address	
General Electric Aircraft Engine Business Group Advanced Technology Programs Department Cincinnati, Ohio 45215	11. Contract or Grant No. NAS3-20643
	13. Type of Report and Period Covered
12. Sponsoring Agency Name and Address	
National Aeronautics and Space Administration Lewis Research Center Cleveland, Ohio 44135	14. Sponsoring Agency Code

15. Supplementary Notes

NASA Project Manager: C.C. Ciepluch G.E. Project Manager: R.W. Bucy

NASA Project Engineer: R.P. Dengler

16. Abstract

The high pressure turbine configuration for the Energy Efficient Engine (E^3) is built around a two-stage design system. Moderate aerodynamic loading for both stages is used to achieve the high level of turbine efficiency.

Flowpath components are designed for 18,000 hours of life, while the static and rotating structures are designed for 36,000 hours of engine operation. Both stages of turbine blades and vanes are air-cooled incorporating advanced state of the art in cooling technology. Direct solidification (DS) alloys are used for blades and one stage of vanes, and an oxide dispersion system (ODS) alloy is used for the Stage 1 nozzle airfoils. Ceramic shrouds are used as the material composition for the Stage 1 shroud.

An active clearance control (ACC) system is used to control the blade tip to shroud clearances for both stages. Fan air is used to impinge on the shroud casing support rings, thereby controlling the growth rate of the shroud. This procedure allows close clearance control while minimizing blade tip to shroud rubs.

17. Key Words (Suggested by Author(s))

Two-Stage, High Pressure Turbine
Energy Efficient Engine
Turbofan Engine

19. Security Classif. (of this report)	20. Security Classif. (of this page)	21. No. of Pages	22. Price*
Unclassified	Unclassified	186	

TABLE OF CONTENTS

TABLE OF CONTENTS (Concluded)

LIST OF ILLUSTRATIONS

LIST OF ILLUSTRATIONS (Continued)

LIST OF ILLUSTRATIONS (Continued)

LIST OF ILLUSTRATIONS (Concluded)

LIST OF TABLES

1.0 INTRODUCTION AND SUMMARY

The General Electric Energy Efficient Engine (E^3) High Pressure Turbine (HPT) represents advanced technology aimed at achieving high efficiency while still meeting the component objective "lives" required for commercial applications.

The turbine design evolved from overall engine-integration and systems studies conducted by the General Electric Company for NASA (References 1 through 5). These programs studied improvements and evaluated four promising engine configurations. The evaluation of these engine configurations developed technology and refined advanced engine cycles and conceptual designs (Reference 6). Advanced features for the turbine design were developed within the Reference 6 work effort: directionally solidified (DS) alloys for blades, expander cooling system for a two-stage turbine, active clearance control (ACC), ceramic shrouds, and high-strength alloys with low coefficients for thermal expansion.

The E^3 Preliminary Design and Integration Studies (Reference 6) combined and integrated the technologies developed in the programs cited above. This study established the background for the design of the HPT under the present contract for the Design, Component Integration, and Test Program.

The HPT work scope covered all technology disciplines related to high turbine efficiency. These include aerodynamics, mechanics, heat transfer, metallurgy, manufacturing, and tests. Turbine performance efforts are aimed at achieving a high pressure turbine efficiency of 92.4% at Mach 0.8, 10.67-km (35,000-ft) altitude, standard day, maximum cruise power setting. The airfoils in the two-stage turbine design are moderately loaded.

To establish the level of turbine performance expected in the core engine test and in the Integrated Core and Low Pressure Spool (ICLS) engine tests, an air-turbine test was planned as part of the program. The air-turbine program consisted of two major tests, and both of these have been successfully completed. The first test consisted of evaluating the Stage 1 nozzle performance in an annular cascade. The results of this test were used to compare predicted versus actual Stage 1 nozzle efficiency. The second test consisted of running both stages of nozzles and blades in a rotating rig. Evaluation of test results indicated a turbine efficiency of 92.5%; this is 0.1% higher than predicted for the FPS engine (92.4%).

The air turbine was built using the simulated turbine design features selected for the core and ICLS engine tests. This provides assurance that the measured efficiencies in the air turbine can be expected to be realized during the engine tests.

The overall design for the high pressure turbine consists of two phases as follows:

Phase I - Preliminary Design - Phase I design effort started in January 1978 and ended in April 1978. Phase I was a preliminary analysis to define geometry and systems integration of the two-stage turbine. The integration consisted of establishing methods for determining rotor and stator configurations, cooling flow, and turbine geometry. The preliminary design was presented to NASA, and their approval was obtained to proceed to Phase II - Detailed Design.

Phase II - Detailed Design - The detailed design consisted of an effort to integrate all the experience from the material-development programs, the heat-transfer cascade tests, the air-turbine tests, and the preliminary mechanical and systems designs. A Detailed Design Review of the High Pressure Turbine was presented to NASA on October 10, 1980. Approval was received from NASA to procure all necessary hardware for the core and ICLS engine tests.

2.0 AERODYNAMIC DESIGN

2.1 PERFORMANCE REQUIREMENTS

Historically, turbomachinery component efficiencies in prototype engines fall short of design goals by significant amounts. The consequent cycle rebalancing causes turbomachinery components to operate off-design and further reduces component efficiency. In an attempt to alleviate this trend, the ICLS cycle was constructed with appropriate derating of component efficiencies. Depending on the accuracy of the efficiency derates, turbomachinery components designed to the requirements of the resultant cycle will avoid off-design penalties. Critical HPT operating-point data are summarized in Table I. Comparison of ICLS and Flight Propulsion System (FPS) requirements indicates the ICLS maximum climb conditions to be most stringent. While the differences are relatively small, the ICLS maximum climb condition was selected as the design point on the basis of these comparisons. In Table I, note that the ICLS efficiency level is 0.5% below that of the FPS design, reflecting the HPT derate at the time of the aero design execution.

Subsequent to completion of the turbine aerodynamic design, early compressor aerodynamic testing indicated the potential of a stall margin deficiency relative to the pretest prediction. Consequently, in recognition of this potential deficiency in stall margin, the HPT first-stage stator flow area (A_{41}) was increased by 4%. Requirements for the rebalanced cycle to incorporate this change are indicated in Table I. Note that no net change in turbine efficiency results from the cycle rebalance.

2.2 DESIGN STUDIES

With mimimum cruise specific fuel consumption (sfc) as the primary evaluation criterion, a series of system trade studies was performed with the objective of identifying the turbine configuration and the major flowpath dimensions for use in subsequent detailed design analyses. The following summaries present the results of these studies.

2.2.1 Number of Stages

Based on comparison of the E^3 cycle thermodynamic parameters with core engines employing single-stage or two-stage HPT's, selection of a two-stage configuration was made during preliminary design studies. In order to verify the preliminary design selection, a brief pitch-line study was conducted. The results of this study are summarized in Table II. Assessing the high loading and Mach numbers in light of current single-stage HPT experience and the E^3 turbine efficiency goal, it was concluded that the level of risk associated with the single-stage turbine is inappropriate for the E^3 program goal. This established the rationale for a two-stage turbine in the ICLS application.

Table I. HPT Aero-Thermodynamic Design Requirements.

Parameter	Units	ICLS		FPS		
		Max Climb	Max Climb + 4% A_{41}	Max Climb	Max Cruise	Sea Level Takeoff + 27° F
Inlet Temp, T_{41}	K	1588	1591	1557	1515	1618
	° R	2858	2863	2802	2728	2913
Energy, $\Delta h/T$	J/kg•K	353.4	353.4	355.5	353.4	354.6
	Btu/lbm/° R	0.0844	0.0844	0.0849	0.0844	0.0847
Speed, $N/\sqrt{T}$	rad/sec•$\sqrt{\text{K}}$	33.19	33.78	33.56	33.68	34.22
	rpm/$\sqrt{\text{° R}}$	236.2	240.4	238.9	239.7	243.6
Corrected Flow, $W\sqrt{T}/P$	g$\sqrt{\text{K}}$/sec•Pa	0.8648	0.8913	0.8643	0.8638	0.8628
	lbm$\sqrt{\text{° R}}$/sec•psi	17.65	18.19	17.64	17.63	17.61
Loading, $\Delta h/2U^2$		0.635	0.625	0.624	0.616	0.599
Efficiency, η_T %		91.9	91.9	92.4	92.4	92.1

Table II. Single-Stage Versus Two-Stage Turbine.

	Two-Stage*		One-Stage
Stage	1	2	1
Pressure Ratio	2.25	2.11	5.01
Loading, $\Delta h/2U^2$	0.74	0.56	0.92
Vane Exit Mach No.	0.89	0.82	1.36
Blade Exit Mach No.	0.84	0.83	1.2
Blade Turning	118	99	132
Swirl, Γ	17	1	24
Stage Exit Mach No.	0.36	0.41	0.57
Efficiency, %	92.4		?

*Preliminary, free-vortex calculations

2.2.2 Diameter

The turbine diameter established during preliminary design, together with the core engine thermodynamic parameters, resulted in light to moderately loaded, low-aspect-ratio blading. A study was undertaken to determine the benefits that might be gained by increasing the turbine diameter. Increased turbine diameter would reduce blade loading and thereby increase efficiency. However, a larger diameter would also increase weight, reduce blade aspect ratio, increase tip clearance, and lead to greater windage effects. The study concluded that the efficiency to be gained by increased turbine diameter would certainly be diminished and possibly exceeded by related penalties.

A similar study was undertaken to investigate the benefits that might be gained from a decrease in turbine diameter. The object of this study was to determine whether the small efficiency loss associated with higher loading in a smaller diameter turbine might not be offset by a gain due to decreased weight, increased aspect ratios, and tighter tip clearance. Reducing the diameter of the HPT would also necessitate a reduction in the low pressure turbine (LPT) diameter or an increase in transition-duct length. Both of these changes would introduce considerable performance penalties. Based on the above rationale, it was concluded that the diameter selected in preliminary design was sufficiently close to the optimum for the overall HPT/LPT system and that further study was unwarranted.

2.2.3 Annulus Height

A system trade study of the effect of annulus height was conducted by making vector-diagram calculations in which stage-exit annulus heights were varied individually. The effects on efficiency of the consequent variation of tip clearance, aspect ratio, edge blockage, aerodynamic loading, and gas deflection were evaluated by a loss system sensitive to these parameters. Variation in flowpath wetted area and the consequent effect on cooling air consumption and loss were evaluated concurrently and included in the turbine efficiency evaluation. Results of the annulus-height study are summarized in Figure 1. The design values of annulus area were selected slightly below the optimum in order to minimize the high weight penalty that would be imposed for relatively small (if any) gains in efficiency.

2.2.4 Stage Work Distribution

Using the flowpath developed above, further studies were conducted to identify the most appropriate stage-energy distribution. The calculations were executed in a manner similar to the annulus-height studies with the exception that stage-energy split was varied while maintaining constant blade aerodynamic loading. The loss system was then employed to evaluate the effect on overall efficiency. As with the annulus studies, cooling-flow variation was included in the overall efficiency assessment. Figure 2 shows the results of these studies in terms of Δsfc. The effect of stage-energy distribution was calculated assuming extraction of HPT second-stage stator cooling air from either the seventh or eighth stage of the compressor. It is seen that an optimum distribution would exist at approximately 48% to 50% energy extraction in the first stage. However, given the requirement that the second stage vane coolant supply pressure exceed gas total pressure, it would have been necessary to shift from seventh- to eighth-stage cooling-air extraction with a net increase in fuel consumption. Therefore, the stage work distribution was selected at 56.5% in the first stage, as shown in Figure 2, to improve sfc.

Results of the annulus-height trade studies are summarized in Figure 3 and Table III; turbine flowpath geometry and stage aerodynamic parameters are shown, respectively. The primary features of the flowpath are the converged annulus through the first-stage stator and smoothed end-wall contours. The stage aerodynamic parameters are well within empirical limits established from other successful two-stage turbines.

The effects of the 4% first-stage stator flow-area increase were determined by off-design, vector-diagram calculations. These calculations are summarized by the values shown in parentheses in Table III. The significant aerodynamic effects are increased reaction and stage work shift toward the second stage. These effects, although small, are in the direction of improved efficiency.

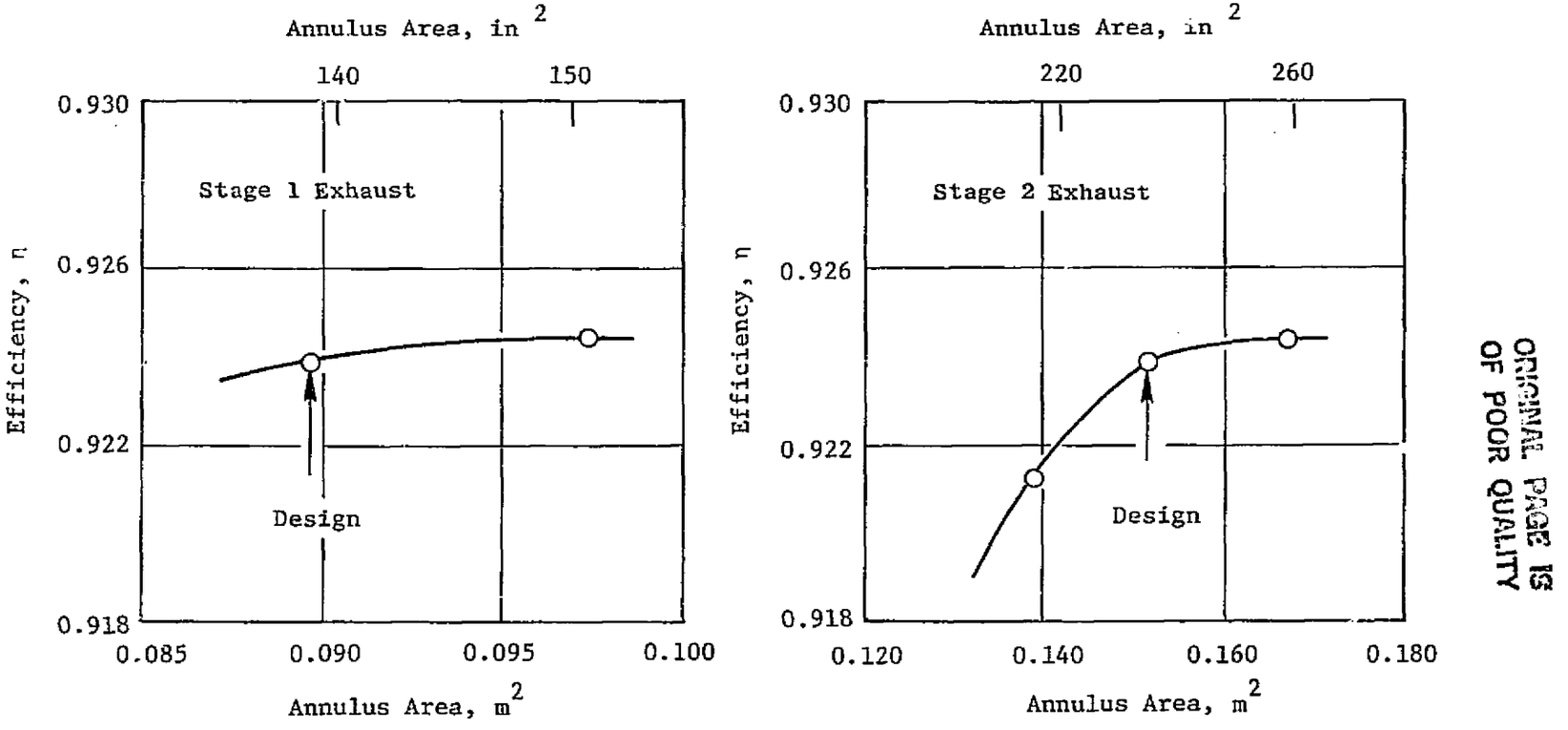

Figure 1. Annulus Trade Study.

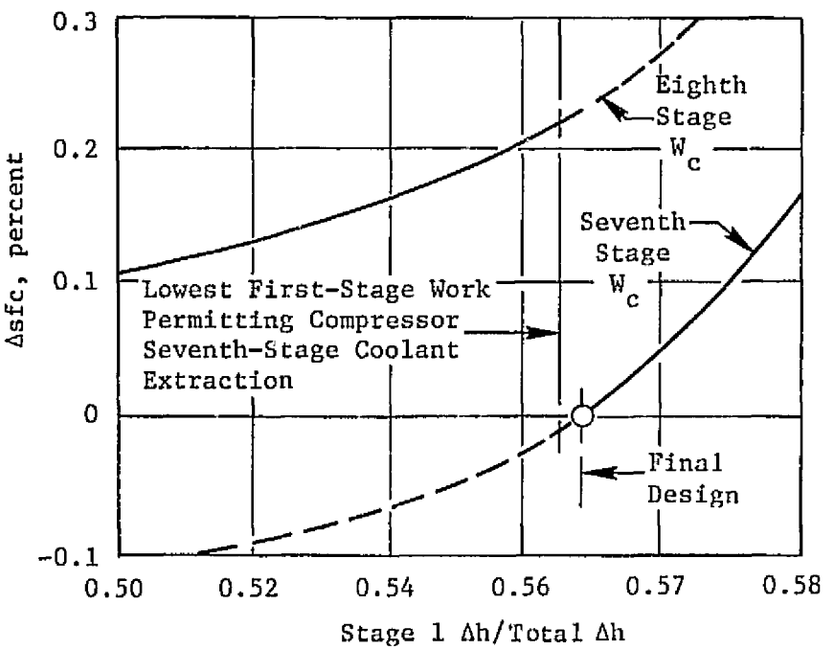

Figure 2. Stage Work Distribution.

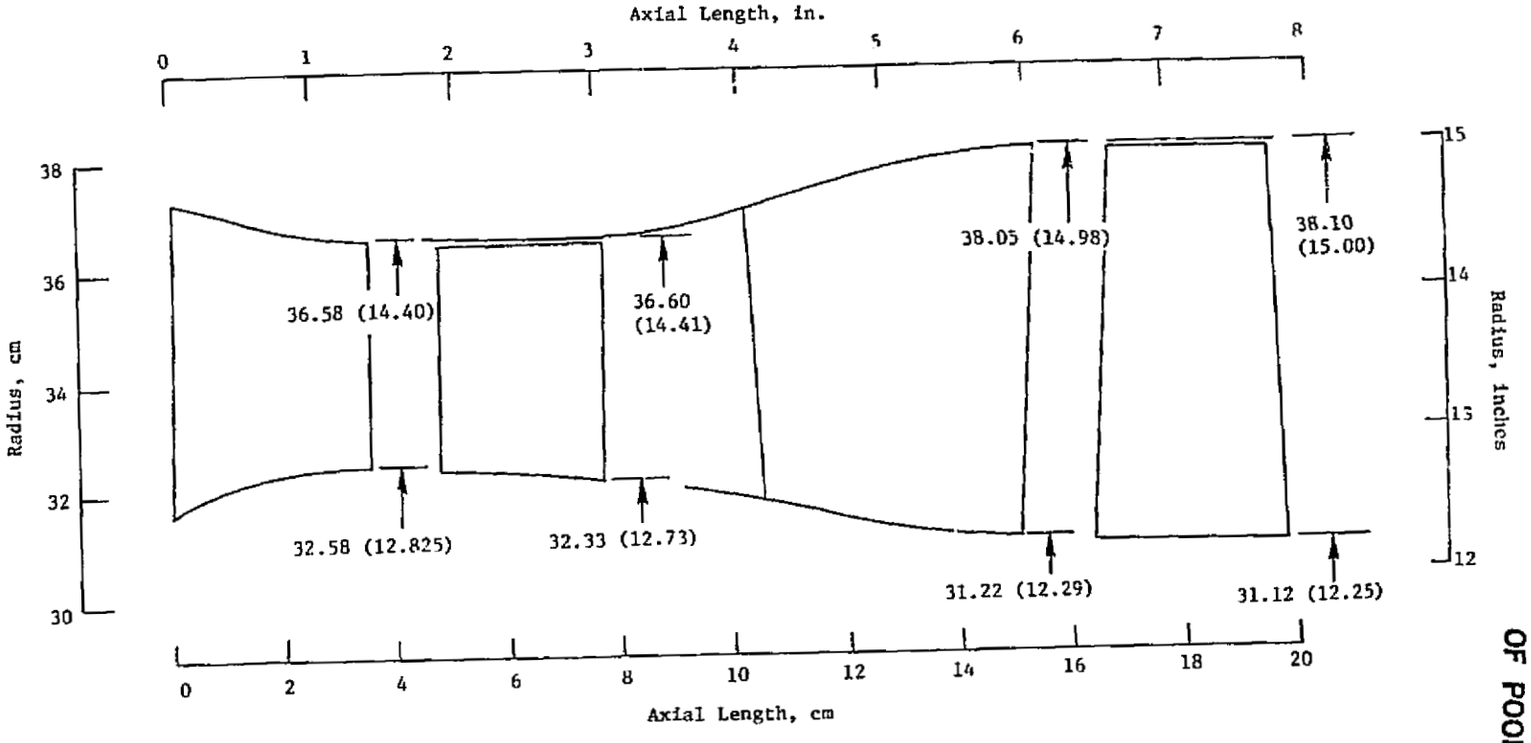

Figure 3. Turbine Aerodynamic Flowpath.

Table III. Stage Aerodynamics Summary.

Parameter	Stage 1	Stage 1*	Stage 2	Stage 2*
Pressure Ratio	2.25	(2.18)	2.11	(2.18)
$\Delta h/2U^2$	0.74	(0.69)	0.56	(0.56)
Tip Speed (Takeoff), m/sec	513.9		535.2	
ft/sec	1686		1756	
Cooling and Leakage, $\%W2_C$	18.2			
Exit Mach No.	0.34	(0.34)	0.42	(0.43)
Reaction	0.34	(0.38)	0.33	(0.35)
Swirl, Degrees	16	(15)	0	(1)
Number of Vanes	46		48	
Number of Blades	76		70	
Radius Ratio, D_n/D_t	0.88		0.82	
% Tip Clearance	1.0		0.6	

*A_{41} increased by 4%.

2.3 DETAILED AERODYNAMIC DESIGN

The objective of the detailed aerodynamic-design analysis was to obtain detailed geometry specifications of the flowpath and airfoils for use in demonstrator-engine hardware fabrication. This process was based on flowpath and other aerodynamic data established in the design trade studies. The design process consisted of a through-flow or vector-diagram analysis, for the purpose of establishing radial gradients of flow properties consistent with loss and desired work gradients, followed by the airfoil design analysis in which final airfoil geometry was determined.

The gas path through-flow or vector-diagram analysis was accomplished using a procedure that solves the full, three-dimensional, radial-equilibrium equation for axisymmetric flow. The procedure accounts for streamline slope and curvature, effect of the radial blade-force component data to airfoil sweep and dihedral, airfoil blockage, and radial gradient of flow properties. Calculations were made with radial gradients of blading losses, to simulate end-loss effects, and also with local flow addition to simulate ejected-film cooling. Temperature, dilution, and momentum-mixing losses associated with cooling-flow injection were accounted for within the calculation. The calculation model for the E^3 HPT, showing meridional streamlines and intrablade-row calculation stations, is shown on Figure 4. Final flow angle Mach

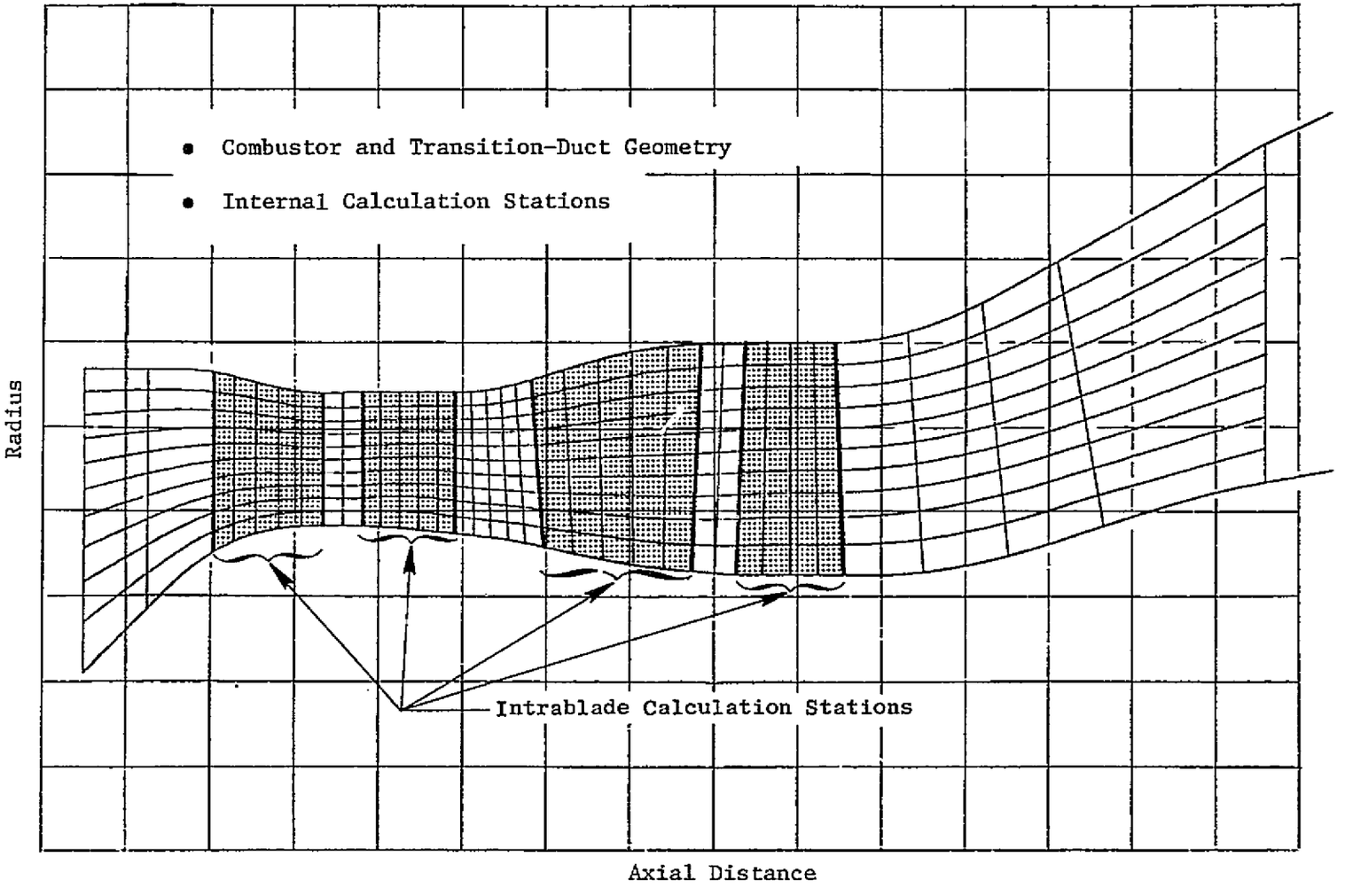

Figure 4. Axisymmetric-Flow Analysis Model.

numbers and energy extraction distributions are summarized in Figure 5. The overall gradients characterize the forced-vortex flow distribution and small gradients in stage energy extraction. The effect of loss gradients is seen in local angle and Mach number variations adjacent to the end walls. These data served as boundary conditions for the airfoil design analysis.

2.3.1 Airfoil Design Analysis

Airfoil aerodynamic design analysis was initiated based on vector-diagram data from the through-flow analysis and on preliminary solidities determined during design studies. A summary of the blading aerodynamic geometry is presented in Table IV. The design process was initiated by generating approximate airfoil shapes using a numerical procedure that applies a thickness distribution to a mean camber line as a function of flow angles and appropriate input coefficients. Mechanical constraints [such as edge thickness (including coating), thickness distribution, and radial taper] were observed along with the aerodynamic requirements in generating these shapes. These preliminary airfoil shapes were analyzed using a procedure that calculates the compressible flow along the stream surfaces, determined from the through-flow analysis, accounting for variations in streamtube thickness.

Table IV. Blading Aerodynamic Geometry.

Parameter	Stage 1 Vanes	Stage 2 Vanes	Stage 1 Blades	Stage 2 Blades
Number	46	48	76	70
Solidity, $\sigma = AW/t$	0.71	1.07	0.96	1.06
Zweifel No., ψ_Z	0.67	0.79	1.08	1.03
% Trailing-Edge Blockage	7.2	6.6	8.1	7.4
Aspect Ratio, $AR=h/d_o$	3.3	4.4	3.8	4.6
Unguided Turn, $\Delta\beta_s$	8.4	11.0	13.0	15.5

Undesirable features of the resultant surface-velocity distributions were corrected, and modified surface Mach number distributions were input to the analysis procedure in order to determine the modifications to the airfoil shapes necessary to produce the desired velocity distribution. Final airfoil shapes and velocity distributions are shown in Figure 6 for the hub, pitch, and tip sections. The data are represented by plots of local surface velocity normalized by downstream exit velocity. Peak Mach number is indicated on each velocity distribution.

a. Flow Angles

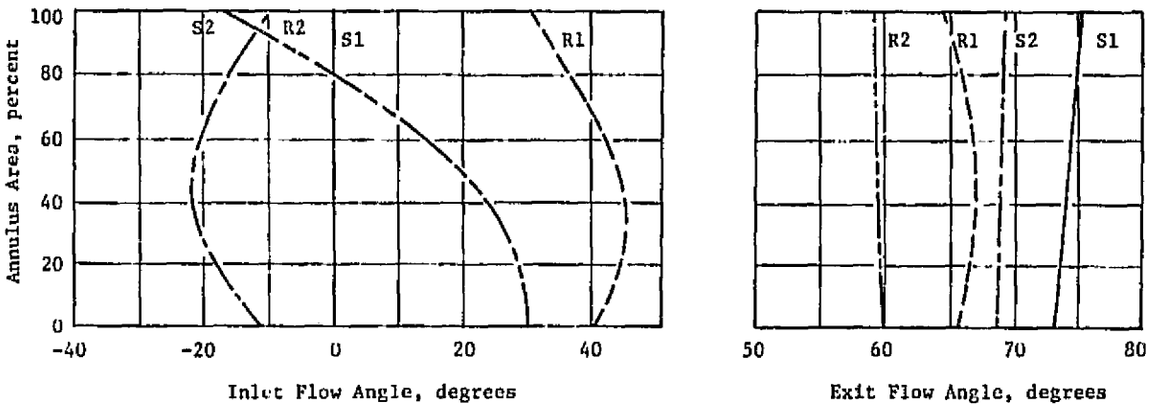

b. Mach Numbers

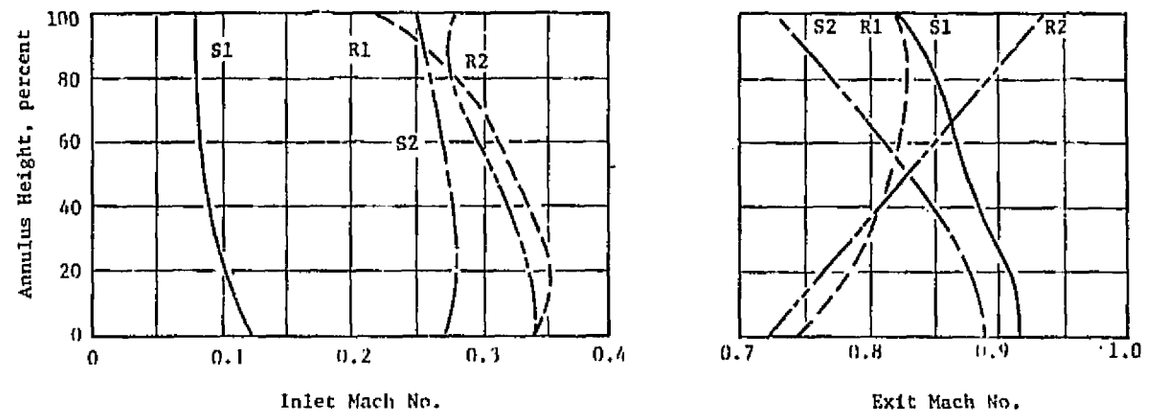

c. Energy Extraction

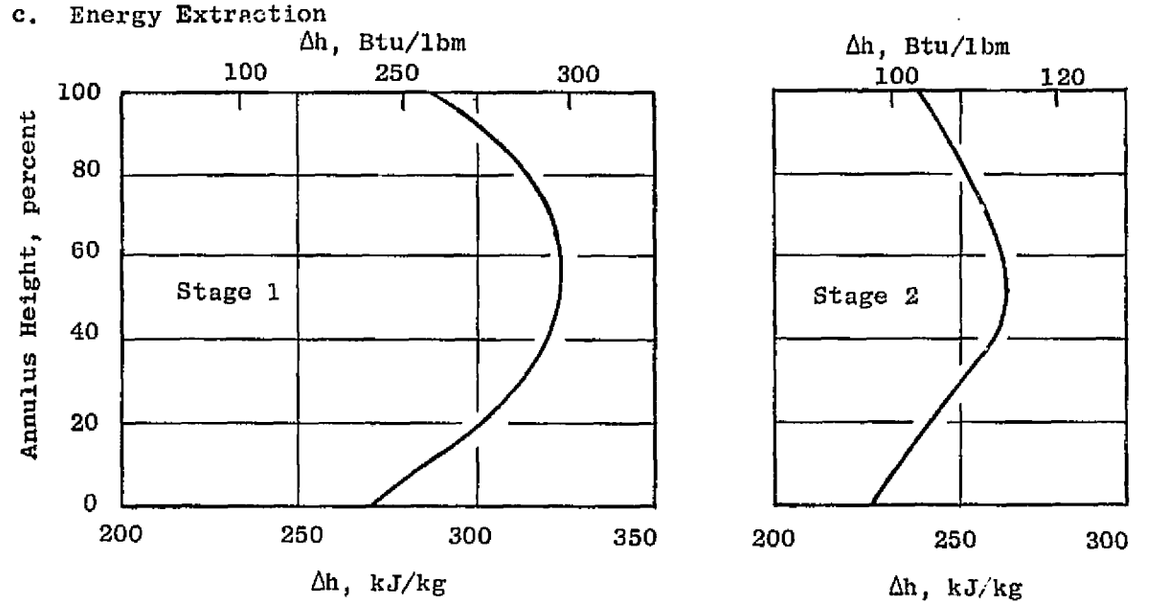

Figure 5. Blading Parameters.

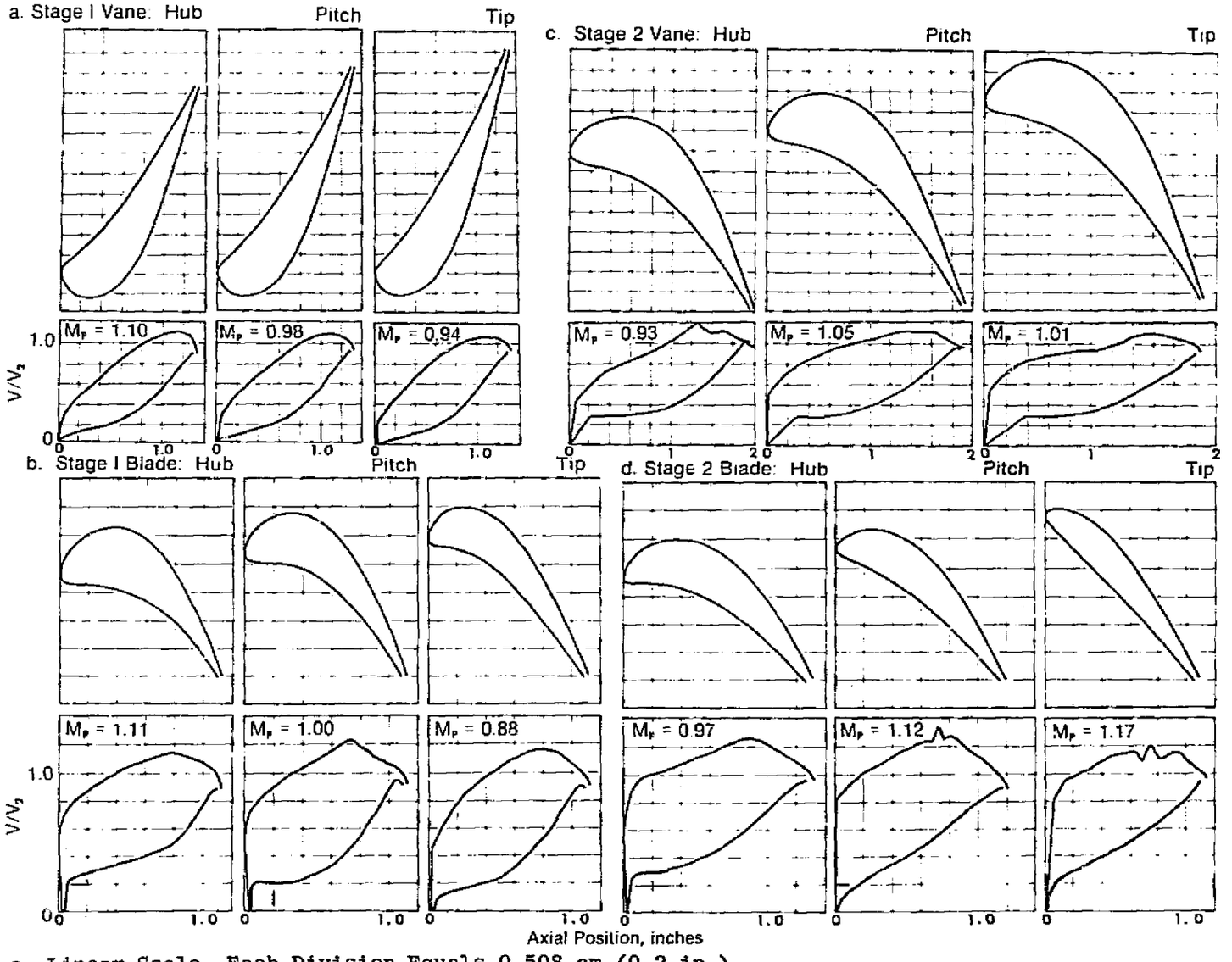

- Linear Scale, Each Division Equals 0.508 cm (0.2 in.)

Figure 6. Airfoil Shapes and Velocity Distributions.

2.3.2 Efficiency Prediction and Verification

After the preliminary design studies, a prediction of the design-point turbine efficiency was made based on appropriate uncooled, two-stage air-turbine test data. Correction factors for significant aerodynamic and cooling-flow effects were included. This prediction, summarized in Table V, shows baseline data and the appropriate corrections which resulted in an efficiency of 91.55%. This represented a deficiency of 0.35% relative to the ICLS goal of 91.9%.

Table V. Efficiency Estimate.

Base Aerodynamic Efficiency (Tight Clearance)	92.65%
Stage Loading	+0.27
Aspect Ratio	-1.04
Tip Clearance	-1.50
Improved Overlap	+0.30
Edge Blockage	+0.37
Improved Aerodynamics	+0.20
Cooling Effects	+0.30
Net Efficiency	91.55%

To verify predicted HPT efficiency, an air-turbine evaluation was completed in September of 1980. This evaluation included test of a full-scale, fully cooled, warm-air-turbine rig. The test rig employed slave hardware with hollow blading drilled to simulate all cooling flows in the prototype hardware. The test rig cross section is shown in Figure 7.

The test was run at an inlet temperature of 806 K (991° F) with shaft speed and power of 8300 rpm and 2.83 MW (3800 bhp), respectively. Power output was determined by measured shaft speed and shaft torque. Detailed analysis of the resulting data is in process; a detailed report will be issued at a later date. Preliminary analysis of the data indicated that the design-point efficiency was 92.5%, exceeding the FPS goal by 0.1%.

A plot of test efficiency versus blade-jet speed ratio (Reference 1) for several values of group pressure ratio is presented in Figure 8; each type of symbol represents a unique pressure ratio.

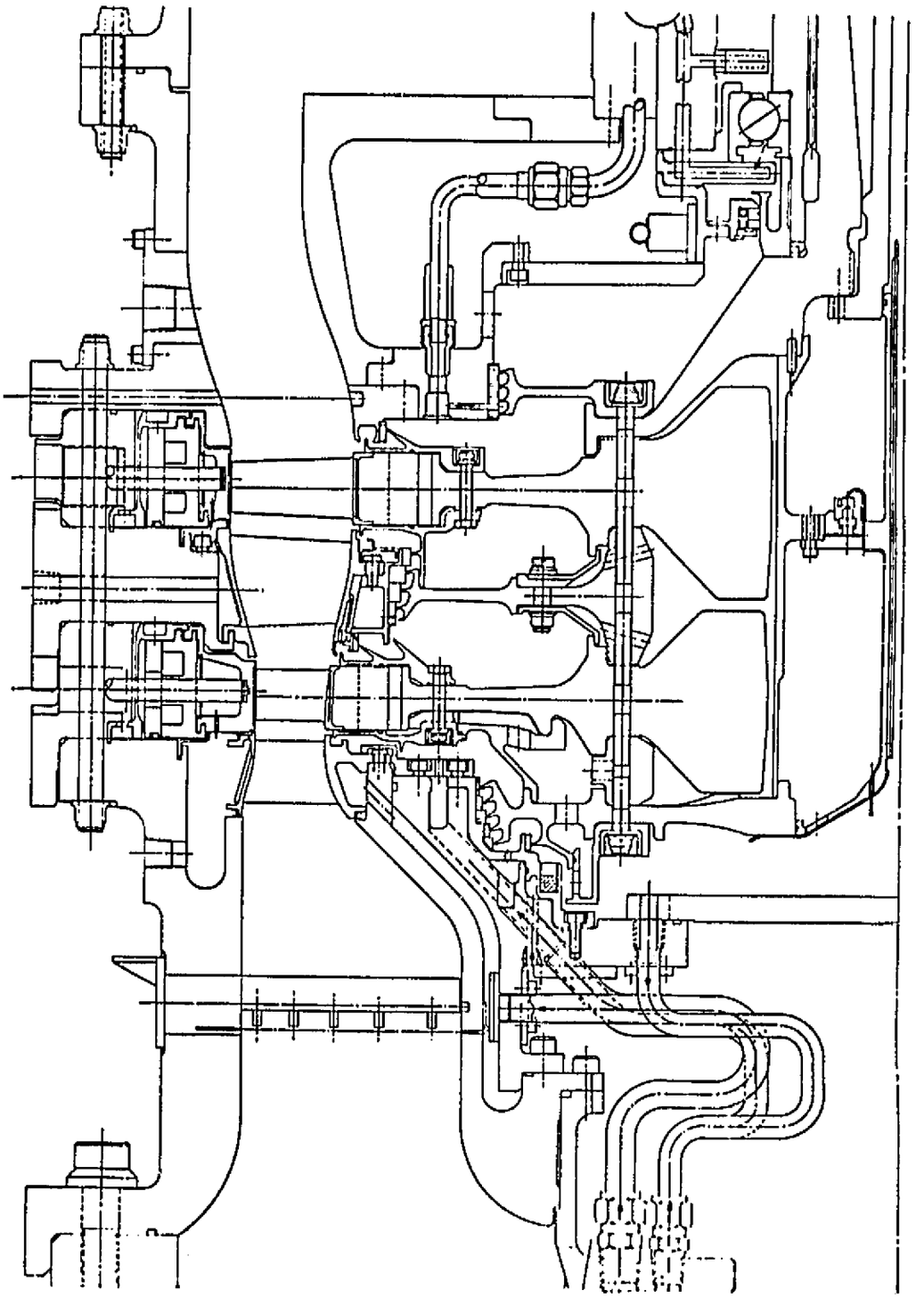

Figure 7. Warm Air Turbine Rig.

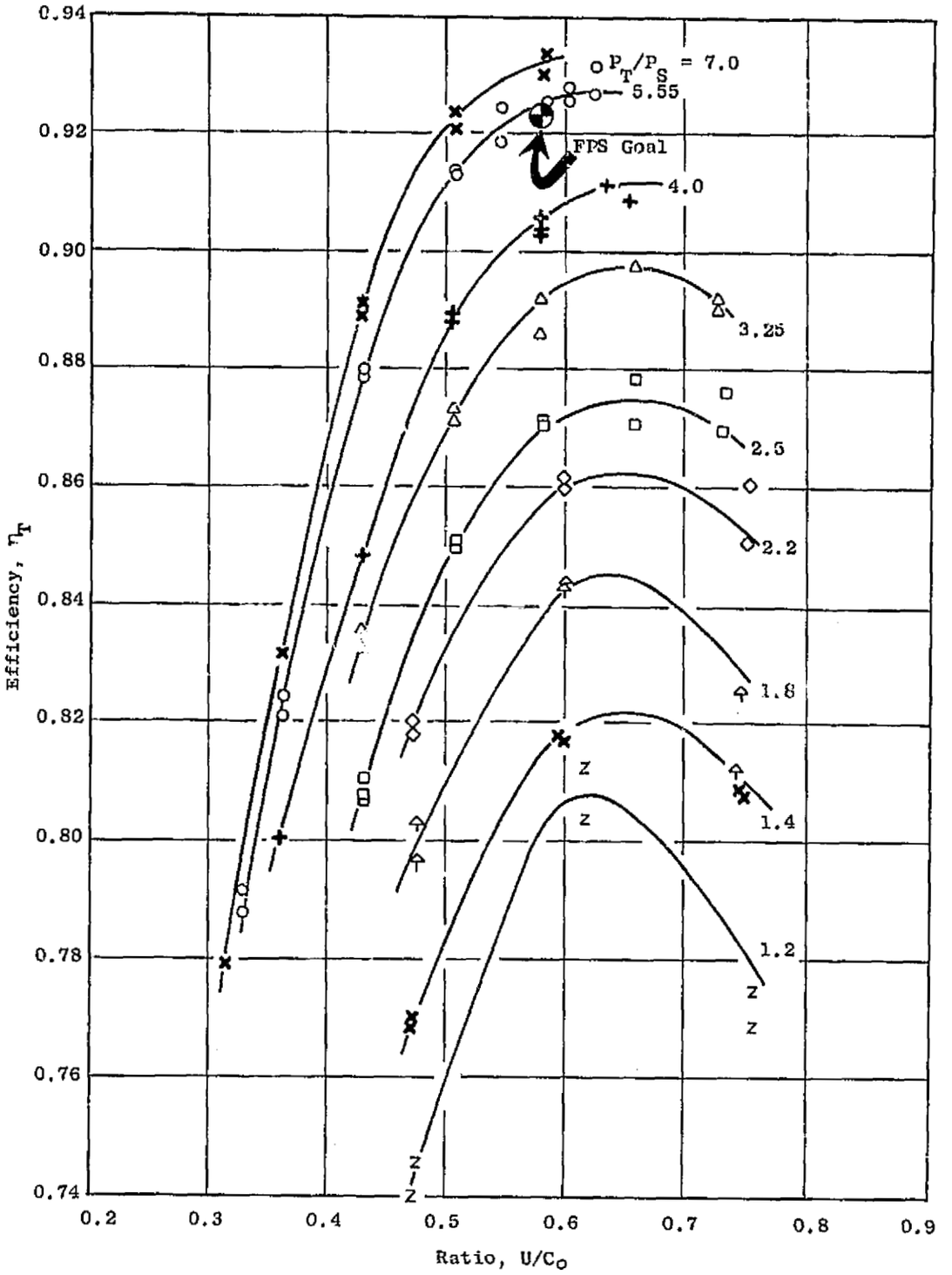

Figure 8. Blade - Jet Speed Performance and Subidle Mapping, Efficiency Versus Velocity Ratio.

3.0 COOLING SYSTEM DESIGN

3.1 FEATURES AND DEVELOPMENT

3.1.1 General Description

The E^3 high pressure turbine presents the challenge of designing components that maintain the life objectives while achieving levels of overall thermodynamic efficiency higher than state-of-the-art turbines. The design of the HPT cooling system is instrumental in achieving these goals. Several of the heat-transfer and cooling system features are shown in Figure 9.

The cooling systems selected for the hot-flowpath components (airfoils and end walls) are high-cooling-efficiency designs; thus the desired metal temperatures are achieved with low coolant-flow rates. The low coolant-flow rates lead directly to high thermodynamic efficiency as long as the coolant is returned to the flowpath without causing large mixing losses.

In Stage 1, where a relatively high level of cooling effectiveness is required, it is necessary to utilize the full potential of the coolant in order to maintain low coolant-flow rates. The design chosen for the E^3 uses the coolant for three separate cooling mechanisms in series. First, the air convectively cools the back side of the flowpath and airfoil walls by impinging on or by flowing through small passages containing turbulence promoters. The air then enters film holes and convectively cools the walls as it passes through. Finally, the air discharges from the holes onto the outside airfoil surfaces and provides film protection from the hot gas.

For the Stage 1 cooling system design, where a low-solidity vane is used, emphasis has been placed on reducing the amount of coolant required and also on injecting the coolant in a manner that minimizes performance penalties. The radially oriented holes are located in regions of very low velocity (leading edges and pressure surfaces) where the resulting performance penalty is slight. Axially oriented holes, that contribute momentum to the mixture, are used in the higher velocity regions (suction surfaces and trailing edges) where they have been shown to give excellent film protection in addition to lower mixing losses.

In Stage 2, where the required airfoil cooling-effectiveness levels are lower, convection-cooling systems were chosen because of several important factors. The use of convection/film systems, as in Stage 1, would theoretically allow lower coolant flow rates; however, film holes sized for discharge of the low Stage 2 coolant flow rates would either be too far apart to give uniform cooling or be too small in diameter. Small-diameter film holes tend to be more expensive to manufacture, are more prone to plugging, and lead to higher effective stresses. In addition, a certain quantity of the Stage 2 nozzle coolant is utilized for tip discharge, trailing-edge discharge, and interstage-seal blockage; when these quantities are expended, very little of the cooling air remains for film cooling.

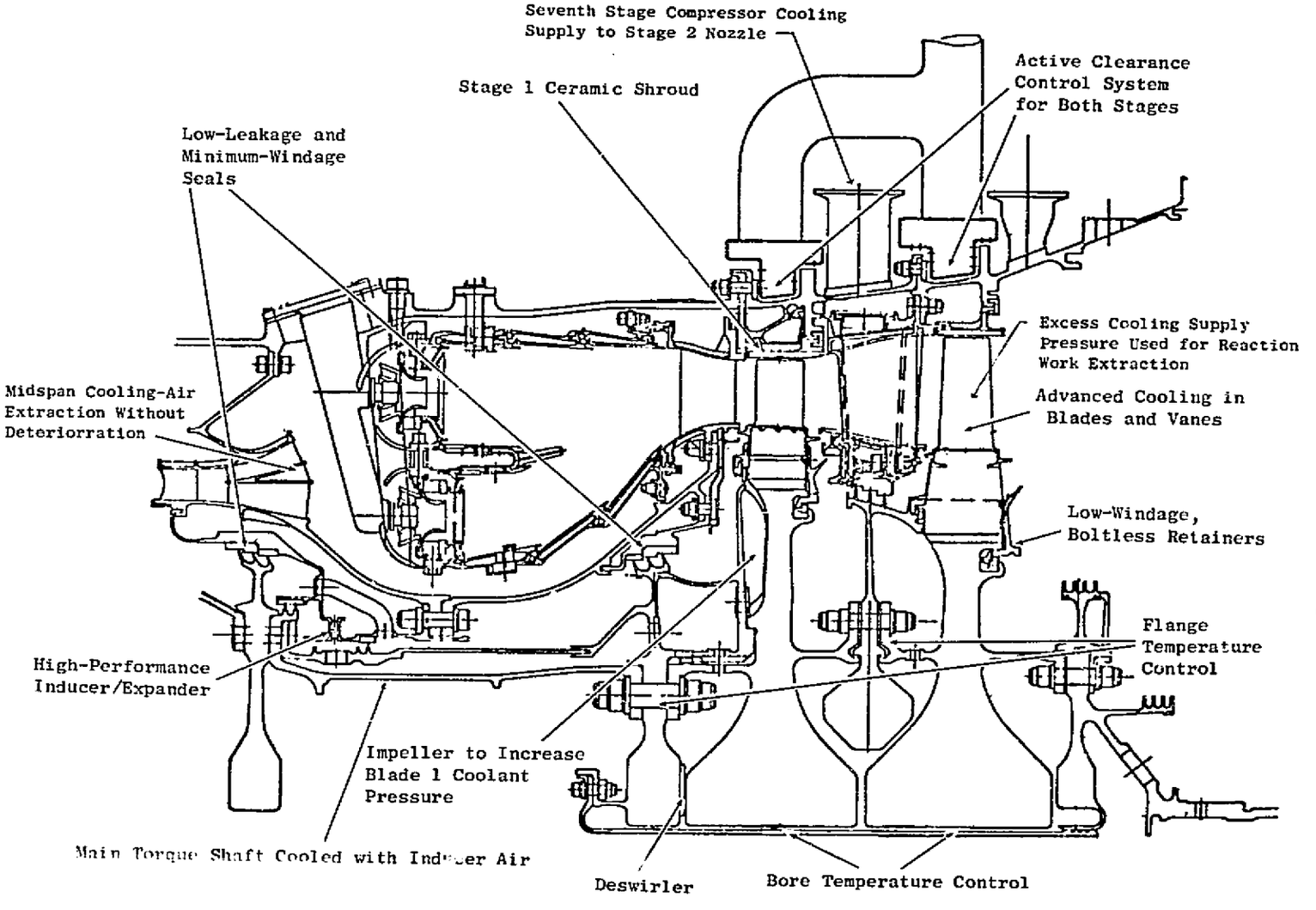

Figure 9. Heat-Transfer/Cooling Design Features.

As part of the turbine cooling system design, it was imperative that the method of injecting the cooling air into the gas stream be improved. The magnitude of the film-mixing losses is determined by the amount of coolant injection, the coolant-to-gas velocity ratio, the angle of injection, and the location of injection. A concerted effort has been made in the E^3 program to reduce the mixing losses of the film-cooling systems while accommodating the constraints imposed by manufacturing, the convective systems, and the need for film protection.

An upstream compressor-bleed location was chosen to supply cooling air to the Stage 2 turbine stator while satisfying backflow criteria. Use of the lower pressure air for coolant improves thermodynamic efficiency because less shaft work has been utilized in compression, and a smaller quantity of the lower temperature coolant is required.

A cooling-air expander, shown in Figure 9, is utilized to accelerate the rotor-blade coolant in the direction of rotation at the location where the coolant enters the rotor. This feature reduces the power required to pump the coolant to the blades and lowers the associated temperature rise. The result is lower blade-coolant temperature and, thus, lower coolant-flow rate. The rotor-coolant source is compressor-discharge air extracted at the mean line of the combustor diffuser. The objective of this scheme, as opposed to extracting cooling air from the compressor end wall, is to obtain lower temperature cooling air and to lower the deterioration rate. The cooling-air expander pressure ratio is chosen to be consistent with the blade-coolant pressure required to satisfy the Stage 1 blade leading-edge backflow criteria utilizing air at compressor discharge pressure. The cooling-air expander accelerates the air to the wheel speed such that the rotor does not have to do any pump work to the air as it is brought on board.

The reduced power required to pump the coolant corresponds to the shaft work that would be saved if the coolant were extracted from an upstream compressor stage at the required coolant pressure. However, the upstream-extraction system would be less efficient due to the low energy of the end-wall bleed compared to the diffuser-mean-line bleed selected.

In each cavity between the rotor and stator, an effort was made to keep the windage drag at a low level. Bolt covers were used where needed, and cavity sizes were reduced where possible. At any point where purge air was injected into a cavity, it was oriented in the direction of the rotor rotation through tangential holes or slots. This effort was directed at keeping the air tangential velocity as close as possible to the wheel speed in order to reduce drag on the rotor.

The number of seal teeth was optimized at all locations in the turbine to yield the lowest performance cost. The performance gains due to seal-leakage reduction associated with more seal teeth were traded off against the performance losses associated with the higher windage-power requirements induced by more seal teeth.

3.1.2 Trade Studies and Heat Transfer

As mentioned earlier in the aerodynamic section, several trade studies were conducted to assure the best turbine-system performance. These studies included aerothermodynamic design, heat transfer, mechanical design, and manufacturing considerations.

Early in the design, the optimun turbine-inlet temperature was set. The results of this trade study, presented in Figure 10, show the optimum, maximum takeoff, turbine-inlet temperature to be 1365° C (2490 F). To accommodate engine-thrust growth potential, the design turbine-inlet temperature was set on the low side of the optimum at 1343° C (2450° F). During this analysis, the turbine cooling-flow requirements and the engine core size were redefined for each turbine-inlet temperature under consideration.

With the optimum turbine inlet temperature at maximum takeoff defined at 1343° C (2450° F), the margin was defined at 78° C (140° F). The breakdown on the HPT inlet-temperature margin is presented in Table VI.

Table VI. $T_{4.1}$ Margin Definition.

	ΔT_{41}	
Direct Adders to Average Engine	° C	° F
Minimum to Average Engine at Power Setting	7.2	13
Engine Transient at Takeoff Power Setting	16.7	30
Open Clearance Schedule at Takeoff	11.1	20
Total Direct Adders (DA)	35.0	63
2σ Events Variation ±		
Humidity	3.8	7
Engine Quality Variations	14.4	26
Control System Tolerance (Includes T_{49} Measurement Tolerance)	13.8	25
Total Root Sum Square (RSS) Adders	20.5	37
Total Adders Required on New Engine (DA + RSS)	55.5	100
Added for Engine Deterioration	22.2	40
Total Adder with Deterioration ΔT_{41} =	77.7	+140

NOTE: Higher fuel cost degrades the advantage of higher turbine inlet temperature.

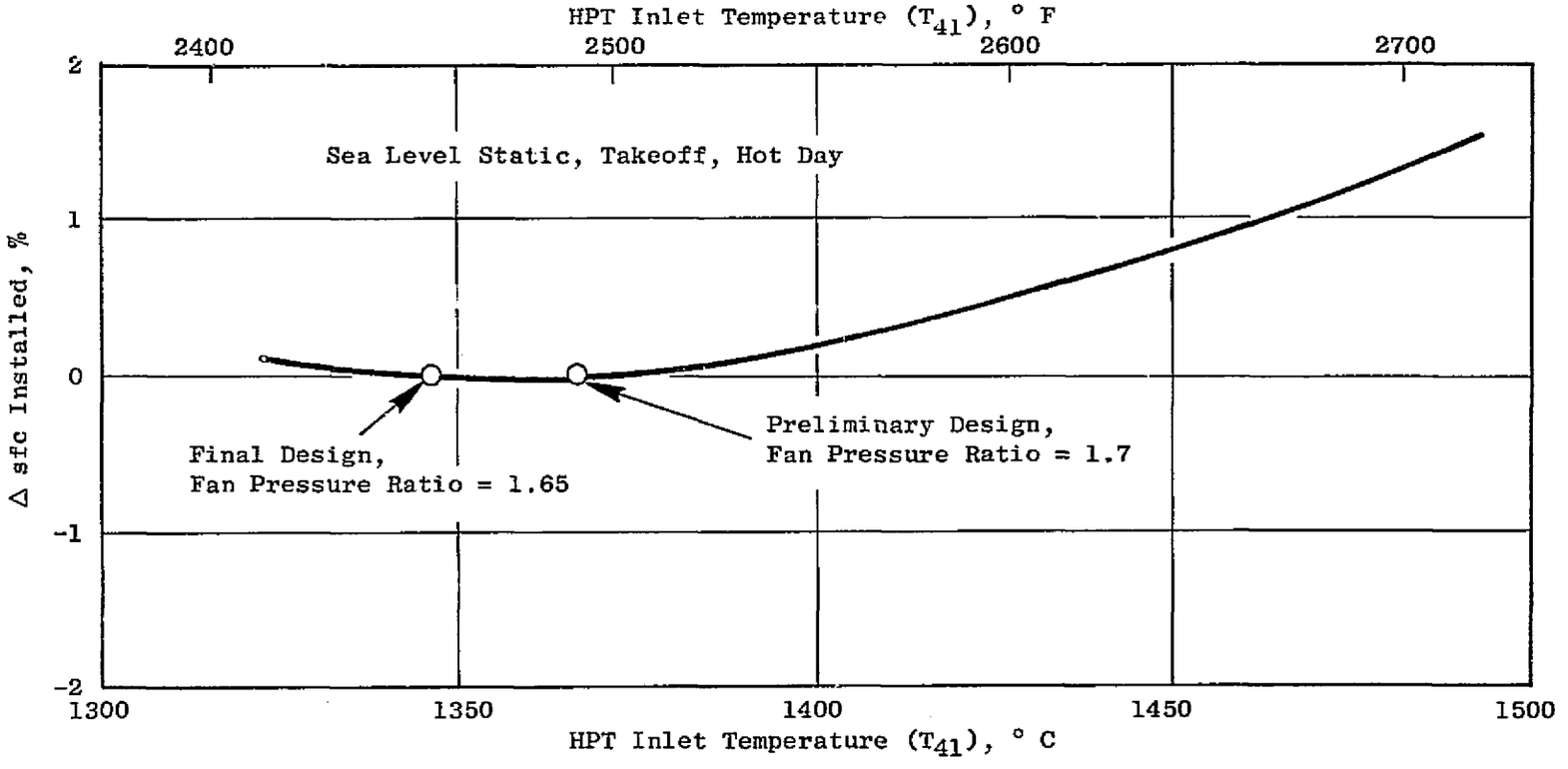

Figure 10. Effect of T_{41} on sfc.

For the E^3 turbine, the 22° C (40° F) margin specified for engine deterioration is somewhat below that established from commercial engine-deterioration experience. The reduction in deterioration should be realized due to the new Active Clearance Control (ACC) system in the compressor, HPT, and LPT along with improvements in core engine compressor blade erosion, the power-management system, and the prediffuser midstream-bleed system for rotor cooling.

3.1.3 Cooling-Supply System and Flows

A schematic of the overall turbine cooling-supply system is shown in Figure 11. The Stage 1 nozzle is cooled by air extracted from the inner and outer combustion-liner cavities. The vane leading-edge cavity is fed from the inner flowpath, and the aft cavity is fed from the outer flowpath. The rib separating the two cavities is slanted aft from tip to hub to provide maximum entrance flow area for the two impingement inserts.

The Stage 1 rotor is cooled by air extracted at the diffuser mean line. The expander, used to accelerate the coolant in the direction of rotation, and the coolant supply-system seals are combined with the seal at the compressor-discharge plane (CDP) into one balanced sealing system located radially to provide adequate rotor thrust balance. The diffuser mean-line bleed flow is also used to back-pressure the compressor-discharge seal. This results in a cooler seal operating temperature since the mean-line bleed is cooler than the end-wall flow upstream of the compressor outlet guide vane. The compressor-discharge seal leakage bypasses the expander feed cavity to prevent heating of the rotor-blade coolant. The bypass system routes the leakage to the aft expander seal. The expander seal leakage then is used to purge the Stage 1 disk forward-wheel-space cavity.

The Stage 2 nozzle coolant is extracted from the compressor at the Stage 7 stator exit. This flow is collected in manifolds and routed by pipes to the turbine. The Stage 2 rotor coolant is supplied through the Stage 1 rotor inducer system.

Once the local gas temperatures and life requirements for each component in the turbine were set, the required chargeable and nonchargeable cooling-flow rates could be defined. These flows are presented in Table VII.

The nonchargeable cooling flow and leakage in the Stage 1 nozzle is 9.46% of the core inlet flow, and the total chargeable cooling and leakage flows amount to 9.41%. The chargeable cooling and leakage is further broken down into 6.91% of compressor discharge air, 2.35% of seventh-stage compressor bleed air, and 0.15% of fifth-stage compressor bleed air.

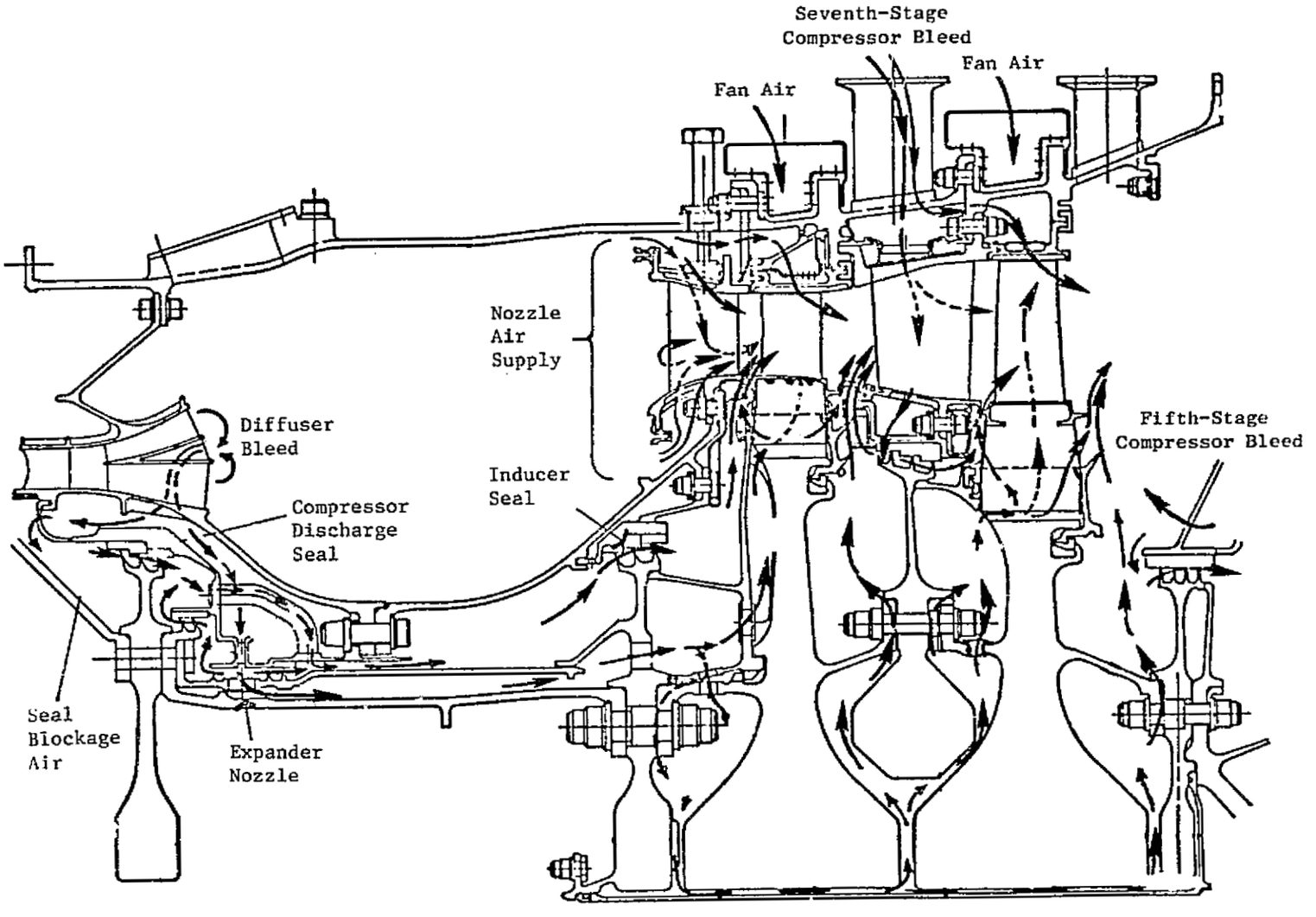

Figure 11. Rotor and Casing Cooling-Supply System.

Table VII. Cooling and Leakage Flows.

• Constant-Life/Fixed Engine • Max Climb, 10.67 km (35,000 feet)	
Flow	%W25
Nonchargeable Cooling and Leakage	9.46
CDP Leakage and Purge Air	2.25
Stage 1 Shroud (CDP)	0.6
Stage 1 Blade (CDP Ind)	3.3
Stage 2 Vane and Interstage Seal Blockage Air (Compressor Stage 7)	2.0
Stage 2 Shroud (Compressor Stage 7)	0.35
Stage 2 Blade (CDP Ind)	0.76
Disk 2 Aft-Cavity Purge Air (Compressor Stage 5)	0.15
Total	18.87

3.1.4 Flight Mission

In order to properly define the heat-transfer design of each component in the turbine, it is necessary to define an appropriate aircraft/engine mission. The mission that was chosen for the E^3 was a 2-hour flight typical of a domestic commuter airline. This mission is presented in Figure 12. It should be noted that each component has its own worst mission. In doing the turbine heat-transfer analysis, variations to the mission were considered for each component. The complete mission, including start and shutdown, had to be analyzed for the rotor structure while the idle, takeoff, and thrust-reverse missions were analyzed for the blades and vanes. The gas-temperature profiles associated with the double-annular-combustor fuel schedule during starting were evaluated for the blades and vanes.

The mission mix evaluated data for sea level hot day 50°C (122°F), flat rating day 30°C (86°F), standard day 15°C (59°F), and cold day -2°C (29°) take-off conditions. The engine thrust is constant (flat rated) up to the corner point temperature and then is limited by a constant turbine rotor inlet temperature of 1343°C (2450°F). At the hot day temperature, the turbine will run at the same temperature as the corner point but at a lower pressure. A comparison of the significant heat transfer parameters for the hot day and corner point day is shown in Table VIII.

- One Cycle Start-Stop

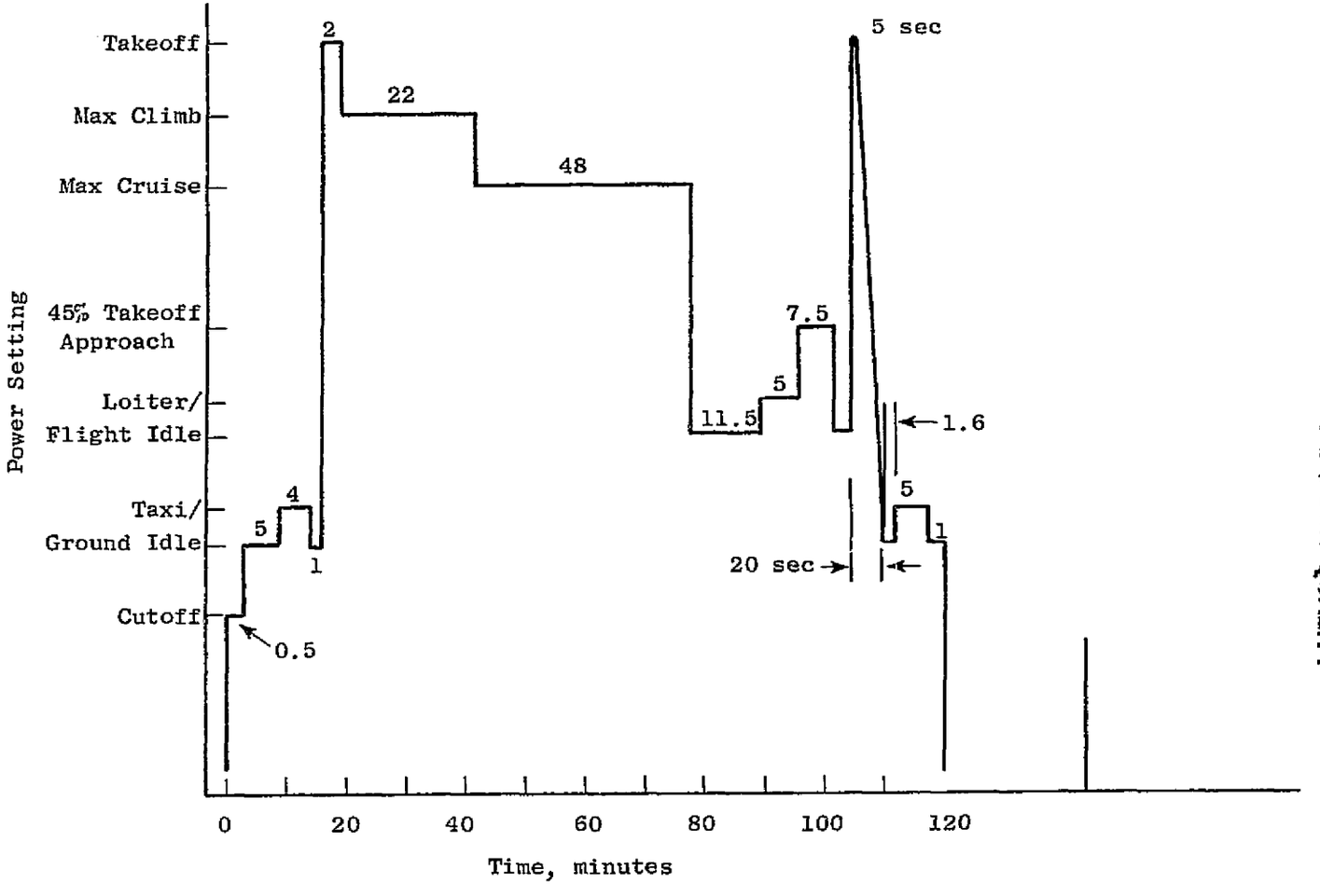

Figure 12. Flight Cycle Mission.

Table VIII. Heat-Transfer Design Parameters.

• Mach 0.3, Sea Level Takeoff		
Parameter	Max $T_{Coolant}$ 50° C (122° F) Day	Max P_{Gas} 30° C (86° F) Day
P_3, MPa (psi)	2.66 (385.76)	3.08 (446.66)
T_3, ° C (° F)	597 (1107)	583 (1081)
T_{41} (Cycle), ° C (° F)	1343 (2450)	1343 (2450)
ΔT_{41} Margin, ° C (° F)	77.7 (140)	77.7 (140)
T_{41} Design, ° C (° F)	1421 (2590)	1421 (2590)
T_{40} Max Peak, ° C (° F)	1739 (3163)	1747 (3177)
T_{tb} Design, ° C (° F)	1396 (2545)	1396 (2545)
Rotor Speed, rpm (Cycle)	13,287	13,179
$W_{Cooling + Leakage}$, % W_{25}	18.87	18.87
ΔT (Max Takeoff-Max Climb), ° C (° F)	158 (285)	158 (285)

3.2 DETAILED COOLING SYSTEM AND HEAT TRANSFER DESIGN

3.2.1 Stage 1 Nozzle

The first-stage nozzle is cooled with combustor bypass air from the compressor-diffuser exit as shown on Figure 13. The coolant for the vane leading-edge region and inner band bypasses the inner combustor liner. The vane is separated into two cavities by a rib that runs from the root to the tip of the vane in the general region of the airfoil midchord. The rib is oriented such that the coolant flow area is maximized as it enters the vane in order to reduce any pressure losses that are not used for generating coolant heat transfer. The coolant for the aft section of the vane bypasses the outer combustor liner before entry into the vane. The prime function of the dual coolant-supply system is to maintain a balanced bypass flow around the inner and outer combustor liners. This makes the pressure losses insensitive to tolerance stackup and thermal growth mismatch problems between the combustor and surrounding structure.

The Stage 1 vane and band (stator end walls) cooling schemes have been designed to meet the specified metal-temperature requirements with emphasis on reducing the mixing losses and coolant usage while operating in a high-temperature environment. The design conditions for the Stage 1 nozzle components are given in Table IX.

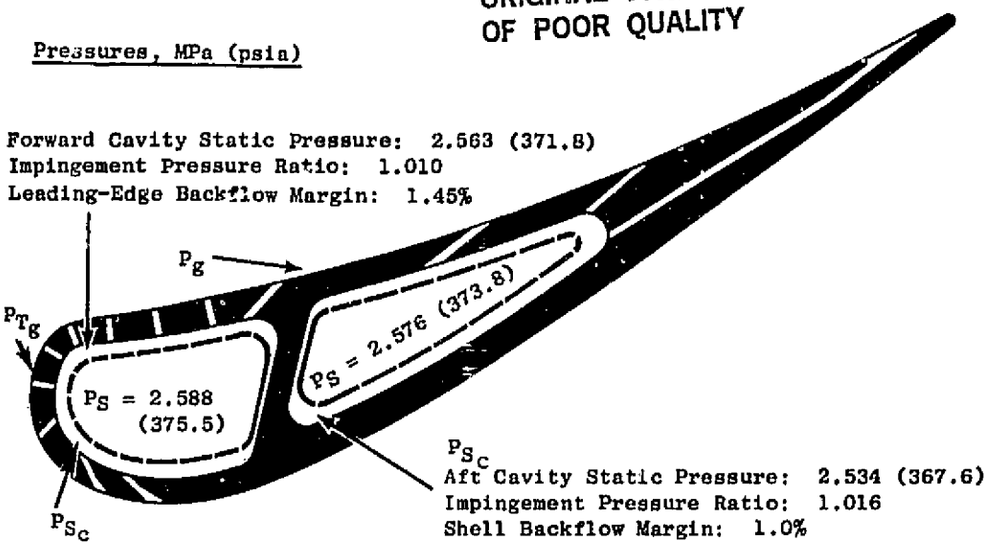

(a) Vane Cavity Pitch-Line Pressures

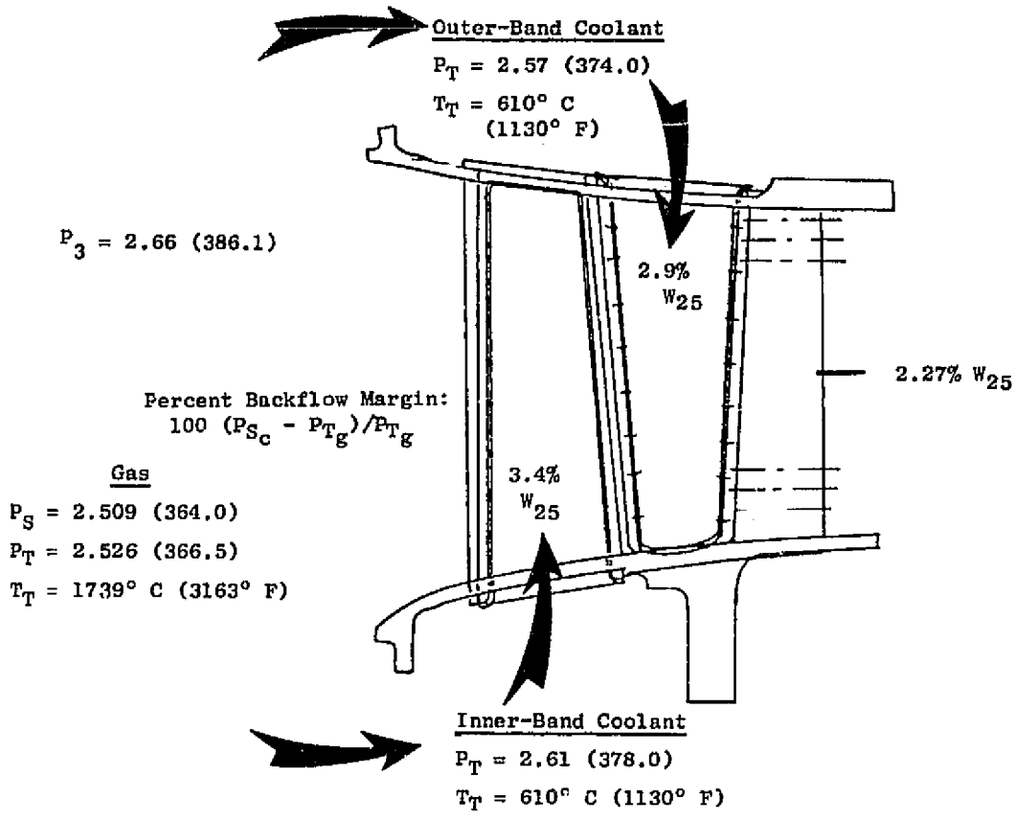

(b) Nozzle Cooling Air Supply

Figure 13. Stage 1 Vane.

Table IX. Stage 1 Vane Cooling Parameters.

Nonchargeable Flow, % W_{25}	9.24
Pattern Factor	0.26
$T_{4.0}$ Max Peak, ° C (° F)	1739 (3163)
$T_{Coolant}$, ° C (° F)	610 (1130)
Leading-Edge Backflow Margin, %	1.45
W_C Vanes, % W_{25}	6.3
W_C Bands, % W_{25}	2.80
$W_{Leakage}$, % W_{25} (Nonchargeable)	0.36
$W_{Leakage}$, % W_{25} (Chargeable)	0.21
Number of Vanes	46

A detailed schematic of the cooling system for the Stage 1 vane is shown in Figure 13. This design includes two impingement inserts and trailing-edge, pressure-side-bleed (PSB) slots. The cooling design makes extensive use of film cooling and impingement cooling at the vane leading edge and the midportion of the vane and efficient, convective, long slots in the vane trailing edge. The cooling air, drawn from the combustor liner, is fed from the stator inner flowpath for the leading-edge insert and from the stator outer flowpath for the aft insert. This arrangement takes advantage of the compressor-discharge total pressure profile to provide a higher coolant feed pressure at the combustor inner liner and maintain a positive pressure ratio across the leading-edge film holes, as shown in Figure 13. In addition, the rib separating the two inserts is slanted to create larger entrance flow areas for both inserts.

The two impingement inserts, shown in Figure 14, have a prescribed pattern of small holes that provide highly effective cooling by impinging cooling air normal to the inside surface of the vane shell. The impingement-hole spacing varies between four and eight diameters in the leading-edge insert and between six and eight diameters on the aft insert. This impingement-hole pattern variation is used to balance the temperature gradients between a high-heat-flux, low-film location and the low-heat-flux, high-film location on the vane gas side.

Considerable attention was directed to the cooling-air pressure losses of the outer and inner combustor liners. Because of the compressor prediffuser dump pressure losses and the fuel-nozzle/skirt blockage, the outer-liner pressure losses were 3% as indicated by the combustor model tests. The inner-band pressure losses were 2%. The total pressure losses for the complete system amounted to 3.15% at the outer band and 2.12% at the inner band. In order to help overcome the larger than expected pressure loss in the combustor outer liner, a bellmouth was designed for the inlet to the aft insert, as shown in Figure 14. This feature reduced the velocity-head loss by 35% and holds the aft-insert impingement pressure drop to 1%; this is comparable to that of the leading-edge insert. Vane-shell backflow margins of 1% in the aft cavity and 1.45% in the forward cavity resulted.

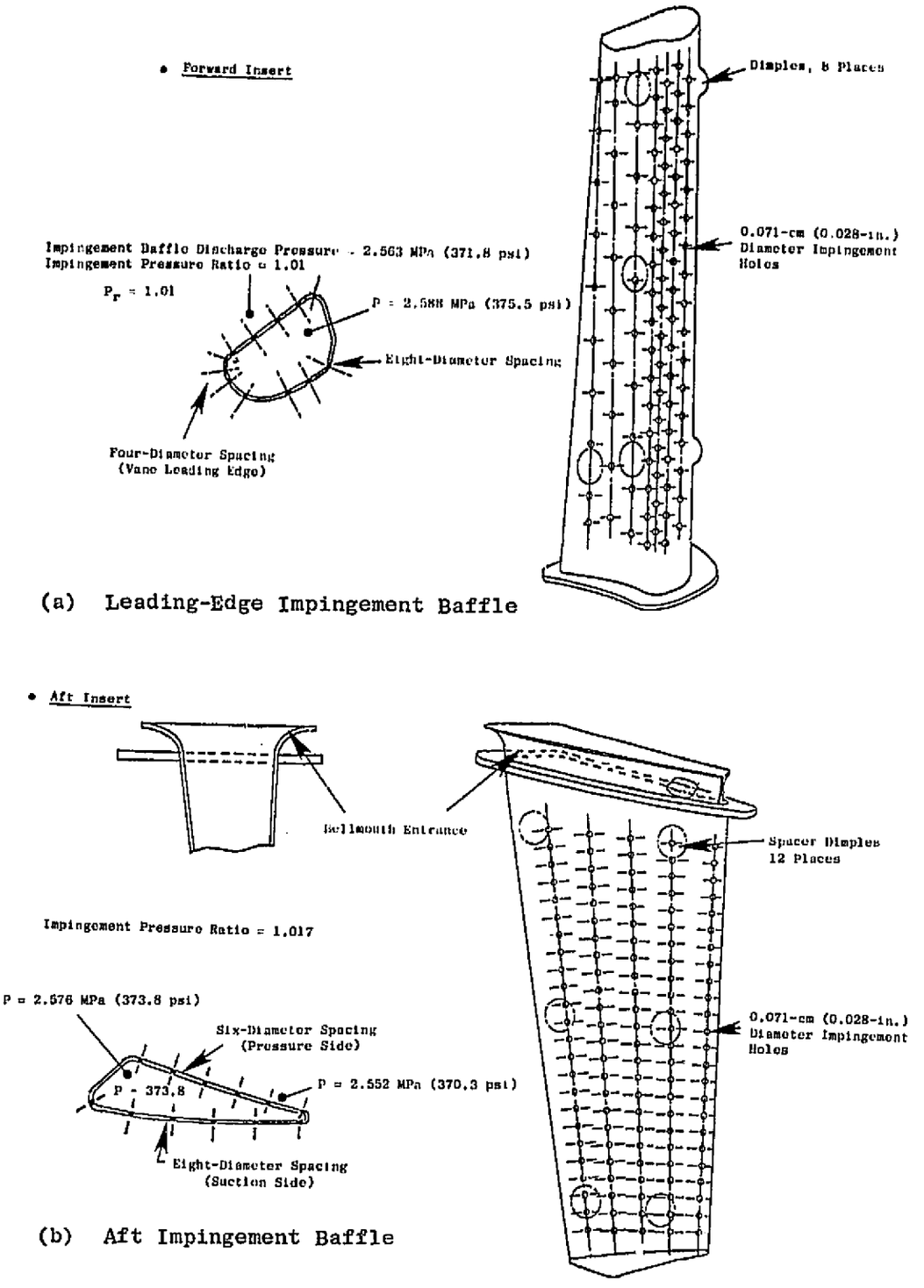

Figure 14. Stage 1 Nozzle Impingement Baffles.

After the impingement, the coolant is injected into the hot-gas stream for film cooling through various types of film holes drilled in the vane shell. The film-hole pattern is shown in Figure 15.

The pressure-side-bleed slots incorporated in the current vane design for cooling the trailing edge offer improved stator performance. The slots discharge cooling air to a lower gas-side Mach number area and result in a smaller coolant/mainstream mixing loss compared to conventional, trailing-edge bleed.

The vane is designed for the local maximum turbine-inlet temperature of 1739° C (3163° F). The total cooling flow required is 6.3% W_{25} of which 3.4% W_{25} is for the forward insert and 2.9% W_{25} is for the aft insert. The vane pitch-line bulk material temperature is 947° C (1737° F) with the local leading and trailing-edge surface temperatures under 1093° C (2000° F) in the hot streak. The thermal-node breakdown used in the heat-transfer analysis is presented in Figure 16 and consists of 164 nodes and 68 separate temperature and heat-transfer coefficient tables of 35 time steps. Vane steady-state temperatures at hot-day takeoff are also shown in Figure 16. The hot-day takeoff transient was also analyzed since the transient temperature gradients appear to be the most life limiting. The transient analysis accounted for the combustor fuel schedule at idle and transient maximum takeoff.

The momentum mixing losses associated with film injection into the gas stream were evaluated in detail. This study showed that the major losses occur at the pressure-side trailing edge and at the suction-side film holes. Annular-cascade data verified the losses from the suction-side film holes, as shown in Figure 17, and indicated a need to decrease the tolerance in the trailing-edge, pressure-side slots. The annular-cascade hardware incorporated slots with excessive diffusion. Even though they met the flow-check requirements, the velocity of the air leaving the slots was low enough to double the mixing losses of the trailing-edge flow. The tolerances on the slots were subsequently reduced on both the air-turbine rig and the engine hardware.

The cooling design for the stator inner band is illustrated in Figure 18. The inner and the outer bands are both designed to be cooled on the back side by an array of coolant jets impinging from a baffle plate fed by a coolant plenum. The spent impinging air is then collected and discharged from rows of film holes inclined to the main gas flowpath to create a film over the band hot surface. With the emphasis on reducing the stator performace mixing-loss penalty, all film holes are selectively located upstream of the vane flowpath throat where the local gas Mach numbers are relatively low. This characteristically results in lower coolant/gas-stream mixing losses. The placement and orientation of the film holes also take into account end-wall, secondary-flow effects on the film.

The details of the outer-band cooling system are presented in Figure 19. The outer band used a cooling flow of 1.5% W_{25} and the inner-band cooling design requires 1.3% W_{25}. The band flowpath intersegment seals are of the hour-glass type from the band leading edge back to the nozzle throat; spline

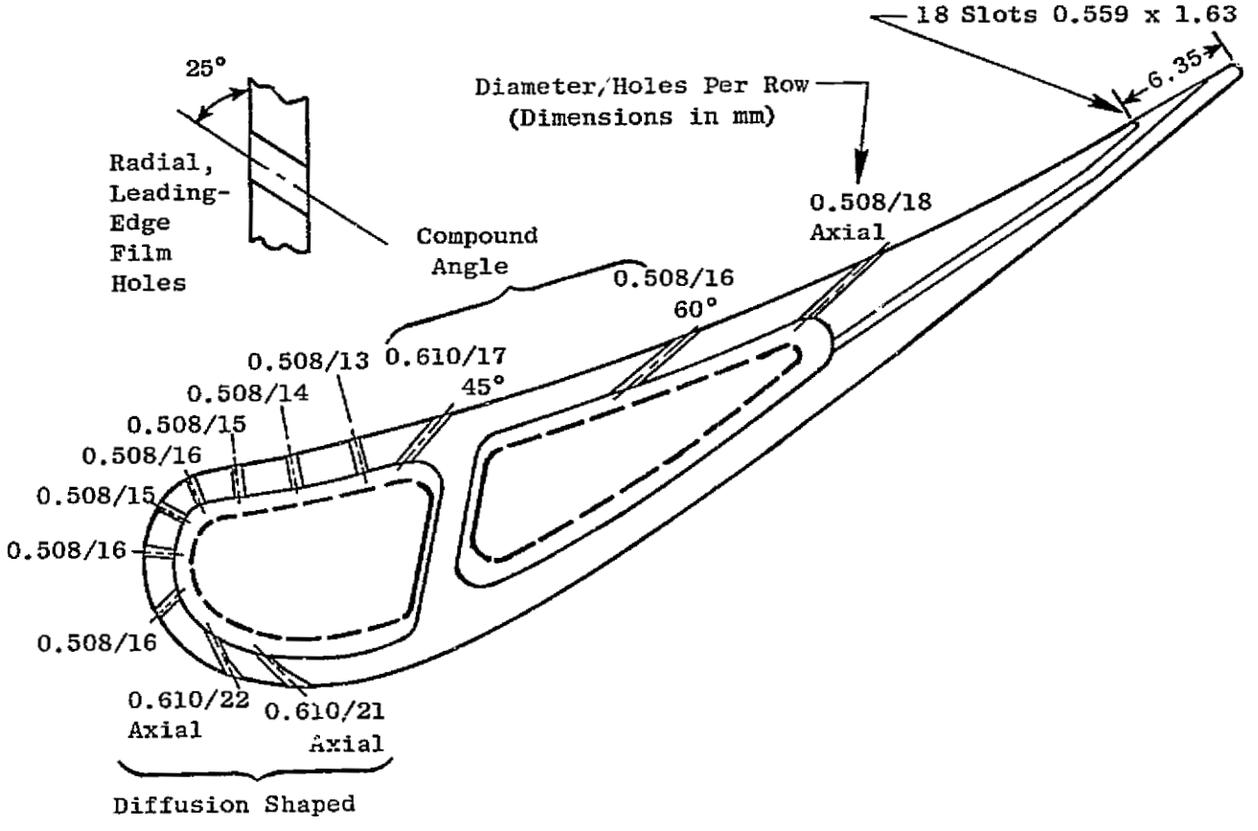

Figure 15. Stage 1 HPT Vane Cooling Geometry.

Thermal Model at Pitch Section

- 164 Nodes
- 68 Boundary Conditions
- 35 Transient Time Steps

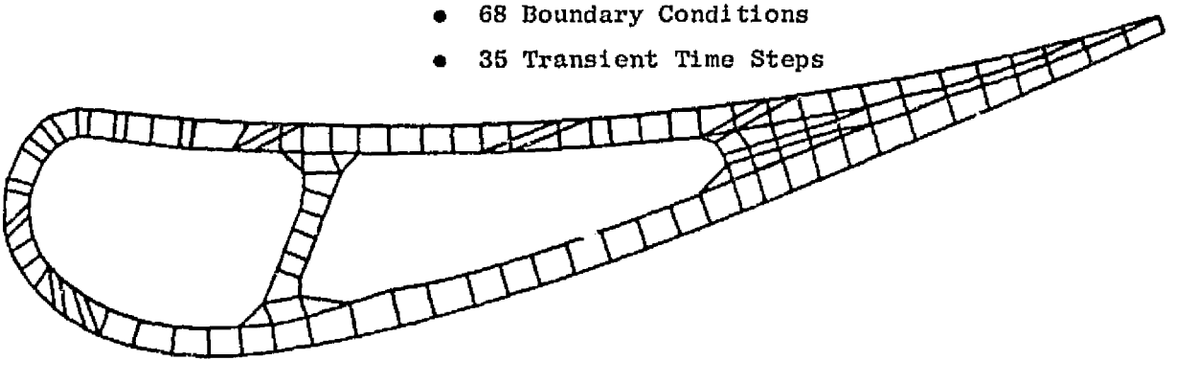

Detailed Temperatures at Pitch Section

° C (° F)

T_{Bulk} = 947 (1737)

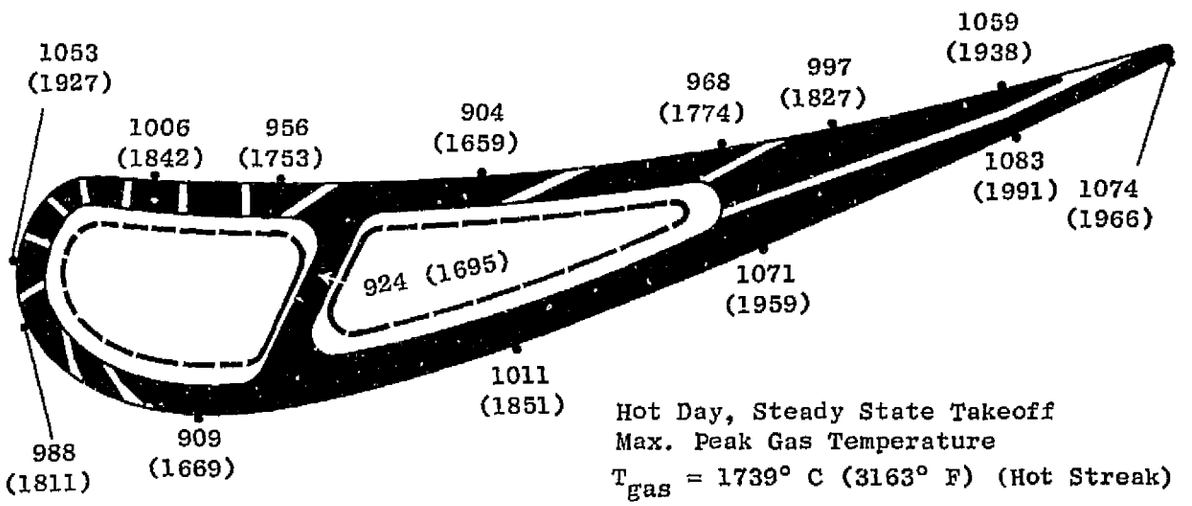

Hot Day, Steady State Takeoff
Max. Peak Gas Temperature

T_{gas} = 1739° C (3163° F) (Hot Streak)

$T_{coolant}$ = 610° C (1130° F)

$W_{coolant}$ = 6.30% W_{25}

Figure 16. Stage 1 Vane Thermal Model and Detailed Temperature Distribution.

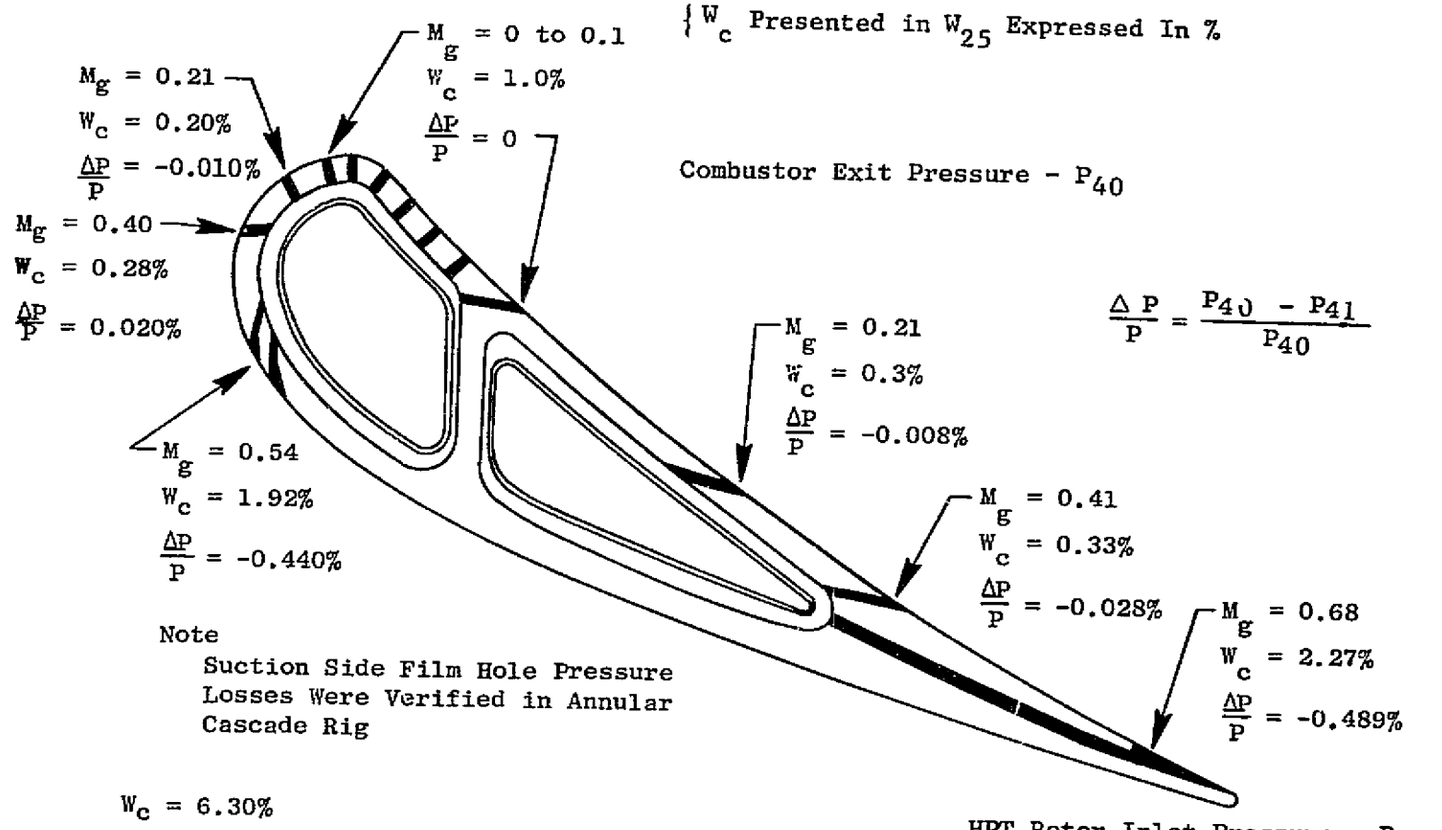

Figure 17. Stage 1 HPT Vane Cooling Air Mixing Losses.

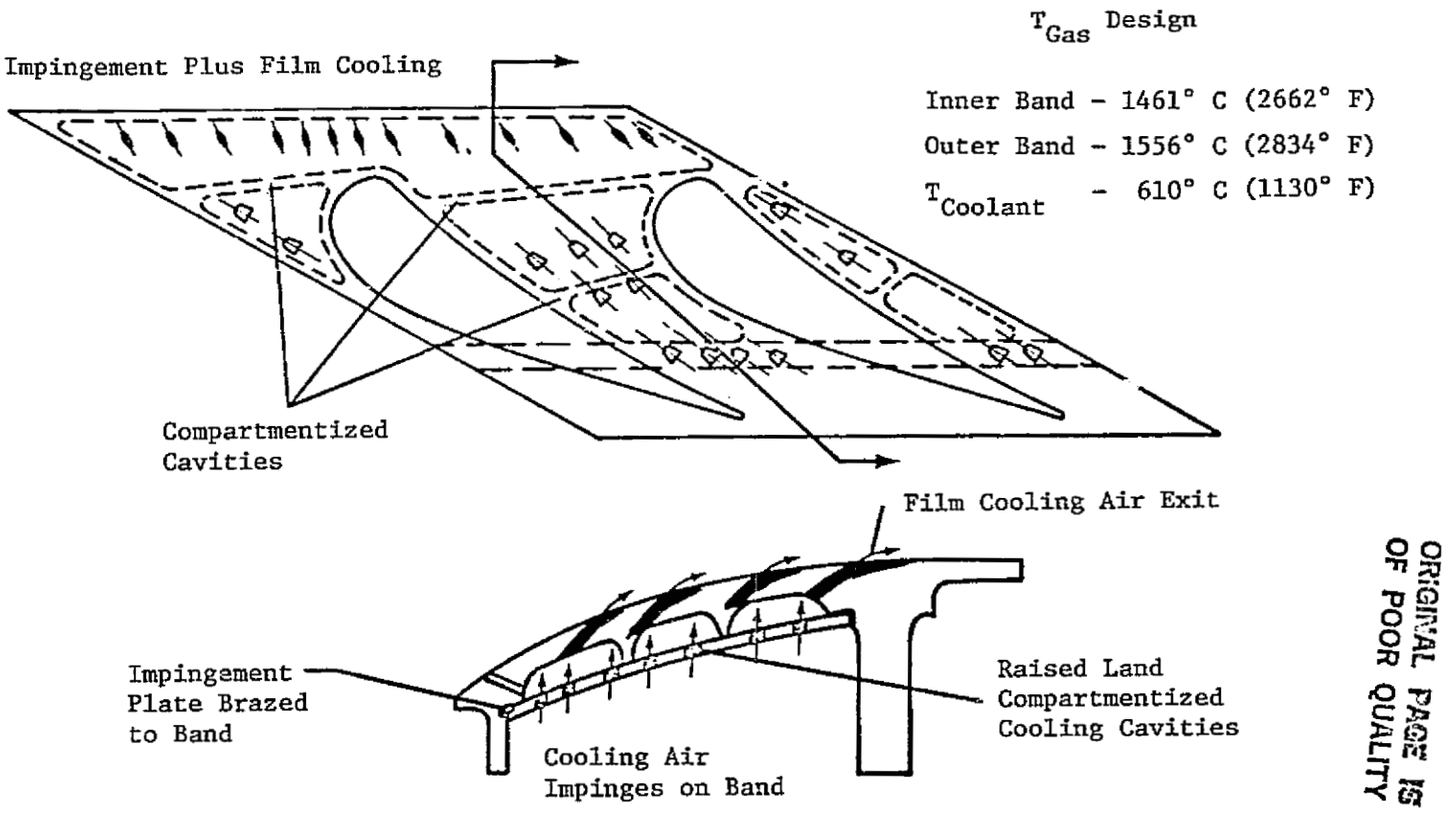

Figure 18. Stage 1 Vane, Inner Band.

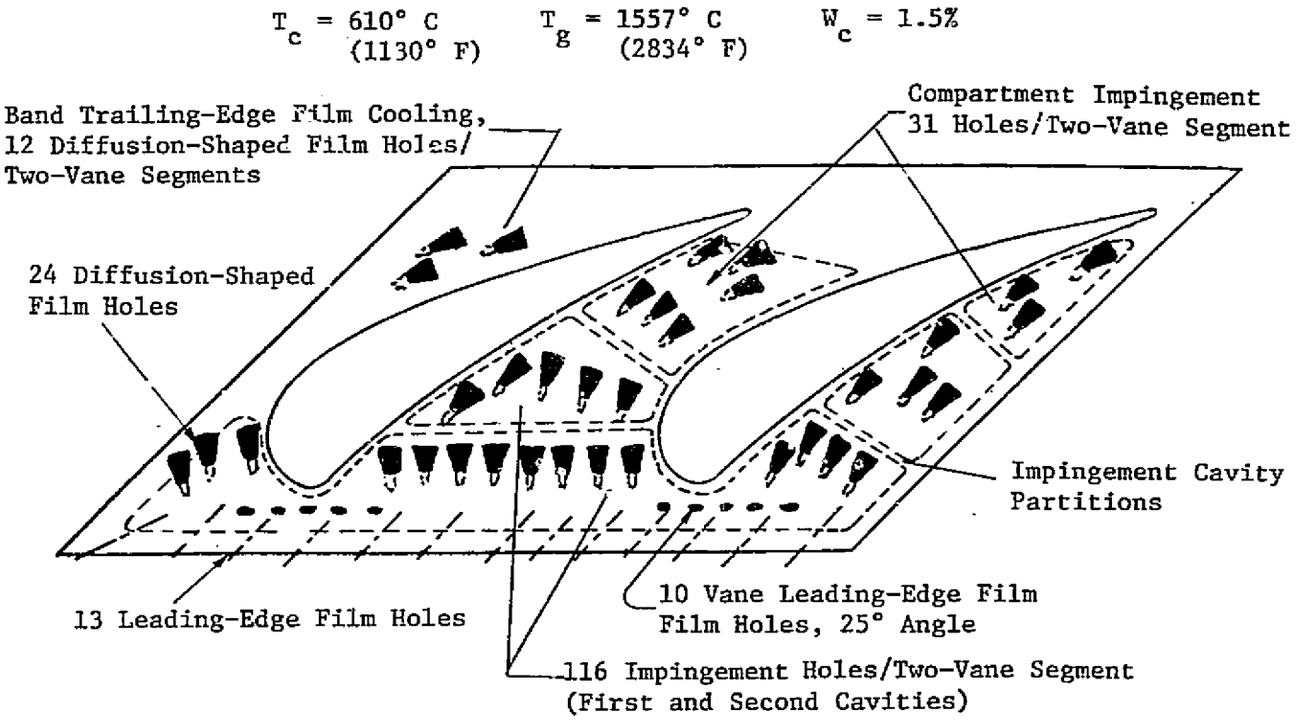

Figure 19. Stage 1, Nozzle Outer Band Heat Transfer Design.

seals are used from the throat back to the trailing edge. The flanges also incorporate spline seals. The leakage through these seal arrangements results in a total nozzle leakage flow of 0.67% W_{25}.

3.2.2 Stage 1 Rotor

The design goal of the cooling-air-supply system for the Stage 1 rotor is to deliver coolant at the lowest possible temperature at the required design pressure. The high efficiency requirements of the E^3 necessitated the design of a cooling system that is more effective than current, commercial designs. Stage 1 rotor coolant is extracted from the compressor diffuser exit at the midspan, as shown in Figure 20. Relative to existing systems, this source yields a cooler supply of air to the rotor. This cooler air [19 to 22° C (35 to 40° F)] allows a reduction in blade cooling-air usage and results in a direct engine-efficiency gain. Midspan extraction also tends to stabilize the diffuser dump flow since the air is extracted from the wake region of the diffuser. As the engine deteriorates due to the compressor flowpath seals opening up, the midspan temperature will be affected the least. In terms of design specifics, the extracted rotor cooling air is 6% of the compressor inlet flow. The extracted air is routed through 28 struts into the inducer feed cavity. The inducer accelerates 80% of the extracted air to the rotor wheel speed; the other 20% is metered into the cavity ahead of the compressor-discharge seals for blockage of the compressor inner flowpath hot leakage air as previously shown in Figure 11. This metered air is directed tangentially in an effort to also reduce the frictional windage. Proper blockage of the inner flowpath leakage reduces the leakage-air temperature about 55° C (100° F) and prevents the hot leakage air from making contact with the torque cone. A secondary feature of this design is the improved engine performance which results from the fact that the air delivered to the combustor is now better since the cooling air removed is at a lower temperature.

The compressor-discharge seal leakage air is allowed to bypass the inducer through 64 pipes of 0.8 cm (0.315 in.) diameter and is thus kept away from the rotor shaft cover. This compressor-discharge seal leakage air is then injected upstream of the inducer seal to satisfy the leakage requirements of that seal.

The inducer accelerates the flow to a slightly higher velocity than the wheel speed; then it is collected on board the rotor and routed along the main shaft to the turbine disk. Taking the cooling air on board the rotor ahead of the combustor permits the main shaft to operate at a temperature of approximately 538° C (1000° F) even during the hot-day takeoff conditions. This temperature limitation will allow use of Inco 718 material for the growth engine where T_3 will achieve a level of 649° C (1200° F). At the turbine disk, the flow is pumped up to the required coolant pressure through a radial-outflow impeller scheme between the first-stage turbine disk and the cover disk.

Significant design features of the Stage 1 blade-cooling system are illustrated in Figure 21. The blade cooling system is divided into two separate

- Pitch Cooling Source Reduced 21° C (37° F)
- Pitch-Line Temperature Constant, Less Deterioration
- No Heat Pickup from Combustor

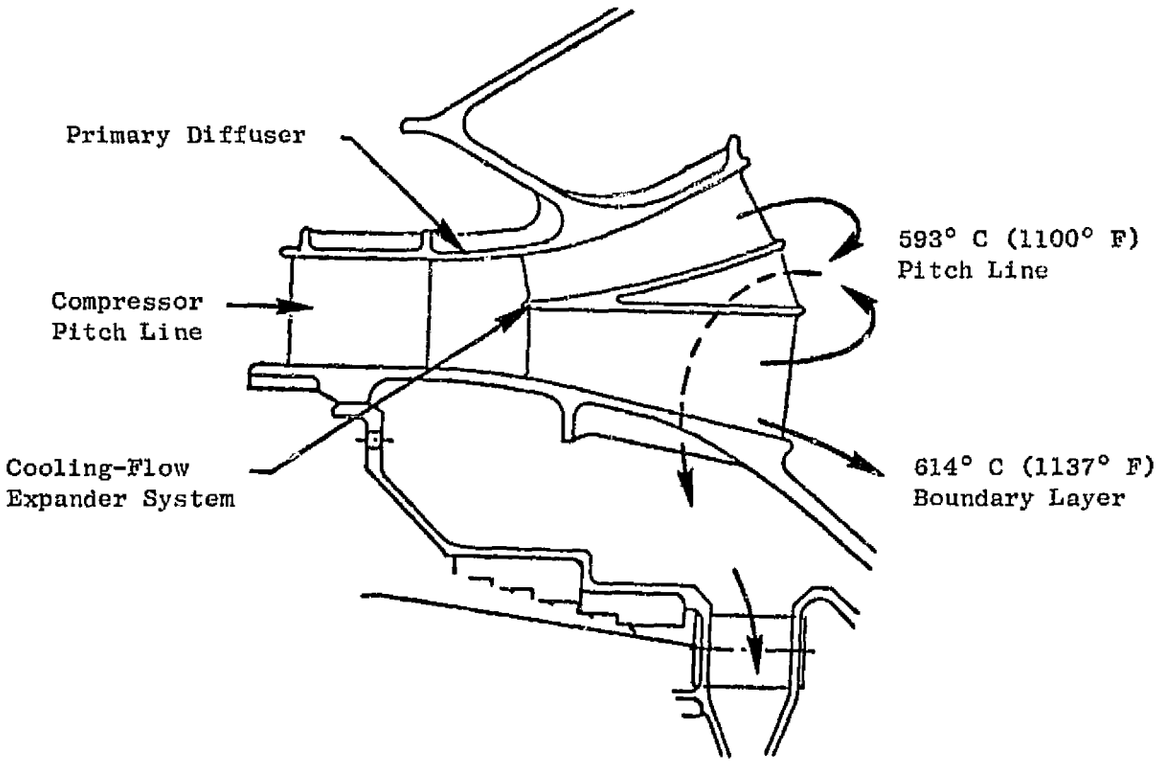

Figure 20. Turbine Rotor Cooling Source.

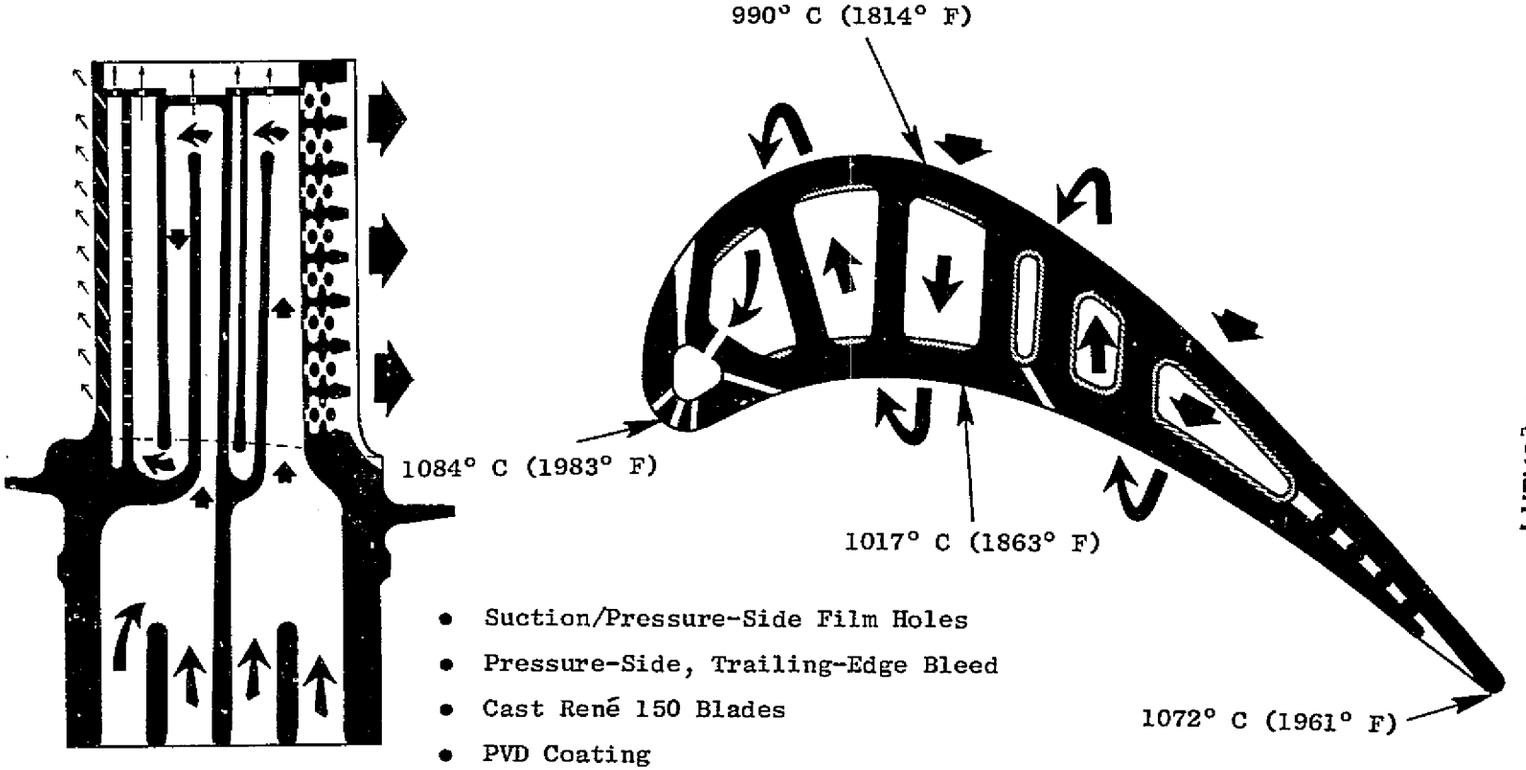

- Suction/Pressure-Side Film Holes
- Pressure-Side, Trailing-Edge Bleed
- Cast René 150 Blades
- PVD Coating
- Warm Air Impingement on Leading Edge
- Serpentine Convection Cooling
- Trailing-Edge Cold Bridge
- Turbulence Promoters on Ribs and Airfoil
- Impinged-Pin-Fin, Trailing-Edge Slot

Figure 21. Stage 1 Blade Design Features.

circuits for the leading and trailing edges of the blade. The leading-edge circuit cools the forward portion of the airfoil by means of a serpentine and cast impingement scheme. The trailing edge is cooled by means of a serpentine circuit in the midchord region and by an impingement/pin-fin configuration at the trailing edge. The extreme trailing edge of the blade is cooled by pressure-side slot film-cooling from the impingement pin-fin cavity. Substantial heat-transfer improvements have been gained by using turbulence promoters on the ribs and by incorporating a new, impinged-pin-fin, trailing-edge-slot design. The impinged-pin-fin, trailing-edge slot uses the pressure available to generate high internal heat transfer and offers a 50% heat-transfer improvement over a conventional pin-fin design. Other, more subtle, improvements occur due to the reduced adverse pressure gradient on the pressure side of the airfoil. As shown in Figure 22, the velocity along the pressure side accelerates all the way from the leading edge to the trailing edge. This should reduce the potential for the boundary layer to separate and reattach. The end result is an airfoil with lower gas side heat transfer compared to the production engine family of blades. The exterior heat transfer coefficients that were used in the analysis are presented in Figure 23.

Stage 1 blade cooling-system geometry details are illustrated in Figure 24. The Stage 1 blade-cooling system utilizes a two-circuit, convection/film-cooled design. In the forward circuit, leading-edge impingement holes are supplied by a three-pass, convection serpentine. Heat transfer on the side wall in the serpentine is significantly improved by turbulence promoters. The leading edge of the blade is cooled by a combination of impingement, convection, and film cooling. After being heated in the serpentine, the cooling air is impinged on the leading edge. Spent impingement air provides additional cooling through convection in the film holes as well as through external film cooling. Leading-edge film cooling is supplied by three rows of radial holes. Pressure-side, film-cooling air is supplied through a single row of round, axial, film holes. Suction-side, film-cooling air is provided from spent impingement air through a single row of diffusion-shaped, axial, film holes.

The aft circuit consists of a three-pass, forward-flowing serpentine. Due to temperature/life constraints, the trailing-edge cooling air is supplied from the first pass of the serpentine. After flow metering through axial holes in the crossover rib, trailing-edge cooling air is impinged twice on two rows of equally spaced pins. The impinged-pin-fin design reduces flow area, increases convection heat-transfer area, and increases flow turbulence. This combination of features results in excellent cooling effectiveness. Spent trailing-edge cooling air exits through 11 pressure-side bleed slots and provides external film cooling for the remainder of the trailing edge.

The balance of the aft-circuit cooling air continues through the turbulated serpentine and exits through a single row of pressure-side, midchord, film holes. These angled holes provide local convection cooling as well as reinforcing the pressure-side film cooling from the upstream, pressure-side, gill holes. Tip-cap and squealer-tip cooling are accomplished by bleeding a small portion of the cooling air through holes in the tip cap as shown in Figure 25.

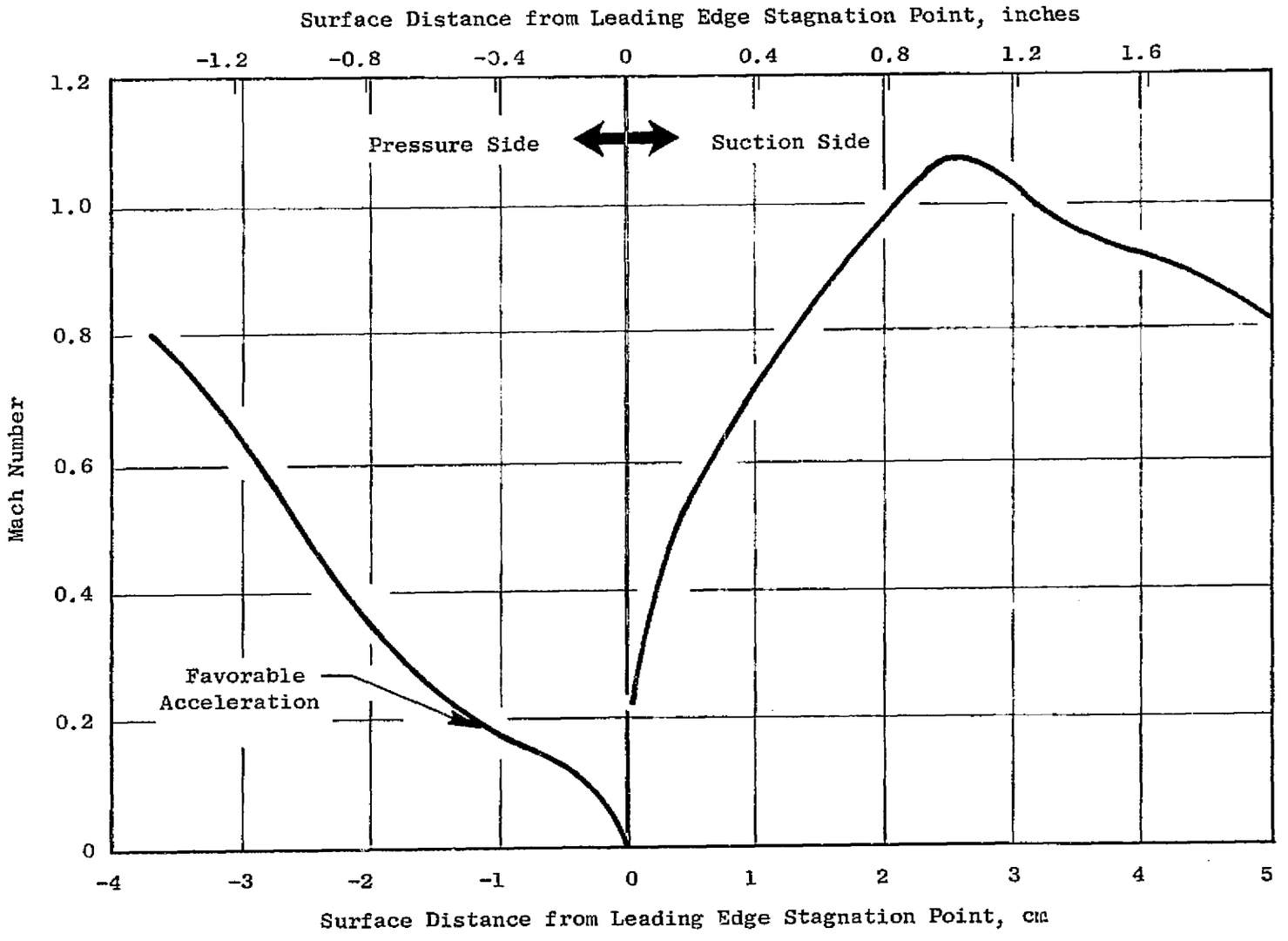

Figure 22. Stage 1 Blade Pitch-Line Mach Number Distribution.

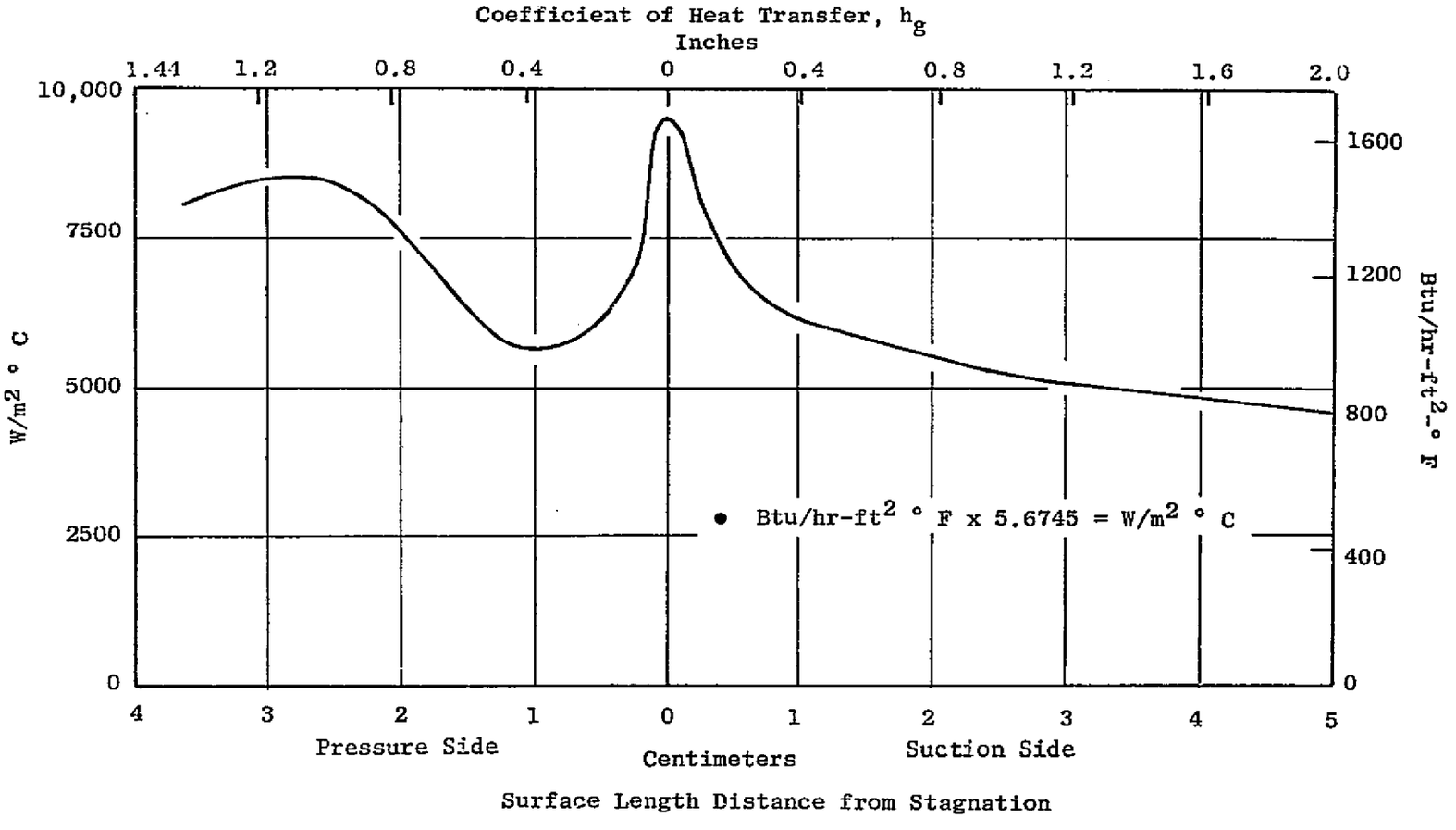

Figure 23. External Heat Transfer Coefficient.

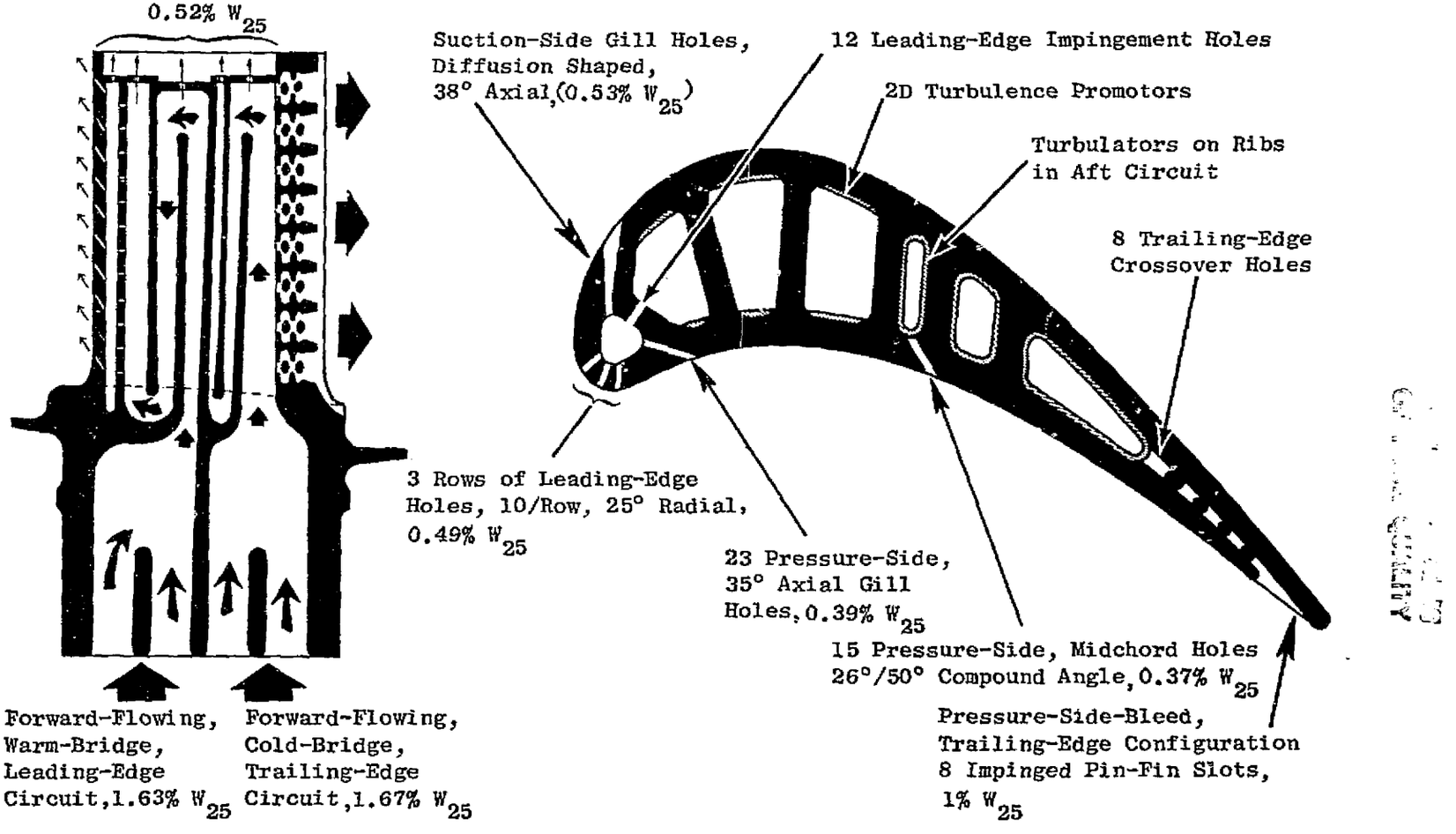

Figure 24. Stage 1 Blade Cooling System.

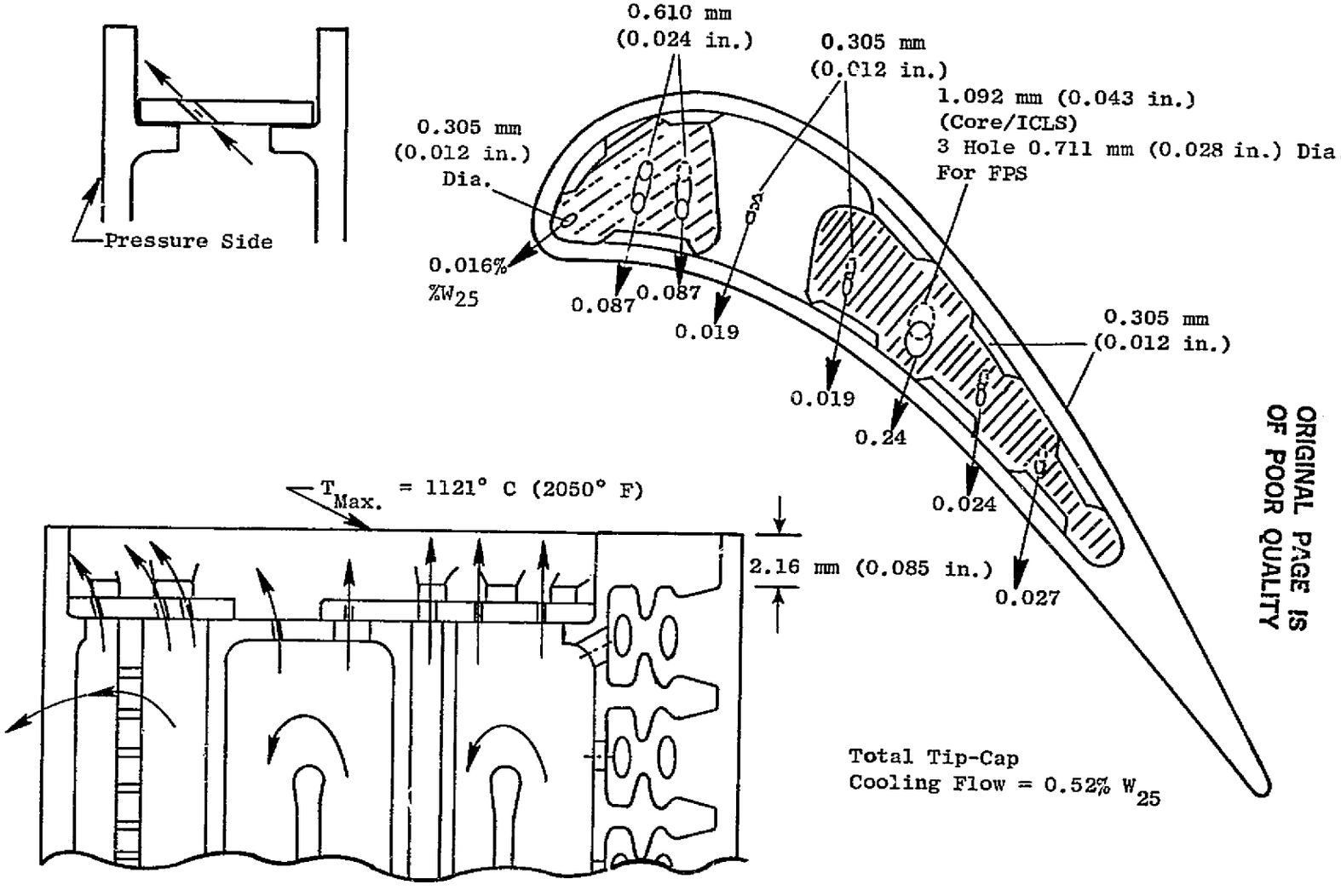

Figure 25. Stage 1 Blade Tip Cap Cooling Design.

Blade cooling-flow characteristics are crucial when the supply pressure drops below design intent. This would occur, for example, if damage incurred by the inducer seal resulted in a drastic increase in seal leakage flow. In order to evaluate the impact of the reduced supply pressure on the Stage 1 blade, a compressible network computer program was used. The supply pressure was dropped, and the impact on the blade leading-edge backflow margin was evaluated. The results of this analysis are presented in Figure 26. The tip leading-edge backflow margin, which is most limiting at design conditions, drops to 9% when the dovetail-cooling pressure ratio drops from the design values of 1.35 to 1.24.

The blade node breakdown and the corresponding temperature at steady-state, hot-day takeoff are presented in Figure 27. The maximum temperature of the coating is 1084° C (1983° F) at the leading edge and 1072° C (1962° F) at the trailing edge. Pitch-line bulk temperature is 953° C (1748° F) based on the design cooling flow of 3.3% W_{25}. The engine start-up, takeoff, acceleration, and deceleration to ground idle transients were also investigated. This was done in an effort to define the local temperature distribution for LCF analysis. The results of the thermal transient analysis are shown in Figure 28 which shows the transient local temperatures for five selected points on the blade.

The blade cooling-flow mixing losses were also evaluated on the Stage 1 blade. The biggest contribution to the momentum losses occurred at the trailing-edge, pressure-side slots. The Mach number of the coolant air leaving the slots is 0.45; the gas-stream Mach number is 0.75. This high gas-stream velocity in conjunction with the low coolant velocity is the primary cause of the loss. Every effort has been made to keep the slot-cooling velocity as high as possible while cooling the trailing edge to the required level. The slot-cooling velocity, however, is influenced by the casting-process limitations. If the slot width is reduced significantly, the blade ceramic core and casting yields drop significantly. During the E^3 demonstrator program, the reliability of the ceramic core and the blade casting yield will be watched very closely to define the possibility of reducing the trailing-edge slot for the FPS.

3.2.3 Stage 1 Shroud

The Stage 1 shroud is cooled with air supplied from the compressor discharge. Like the Stage 1 nozzle outer-band and vane trailing-edge cooling supply, the air bypasses the outer combustor liner as it flows to the turbine. Since the cooling pressure requirements are not nearly as large as those of the Stage 1 nozzle, the shroud-cooling air is orificed after it passes the Stage 1 nozzle outer band and flows through the shroud-support structure. The prime purpose of orificing the flow is to reduce excess pressure that would cause unnecessary leakage at the shroud.

The shroud-cooling air is also used to improve temperature control of the shroud-support rings. With the active clearance control that is being developed in this engine, it is imperative that the shroud-support rings be heated uniformly from inside the casing. This allows uniform cooling from the outside of the casing when the ACC system is activated.

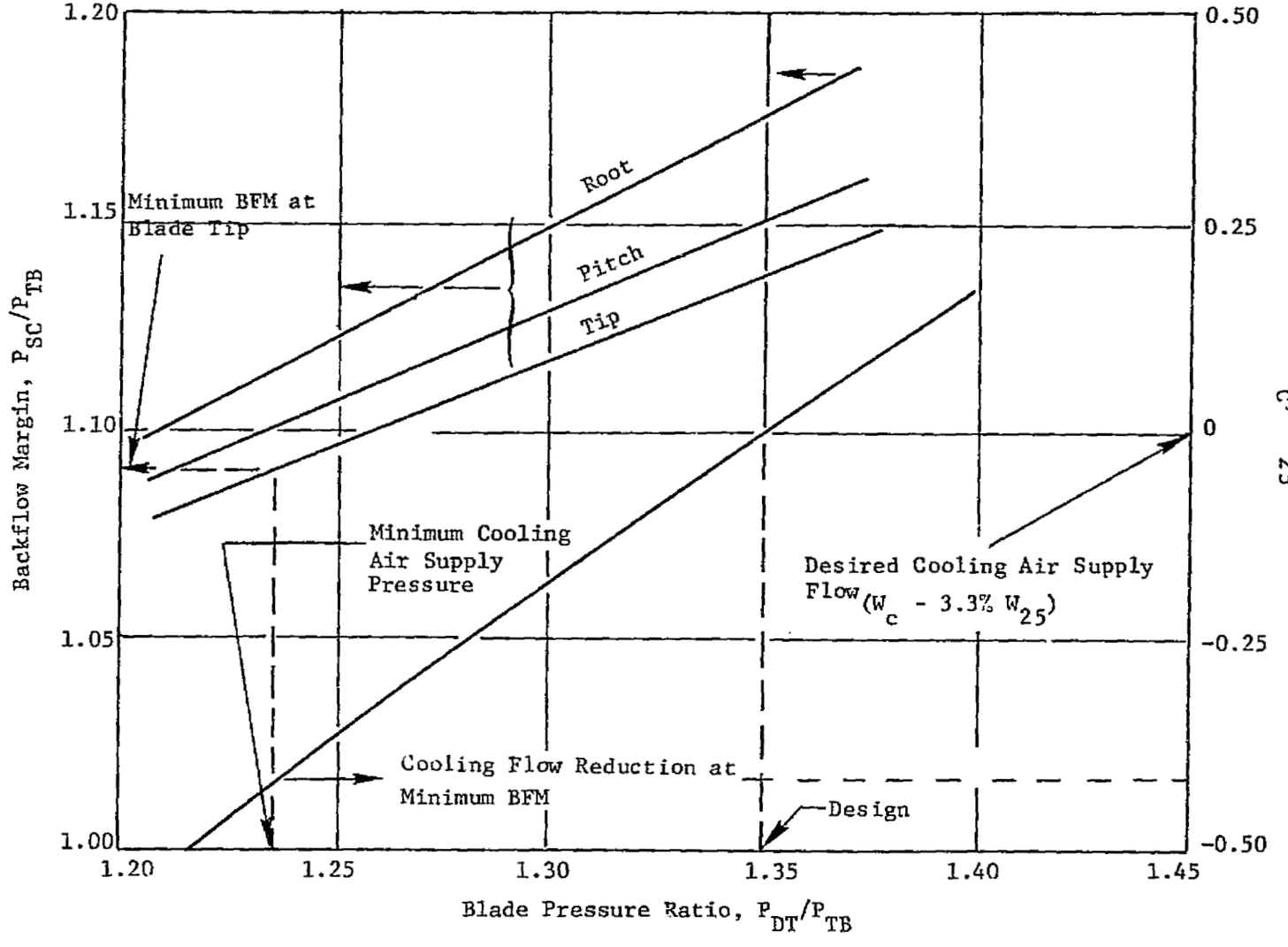

Figure 26. Stage 1 Blade Flow Characteristics.

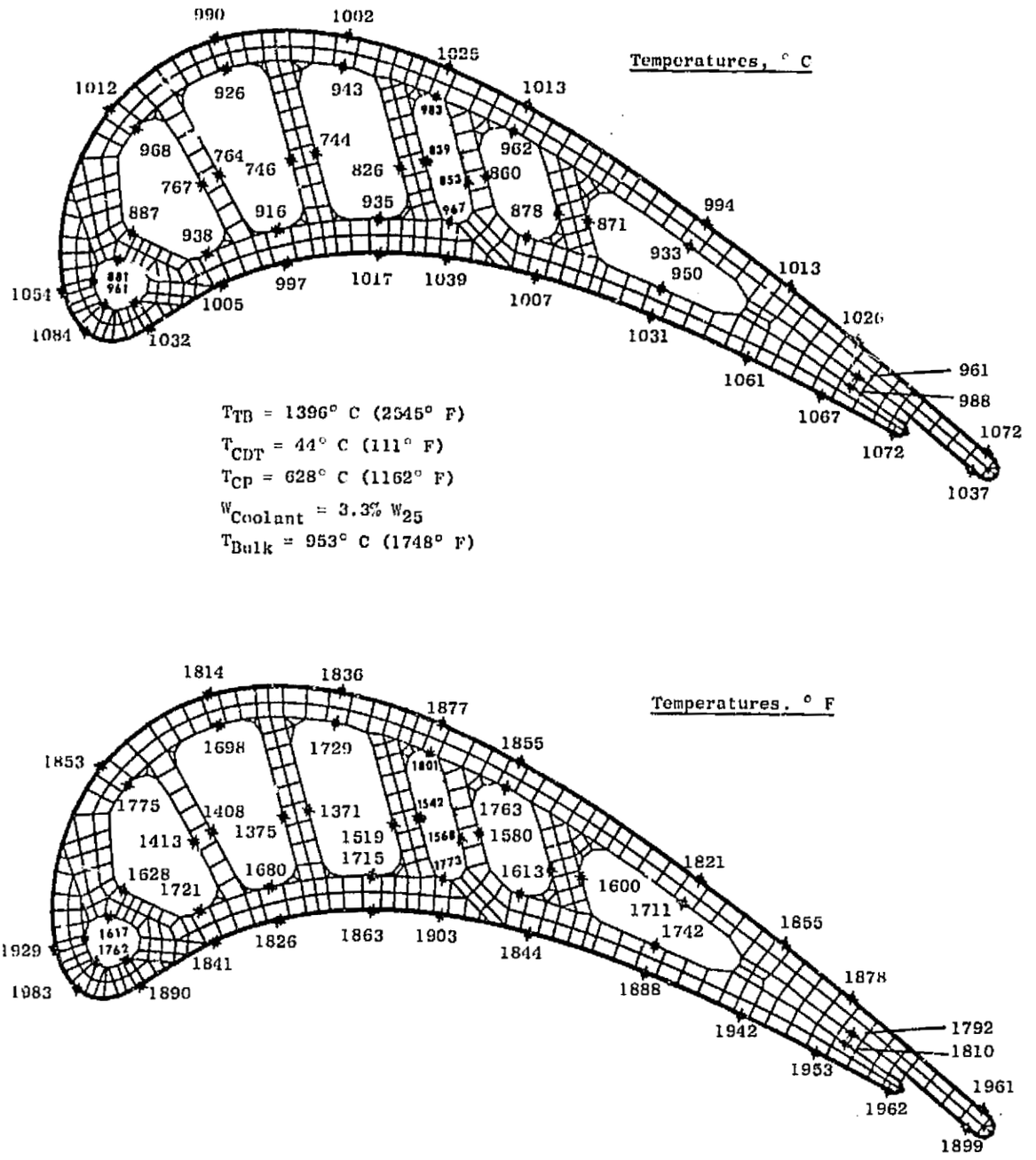

Figure 27. Stage 1 Blade Pitch-Line Temperature Distribution at Steady-State Takeoff.

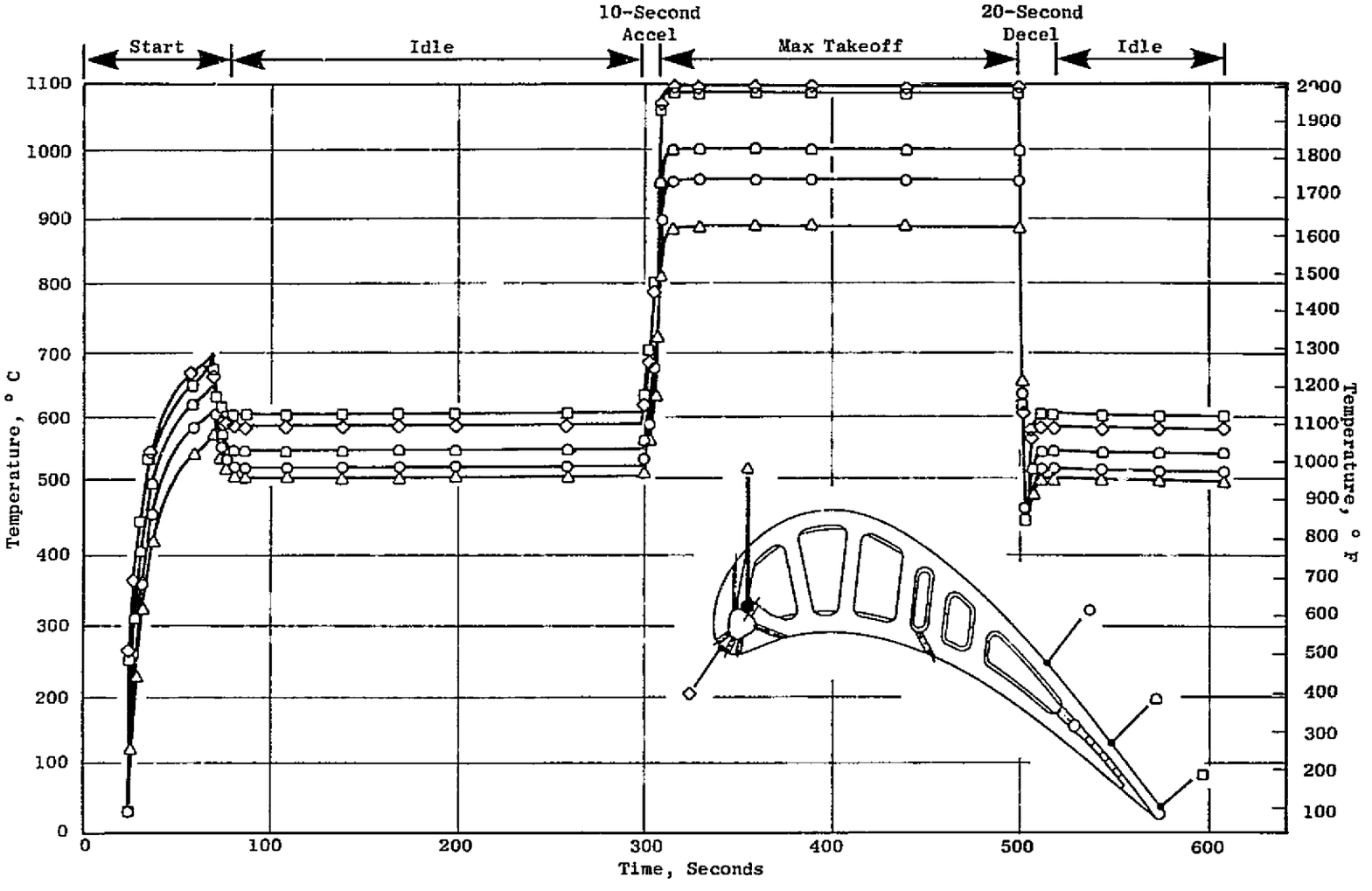

Figure 28. Stage 1 Blade Transient Thermal Analysis

The detailed cooling design of the Stage 1 shroud is presented in Figure 29. Significant features of this shroud design are the thermal-barrier coating (zirconia) that reduces the cooling-flow requirements by half and the 360° impingement manifold that allows all the air (leakage and film) to be used for impingement cooling. The thermal conductivity of zirconia is so low [1.04 W/m·° C (0.6 Btu/hr·ft·° F)] that the 1.02 mm (0.014 inch) thick coating reduces the heat load by half. The design of the thermal-barrier-coated shroud is similar to that of hardware which has been successfully tested in a CF6-50 engine. These test results were instrumental in the choice of this shroud design for the E^3. The 0.6% W_{25} shroud-cooling air is also used to cool the aft-casing ring of the shroud support. This allows a better match between forward and aft rings with and without ACC air cooling the outside casing. The maximum temperature of the zirconia surface of the shroud will be as high as 1349° C (2461° F); the René 77 backing will be held to 1077° C (1970° F) at the shroud leading edge. These are steady-state, maximum-takeoff temperatures for a deteriorated engine with the worst expected hot-streak, gas-stream temperature of 1471° C (2680° F) at the outer wall. Temperatures for various locations on the shroud components are presented in Figure 30.

The primary method of cooling is by impingement from the 360° baffle. After cooling the back side of the shroud, about 70% of the spent impingement air is used to cool the forward and aft shroud hangers. The remaining impingement air is used to block the 24 intersegment seals.

3.2.4 Stage 2 Nozzle

The Stage 2 nozzle cooling air is extracted from the compressor at the exit of the seventh-stage stator. The cooling-air-extraction port is combined with the engine-start-bleed port. Since the start-bleed ports have been sized to flow 30% of the engine core flow into the fan duct, the Stage 2 bleed does not pose any pressure-loss problem at the compressor flowpath. After the Stage 7 bleed air is extracted from the compressor, it is routed back to the turbine through four pipes feeding into eight HPT casing inlet ports. The air enters the HPT casing at the Stage 2 stator location and then flows circumferentially around the engine to supply coolant to the complete Stage 2 nozzle.

The cooling system for the Stage 2 vane is illustrated in Figures 31 and 32. The design utilizes convection cooling with a single impingement insert in the vane. Pressure-side-bleed slots are used to cool the trailing-edge region and inject the spent coolant back into the flowpath with low aerodynamic mixing loss. Significant features of the design are the use of preferential cooling and a low-leakage, air-delivery system.

The required 1.85% W_{25} cooling flow impinges on the inside of the vane through 0.51 mm (0.020 in.) holes that are spaced between 4 and 12 diameters apart. After impingement, 0.75% W_{25} cooling air is vented through the inner diameter of the vane to provide purging for the interstage seal. The remaining 1.1% W_{25} cooling air is discharged through the pressure-side, trailing-edge bleed slots as shown in Figure 32.

- Zirconia Coating, Recessed Pegs, and Wire Screen Design
  (See Figure 106)

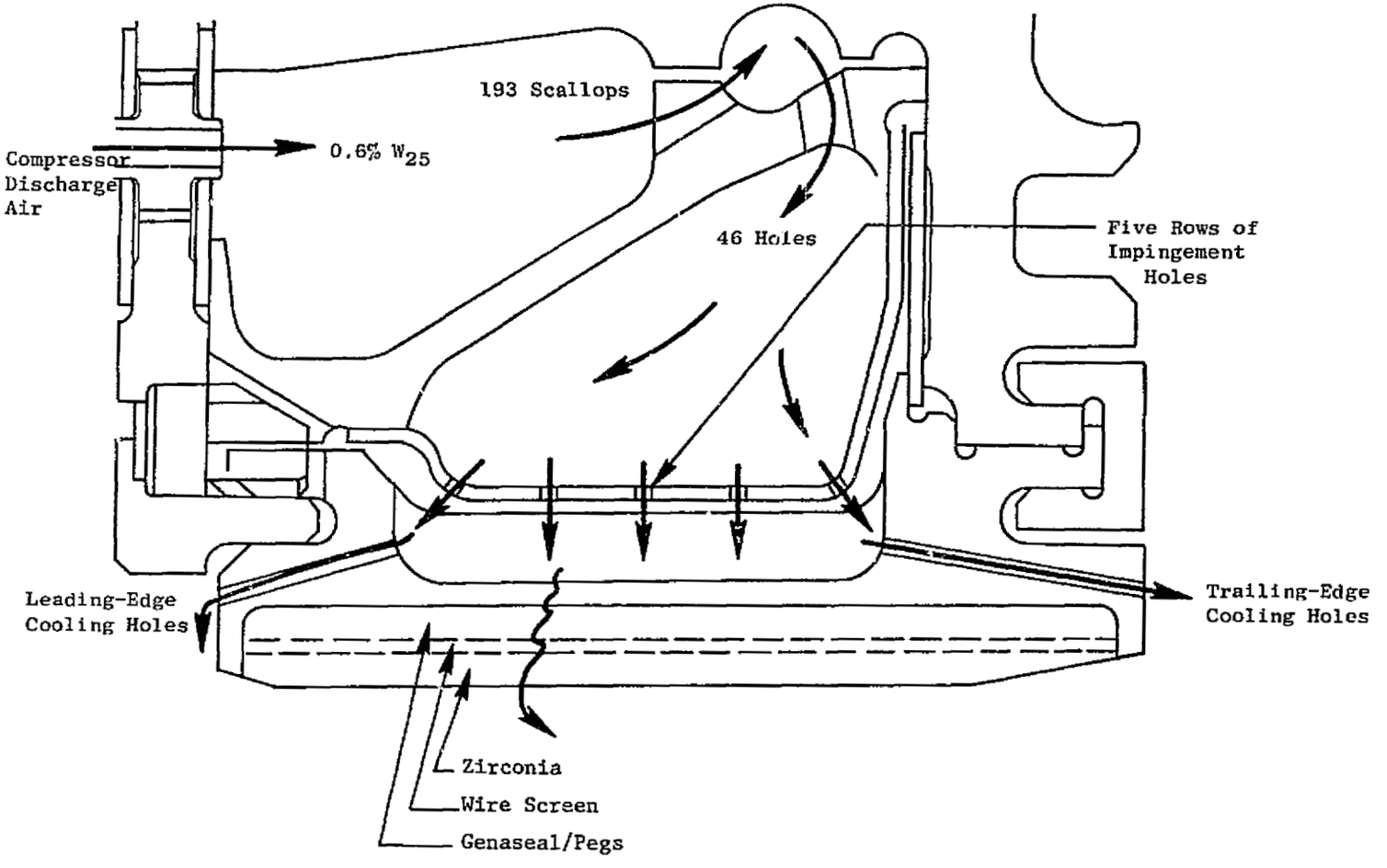

Figure 29. Stage 1 Shroud - Cooling Geometry.

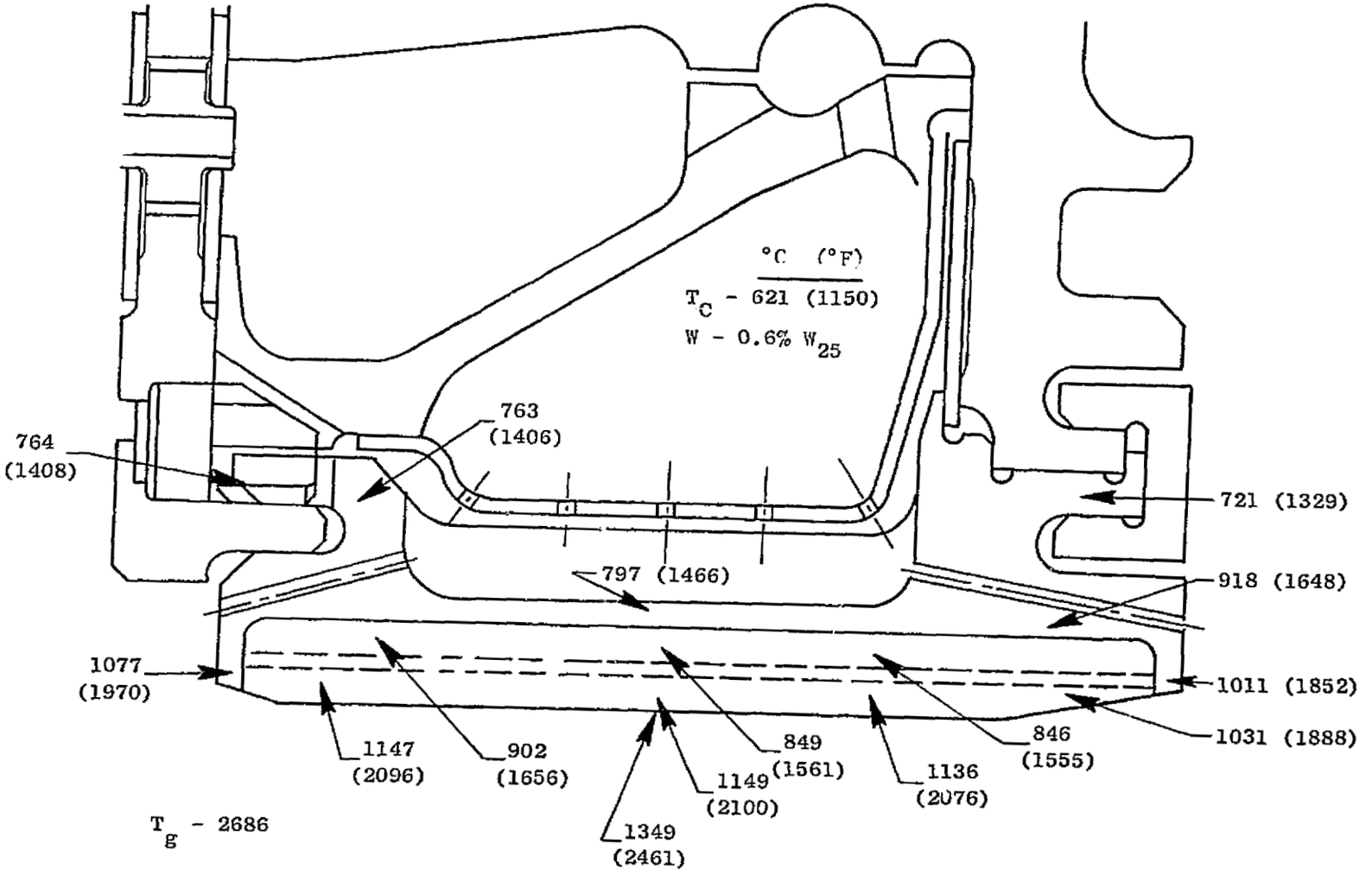

Figure 30. Stage 1 Shroud Temperature Distribution.

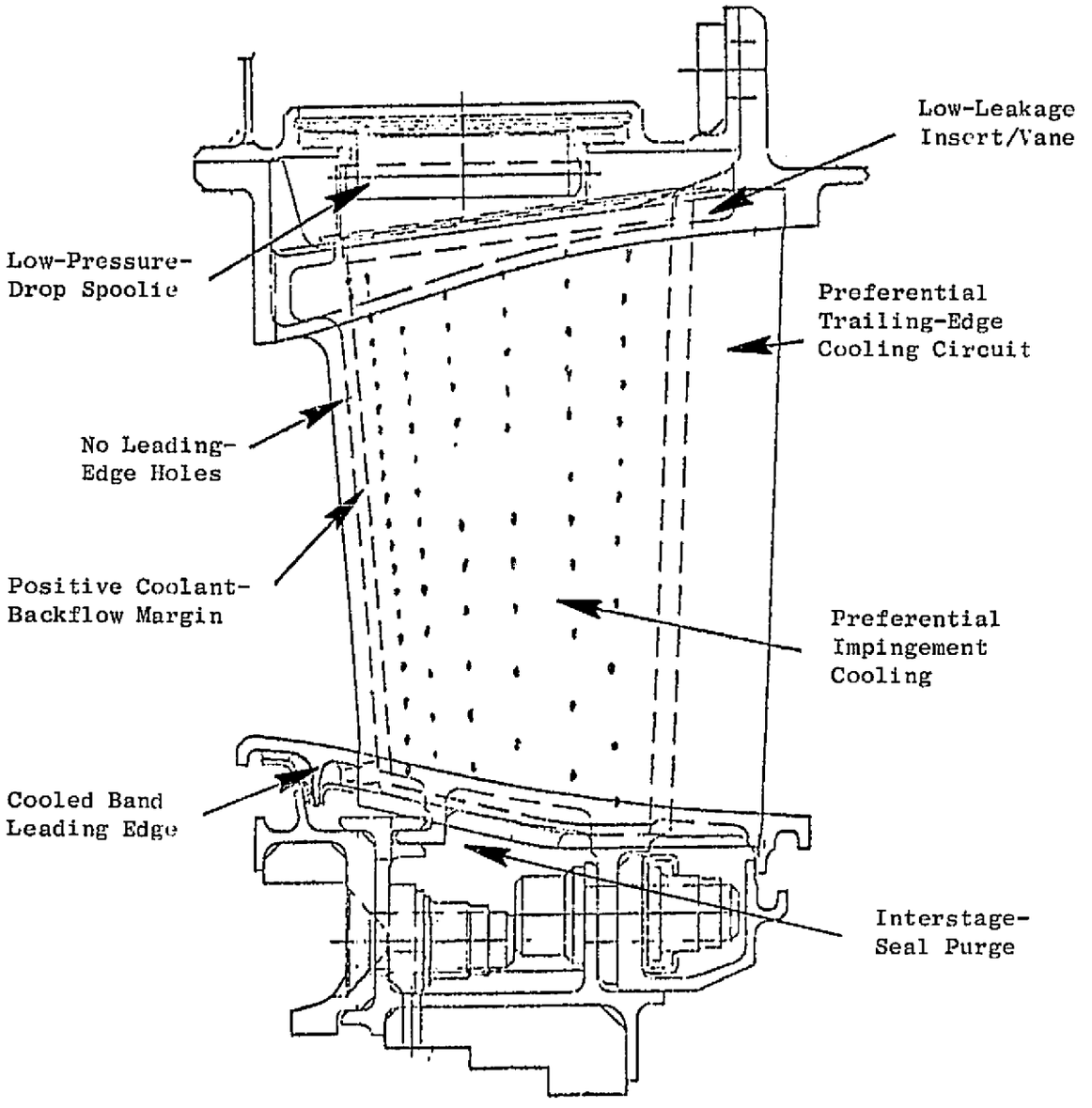

Figure 31. Stage 2 Nozzle Design Features.

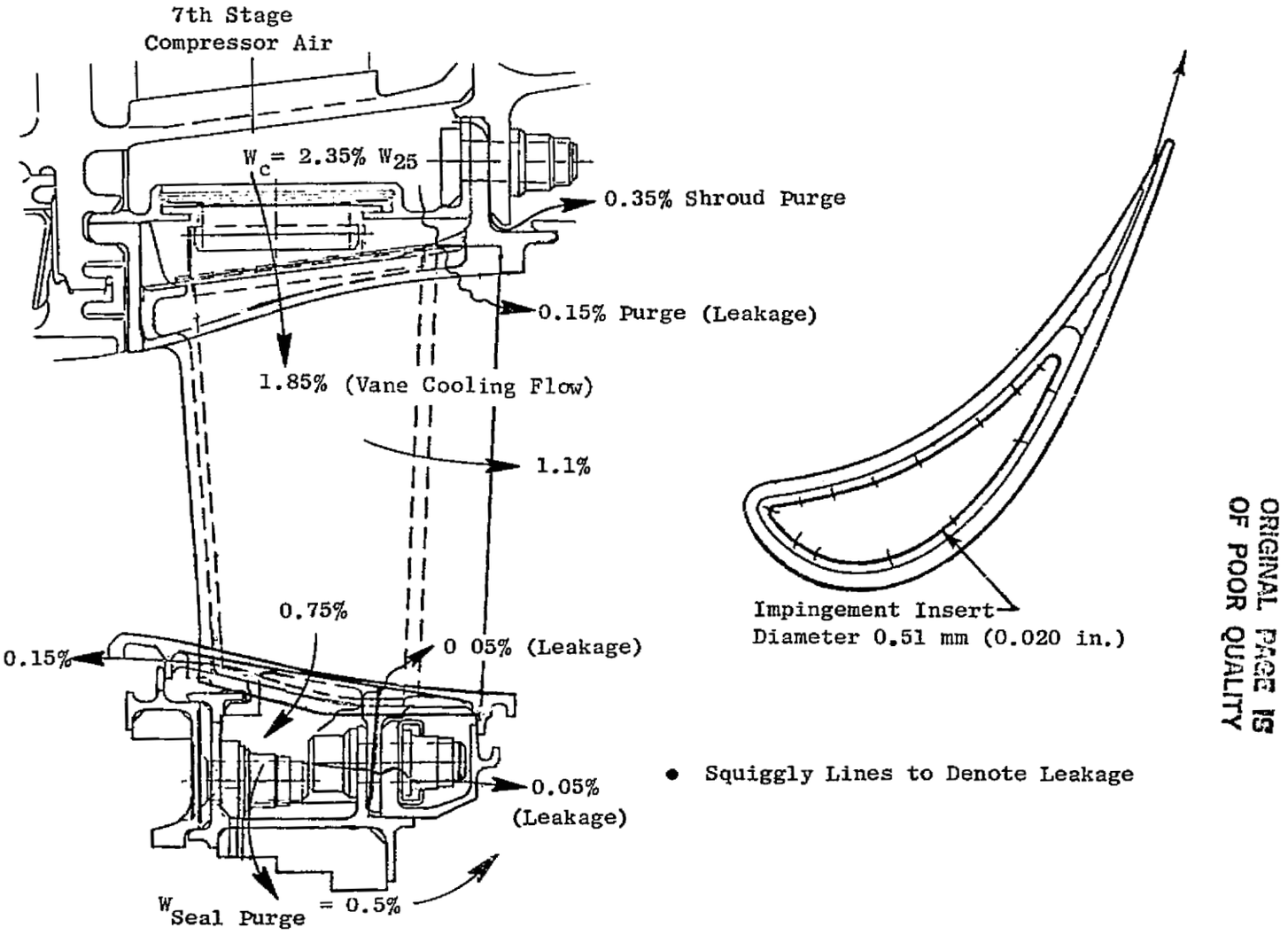

Figure 32. Stage 2 Nozzle Cooling Flows.

The gas-temperature profile analysis indicated a maximum peak temperature of 1337° C (2439° F) at 65% span and 1190° C (2174° F) at 95% span. From production-engine experience, the life-limiting area of the Stage 1 vane is expected to be the 95% span. The gas-bending loads on the nozzle result in high stresses in the vane leading edge at this section. The vane thermal anslysis was conducted not only at the high-gas-temperature vane section but also at this high-mechanical-load section. The impingement cooling was adjusted by changes in hole spacing to accommodate the expected variation in heat load and required temperatures. The node breakdown and temperature distribution at the 65% and 95% span are presented in Figure 33. The bulk metal temperatures at these vane sections are 928° C (1702° F) and 972° C (1781° F), respectively.

3.2.5 Stage 2 Rotor

The Stage 2 rotor blade is cooled with compressor-discharge air supplied through the Stage 1 rotor expander nozzle system and delivered to the Stage 2 blade by means of flow passages down the front side and under the Stage 1 disk. The air is then pumped up the front side of the Stage 2 disk and enters the dovetail disk slot from the front side.

The Stage 2 blade cooling system, as shown in Figure 34, is a two-circuit, internal-convection design. In the forward circuit, cooling air is forced through a three-pass serpentine. A high leading-edge cooling effectiveness is achieved by flowing fresh cooling air through a small area near the leading edge. The cooling effectiveness in the serpentine passages is improved by two-dimensional (rib-type), turbulence promoters. The aerodynamic mixing losses have been reduced by means of a pressure-side-tip, midchord slot. The high velocity of the slot cooling air energizes the mainstream gas flow and improves turbine efficiency.

The aft circuit is very similar to the forward circuit. Cool, fresh air is brought from the blade dovetail through a small, serpentine passage located near the trailing edge. After cooling the trailing edge, the air continues to cool the blade in two additional passages. As in the forward circuit, turbulence promoters are extended onto the ribs for increased cooling effectiveness. The spent air from the aft circuit also exits through a single slot on the pressure side near the tip.

The gas-temperature profile analysis indicated a pitch-line design value of 1038° C (1900° F) with a coolant-supply temperature of 593° C (1099° F). The detailed analysis indicated that a satisfactory 929° C (1705° F) bulk metal temperature could be achieved with 0.76% W_{25} for blade cooling.

The detailed thermal-model node breakdown and the local metal temperatures at the hot-day, steady-state, takeoff condition are presented in Figure 35. The maximum temperature of 1013° C (1855° F) occurs at the trailing edge on the environmental coating. The trailing edge was the most difficult part of the blade to cool because it is in a high-heat-transfer-coefficient environment. Because of the distance of the trailing edge from the last radial

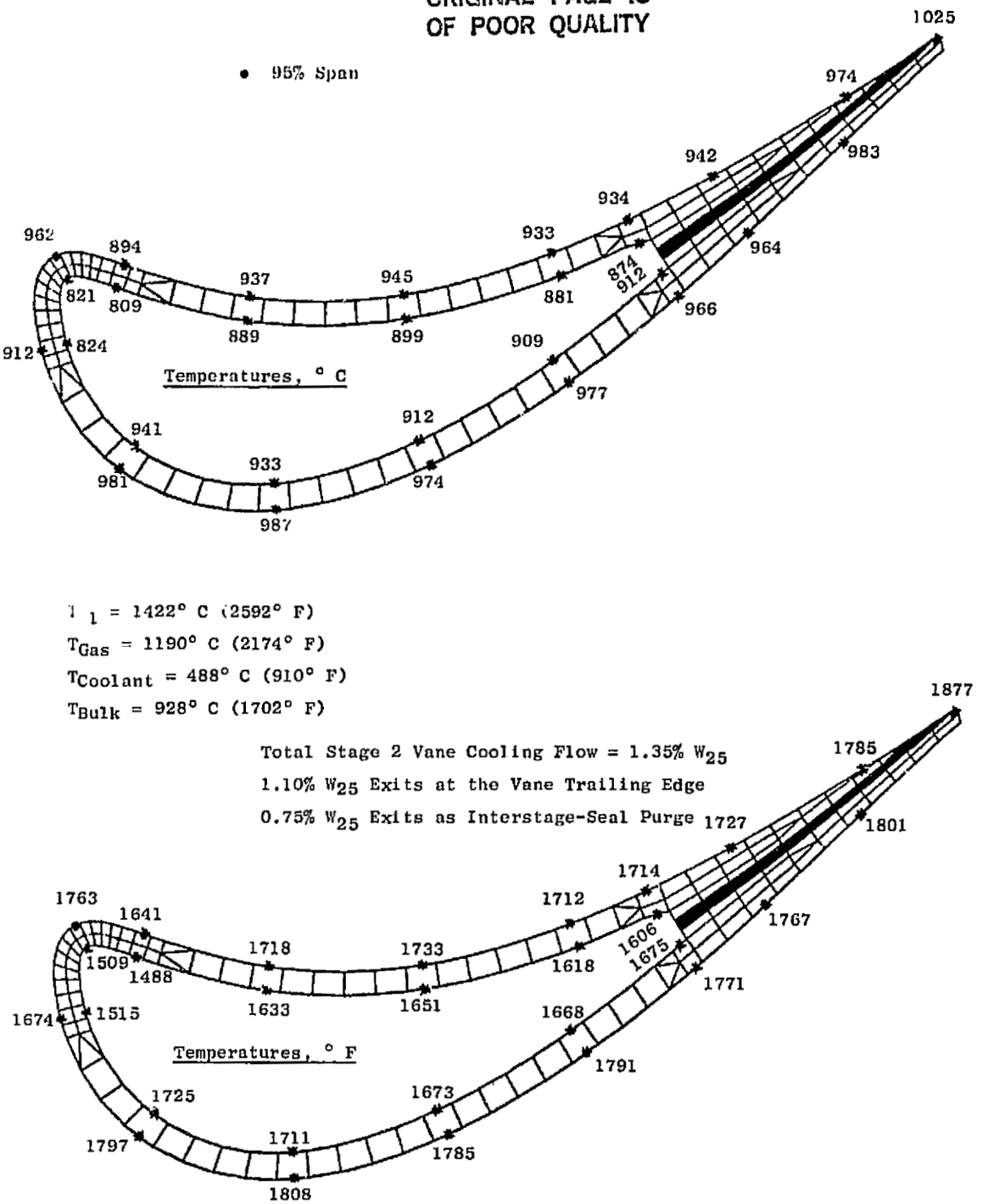

Figure 33. Stage 2 Vane Temperature Distribution.

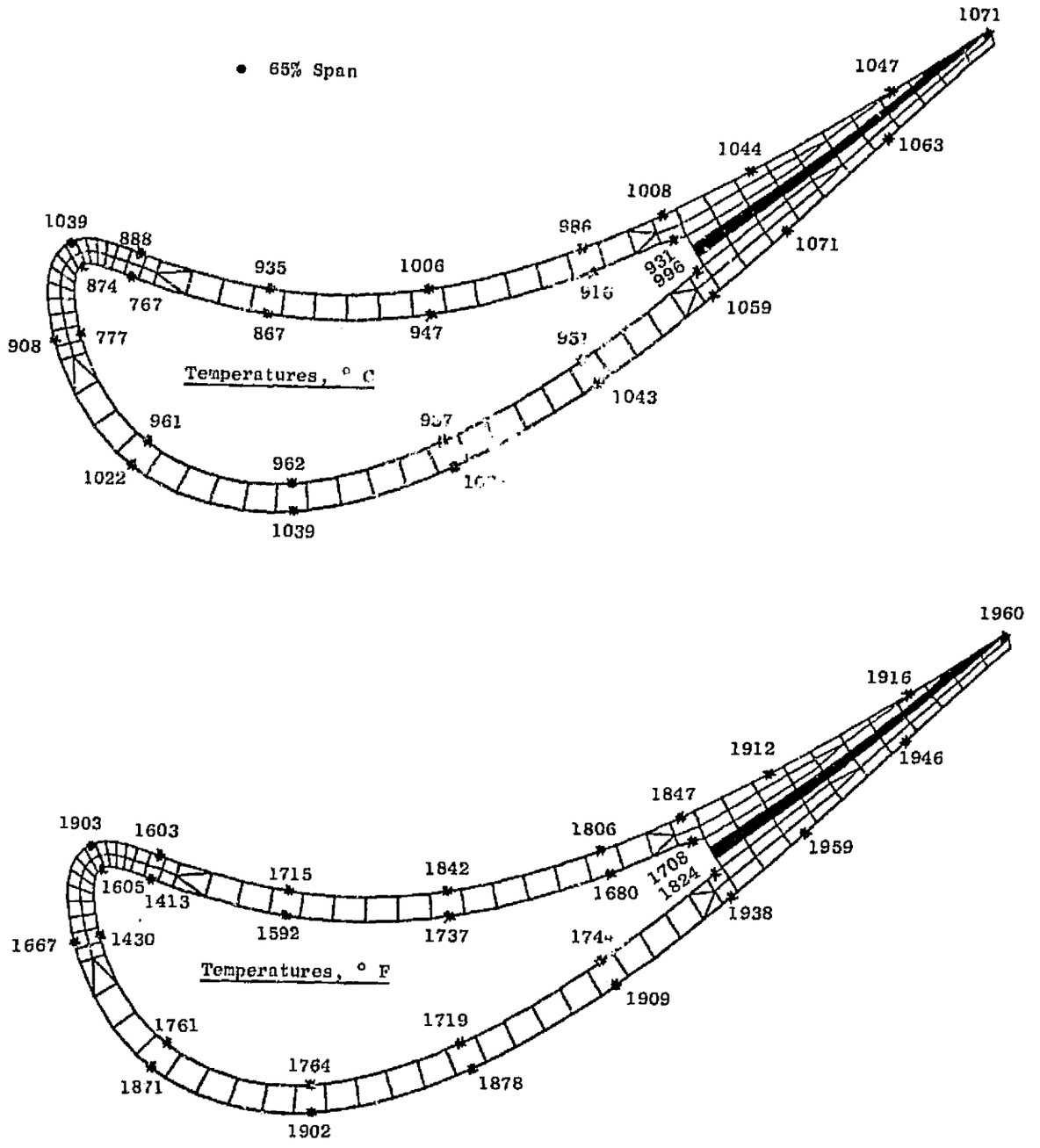

Figure 33. Stage 2 Vane Temperature Distribution (Concluded).

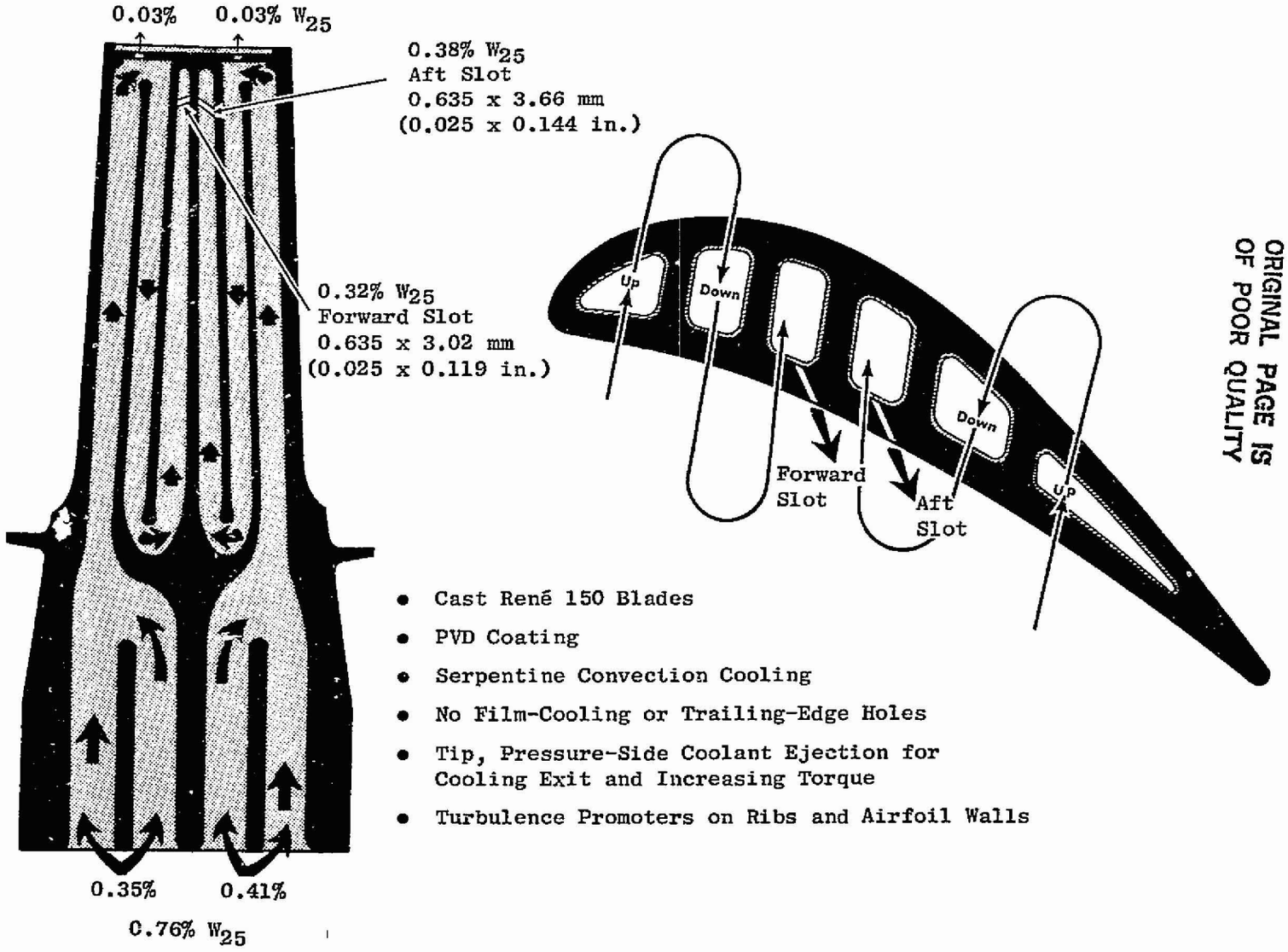

- Cast René 150 Blades
- PVD Coating
- Serpentine Convection Cooling
- No Film-Cooling or Trailing-Edge Holes
- Tip, Pressure-Side Coolant Ejection for Cooling Exit and Increasing Torque
- Turbulence Promoters on Ribs and Airfoil Walls

Figure 34. Stage 2 Blade Design Features.

Temperatures, ° C

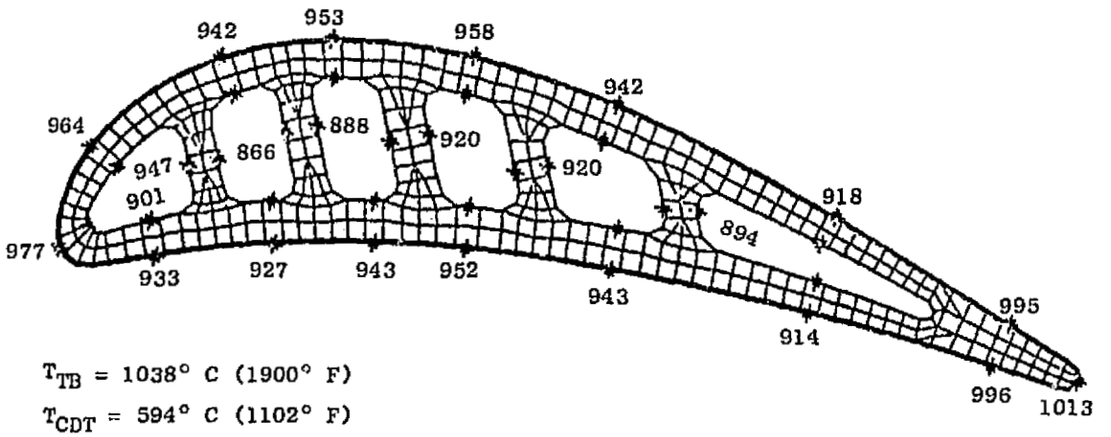

T_{TB} = 1038° C (1900° F)

T_{CDT} = 594° C (1102° F)

T_{CP} = 628° C (1163° F)

W_C = 0.76% W_{25}

T_{Bulk} = 929° C (1705° F)

Temperatures, ° F

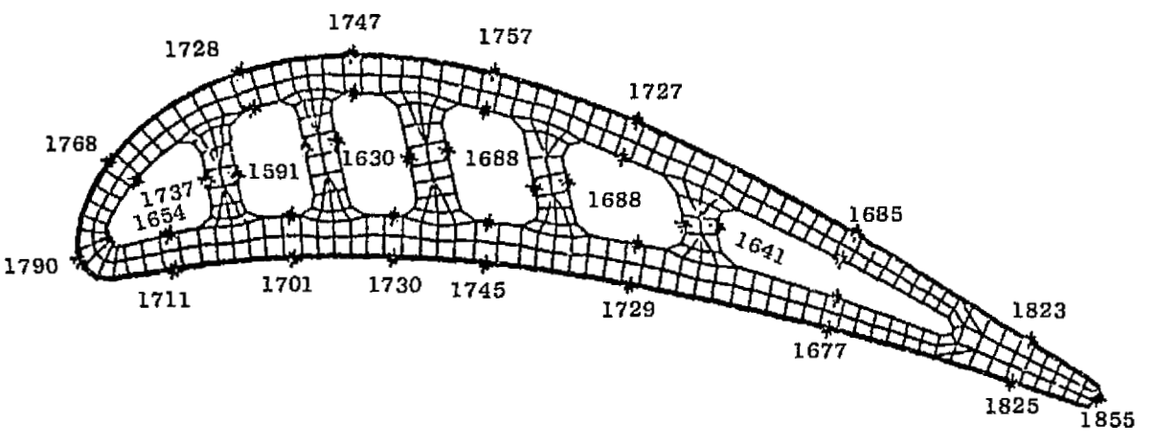

Figure 35. Stage 2 Blade Pitch-Line Temperatures at Steady-State Takeoff.

cavity, internal cooling air in the original configuration had a minimum impact on the trailing-edge temperature. Subsequently, the trailing-edge wedge angle was increased to the present value to improve conductive cooling and allow the last radial cavity to be moved closer to the trailing edge. With these improvements, the needs for a fatter trailing edge and trailing-edge, convection-slot cooling were both eliminated.

Production-engine experience indicates that turbine hardware can experience foreign object damage (FOD). Because of this and the unique nature of the Stage 2 blade cooling circuit, an FOD analysis was conducted. The purpose of this analysis was to define the cooling-flow variation to the blade if a hole caused by FOD penetrated the leading-edge, radial, cooling passage. With an assessed FOD hole up to 0.63 cm (0.25 in.) in diameter at the 60% span, the leading-edge flow circuit flow is increased quite drastically. At the same time, the flow to the second and third radial cavities drops. The corresponding pitch-line temperature distribution with and without the 0.63 cm (0.25 in.) diameter hole is presented in Figure 36. This analysis shows a 37° C (67° F) drop in the bulk metal temperature. The biggest variation occurs at the leading edge where the inside surface of the airfoil wall drops as much as 101° C (182° F). This analysis indicates that a catastrophic loss of Stage 2 blades due to typical FOD is very unlikely.

A similar analysis was conducted on the blade tip cap. The tip cap will be made in one piece and brazed in place with no mechanical retention device. This concept is feasible because the blade-tip gas temperatures in Stage 2 are relatively low. A thermal analysis was conducted to determine the impact of a braze failure and tip cap loss. A compressible-flow network program, as in the previous analysis, was used for this analysis. Without the tip cap, the core support holes became the flow-circuit restriction, and the blade flow increased from 0.76% W_{25} to 2.39% W_{25}. The flow increased in all radial cavities. This analysis indicated no problem if a Stage 2 blade lost its tip cap.

3.2.6 Stage 2 Shroud

Detailed temperatures for steady-state takeoff and the idle - takeoff - idle transient have been calculated for the Stage 2 shroud. Because of the low gas temperature at the Stage 2 shroud, 1140° C (2084° F), no significant cooling was required. A total of 0.35% W_{25} seventh-stage compressor bleed air is used to purge the cavity around the Stage 2 shroud in order to prevent hot-gas ingestion from overheating the HPT casing. There are 24 shroud segments; the gaps between each segment will be sealed with one axial hour-glass seal and one spline seal.

3.2.7 Rotor Structure

The manufacturing cost of HPT rotor structure is relatively high and usually becomes one of the limiting items in the thrust-growth development of an engine. In order to overcome this problem, the E^3 turbine rotor has been

- Pitch Section at Sea Level, Hot Day, Takeoff Steady-State Conditions With Puncture at 60% Span, 0.635 cm (0.25 in.) Diameter Hole

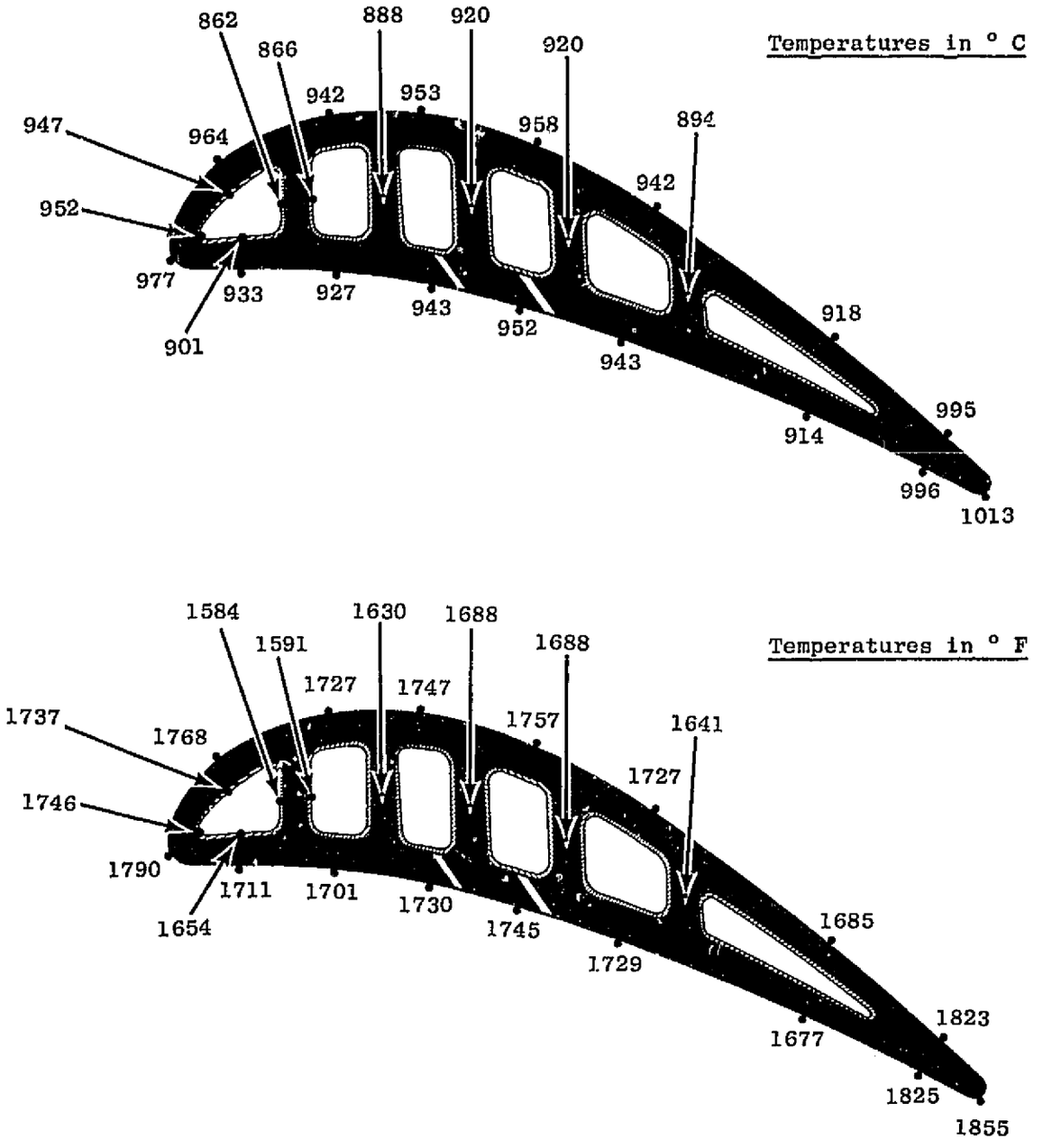

Figure 36a. Stage 2 Blade Design Metal Temperatures.

- Pitch Section at Sea Level, Hot Day, Takeoff Steady-State Conditions With Puncture at 60% Span, 0.635 cm (0.25 in.) Diameter Hole

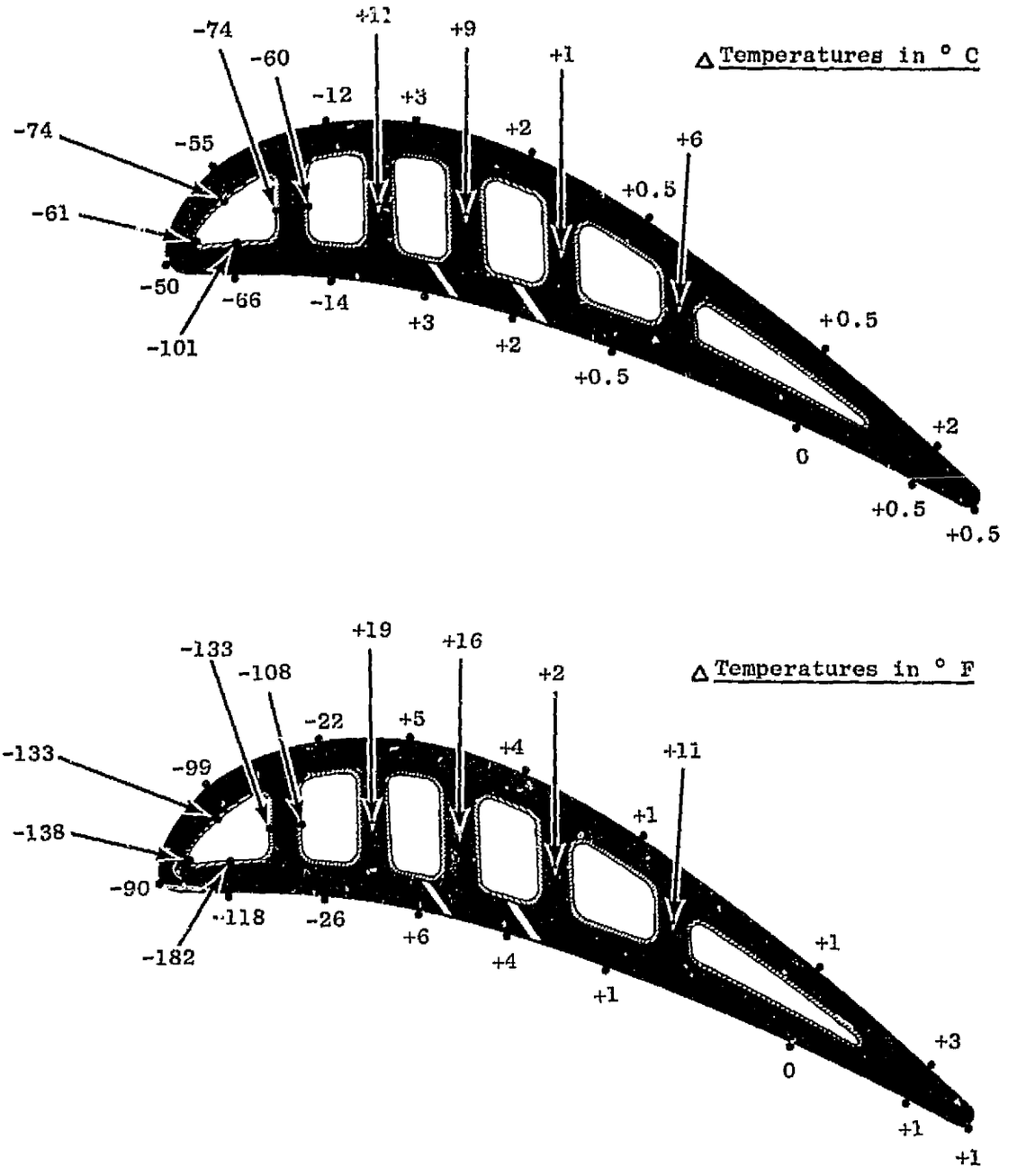

Figure 36b. Stage 2 Blade Metal Temperature Change Due to FOD Leading Edge Puncture.

designed for a growth engine that has a 15% to 20% higher thrust level. The growth engine has higher compressor-exit temperature, turbine-inlet temperature, pressure, and rotor speed. This growth condition was used to define the rotor structure design and temperatures. The FPS rotor was analyzed, but in all cases the growth engine was more limiting.

For the heat-transfer analysis, the transient boundary conditions were evaluated by means of fluid nodes in a simplfied, transient, thermal model. The results of this model were checked against the ACC transient model of the rotor structure. These transient air temperatures and heat-transfer coefficients were then used in the detailed thermal model presented in Figure 37. This detailed model extended from the aft end of the compressor to the LPT bearing and included the LPT shaft. The model contains 908 nodes, eight different materials, and 183 boundary-condition tables covering 44 time inputs of temperature and heat-transfer coefficients.

The transient analysis consisted of a complete mission from cold engine start through the flight mission and engine shutdown, as presented earlier in Figure 11. Extensive iterations and feasibility studies were conducted in an effort to yield a transient temperature distribution that would not overstress any component. The areas that presented the biggest challenges were:

- Compressor Discharge Seal Disk Bolt Flange
- Inducer Seal Disk Bolt Flange
- Impeller Disk Bore and Rabbet
- Stage 1 Disk Bore
- Interstage-Seal Disk Bolt Circle and Seal Teeth
- Stage 2 Disk Bore
- Aft-Seal Disk Bolt Circle

All problem areas were the result of transient temperature gradients except at the interstage disk seal teeth (temperature limited).

Because of the massiveness of the disk bores, the thermal responses of these components were very slow. This condition created large temperature gradients during the early part of the takeoff transient. The interstage-seal bolt circle also presented a severe thermal-stress problem caused by the massiveness of the bolts, flange, and disk as compared to the outer seal ring. The thermal response of the outer portion of the disk was very quick after an accel, but the bore and bolt circle responded sluggishly. In order to overcome this problem, slots were machined in the bolt flanges, and a small quantity of air was used to convectively heat the bolt flange from both sides, as shown in Figure 38. This modification increased the flange temperature by 56° C (100° F) at the critical condition. When the improved cooling of the bolt flange was combined with an improved mechanical design, the life objective was achieved.

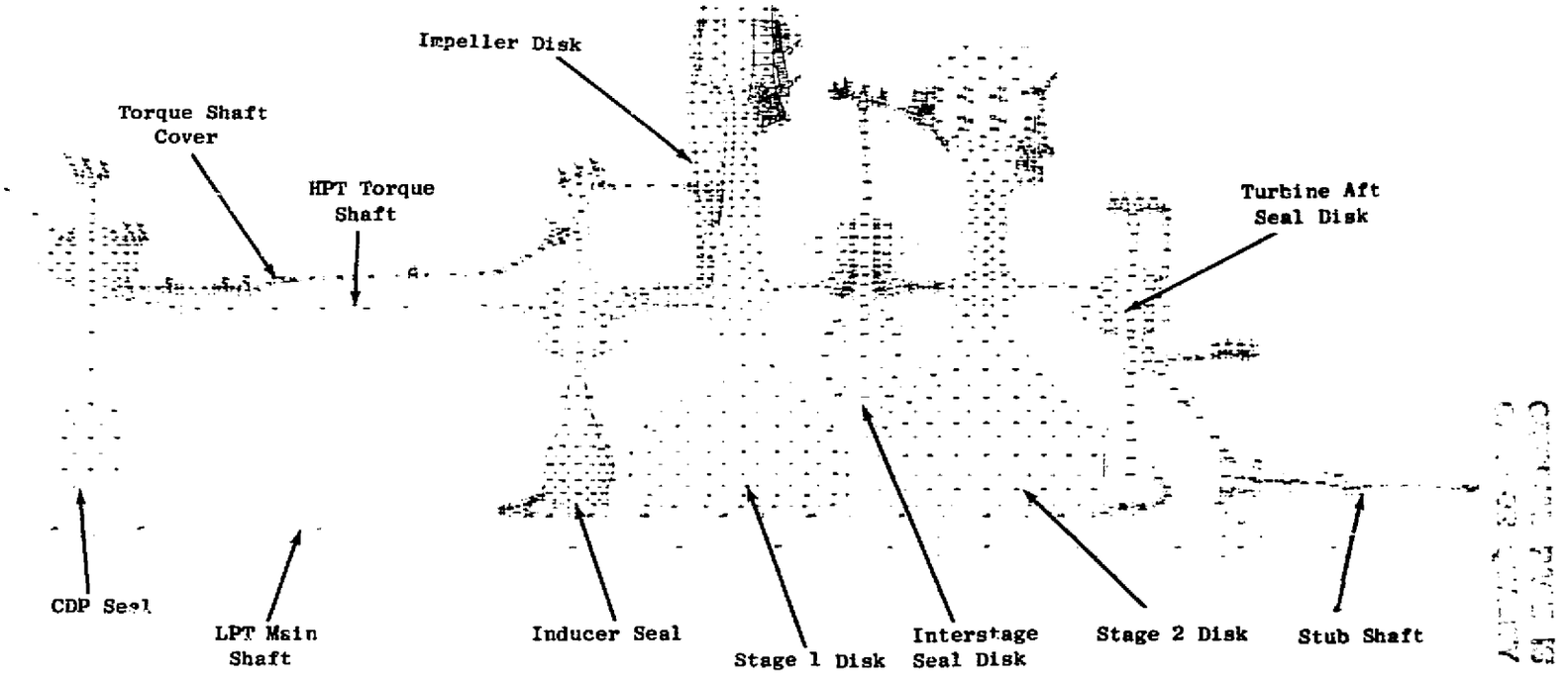

Figure 37. Rotor Structure Detailed Heat Transfer Model.

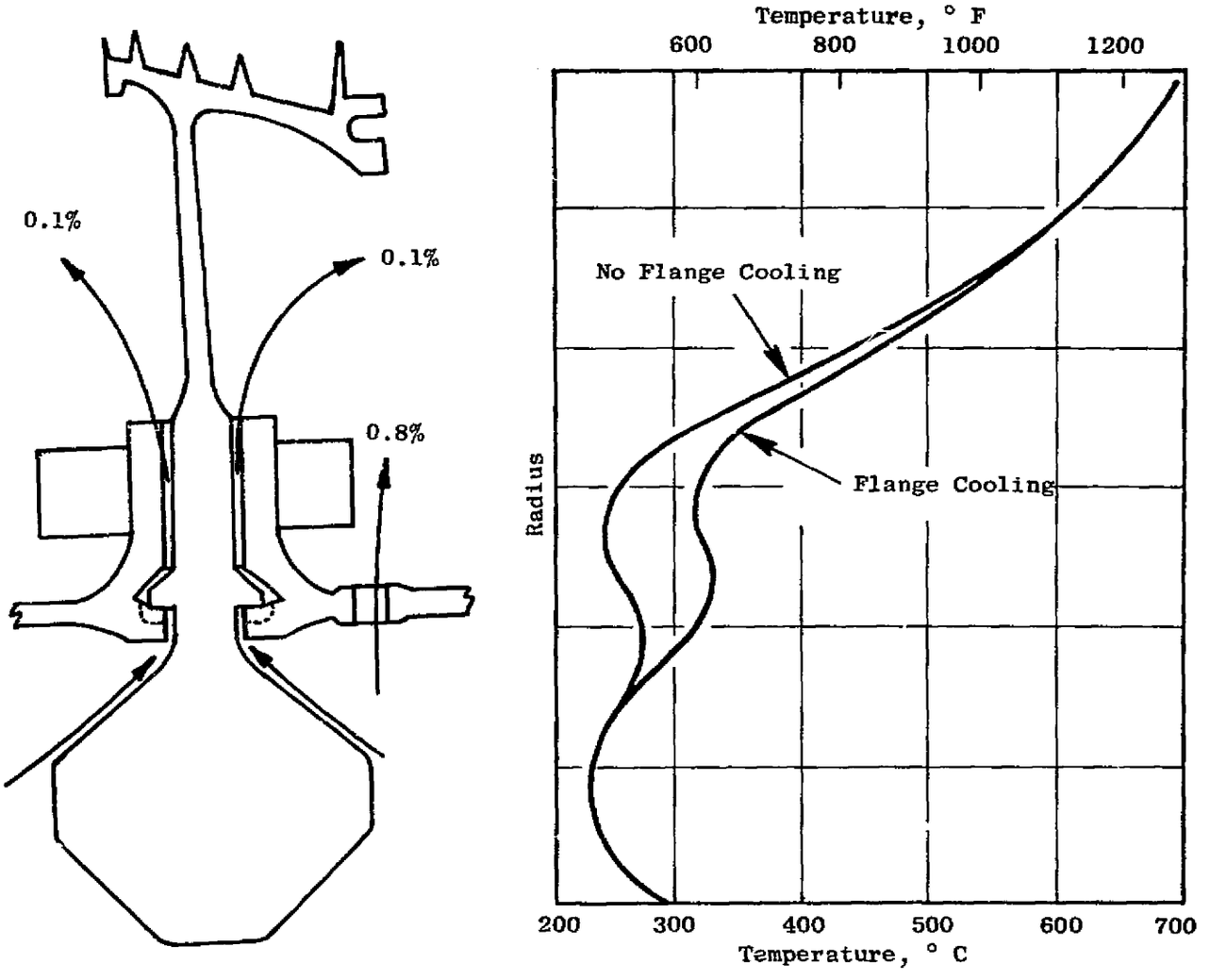

Figure 38. Interstage Seal Disk.

Another problem occurred at the bore of the Stage 2 disk. The axial and radial thermal stresses combined to limit the transient rupture life at that location. This problem was overcome when the heat transfer to the bore was increased. This increased the transient temperature at the bore surface and caused a higher thermal compressive stress. When combined with the mechanical tensile stress, the effective stress was reduced. The end result was a disk that met the rotor structure-life objectives of the growth engine. The improved heat transfer to the bore was accomplished by increasing the flow under the disk to 0.2% W_{25} and reducing the radial gap from 0.254 to 0.127 cm (0.10 to 0.05 in.).

3.2.8 Casing

The thermal analysis of the HPT casing is presented in Figure 39. During this analysis, particular emphasis was placed on evaluating the transient temperature gradients in the rings/flanges. The original analysis indicated that the transient-induced temperature gradients were resulting in high effective tensile hoop stresses in the casing flange bolthole edge over the Stage 2 nozzle even without ACC. The rabbet was moved from the outside of the flange to the inside, and the flange was thickened to enhance conduction and reduce the dead weight of the bolt spacer. The 0.35% W_{25} allocated for Stage 2 shroud purge was used first to cool the Stage 2 nozzle bolt flange by delivering the air to the shroud cavity through 0.381 x 0.127 cm (0.15 x 0.05 in.) slots in the bolt flange. This approach results in a cooler bolt flange and a reduced transient-temperature gradient.

This thermal analysis was performed on the casing hardware that extended from the combustor aft casing through the HPT and back to the LPT nozzle support structure. The coolant/leakage flows were defined along with the geometry required to achieve the objective flows. The thermal model (Figure 40) contained 180 nodes, 35 temperature and heat-transfer-coefficient boundary conditions, and 35 input time steps. A few of the temperatures at steady-state, hot-day takeoff for the base FPS engine are presented in Figure 40. The transient heat-transfer analysis included the effects of the nominal ACC cooling on the outside of the casing. This ACC cooling was initiated at the end of the 2-minute takeoff and continued to the steady-state cruise condition at 10.67-km (35,000-ft) altitude.

3.2.9 Stage 1 Nozzle Support Structure

The thermal analysis of the Stage 1 nozzle support structure consisted of the thermal-transient evaluation of the outer combustor casing, compressor exit prediffuser, inner combustor-discharge seal, inducer, and inducer seal. The transient included the complete engine flight mission.

Of particulsr interest were the inducer and inducer seal since they are both critical to the turbine-rotor, air-supply system. The inducer airflow obtained in the air-turbine test was evaluated and found to be high. Therefore, the inducer width was reduced in an effort to increase the velocity leaving the inducer and thus improve the velocity match with the rotor.

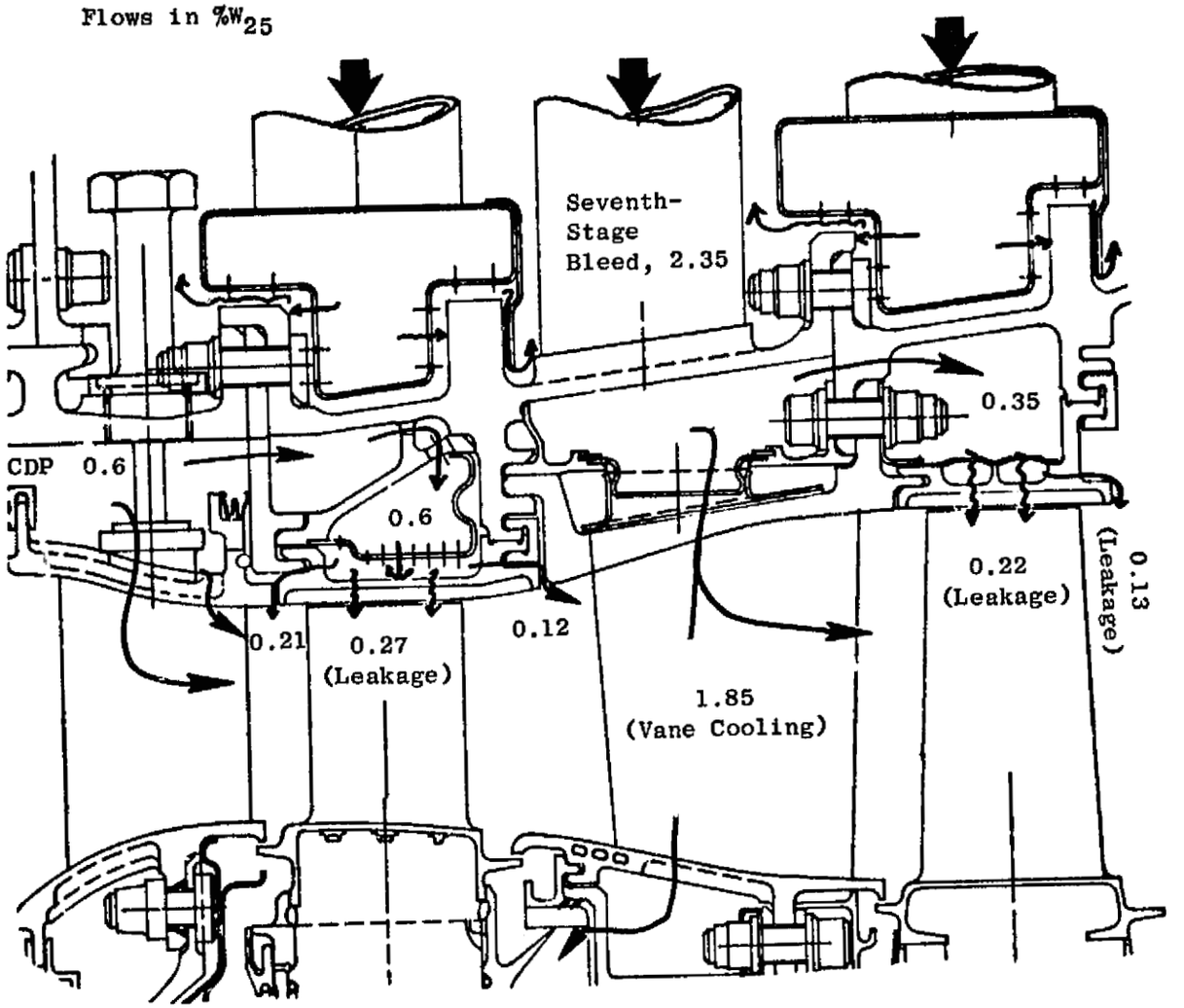

Figure 39. Casing Cooling Flow Distribution.

- No Active Clearance Control

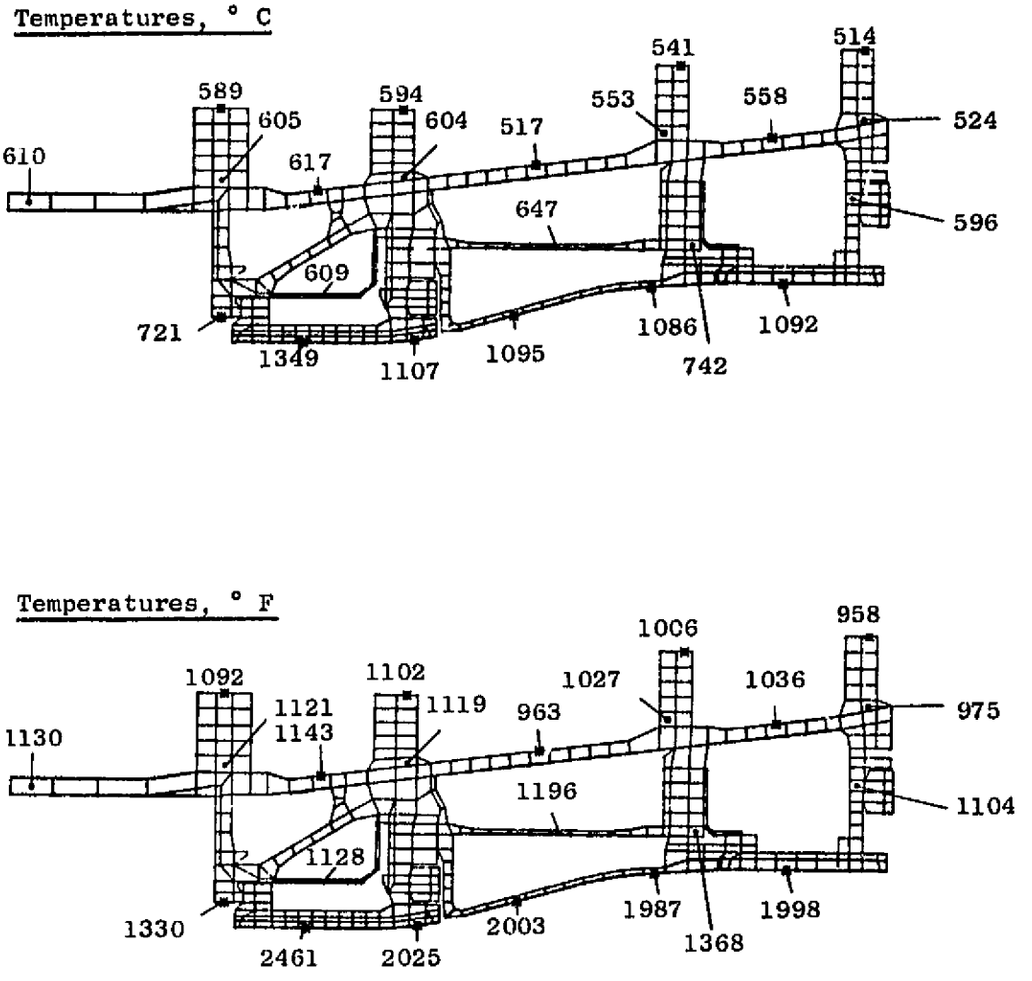

Figure 40. Casing Steady-State Takeoff Temperature Distribution.

Inducer seal leakage can significantly affect the performance of the turbine-cooling system as well as the turbine aerodynamic performance. Because of this, extensive studies were conducted to define the best approach to minimize the leakage of the inducer seal. A dynamic clearance model was set up and used to define the transient clearances during the engine mission. Of particular interest were the engine start/warm-up/accel-to-max takeoff mission cycle and hot rotor reburst at cruise. The engine-acceptance, takeoff, hot-rotor reburst was also evaluated.

Since there is no ACC system on the seal, it was imperative that the best passive system be found. Early in the analysis it became evident that a material with a low thermal coefficient of expansion was needed for the stationary seal. Inco 903A had been selected for the compressor-discharge seal, but the inducer seal temperature [over 649° C (1200° F)] prohibited the use of this unique material. The problem was resolved by the introduction of 0.1% W_{25} compressor discharge air to cool the back side of the seal. This reduced the base engine temperature below 649° C (1200° F) and allowed the use of Inco 903A material which reduced the clearances dramatically.

The mass of the stationary inducer seal was also evaluated. The analysis showed that a more massive seal improves the clearance at cruise by 0.005 cm (0.002 in.) since the hot rotor reburst is not as severe. However, at takeoff pinch clearance is reduced 0.010 cm (0.004 in.) and may be a more limiting condition than at cruise. During the core and ICLS tests, the thermal-transient response of this seal will be monitored very closely to verify the need of the increased seal mass. The worst transient will be evaluated, and the seal-tooth rubs will be checked after test so that a bench mark can be obtained to define transient clearances.

4.0 ACTIVE CLEARANCE CONTROL SYSTEM

4.1 GENERAL DESCRIPTION

One of the prime features of the E^3 HPT is active clearance control. Extensive efforts have been made to understand and implement the ACC system. To understand the system, it is imperative that the relationship of radial clearance between the turbine rotor and stator be defined along with the effects on performance.

In an aircraft engine these clearances tend to vary considerably because of operation over wide ranges of rotor speed and temperature. During a typical flight, many changes in power are made which cause relative mechanical and thermal movement between seal teeth, overlaps, and blade tips. Additional deflections arise due to transient flight loads, imposed on the engine, and engine vibration. When the normal manufacturing tolerances of the many mating engine parts are considered, especially those which affect rotor/stator eccentricity, it can be extremely difficult to maintain close running clearances throughout the operating envelope.

In allowing for random flight loads, engine vibration, and tolerance variations, a desired minimum running clearance can be calculated. This clearance can vary at different operating points, but in general it can be shown that a larger clearance is required at takeoff than at cruise.

After the factors that lead to a minimum running clearance are determined, the clearance effects of rapid engine power changes must be determined. These transient clearance requirements can be larger than all other effects combined. A sketch indicating the variation of clearance during an engine transient is shown in Figure 41. During acceleration, the rotor diameter increases with increasing centrifugal force. After a steady-state speed is achieved, the rotor diameter continues to increase at high power as the rotor mass temperature increases. At the same time, the casing diameter increases during operation at high power as the mass approaches internal-airflow temperatures. Reverse effects occur during deceleration with the rotor diameter again responding initially faster than the stator. With an uncooled casing, a minimum blade clearance must be maintained for the smallest transient clearance; that occurs a few seconds after accelerating the engine to takeoff power. As a result, the tip clearance which occurs over most of the remaining mission is larger than the desired minimum running clearance. To mitigate the excess clearance, the casing is uncooled during takeoff; then cooling is gradually applied through the climb and cruise portions of the mission to reduce tip clearance toward the minimum desired running clearance, as illustrated by the dashed line in Figure 41. With the cooling system employed in this example, even tighter clearances are possible, as shown by the dotted line, but applying this much cooling may result in excessive wear and deterioration under normal flight and engine-operating conditions. The only time that the maximum cooling would be applied would be at a minimum cruise power setting.

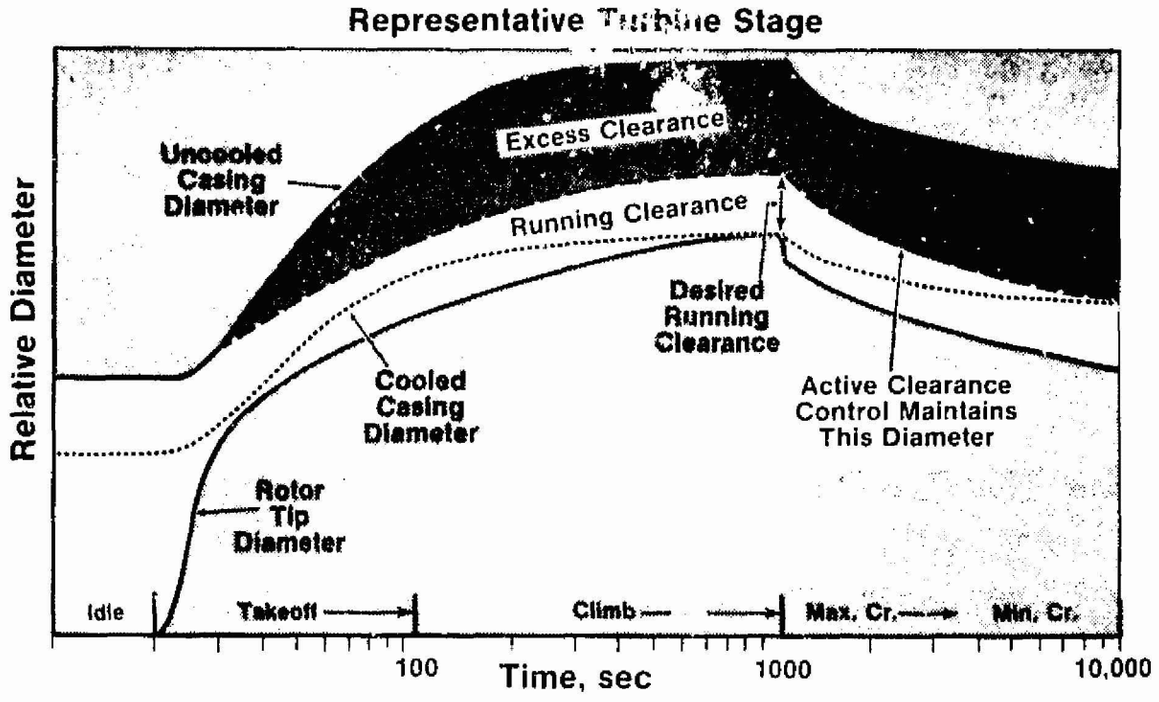

Figure 41. Active Clearance Control Operation.

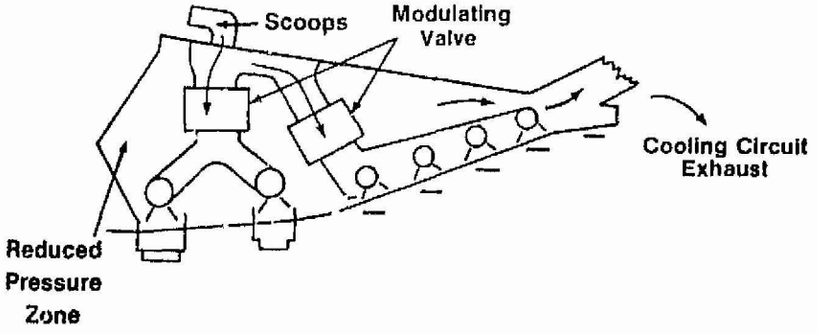

- **Operation**
  - Separate Fan-Air Modulating Valves (2) for HPT and LPT
  - Some Opening of Clearance at SLTO
  - Control by FADEC

Figure 42. HPT/LPT ACC Cooling System.

The turbine clearance-control system uses cooling air extracted from the fan duct as schematically presented in Figure 42. The air is returned to a low-pressure region in the exhaust for partial energy recovery. Because low-pressure fan air is used as a source for casing cooling, the engine cycle penalties are low. Flow of this air is independently controlled by a modulating valve. Maximum cooling flow to the turbine is equivalent to 0.3% of core compressor flow.

In establishing a control system for the ACC, it was clear at the outset that it should be integrated closely with the basic engine control. This can be done without difficulty because the primary engine-control element, the Full Authority Digital Electronic Control (FADEC), incorporates a digital computer capable of handling a multitude of functions on a "time sharing" basis. The clearance-control functions are incorporated by adding clearance-control strategy to the control program memory, making provisions for sensing clearance-control parameters, and providing appropriate output devices for positioning the clearance-control air valves. The primary inputs for the HPT ACC system are core speed, fan-discharge temperature, compressor-discharge temperature, and fuel flow. During the core and ICLS tests, the casing temperature will also be used as the primary means of stator growth definition.

4.2 DETAILED DESIGN AND FEATURES

The details of the HPT ACC system are presented in Figure 43. Fan air is extracted from the bypass duct through a split scoop that separates the HP and LP ACC air. The air, once inside the scoop, is slowed efficiently through a 2:1 area-ratio diffuser in an effort to recover as much as possible of the Mach 0.5 fan-duct dynamic head. After diffusion, the HP ACC air is ducted to the modulation valve in the pylon. After flowing through the valve, the air is delivered to a 270° circumferential rectangular duct built into the core cowl outside the HPT. From this circumferential duct the air is routed through four pipes to the impingement manifold surrounding the HPT casing. There are four impingement-manifold segments surrounding each of the two turbine stages. The impingement manifolds have rectangular cross sections and allow the required proximity of small impingement holes to the casing clearance-control rings and bolt flanges. The clearance of each stage in the HPT is accomplished by impinging the fan air on the casing, ACC rings, and bolt flanges.

The compartment outside the HPT is isolated from the rest of the engine volume between the core engine and the inner fan-duct flowpath by the fire safety wall. This is necessary because the pressure of the spent impingement air is lower than the fan-duct static pressure at maximum ACC flow rates. From this isolated cavity, the spent ACC air can flow inward through the struts of the rear frame to the aft center body and discharge out the vent stinger at a velocity such that most of the thrust is recovered.

A means of heating the casing during engine warm-up was also devised. The heating system impinges 0.3% W_{25} of compressor discharge air on the outside of the casing. This is done for 200 seconds after the engine is at stablized

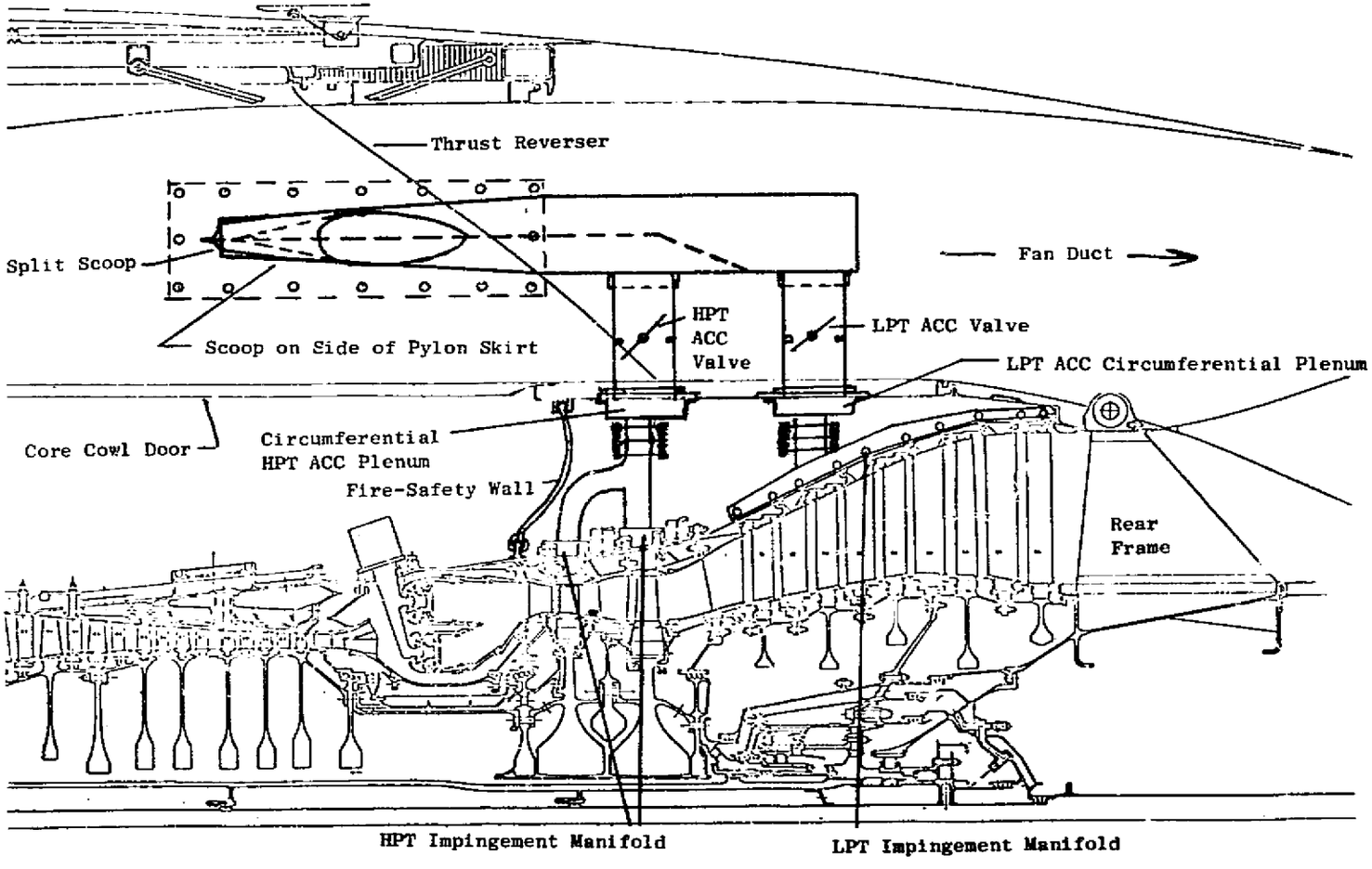

Figure 43. Active Clearance Control Design Features.

idle-power conditions. The purpose of heating the casing is to prevent blade tip rubs if the engine were to be accelerated to full power while the casing was relatively cool compared to the rotor.

Extensive studies have been conducted on the HPT to evaluate the characteristics and possible problem areas of the ACC system. Typical results of a few of these studies are presented in Figures 44 through 46. The Stage 1, interstage seal, and Stage 2 clearance analyses at start, takeoff, and cruise are summarized for hot-day conditions. In this particular analysis, the casing was allowed to heat-up during start, idle (8.3 minutes), and takeoff (2 minutes) before the ACC air was turned on as the engine was throttled back to maximum climb. The ACC air was left on at that rate up to 10.67 km (35,000 ft), and the engine was allowed to thermally stabilize at maximum cruise before going through a throttle chop to flight idle and reburst back up to maximum cruise. This mission includes a few of the most severe transient cycle variations that can be expected in airline service and can be used as an indication to show the deficiencies and capabilities of the ACC system.

The design approach used was to set a 0.64 cm (0.025 in.) clearance at takeoff for both the first-stage and the second-stage blade tips. This also sets the buildup clearance. The interstage-seal buildup clearance will be such that a slight rub will occur at takeoff; this will ensure mimimum seal clearance for all conditions.

The results of this analysis are presented in Figures 44 through 46. Table X summarizes the analysis and shows the expected performance requirements.

Table X. Active Clearance Control System Payoff.

- Based on Air-Turbine Data and 0.041 cm (0.016 in.) Clearance
- Maximum Climb, 10.67 km (35,000 ft) Altitude

	$\Delta\eta_T$/mm	$\Delta\eta_T$/mil	Clearance No ACC		Clearance Reduction		$\Delta\eta_T$
			cm	in.	cm	in.	
Stage 1	1.732	0.044	0.094	0.037	0.053	0.021	0.924
Stage 2	0.669	0.017	0.109	0.043	0.069	0.027	0.459
Interstage Seal	0.472	0.012	0.102	0.040	0.033	0.013	0.15
						$\Delta\eta_T$ Total	+1.533
						Δsfc_{η_T}	-1.24%
W_c (Fan Air) - 0.15% W_{25}						Δsfc_{W_c}	+0.02%
					Net	Δsfc	-1.22%

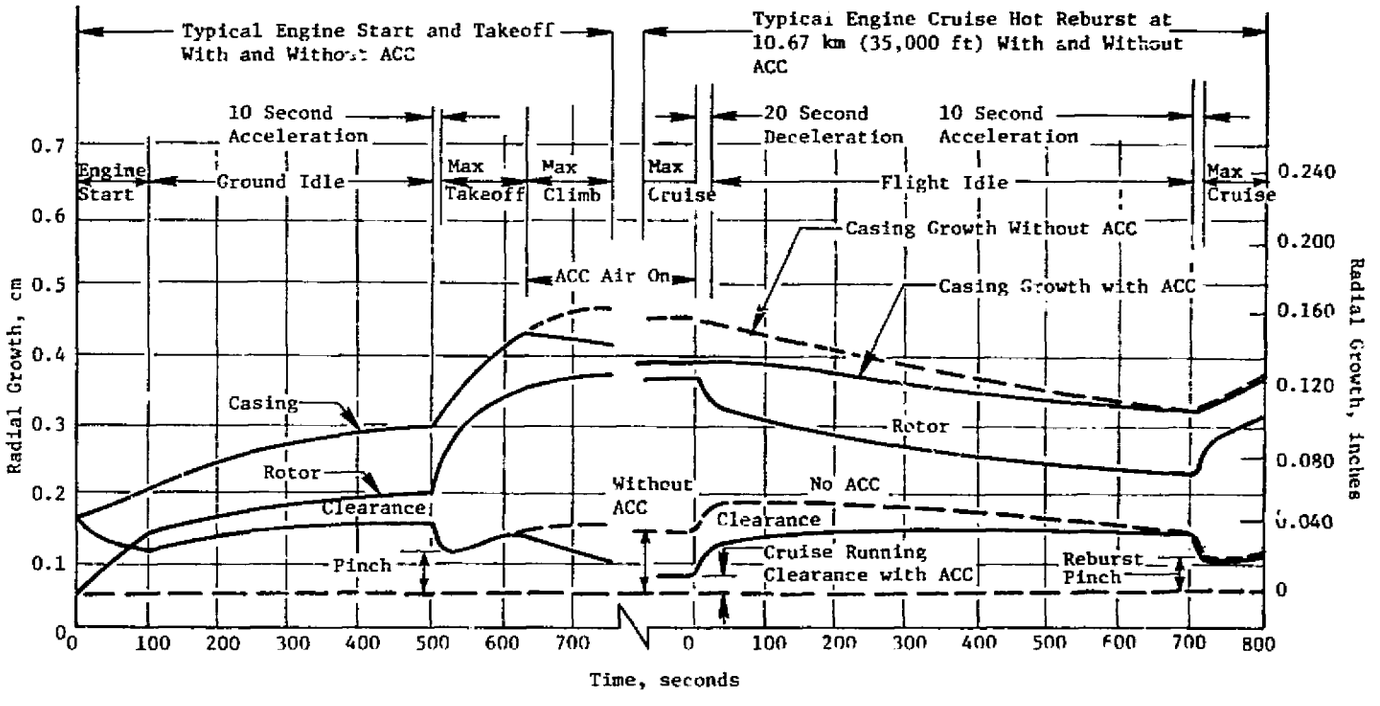

Figure 44. Stage 1 Blade-Tip Clearances.

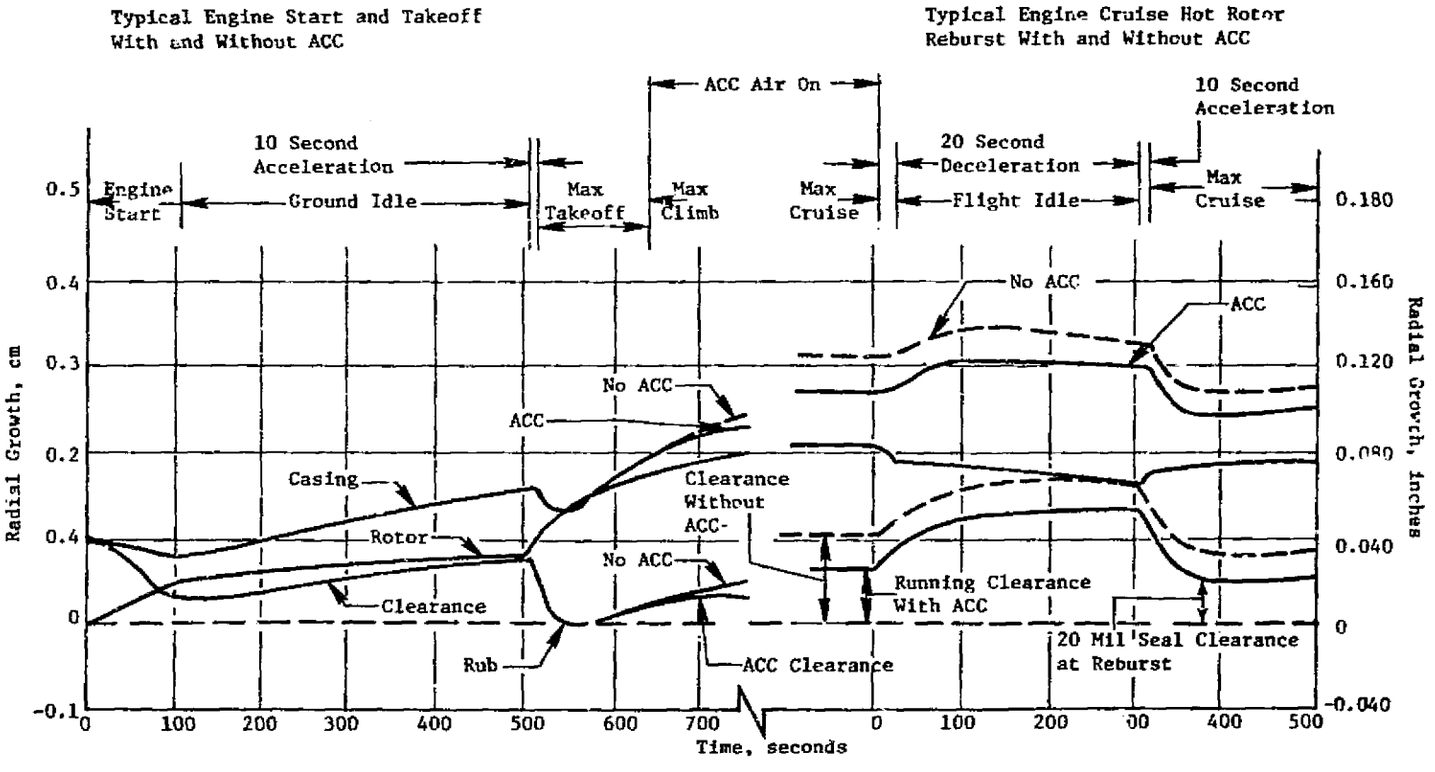

Figure 45. Interstage Seal Clearances.

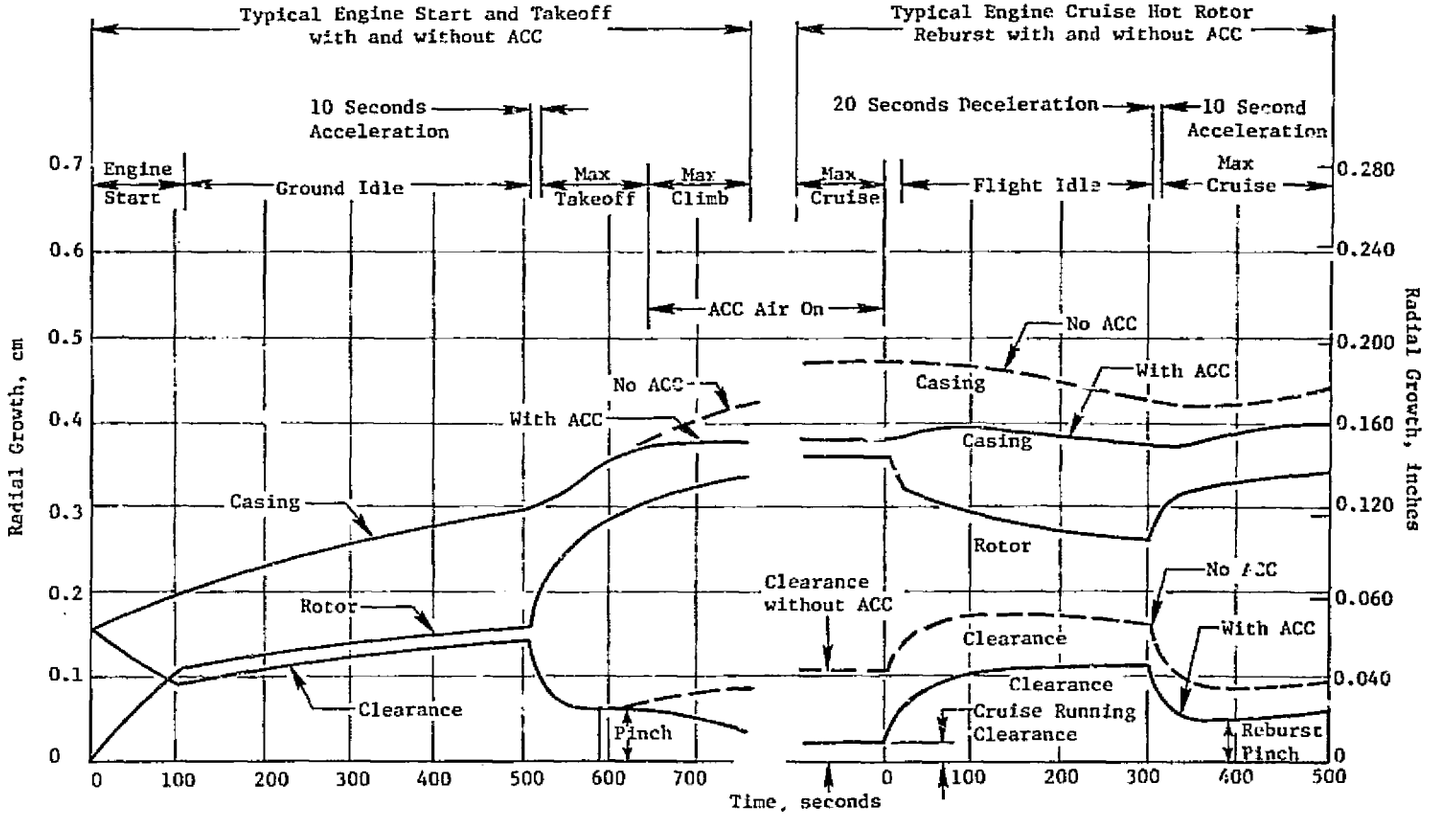

Figure 46. Stage 2 Blade-Tip Clearances.

This analysis shows that the hot rotor reburst (maximum cruise - flight idle - maximum cruise) is not the most limiting condition when ACC is being used. It also shows that the ACC system can reduce the clearance to the prescribed 0.041 cm (0.016 in.) at maximum cruise conditions. The flight condition that tests the full capability of the ACC system is the minimum cruise power condition, about 40% maximum cruise thrust level. Figure 47 shows the blade-tip clearance for both stages at various thrust levels and various quantities of ACC cooling. At the 40% thrust level, Stage 1 has 0.02 cm (0.008 in.) of margin, and Stage 2 has 0.005 cm (0.002 in.) of margin when comparing the maximum closure capability and desired 0.041 cm (0.016 in.) clearance. It is not enough, however, to compare the individual stages independently because the two stages will be modulated jointly. Figure 47 shows that when the Stage 1 blade clearance is 0.041 cm (0.016 in.) at the 40% power point, the Stage 2 clearance is 0.051 cm (0.020 in.) using 65% of maximum ACC coding flow.

The above analysis is based on the assumption that the cold engine, in airline service, has been allowed to warm up at least 8.3 minutes after start. Production-engine experience indicates that this is not always the case, and shorter warm-up times are quite possible. Because of this, an extensive study of the cold and warm engine start, short idle, and maximum takeoff transient has been conducted. The purpose of this analysis, summarized in Table XI, was to define the impact of these start conditions on the minimum clearance after acceleration to maximum takeoff power. The warm engine start occurs, in airline service, when the engine has been shutdown for a short time (such as one-half hour) before being restarted. The rotor structure and casing both cool during the engine shutdown, but the casing cools at a faster rate since it is less massive. The shutdown heat-transfer analysis indicated that in one-half hour, the Stage 1 casing cools to 69° C (125° F) below the Stage 1 rotor average temperature while the Stage 2 casing cools to 111° C (200° F) lower than the Stage 2 disk.

Table XI. Maximum Takeoff Pinch Clearance After Short Start.

	Time at Idle, Seconds	Cold-Start Pinch		Warm-Start Pinch	
		cm	in.	cm	in.
Stage 1 Blade	200	0.041	0.016	0.030	0.012
	300	0.053	0.021	0.041	0.016
	400	0.058	0.023		
	500	0.064	0.025		
Interstage Seal	200	-0.038	-0.015	-0.020	-0.008
	300	-0.023	-0.009	-0.010	-0.004
	400	-0.010	-0.004		
	500	0	0		
Stage 2 Blade	200	0.038	0.015	0.015	0.006
	300	0.048	0.019	0.041	0.016
	400	0.061	0.024		
	500	0.064	0.025		

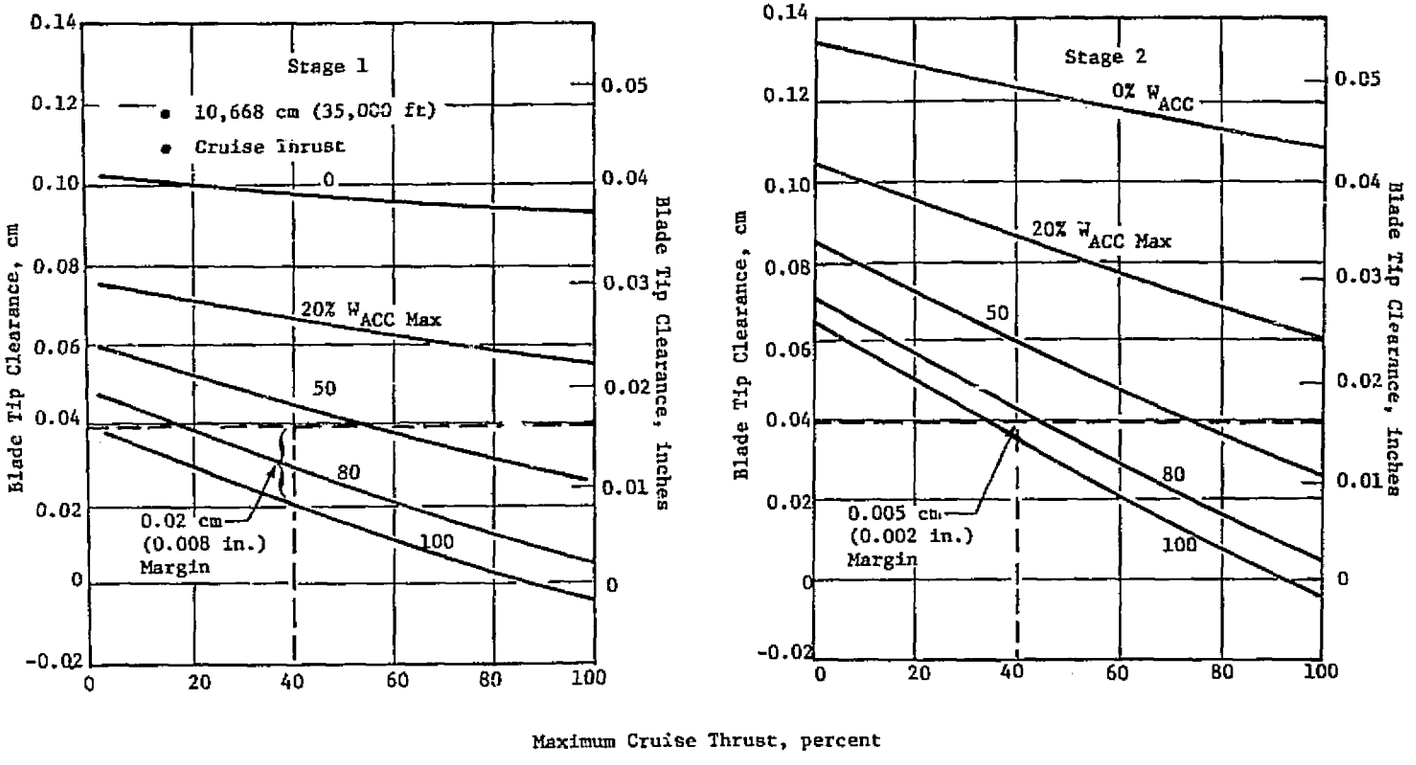

Figure 47. Blade-Tip Clearance Reduction with ACC.

The results of the analysis indicate that a substantial reduction in the turbine blade pinch clearance occurs at takeoff on both cold and warm engine starts when the engine is not given sufficient time to warm up. If the engine accel from idle to maximum takeoff occurs after only a 2 to 3 minute start and warm up, the pinch clearance can easily be reduced from the desired 0.064 cm (0.025 in.) to 0.025 cm (0.010 in.). This could easily produce a blade-tip rub since the pinch will occur in conjunction with high engine maneuver loads and vibration.

In order to overcome this potential problem, a means of heating the casing after start has been devised. The casing-heating scheme is accomplished by impinging 0.3% of compressor-discharge air on the outside of the casing during the idle power condition for 200 seconds. After 200 seconds of casing heating, a valve would turn the warm compressor-discharge air off, and the valve would remain closed until the engine had been shutdown for at least 15 minutes. If an accel to maximum takeoff occurred while the casing heating valve was open, it would remain open for 30 seconds after reaching full power. There is no advantage in continuing to heat the casing beyond the 30-second point since the clearance pinch has already occurred; continued heating of the casing would result in extra power loss from the compressor-discharge air being taken from the cycle and the excess clearances in the turbine. Under normal engine operation, the casing-heating valve would open just after the engine achieved idle rpm and would remain open for 200 seconds. The valve would then be shut for the rest of the engine mission. This would have virtually no impact on engine cycle performance and would yield significant improvement in pinch clearances during takeoff. Table XII presents the pinch clearances for cold and warm engine starts with external casing heating for 200 seconds or 30 seconds after accel to full power, whichever occurred first.

The data from Table XI show that the warm engine start/short idle/maximum takeoff cycle produces the most limiting pinch during takeoff. The improvement that can be achieved with the casing-heating scheme becomes evident when a comparison is made between the two configurations. For the 200-second start/idle, there is a 0.023 cm (0.009 in.) increase in the pinch clearance for both the first- and second-stage blade tips and a 0.005 cm (0.002 in.) increase for the interstage seal during takeoff. This casing-heating system still does not get the minimum turbine pinch clearance back to the desired 0.64 cm (0.025 in.) during maximum takeoff. The minimum pinch clearance is now 0.048 cm (0.019 in.) and 0.038 cm (0.015 in.) on the first and second stages, respectively, with the casing-heating scheme. This indicates that it may be necessary to increase the buildup clearances if 0.64 cm (0.025 in.) is truly required at maximum takeoff. Since this analysis is completely analytical and only has heat-transfer analysis practice from other engines factored in, it is necessary to define specific E^3 turbine thermal characteristics before the optimum FPS ACC can be clearly defined. The casing-heating system is being incorporated into the ICIS engine. This will allow a complete evaluation of the ACC both with and without the casing-heating system. A true system evaluation can then be made to define the need for the heating system in the FPS.

Table XII. Maximum Takeoff Pinch Clearance With External Heating During Engine Warm Up.

	Engine Warm-up Time, sec	Heating Time, sec	Cold Engine Pinch		Warm Engine Pinch	
			cm	in.	cm	in.
Stage 1 Blade	200	100-230	0.064	0.025	0.053	0.021
	*300-	100-330	0.074	0.029	0.056	0.022
	**300+	100-300	0.066	0.026	0.048	0.019
	400	100-300	0.069	0.027		
	500	100-300	0.071	0.028		
Interstage Seal	200	100-230	-0.025	-0.010	-0.015	-0.006
	300-	100-330	-0.008	-0.003	-0.005	-0.002
	300+	100-300	-0.015	-0.006	-0.010	-0.004
	400	100-300	-0.005	-0.002		
	500	100-300	-0.005	-0.002		
Stage 2 Blade	200	100-230	0.069	0.027	0.038	0.015
	300-	100-330	0.079	0.031	0.048	0.019
	300+	100-300	0.061	0.024	0.043	0.017
	400	100-300	0.066	0.026		
	500	100-300	0.071	0.028		

*Indicates that the takeoff occurred prior to the heating-system, valve-closure signal; this allowed the heating to continue 30 seconds into takeoff mission.

**Indicates the heating system valve closed at the 300-second point prior to takeoff accel.

4.3 MECHANICAL DESIGN CONSIDERATIONS

The significant, functional, mechanical features of the ACC system are shown in Figure 48. At the heart of the system are the flanges and rings used for movement of the shrouds to adjust clearance. These flanges and rings also provide stiffening to maintain the shroud roundness essential for control of clearance. The shroud segments, 24 each in Stages 1 and 2, are mounted directly from the casing and move with it in positioning the flowpath wall with respect to the rotor-blade tips. The impingement manifolds are mounted from the flanges and rings. They are accurately positioned by dimples that contact the flat boltheads forward of each manifold to maintain control over the hole-to-surface length of the impingement jets.

There are four 90° segments of manifold for each stage, as shown in Figure 49. Adjacent Stage 1 and Stage 2 segments branch from a common feed pipe from the fan duct. The section of feed pipe crossing over from Stage 2 to

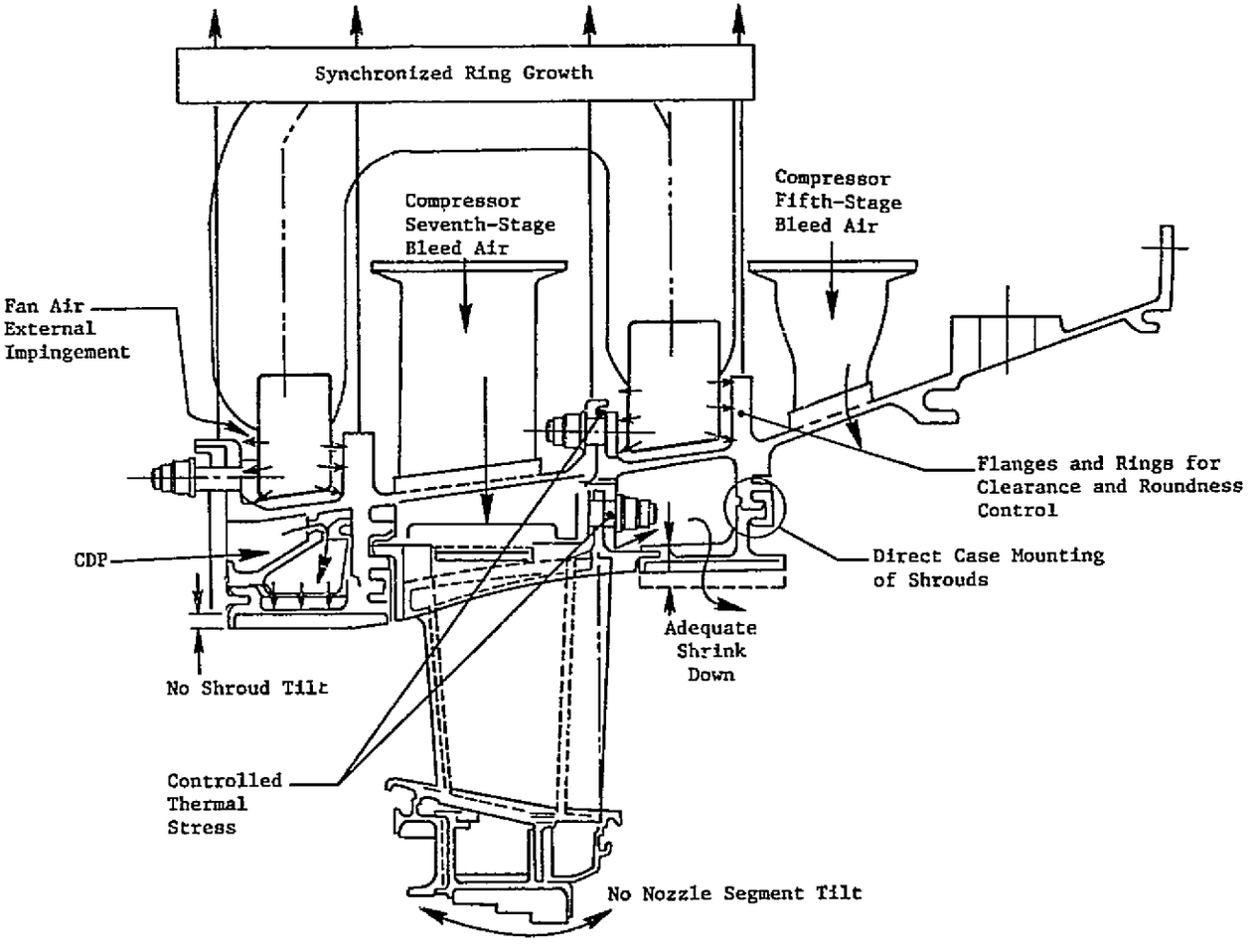

Figure 48. Active Clearance Control Design.

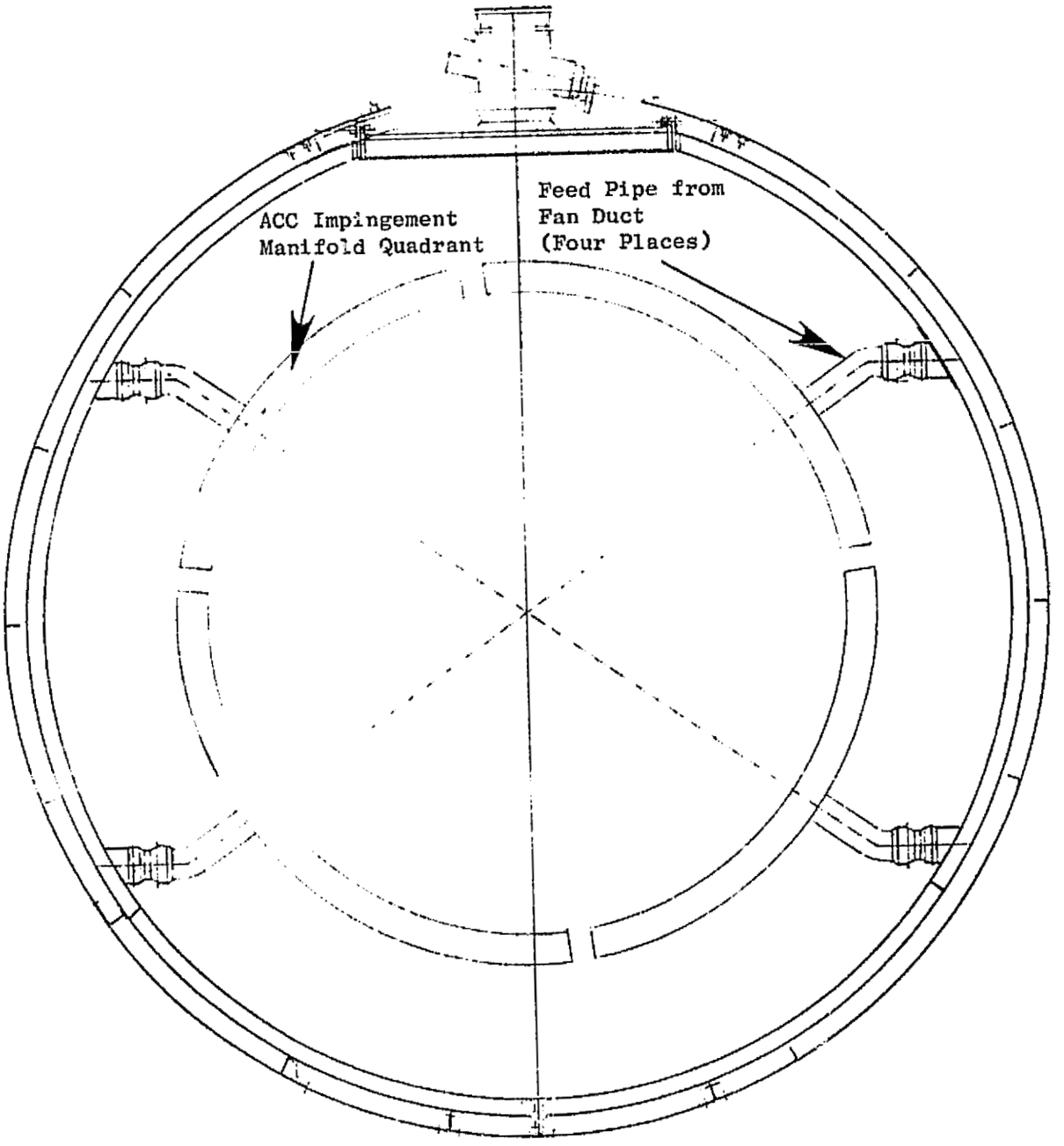

Figure 49. ACC Impingement Manifold Circumferential Arrangement.

Stage 1 has a slipjoint to accommodate differential axial growth between the cool pipe and the hotter casing.

The HPT casings (forward and aft) contain the control rings. Internally, the casings are influenced continuously by air at three different temperature and pressure levels: compressor discharge, compressor seventh-stage bleed, and compressor fifth-stage bleed. They are also acted on externally during ACC operation by fan-air impingement. The depth and cross-sectional distributions of the flange sections and the convection on the surfaces of these flanges have been balanced to produce synchronized movement of the flanges and maintain an axially uniform clearance between the shroud and blade tip at each stage. Axial tilt of the Stage 2 nozzle segments, supported between the Stage 1 aft and Stage 2 forward rings, is also controlled by this balance.

Potential transient clearance changes are listed in Table XIII for the most critical flight conditions. The most severe transient clearance reduction is in the vertical plane, and the implications of this are explored further in Table XIV. Closures from bending of rotor and static structures due to maneuver loads ("g" and gyro) are combined statistically (root sum square, RSS), and all other closure values are combined arithmetically to arrive at probable net values of -0.032 cm (-0.0126 in.) and -0.050 cm (-0.0195 in.), shown for 12:00 and 6:00 o'clock. It is assumed, as a limit, that all wear would come off the blades in case of rubs. Therefore, any rub-caused clearance increase would be carried around the annulus in the form of shortened blades rather than remaining localized in the form of a local depression in the shrouds. On this basis, the minimum clearance that could be maintained under the most severe closure conditions would be 0.041 cm (0.016 in.) average with 0.032 cm (0.0126 in.) at 12:00 o'clock and 0.050 cm (0.0195 in.) at 6:00 o'clock. This is achieved by offsetting the shroud centerline by 0.010 cm (0.004 in.) vertically, relative to the rotor centerline.

Table XIII. Stage 1 Clearance Change for Maximum Closure.

Flight Conditions	Out-of-Round Factors	Horizontal Extreme				Vertical Extreme			
		3:00		9:00		12:00		6:00	
		μm	mils	μm	mils	μm	mils	μm	mils
Takeoff	Beam Bending (RSS)	-125	-4.9	-125	-4.9	- 15	- 0.6	- 58	- 2.3
	Vibration (Unbalance)	- 76	-3.0	- 76	-3.0	- 76	- 3.0	- 76	- 3.0
	Ovalization	- 11	-0.45	- 1	-0.05	+ 23	+ 0.90	- 13	- 0.5
		212	-8.35	-202	-7.95	- 68	- 2.7	-147	- 5.8
Second Segment Climb	Beam Bending (RSS)	-152	-6.0	-152	-6.0	-261	-10.3	-406	-16.0
	Vibration (Unbalance)	- 76	-3.0	- 76	-3.0	- 76	- 3.0	- 76	- 3.0
	Ovalization	- 8	-0.33	+ 3	+0.13	+ 16	+ 0.65	- 12	- 0.47
		-236	-9.33	-225	-8.87	-321	-12.65	-494	-19.47
Low Mach Cruise	Beam Bending (RSS)	-106	-4.16	-106	-4.16	- 88.9	- 3.5	-269	-10.6
	Vibration (Unbalance)	- 76	-3.0	- 76	-3.0	- 76	- 3.0	- 76	- 3.0
	Ovalization	- 7	-0.31	- 2	-0.09	+ 14	+0.55	- 4	- 0.15
		-189	-7.47	-184	-7.25	-151	-5.95	-349	-13.75

Table XIV. Blade-Tip/Shroud Clearance.

	Cold		Maximum Takeoff		Maximum Clearance and High-Mach Cruise		Low-Mach Cruise	
	mm	in.	mm	in.	mm	in.	mm	in.
Clearance	1.24	0.049	0.889	0.035	0.406	0.016	0.406	0.016
Tolerance Stack			±0.102 mm (0.004 in.)					
Min. Clearance	1.14	0.045	0.787	0.031	0.305	0.012	0.305	0.012
Vibration	0		±0.076 mm (0.003 in.)					
Out of Round, 12:00	0		+0.023	+0.0009	+0.018	+0.0007	+0.015	+0.0006
6:00	0		-0.013	-0.0005	-0.013	-0.0005	-0.005	-0.0002
Beam Bending, 12:00	0		-0.015	-0.0006	-0.262	-0.0103	-0.089	-0.0035
("g," Gyro, Thrust, 6:00	0		-0.058	-0.0023	-0.406	-0.0160	-0.269	-0.0106
Nacelle Air)								
Total Closure, 12:00			-0.114	-0.0045	-0.320	-0.0126	-0.149	-0.0059
6:00			-0.139	-0.0055	-0.495	-0.0195	-0.351	-0.0138
Max. Interference, 12:00			0		0.015	0.0006	0	0
6:00			0		0.190	0.0075	0.046	0.0018
Offset					0.102	0.0040		
Max. Rub, 12:00 and 6:00					0.089	0.0035		
Local Clearance with Rub					0.406	0.016		

5.0 MECHANICAL DESIGN

5.1 GENERAL DESCRIPTION

5.1.1 Configuration

The HPT mechanical configuration, shown in Figure 50, utilizes a high-efficiency, two-stage system. Major design features of the turbine are:

1. Inducer System - Provides lower temperature air for blade cooling.

2. Impeller - Increases coolant air pressure to blade in order to maintain sufficient backflow margin between this air pressure and the hot-gas pressure.

3. Inner Tube - Separates the fan air from cooling air feeding the Stage 2 blade.

4. Deswirler - Rotating vanes built as an integral part of the inducer disk. The purpose of these vanes is to eliminate any potential hazard from acoustic vibration or vortex whistle.

5. Boltless Blade Retainers - This design does not require any bolts through the rim of the disk for support. Elimination of these holes enhances the low cycle fatigue (LCF) capability of the disk.

6. No Bolts in Disks - The main structural portions of the disks do not contain any holes. This feature is essential in achieving long life in the disk.

7. Interstage Disk - Prevents recirculation of hot gases between the Stage 1 blades and Stage 2 blades at the inner flowpath.

8. Single-Wall Structures - The use of a single-wall structure simplifies the geometry configuration for the ACC system. This is due to the direct access of the fan air impinging on the casing. No holes penetrate the casing wall.

9. Stage 1 Ceramic Shrouds - Ceramic shrouds require less cooling air compared to other types of shroud material. Cooling-air reduction increases turbine efficiency.

10. Stage 2 Solid Shrouds - Using a solid-shroud configuration is expected to improve component life relative to present designs.

A major objective in the mechanical design of the turbine components is to achieve long lives for commercial application. Component lives, designed for a growth cycle, are shown in Table XV.

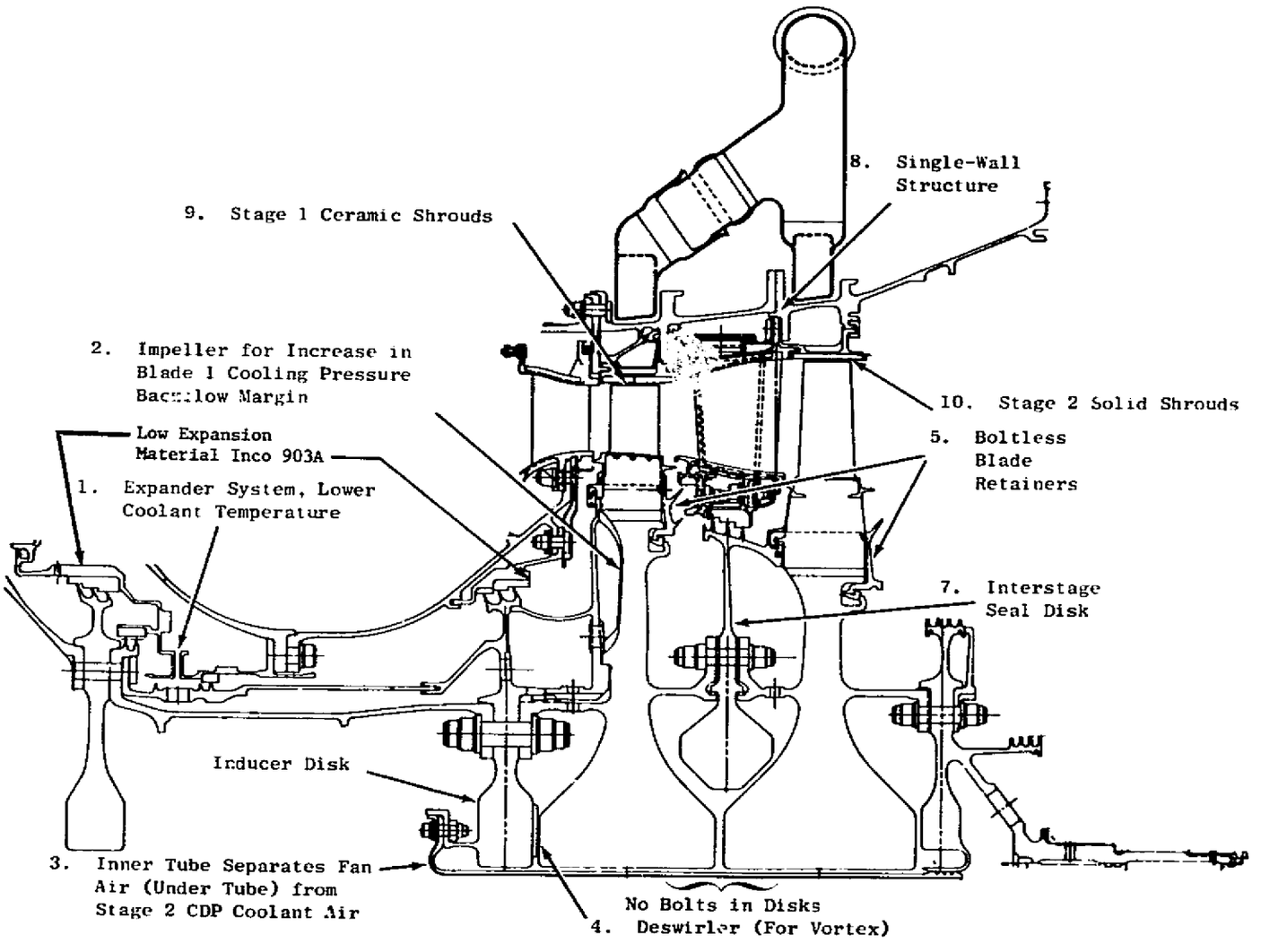

Figure 50. E^3 HPT Major Design Features.

Table XV. Component Design Lives.

	Service	Installed	Total Service Life With Repair	
	Flight Hrs	Flight Cycles	Flights Hrs	Flight Cycles
Flowpath Components/ Blade Retainer	9,000	9,000	18,000	18,000
Disks, Shafts/Seal Disk	18,000	18,000	36,000	36,000

Flowpath components (blades, vanes, blade retainers, interstage disk) are designed for 18,000 hours with repairs permissible after the first 9000 hours of engine operation.

The type of repairs for these components are as follows:

Stage 1 and 2 Blades

Repair would be performed in the following areas:

Blade tip - Weld buildup the tip locally. For abnormally worn tips, the tip is removed and replaced using Activated Diffusion Bonding (ADB). The ADB process was developed for the TF39 and is presently being used by GE for repairing HP turbine blades for other engines, especially for commercial use.

Platform Cracks - Normally cracks in the platform would appear along the edges. These locations are not considered to be highly stressed (mechanically) and can be repaired using the Activated Diffusion Healing (ADH). The difference between ADB and ADH is that ADH is limited to crack repairs not exceeding approximately 0.1016 cm (0.04 inch), and there are no missing pieces within the area to be repaired.

PVD Coating - The PVD coating could be stripped and a new coating applied.

Stage 1 and 2 Blade Retainers

Repair weld would be limited to the labyrinth seal teeth. The repair would consist of removing locally developed cracks that may appear close to the sharp edge surfaces of the teeth. The surrounding area around the crack is removed, polished, and zygloed.

A weld buildup process using René 95 filler material would be used. The aluminum oxide coating would be removed by chemical stripping prior to welding. The coating would then be reapplied after X-ray and Zyglo inspections show no further cracks.

The above procedure is an established and approved process for Inco 718. In the case of AF115 material, this repair process has not been firmly established, and, therefore, further work would be necessary to assure complete approval.

In the even of rabbet wear, the surface can be machined [0.0254 cm (0.01 in.) to 0.0508 cm (0.02 in.)] and a hard metal spray applied and ground down to the original dimensions.

Stage 1 and 2 Disk

Repair would be limited to the flange boltholes, rabbet surface wear, and the local radial scallops located in the flanges used for air passages.

Depending on the size of cracks found, the boltholes would be reamed and polished. This would also apply to the Stage 2 forward disk arm cooling-hole passage.

Forward and Aft Shafts

The two-seal-teeth arrangement on the HP shaft would be repaired using a similar procedure presently used for the CF6-50 engine interstage catenary support. If cracks appear on the flanges, they would be reamed, provided the sizes of the cracks are small.

In the event of rabbet wear, a similar procedure as described for the blade retainers can be used.

Impeller

Repair could be done on the elliptical cooling passages located above the rabbet support. These cooling holes are elliptical in geometry and could be slightly increased in size, if necessary.

Forward Seal Disk

By slightly increasing hole sizes, repairs can be made for the following:

- Cooling hole passages
- Elliptical boltholes (limited size only)
- Inner flange boltholes (fastens the inner tube to this flange).

C-2

5.1.2 Materials Selection

The material selections for the HPT are summarized in Figures 51 and 52 and Table XVI. Material selection differences between the ICLS and FPS base engine are in the HP shaft and aft shaft/disk. Present ICLS engine material for these two components is Inco 718. For the FPS base, advanced "super" processing of Inco 718 will be required to achieve the LCF life goal of 36,000 cycles. Super Inco 718 is presently used in the CF6-50 HPT disks. The basic difference between super and standard Inco 718 processing is improved grain-size control to provide an ASTM grain No. 7 or finer in Super Inco 718.

For the balance of the HPT components, the plan is to continue with René 95 and AF115 Powder-Metallurgy (PM) or Hot Isostatic Pressing (HIP) material. However, other materials will also be explored.

Turbine disks and the forward outer liner are manufactured from René 95 using PM techniques. René 95 has excellent strength and resistance to creep and fatigue at temperatures up to about 650° C (1200° F). The use of HIP to consolidate the powder permits manufacture of a blank that is far closer to the net shape of the finished disk than a forging would be. Thus the machining and powder material required to produce these parts have been substantially reduced.

The inducer disk, interstage-seal disk, impeller, U-clip, and Stage 1 retainer are manufactured from AF115 material using PM techniques. This alloy, developed by General Electric under Air Force Material Laboratory sponsorship, has strength and fatigue resistance similar to those of René 95 at temperatures up to 650° C (1200° F). The creep resistance of AF115 is superior to that of René 95; for the same creep life and stress levels, AF115 can operate 50° C (90° F) hotter than René 95. The E^3 represents the first application of AF 115.

Supplementary mechanical-property data for both René 95 and AF115 were obtained during this program. The testing was needed to support the use of these materials at design points characteristic for the different components. LCF and creep/rupture tests were conducted.

Stage 1 and Stage 2 blades are made from directionally solidified (DS) René 150. This General Electric alloy was developed specifically for DS processing. The grain boundaries are parallel to the tensile loads in these blades. This structure, plus the composition of the alloy, results in superior creep resistance and tensile strength relative to the present turbine blades at metal temperatures of about 1100° C (2000° F). The blades are coated with an oxidation-resistant, nickel-base alloy using a physical vapor deposition (PVD) process. In the PVD process, the part to be coated and a feed ingot of the coating material are placed in a low-pressure chamber. An electron beam directed against the top of the feed ingots evaporates metal from the ingot. The metal vapor condenses onto the part; the part is positioned above the feed ingot and manipulated to expose all specified portions of its surface to the metal vapor. GE experience with PVD coated blades for

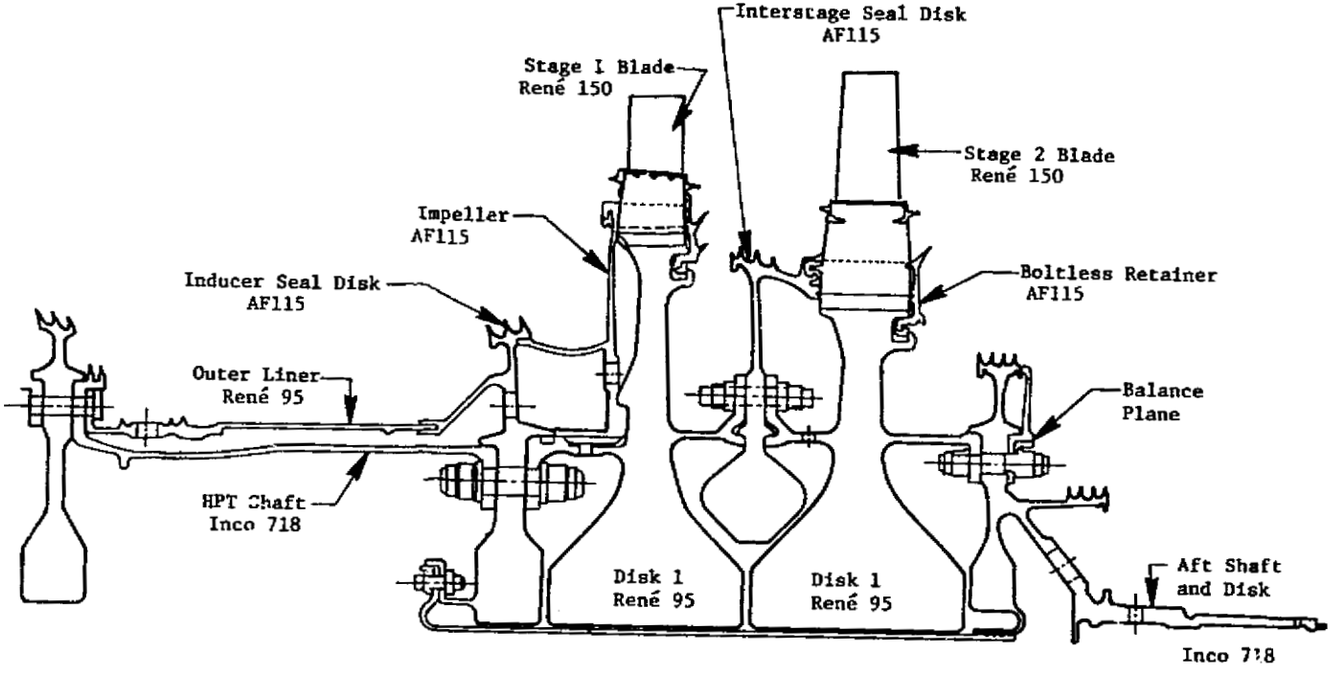

Figure 51. Material Selections for Rotor Components.

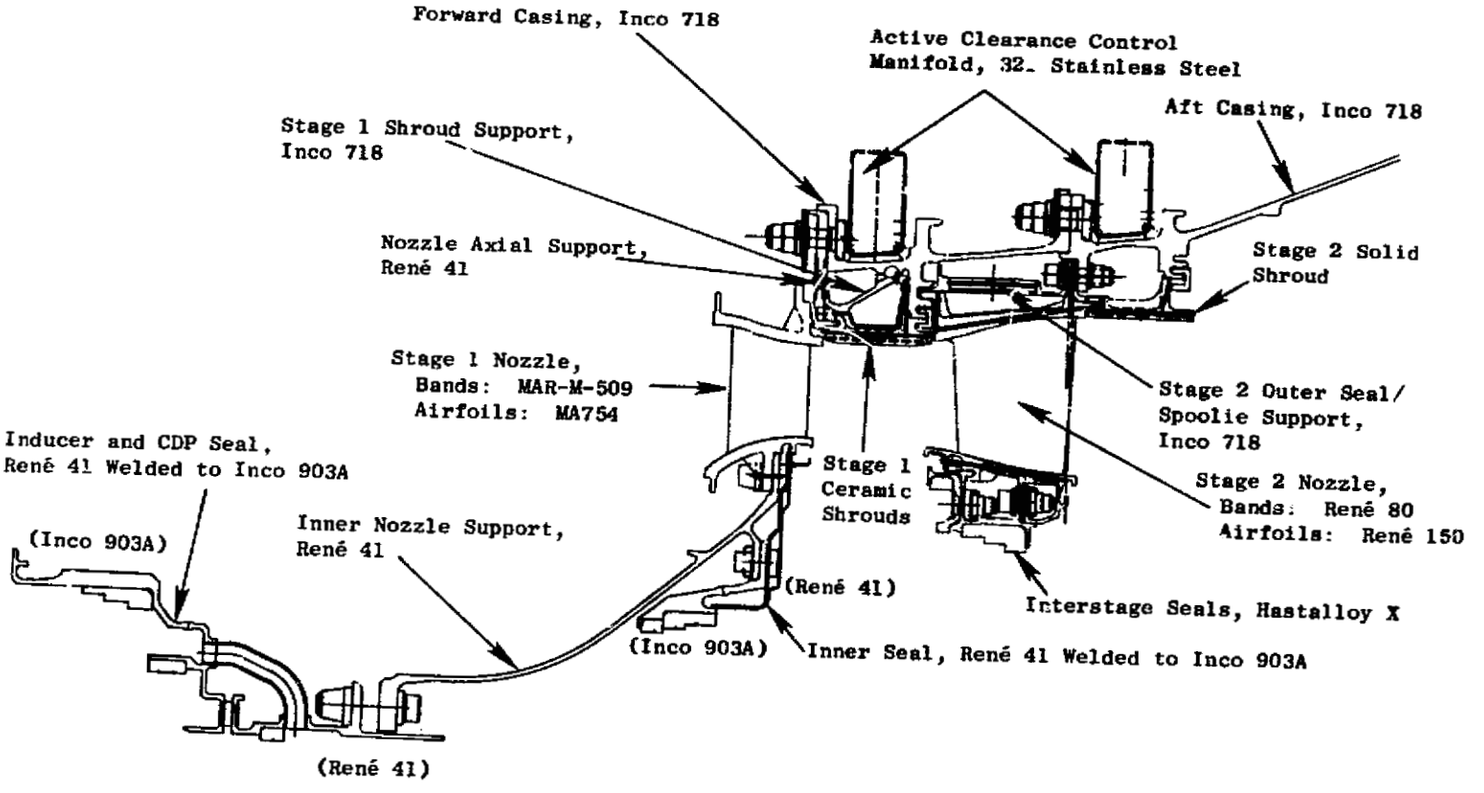

Figure 52. Material Selections for Static Components.

Table XVI. Rotor and Stator Materials.

Part	Material	Form	Reason for Selection
Stage 1 Vanes	MA754	E	Creep, Burnout Margin, LCF
Stage 1 Bands	MAR-M-509	C	Rupture, Cost; Y.S.
Stage 1 and 2 Blades	René 150	C, DS	Rupture, LCF
Stage 1 and 2 Disks	René 95	PM	Tensile (Burst)
Stage 1 Shrouds	Ceramic (Zirconia/Yttria)	---	High Temp >1370° C (2500° F) Capability, Erosion
Stage 2 Shrouds	René 77 (Solid)	C	Cost
Stage 2 Nozzle and Shroud Support	Inco 718	F	Med Temp Strength, Tensile Strength
Outer Casing	Inco 718	F	Med Temp Strength, Tensile Strength
Stage 1 Retainer/Seal (Fwd. and Aft)	AF115	PM	704-760° C (1300-1400° F) Creep, LCF
Interstage Seal Disk and Space/Retainer	AF115	PM	704-760° C (1300-1400° F) Creep, LCF
Stage 1 Inner Nozzle Support	René 41	F	Rupture Vs. Inco 718, Temp.
Stage 2 Vane	René 150	C	LCF, Rupture
Stage 2 Vane Band	René 80	C	Rupture and Castability
Stage 2 Interstage Seal	Hast X	F, HC	Temperature
Impeller	AF115	PM	Temp, LCF, Rupture
Inner Shield	Inco 718	F	538-649° C (1000-1200° F) Tensile
Stage 2 Aft Retainer	AF115	PM	Creep, Rupture Strength
Forward Shaft	Inco 718	F	538-649° C (1000-1200° F) Tensile, LCF
Fwd. Outer Liner	René 95	F	LCF, Rupture
Inducer/Seal Disk	AF115	F, S	Rupture, LCF, Temp.
Aft Shaft/Disk	Inco 718	F	538-649° C (1000-1200° F) Tensile, LCF
Inducer/CDP Seal	Inco 903A/René 41	F/S HC	Low Coeff. of Exansion for Clearance Matching
Stage 1 Inner Seal	René 41/Inconel 903A	F/ H/C	Temp, LCF, Coeff. of Expansion

Nomenclature

E - Extrusion
C - Cast
DS - Directionally Solidified
PM - Powder Metallurgy
F - Forging

long-time usage has been the recently completed testing accomplished in the CF6-50 Engine 455-508 Buildup 21. This engine was test run for 1000 "C" cycles. Some of the CF6-50 engine, Stage 1 HPT blades (René 150 material) were coated with PVD. These blades were a modification of the standard HP blades. The modification essentially consisted of reducing the blade cooling flows. This was accomplished by deleting the center row of leading-edge holes and also the cooling holes on the pressure side, midchord. The effect of the reduction in cooling holes resulted in flows being lowered from present 3.4% to 2.8%. Predicted leading-edge temperature for the PVD coated blades was 1110° C (2030° F).

Test Evaluation

All HP turbine blades went through the full 1000 "C" cycles test. Appearance of the René 150, PVD coated blades after completion of the test was similar to the standard-production, René 80, Codep-coated blades in spite of the 56° C (100° F) hotter blade temperatures of the René 150 blades.

The 1000 "C" cycles CF6-50 engine tests simulate the blade life for the standard CF6-50 blades. The E^3 blade, 9000 hours between coating repair, is therefore attainable. Another factor that enhances obtaining the 9000 hours is that the maximum surface temperature for the E^3 Stage 1 blade is 1074° C (1965° F) versus 1110° C (2030° F) for the modified CF6-50 blade. The difference of 36° C (65° F) is significant in terms of coating life improvement in high-temperature operating range.

Based on the CF6-50 engine experience with the modified Stage 1 blade (René 150 coated with PVD) it is expected that the E^3 HP blade can be designed with 9000 hours of operation prior to recoating.

The coating specified for the ICLS engine is a single-layer, nickel-base coating applied by the PVD process. This process has been found to provide protection against oxidation. The FPS engine will have a two-component coating system: a nickel-base PVD coating (of a different chemical composition) followed by pack aluminiding. This two-component system provides slightly better oxidation resistance but requires two separate manufacturing operations.

The Stage 1 nozzle is assembled from vanes made of MA-754 material and from inner and outer bands made of MAR-M-509 material. The latter is a conventional, cobalt-base, casting alloy and has good strength to resist distortion at metal temperatures of about 1040° C (1900° F). MA-754 is an oxide-dispersion strengthened (ODS) alloy manufactured by a mechanical alloying process; the crystal structure is strongly textured. As a result, mechanical and physical properties vary considerably, depending on the orientation of the test specimens relative to the bar from which they were made. The textured structure is optimized in the spanwise direction to provide improved thermal-fatigue properties. MA-754 has excellent oxidation resistance; it can be used at temperatures above 1100° C (2000° F) without surface protection. The airfoils and bands are conveniently assembled by brazing.

The E^3 Stage 1 nozzle is a fabrication involving a brazed joint at the airfoil-to-band interface. The E^3 braze alloy and the airfoil material are

the same as that used on Stage 1 nozzles of other General Electric development and production engines. The integrity of these joints has been successfully demonstrated in endurance-type engine tests.

In existing General Electric engines containing Stage 1 nozzles processed as a fabricated design, local cracks after extensive testings seem to initiate from the trailing-edge "inner vane" and pressure-side regions. These cracks start at the airfoil-to-band interface, traverse across the braze joint, and continue along the band surface.

These nozzles continue to be used without any repair processing. Only if the inner-band flange support shows yielding (seen through physical axial flange distortion), or if cracks appear on this flange, is the nozzle retired due to this condition.

The Stage 1 shroud is a composite metal/ceramic part. The backing material is cast from René 77. A thermal-spraying process is used to apply the final coat of yttria-stabilized zirconia. Adherence of the coating to the backing is enhanced by a mechanical anchoring system. Because the ceramic coating is an excellent thermal insulator, the amount of air required to cool the shroud is significantly reduced compared to present shrouds.

The Stage 2 nozzle is assembled from airfoils made of DS René 150. The inner and outer bands are made from conventionally cast René 80. The latter alloy is used in a similar application in other engines. The crystral structure of the DS René 150 vanes is highly anisotropic, and this feature is utilized to minimize the effects of thermal fatigue on the nozzle. Individual airfoils are coated with a nickel-base, oxidation-resistant alloy using a physical vapor-deposition process. (The PVD process is described in greater detail in the section on blades.) After the nozzle components are assembled by brazing, the entire assembly is aluminided using a pack coating process. This combination of coatings can protect both vanes and bands for thousands of hours of service.

The Stage 2 shroud is solid René 77, and the configuration is similar to those used in the F101 and CF6-80 engines. A cobalt material base coating is applied by thermal spray to the René 77 backing.

Other components of the HPT are made from materials that have been proved in other engines. They are able to meet the temperature, load, and environmental requirements.

Fracture Mechanics Analysis - The LCF lives predicted for the various areas of the HPT spool in this report are based on conventional -3σ LCF data and indicate the rotor design life requirements have been met. Recent factory and flight-test experience, however, indicates that the minimum cyclic life of as-HIP René 95 PM components can be lower than that predicted by this method. Experience is showing that this material is sensitive to small internal and surface defects inherent in the conventional PM process. These defects act as crack initiations even in virgin material. The reduced cyclic life due

to these initiation points is more accurately predicted using fracture-mechanics techniques.

A fracture-mechanics analysis of the E^3 HPT rotor spool, based on an assumed defect size equivalent to the minimum detection limit of available nondestructive testing (NDT) methods, is now in process. Results of this analysis will be presented at a later date. Process modifications or material substitutions will be considered for the FPS spool configuration to ensure component integrity for the design cyclic life. A substitute material is not under consideration for the E^3 HPT rotor design for either the current or follow-on programs. PM René 95 and AF115 materials will continue to be used for any follow-on E^3 HPT disk designs. Work is currently underway to incorporate processing refinements which will result in improved powder cleanliness and increased low cycle fatigue capabilities. It is expected that the improved powder metal materials will have superior low cycle fatigue life/fracture mechanics characteristics for advanced turbine designs.

5.1.3 Analytical Methods

5.1.3.1 Computer Programs

Analysis of the HPT components was conducted using numerous computer programs developed by the General Electric Company. Table XVII lists the names of the various computer programs that were used in the analysis of the HPT mechanical design. The table also summarizes the mechanical characteristics which the programs analyze or calculate.

5.1.3.2 Procedures

Two of the programs listed in Table XVII were used extensively in the structural analysis of the HPT. The first, called CLASS-MASS, is a mathematical-shell analysis program. In using this program, the rotor structure is divided into shell elements. These shell elements can be cylindrical (shafts, etc.), conical (aft stub shaft), or vertical (disks, etc.). Axially symmetric or asymmetric external load can be applied. The second, called FINITE, calculates very localized stresses as around holes, disk posts, slots, fillets, disk bores, and other types of geometries where surface discontinuities exist.

Boundary conditions used for the FINITE model are the resulting loads or deflections from the CLASS-MASS program. Using FINITE analysis greatly enhances the true local stress field relative to using test data from photoelastic references. This is because, in the use of FINITE, there exists a radial and a circumferential stress gradient along the hole height (or radius). This gradient is due to speed effects, which vary with radius, and also due to the radial temperature variation.

Table XVII. Analytical Computer Methods.

Computer Program	Analysis
BUCKET CREEP	• Predicts Time-Dependent, Localized Values of Stress, Strain, and Creep Damage Due to Temperature and External Loads • Analysis Based on Beam Theory (Plain Sections Remain Plane)
CLASS-MASS	• Stress and Vibratory Solutions Due to Axisymmetric-Shell Structures - Thermal - Mechanical - Maneuver • Can Also Analyze Orthotropic Shell Structures • Centrifugal Recovery Effects • Vibratory Characteristics (Mode Shapes) and Harmonics • Calculates Stresses Due to Axisymmetric or Harmonic Loads
TWISTED BLADE	Calculates: • Natural Frequencies • Relative Vibratory Stress • Steady-State Stresses Due to: - Centrifugal - Axial and Tangential Bending - Shear - Induced Spanwise Stresses Due to Airfoil Untwisting Due to Speed
MULTI-HOOK	• Modified Heywood Stress Method - Radial Stress (P/A) - Tang Bend Stress (MC/I) - Tang Hook Stress • Relative Vibratory Stresses For Corner and Midchord of Dovetail • Stress Concentration - Notch P/A - Neck P/A - Bending

Table XVII. Analytical Computer Methods (Concluded).

Computer Program	Analysis
CYANIDE	• Elasto/Plastic Finite-Element Analysis • Constant Strain Plane-Stress, Plane-Strain, Axisymmetric Ring Elements • Included Speed and Thermal Loads • Creep and/or Large Displacement Analysis • Nonlinear Stress/Strain Curve • Orthotropic Material Properties For Elements in Elastic Range • Determines Plastic Zone • Postprocessing For Contour Plots (Isodisplacements, Stress, Total Effective Strain/Stress, Plastic Strain, Creep Strains)
FINITE	• Elastic Finite-Element Analysis • Constant-Strain, Quadrilateral, Finite Elements • Plane Stress, Plane Strain, Axisymmetric Analysis • Includes Speed and Thermal Loads • Orthotropic Material Properties and/or Elastic Material File Data (ESPEC Codes) • Calculates Stress, Strain, and Displacements
BOLFAN	• Calculates Required Cold Bolt Preload And Assembly Torque • Preload Requirements Based on Hot Operating Loads Including Torque Transmission Through Flange • Criteria: No Separation or Slipping • Axisymmetric Flange Loading • Linear Analysis • Bolt-Relaxation Analysis • Calculates Creep Relaxation of Bolt and Flange • Time Versus Load For Given Mission Mix (Time at Temperature) • Also Rupture Damage Versus Time

In order to determine the minimum life for any component, the local stresses and temperatures must be known. These conditions can only be determined by analyzing the turbine rotor at various flight-time increments. During these increments, the components are subjected to varying engine speeds, pressure loads, and temperatures. The rotor structure was analyzed starting from an idle condition, through a transient takeoff, into a max climb, and max cruise. Table XVIII summarizes the various flight times used for the analysis.

Table XVIII. Flight Times for Rotor Analysis.

Analysis At The Following Flight Condition	Time, sec
Ground Idle	500 (From Zero Speed)
Transient Takeoff (From Ground Idle)	10, 30, 40, 60, 125 Into Takeoff
End of Max Cruise	875 From Ground Idle
Max Cruise	1500
Max Cruise	1700
Max Cruise	2750
Flight Idle	3450
Thrust Reverse	4460

Figure 53 summarizes the various speeds and temperatures as a function of time. All the analyses were performed based on hot-day [50° C (121° F)] takeoff conditions and using the E^3 FPS growth cycle.

Evaluation of the stress/temperature distribution for the various flight times indicated that 40, 875, or 1700 seconds into takeoff resulted in the minimum life predicted for the rotor components. Temperatures and effective-stress distributions for these time-cycle conditions are shown in Figures 54 and 55, respectively.

CLASS-MASS analysis for the disk bore can only calculate hoop stress (radial stresses at bore are zero). There are, however, other types of stresses that must be included to determine the total bore stresses. These stresses are in the axial direction and are compressive; they are induced by:

1. A varying axial temperature and nonlinear temperature gradients.

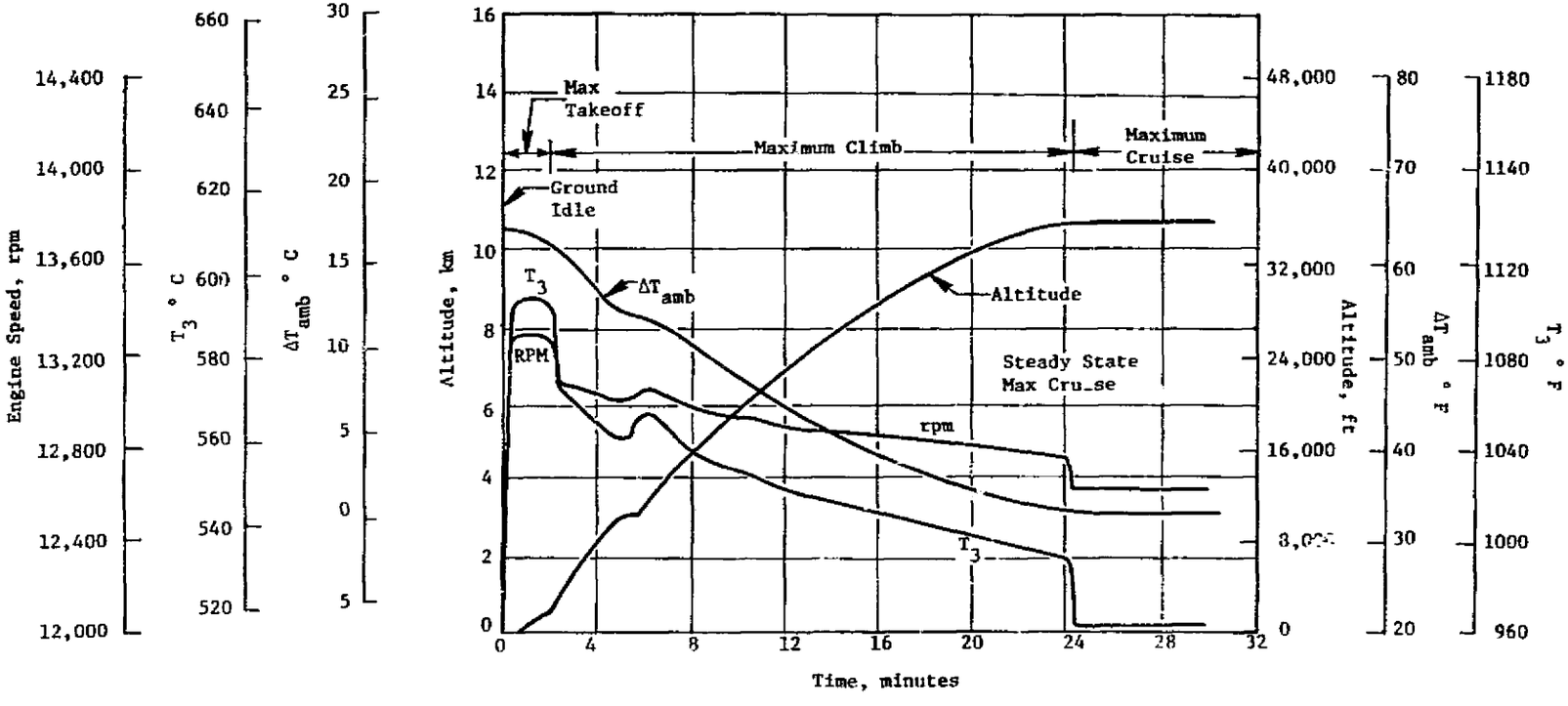

Figure 53. Takeoff/Climb/Cruise Transient Parameters.

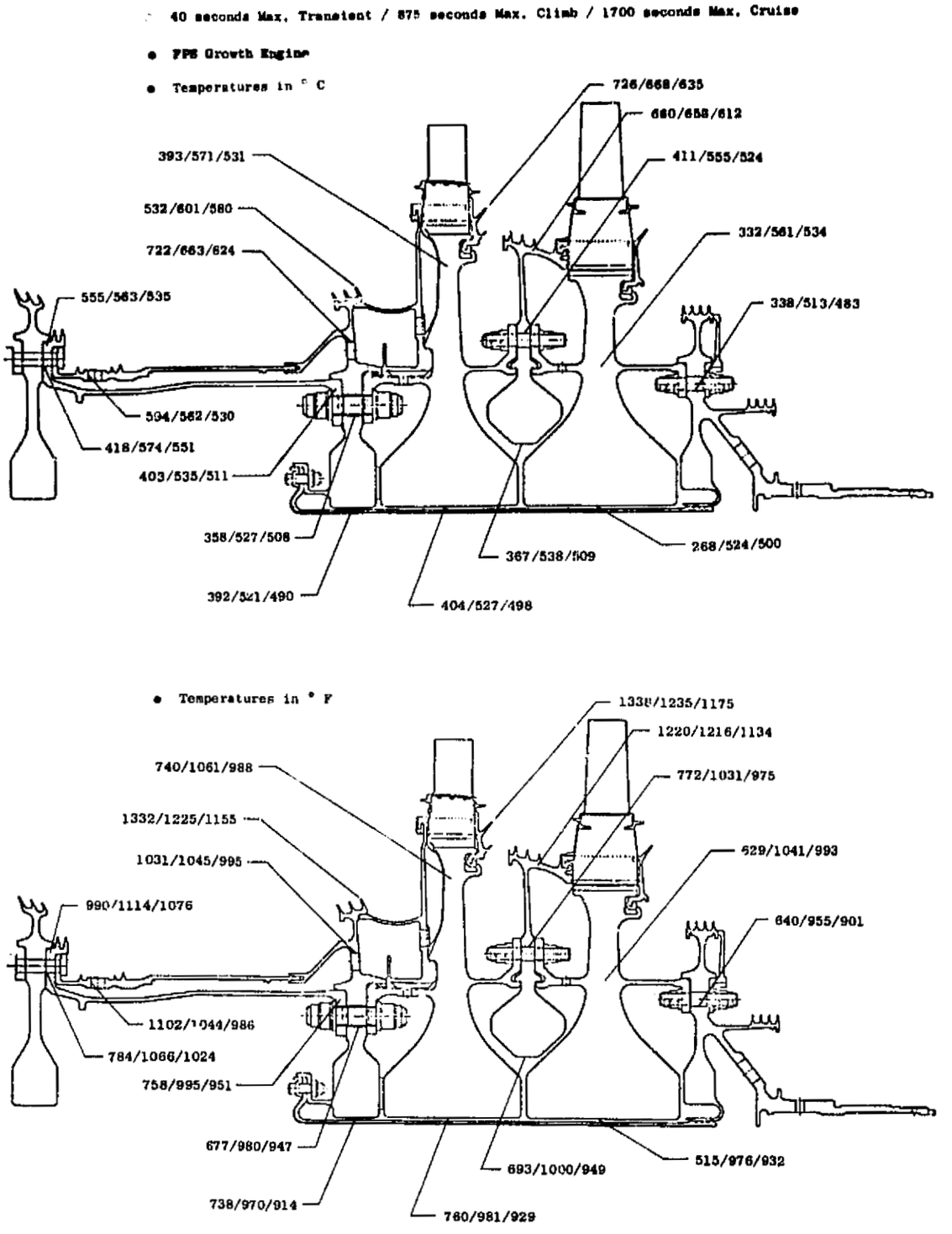

Figure 54. Rotor Temperature Distribution.

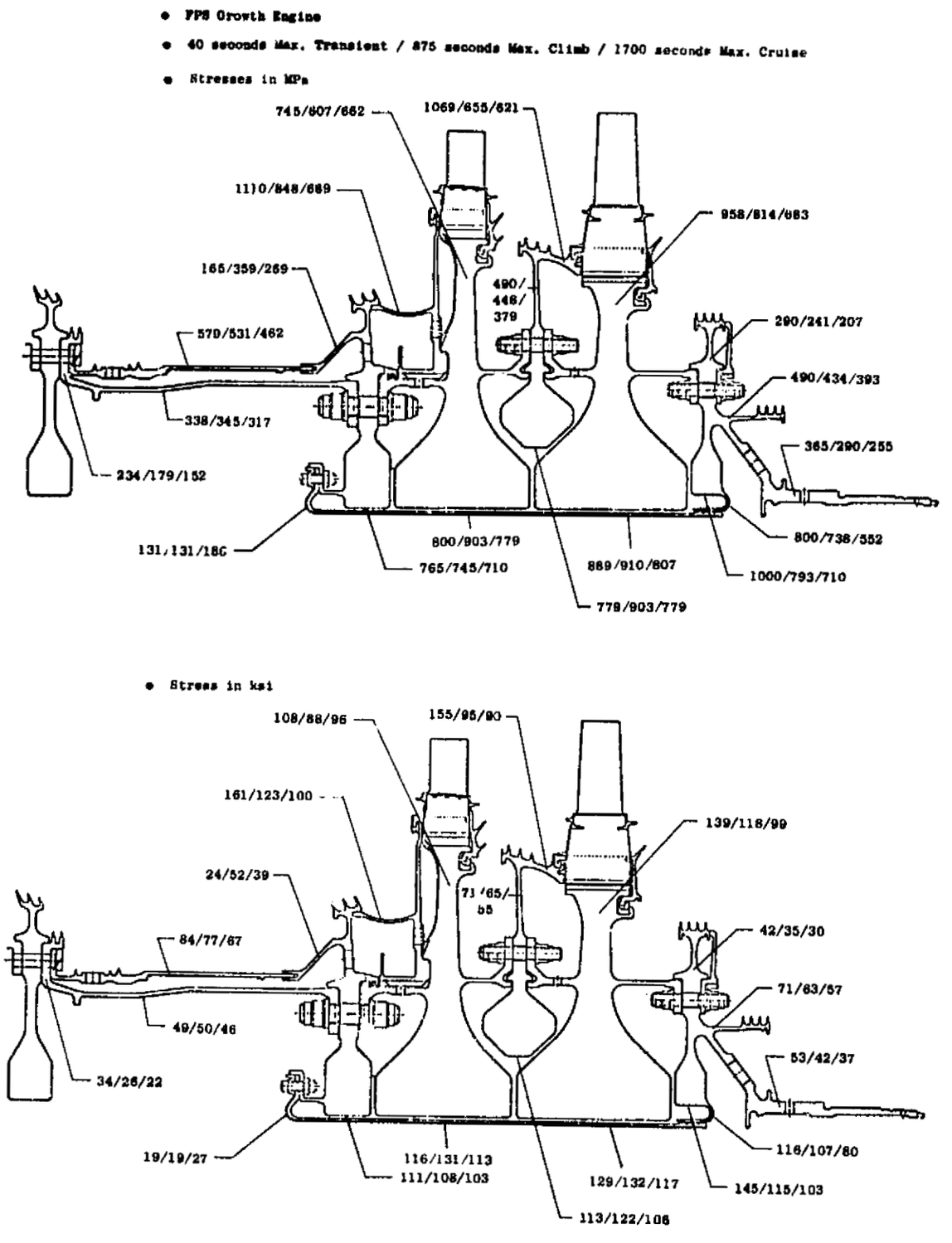

Figure 55. CLASS/MASS Effective Stress.

2. The bore width thickness resulting in a compressive stress at speed. The true bore stress distribution can only be analyzed by using a FINITE computer program.

Stress concentrations in the boltholes and air-slot passages were determined by using the FINITE computer program or by the appropriate stress-concentration factors from Peterson. The finite-element analysis was accomplished by using constant-strain, quadrilateral elements. Due to symmetry of boltholes, the analysis and results can be accomplished by modeling only one-half of the geometry. Using one-half of the symmetrical model requires an appropriate boundary condition along the radial line of symmetry. In addition, the tangential deflection normal to the radial line is restrained. Boundary conditions (displacements) are also applied at the inner and outer radii of the model. These displacements were determined from the CLASS-MASS analysis. The CLASS-MASS model for shell members in the vicinity of holes was modified to account for a reduction in bending stiffness and for simulation as an orthotropic shell. The load of the bolt due to centrifugal forces was applied at specific nodes surrounding the hole. Thermal gradients were considered by applying the appropriate temperatures at the nodes. The critical flight time that would establish the LCF life was determined from the various CLASS-MASS analyses for various time steps.

5.1.4 Design Criteria

The HP turbine was designed to meet the objective life goals defined for the FPS engine. The mechanical analytical methods and procedures follow the General Electric Design Practice.

The designs for the components are based on life predictions by using material test data curves. These curves define the stress at temperature versus life (cycles or hours).

Among the more important factors affecting the life of a component are:

- Stress rupture
- Creep
- Yield
- Low Cycle Fatigue (LCF)
- High Cycle Fatigue (HCF)
- Fracture Mechanics.

Stress Rupture - Stress rupture in materials is a form of failure mode which occurs under the influence of time exposure under a stress and temperature condition. Material test data is used to predict rupture life based on calculated stresses and temperatures.

Creep - Materials subjected to stresses at temperature for prolonged periods of time exhibit some form of deformation. Creep is considered an important criteria, especially for rotating structures. In the turbine design, the total amount of creep is limited to 0.2%.

Low Cycle Fatigue - Structures subjected to repeated loads or thermal stress effects exhibit fatigue failure. This type of failure occurs at a stress level lower than a single stress level application.

The failure originates when a very localized crack is initiated in a material and then propogates until material separation occurs.

Low cycle fatigue is a fatigue failure normally considered to be less than 10^5 cycles. The level of stress at temperature is used to predict the LCF based on material test data. Thermally induced stresses also affect the parts life.

When geometric discontinuities exist in a part, such as boltholes, the stress concentration effects around the holes must be considered. Life predictions therefore include the stress concentration factors.

High Cycle Fatigue - High cycle fatigue is a similar mode of failure to an LCF, except that the number of cycles to failure should exceed 10^7 cycles. HCF failure mode is a function of stress at a temperature level. Stress concentration factors also have a high influence on material life. Therefore, careful attention is always provided to include analysis where stress concentration factors are present.

This is especially the case for blades and blade/disk dovetails. The varying gas load on the blade as it passes through the nozzle gas flow is characterized by a pulsating pressure. This varying gas pressure induces a vibratory stress on every blade. The blade vibratory stress levels when combined with the mechanical stresses (centrifugal, gas bending, and thermal) must meet the requirements for blade life.

Fracture Mechanics - Current GE powder metal alloys used in high-temperature rotor structures exhibit low cycle fatigue strength characteristics which are lower than standard or conventional material forgings. This problem is primarily due to the presence of undetectable surface or subsurface defects. The failure mode characteristics can be predicted by fracture mechanics methods of analysis and must be accounted for in the life analysis of current designs.

Specific improvement programs are in process at GE to define improved materials processing to minimize the impact of small defects on fracture mechanics lives and to improve the cleanliness of the powder for future engine part design, including E^3 HPT follow-on.

5.2 DETAILED MECHANICAL DESIGN

5.2.1 Rotor Components: Stress, Stress Concentration, LCF Life

Figure 56 shows the major components of the HPT rotor assembly. The stress concentrations and LCF life of the turbine rotor components were determined by employing the computer programs, mentioned earlier, to evaluate the effects of load, temperature, and speed.

5.2.1.1 Forward HP Shaft and Outer Liner

The forward portion of the HP shaft, shown in Figure 57, contains two seal teeth slightly overhung from the forward flange. In order to determine the effect of this overhang, specifically around the fillet, a finite-element analysis was made. A maximum stress of 958 MPa (139 ksi) occurs at the forward face of the flange, at 40 seconds into acceleration, resulting in a minimum calculated LCF life of 11,000 cycles for Inco 718.

The maximum concentrated stress in the forward shaft is 931 MPa (135 ksi) at the aft-flange bolt circle. The predicted 3σ LCF life is 14,000 cycles for standard Inco 718 as planned for use in the ICLS engine.

A material change to Super Inco 718 is planned for the FPS. Super Inco 718 is presently used in CF6-50 turbine components; it improves LCF life by means of better grain-size control. The use of Super Inco 718 will assure an LCF life of 36,000 cycles for the forward shaft.

The material for the outer liner is René 95. The maximum-stress location is at the cooling-air holes. The maximum stress is 951 MPa (138 ksi) at 40 seconds into the accel. The calculated LCF life is greater than 36,000 cycles.

5.2.1.2 Inducer Disk

The inducer disk material is AF115. Analysis of the disk design led to the choice of a "race track" shaped bolthole as shown in Figure 58. This shape was chosen for the following reasons:

- Lower hoop stresses with stress concentration relative to a circular hole. Radial stresses with stress concentration are lower than the hoop stresses.
- The "race track" hole prevents bolt stud rotation at assembly. The bolt stud has a similar race track collar and fits within the inducer disk hole. When the assembly torque is induced in the bolt, the disk race track provides the reaction; thus the bolt is not allowed to turn.

The inducer disk stresses and predicted LCF lives for the various critical locations are summarized in Figure 58. At all locations, the disk meets the objective of 36,000 cycles.

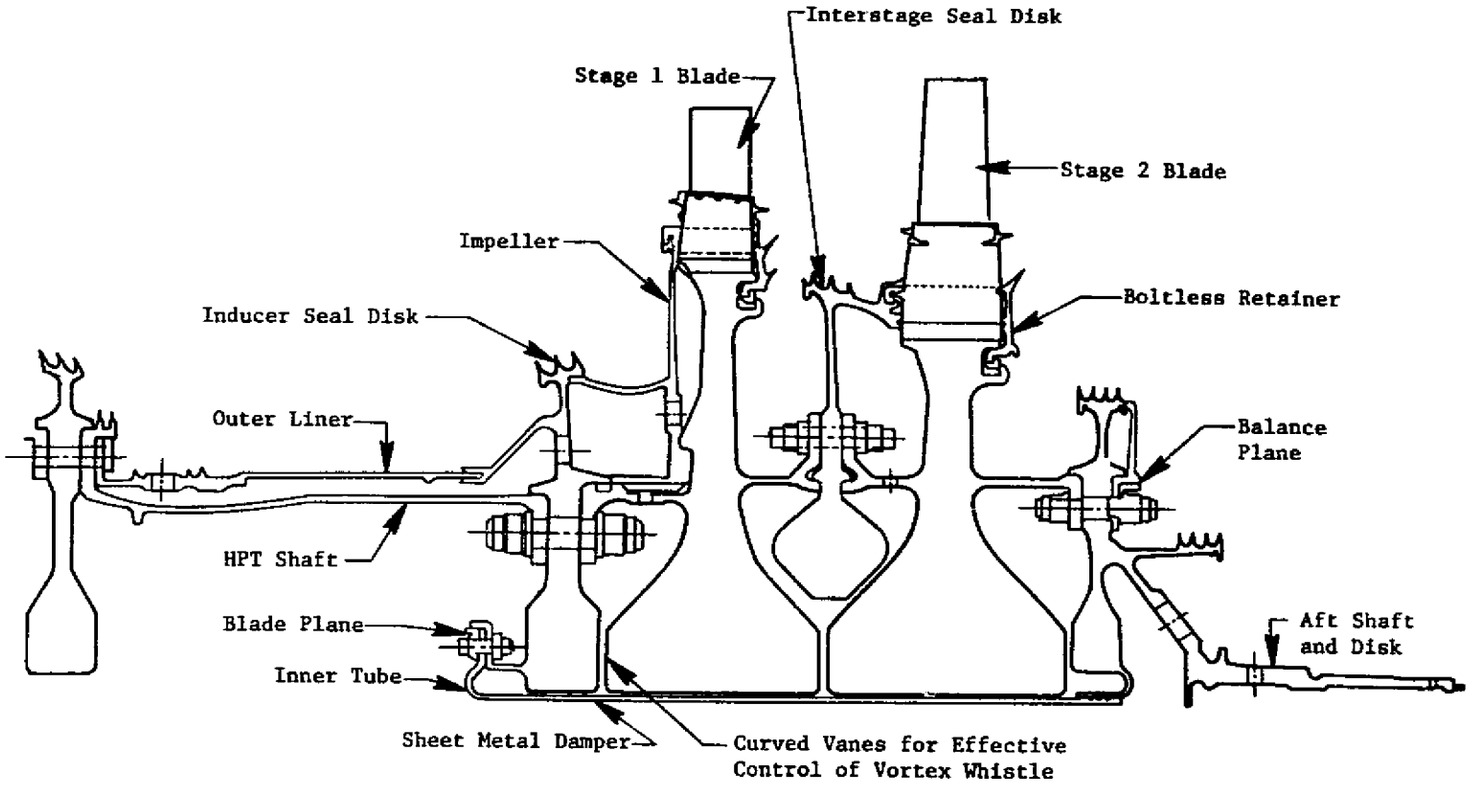

Figure 56. E^3 High Pressure Turbine.

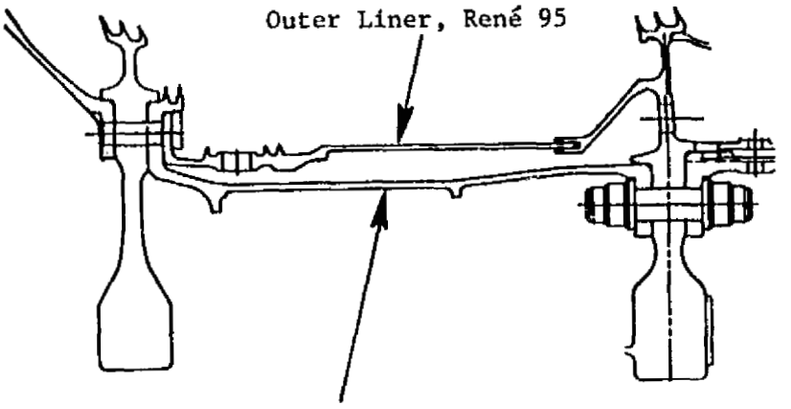

Figure 57. Forward Shaft and Outer Liner.

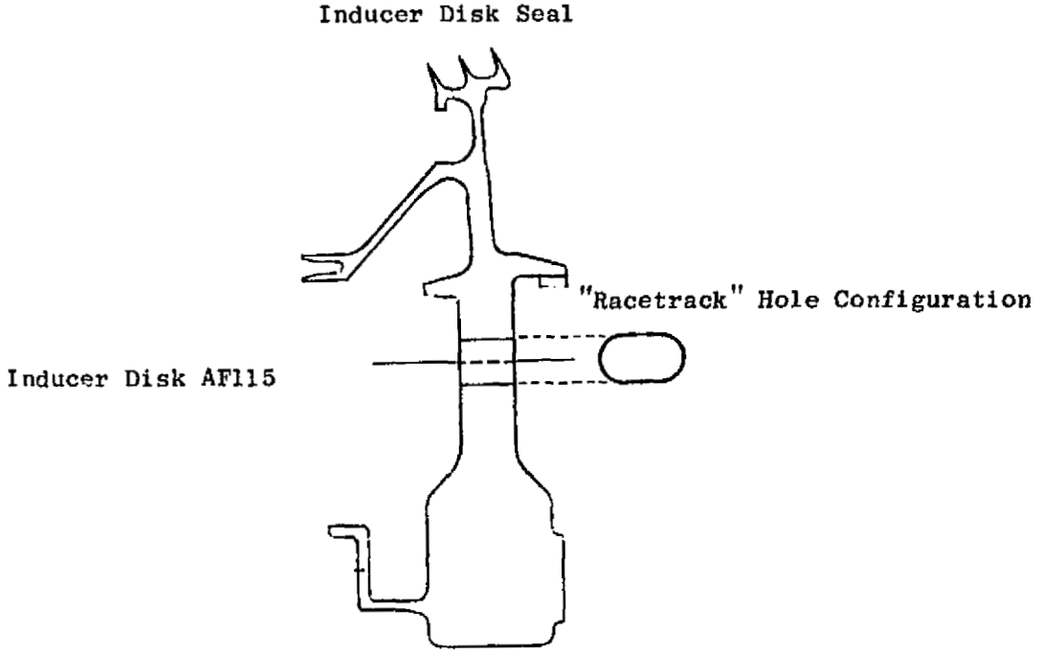

Figure 58. Inducer Disk.

5.2.1.3 Impeller And Stage 1 Retention System

After the 76 Stage 1 blades are assembled from the front of the disk, the 76 seal plates are individually inserted into each dovetail slot engaging the upper tang of the disk. The seal plate functions to minimize purge air in the cavity formed between the front of the disk and Stage 1 inner nozzle support from entering the space between blade shanks. The compressor-discharge air used to purge the cavity and the inner flowpath between Blade 1 and Nozzle 1 is intended to exit into the flowpath at this location.

In addition to coolant-air pumping, the impeller provides axial blade retention and a support for the blade wire seal. The wire seal is used to minimize leakage of blade-coolant air, thereby increasing turbine performance.

The "U" clip functions to axially retain the seal plates and also as a windage cover for the disk post extension. The "U" clip contains one sawcut to allow for assembly. The 360° retaining ring is snapped in place after the "U" clip has been assembled.

The impeller material is AF115. Due to the presence of the radial vanes along the impeller web and the serrations in the horizontal impeller-support arm, the impeller analysis required a more detailed and different type of modeling using the CLASS-MASS analysis. The impeller model is shown in Figure 59. The radial vanes and serrations were simulated by shells (shown shaded) without hoop-carrying capability. The proper weight was simulated by changing the density based on an equivalent shell thickness. The shell thickness simulating the vanes was based on an equivalent shell bending stiffness. The resulting loads from the CLASS-MASS analysis were used to determine the actual vane stress.

Maximum stresses for the impeller, determined from the CLASS-MASS analysis, occur at 40 seconds into the takeoff. These stresses are shown in Figure 60. Stress concentrations occur at the 38 "race track" holes that allow the passage of the expander air, used to cool the Stage 1 blades, and at the interface between the disk web and the impeller vanes. Neither of the areas affect the expected 36,000 cycles LCF life of the impeller.

5.2.1.4 Stage 1 Disk

The Stage 1 disk, shown in Figure 61, is manufactured from René 95 material. The disk is composed of two distinct stress/load-carrying structures. The first consists of the 76 disk posts and dovetail slots at the outer diameter of the disk; these carry the load from the blades (gas bending and centrifugal loads). The second consists of the main body of the disk, or the live disk, and carries all the loads mentioned above and internal forces induced by temperature, axial pressure, and speed effects. In addition, the disk web rabbet, located in the forward face and above the forward cam, radially supports the impeller.

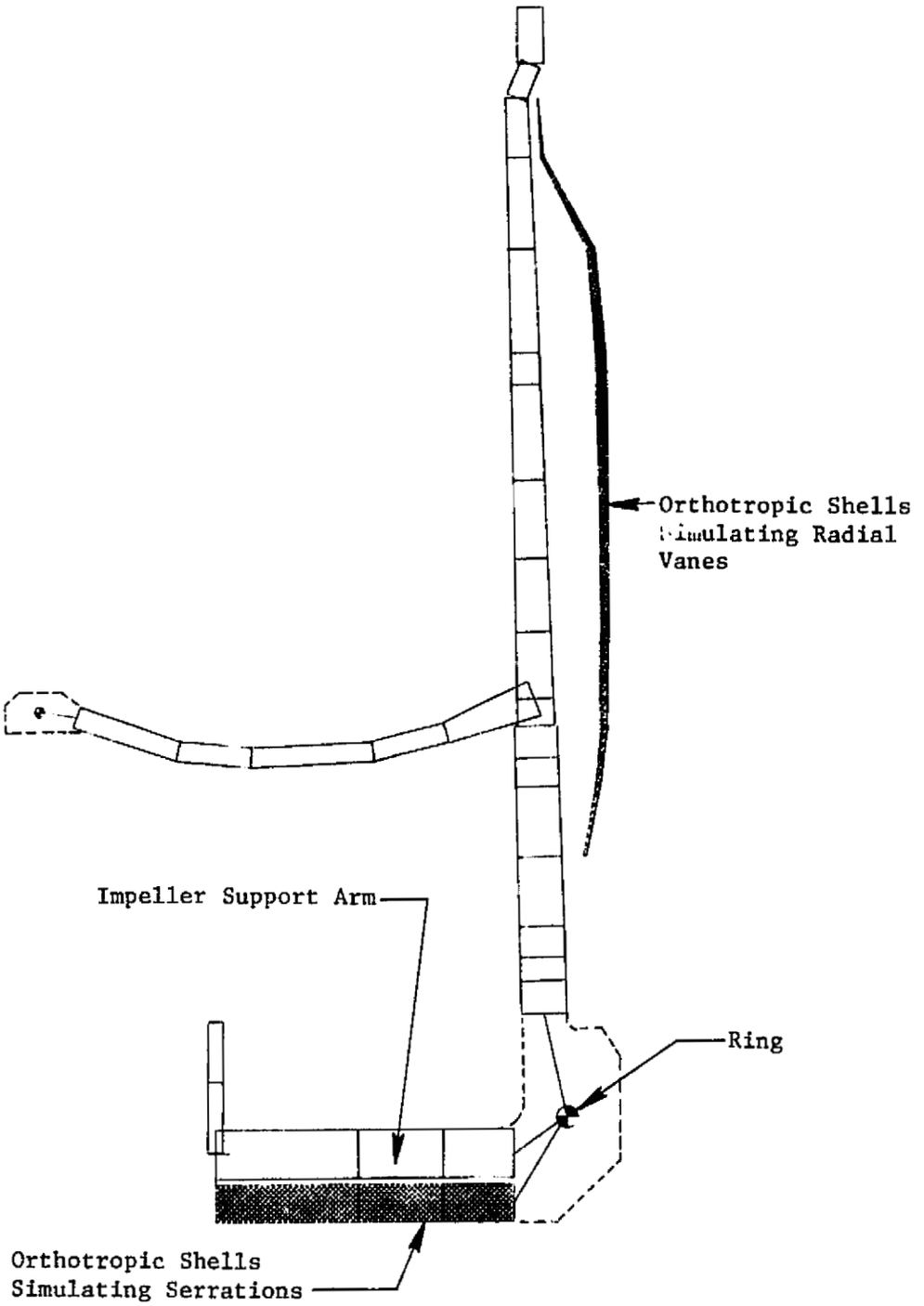

Figure 59. CLASS/MASS Impeller Model.

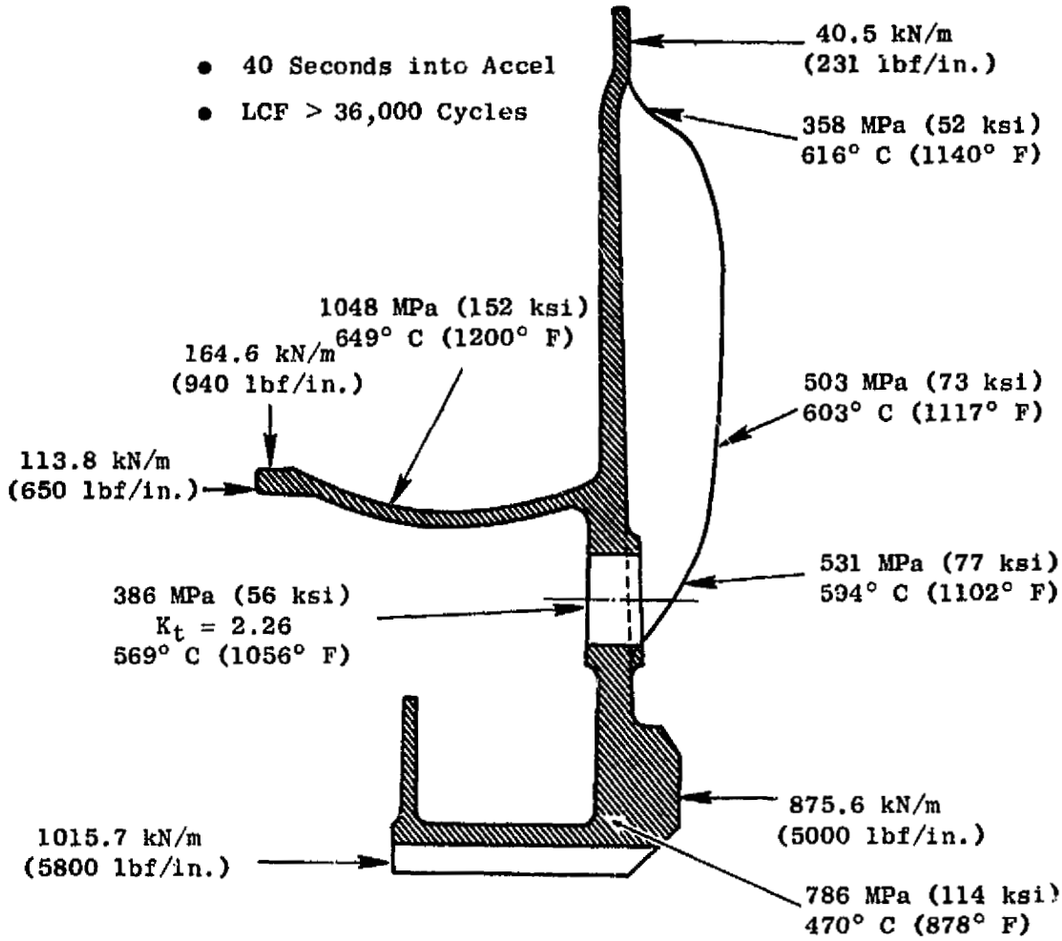

Figure 60. Impeller Loads, Effective Stresses, and Temperatures.

- René 95 Material

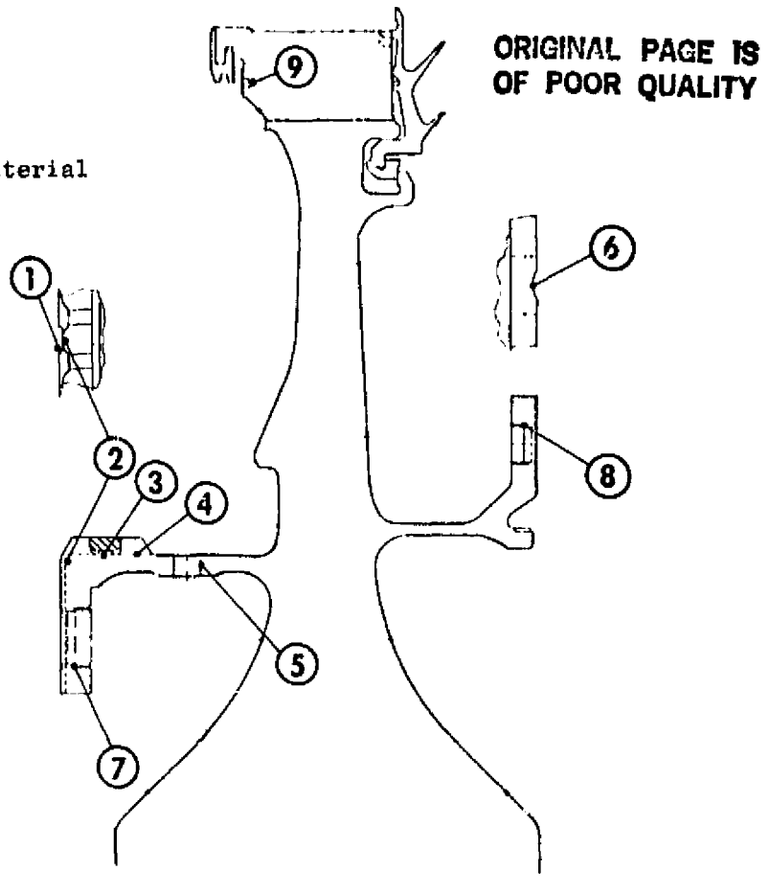

Location	Nominal Stress		$K_t\sigma$		Critical Time	Temperature		LCF Life
	MPa	ksi	MPa	ksi	sec	°C	° F	kilocycles
1. Forward Arm Air-Passage Slot	448	65	841	122	875	541	1006	>100
2. Forward Arm Flange Air-Passage Slot and Scallop	269	39	731	106	40	427	800	>100
3. Forward Arm Ring Container	331	48	945	137	40	458	857	>100
4. Forward Arm Scallop	393	57	565	82	875	545	1013	>100
5. Forward Arm Air Hole	455	66	1103	160	875	544	1012	36
6. Aft Arm Air-Passage Slot	400	58	469	68	875	553	1027	>100
7. Forward Arm Bolt Hole	421	61	938	136	875	541	1006	>100
8. Aft Arm Bolt Hole	434	63	931	135	875	552	1025	>100
9. Disk Post Notch	276	40	827	120	40	527	980	>100

Figure 61. Stage 1 Disk Stress Concentration and LCF Life.

The Stage 1 disk posts and dovetail slots are a two-tang, axial design. Two types of analysis were used to determine the maximum stress and resulting LCF life. MULTI-HOOK analysis was used to determine the preliminary dovetail form. Once this was established, a FINITE analysis was used to determine the localized stresses along the surface of the dovetail and to optimize the dovetail geometry. Figure 62 defines the resultant stress distribution and maximum-stress location.

The effects of temperatures, loads, and pressures on various locations of the disk during engine operation are determined by analyzing the component at various flight times based on the flight cycle. This transient analysis method is used to determine the maximum stresses and life-limiting locations on the disk. The disk temperature distribution was determined first. From the preliminary design, it was determined that the structural components of the rotor were subjected to a maximum combination of stresses and/or temperatures at 40, 875, and 1700 seconds into the flight, measured from a throttle burst from idle. The 40-second point occurs during takeoff; the 875 and 1700-second points occur during maximum climb and maximum cruise.

The finite-element model for the Stage 1 disk is shown in Figure 63. Specific disk locations where the boundary conditions were applied are also shown. Boundary conditions for the finite-element analysis were taken from the CLASS-MASS analyses at various flight times. Effective stresses and corresponding LCF life for the 40-second case are shown in Figure 64.

Figure 61 shows nine points on the Stage 1 disk where stress concentrations were calculated and LCF life determined. LCF life for all nine locations exceeds 36,000 cycles.

5.2.1.5 Interstage Seal Disk

The interstage disk material is AF115. Figure 65 shows the temperatures, stresses, and LCF lives for various areas on the disk. The disk meets the design objective of 36,000 cycles.

5.2.1.6 Stage 1 and 2 Blade Retainers

The Stage 1 and 2 blade boltless retainer is a design concept whereby no bolts are used to restrain the axial movement of the part. Eliminating the bolts and the through holes to fasten the retainer to the disk improves the LCF life capabilities due to the absence of any stress concentration factors associated with boltholes.

The retention feature is accomplished by a split lock ring which is mounted between the blade retainer and disk web "ear" (Figure 66). Axial blade loads are transmitted to the outer end of the retainer. Reaction loads within the retainer occur at the retainer ring and disk web ear. The retainer is radially supported by the rabbet interface with the disk post.

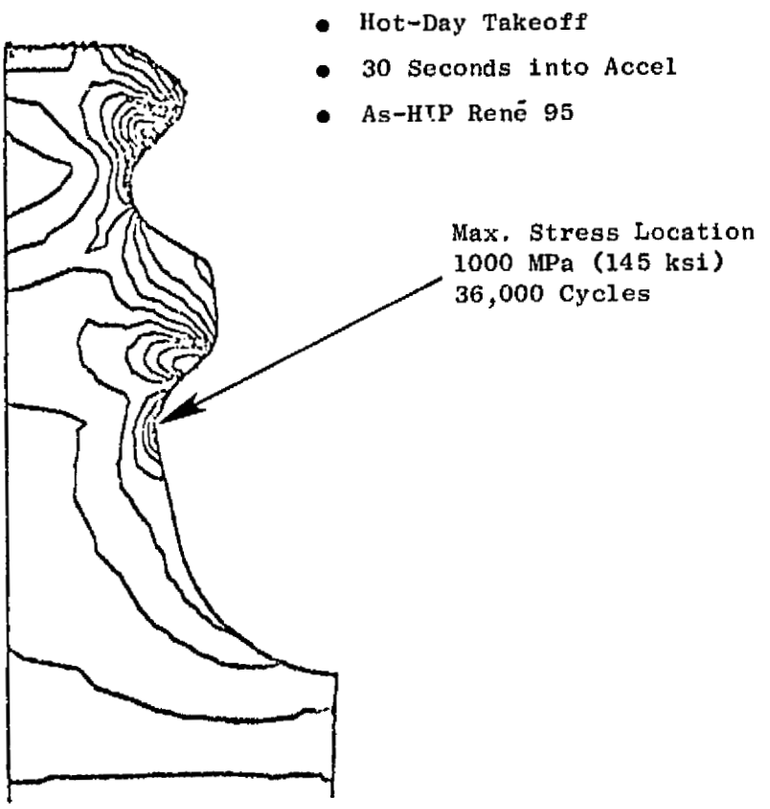

Figure 62. Stage 1 Disk Dovetail Elastic/Plastic (FINITE) Stress Analysis.

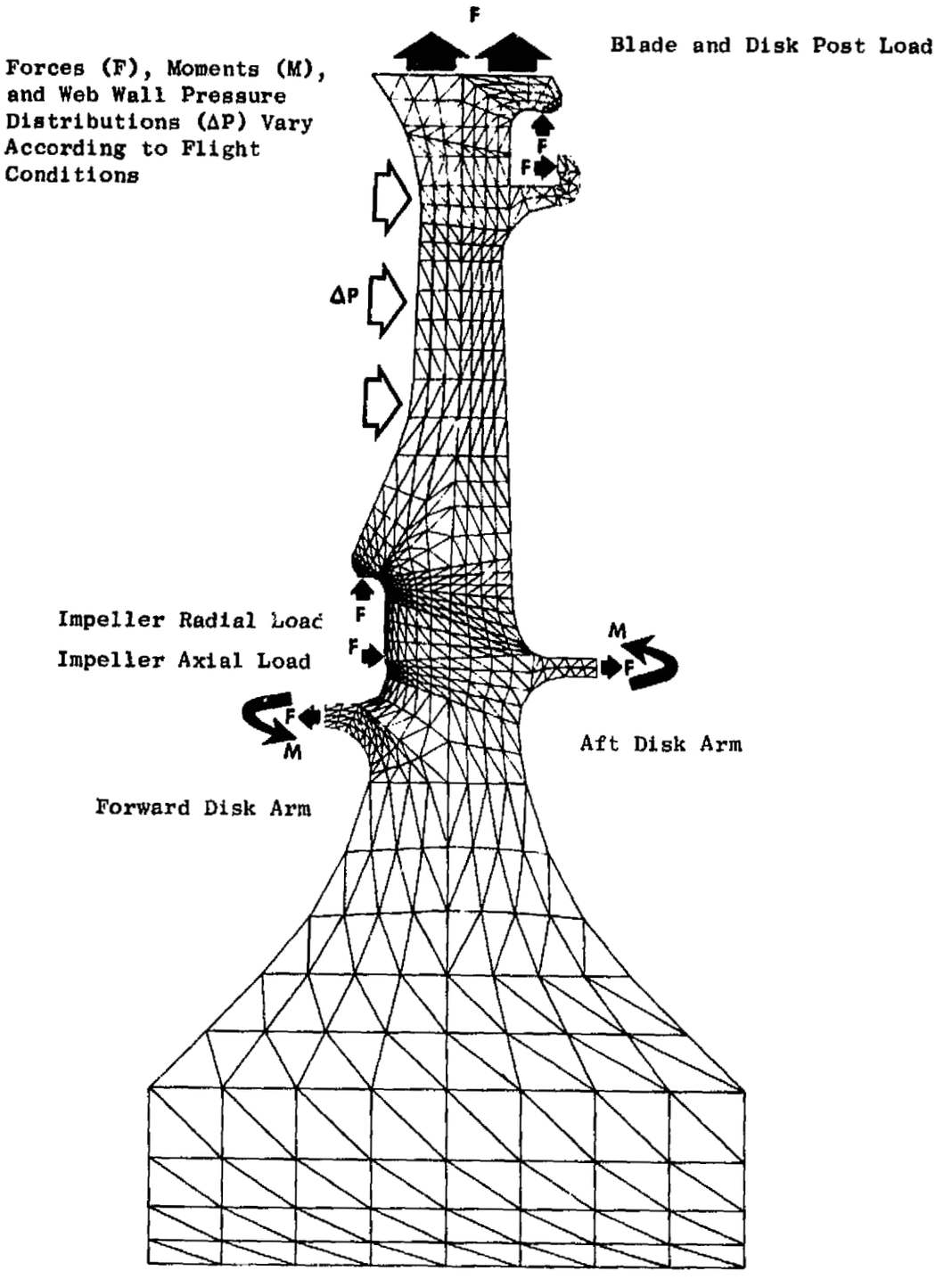

Figure 63. Stage 1 Disk Finite-Element Model.

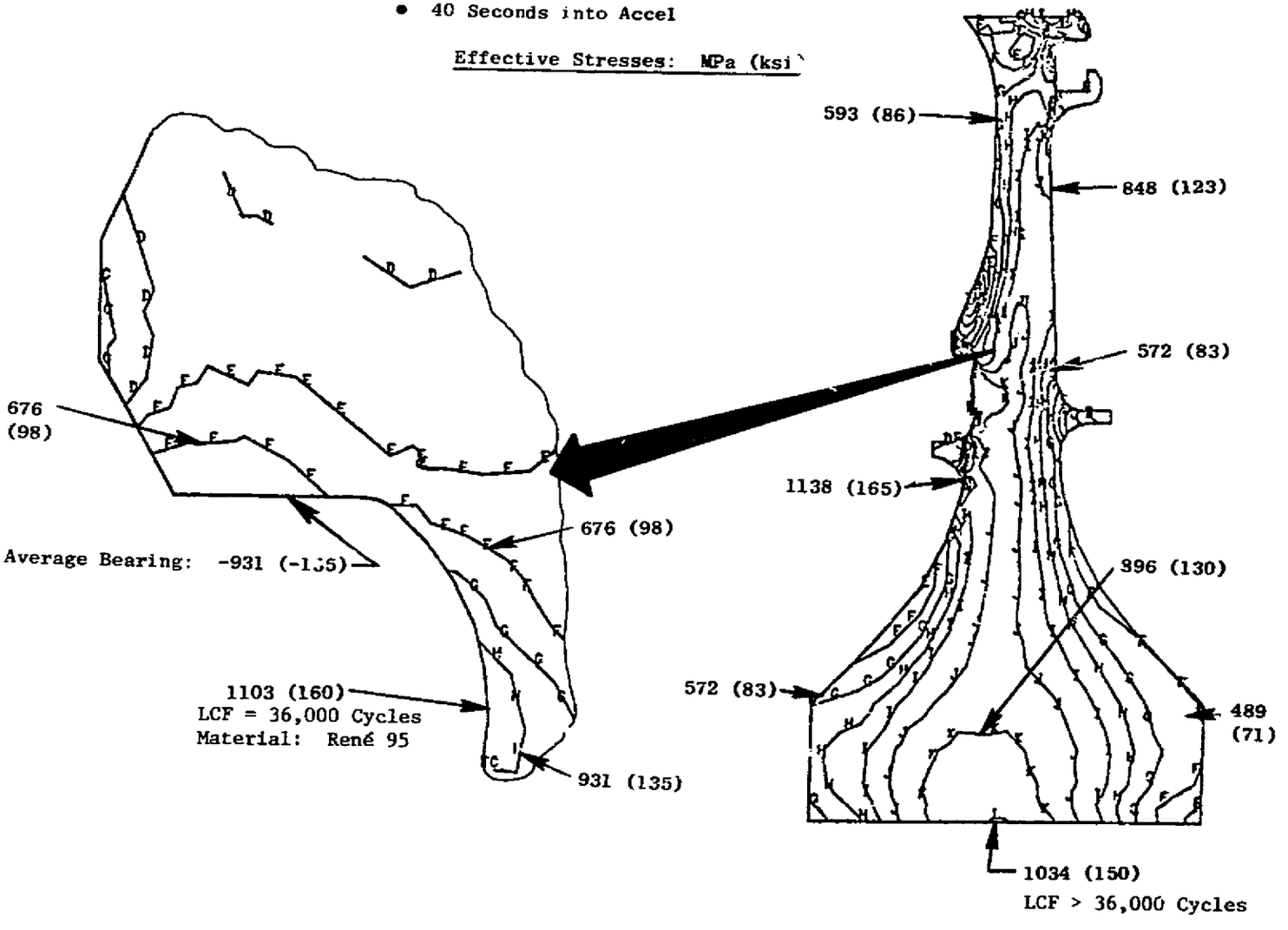

Figure 64. Stage 1 Disk Stress/Life.

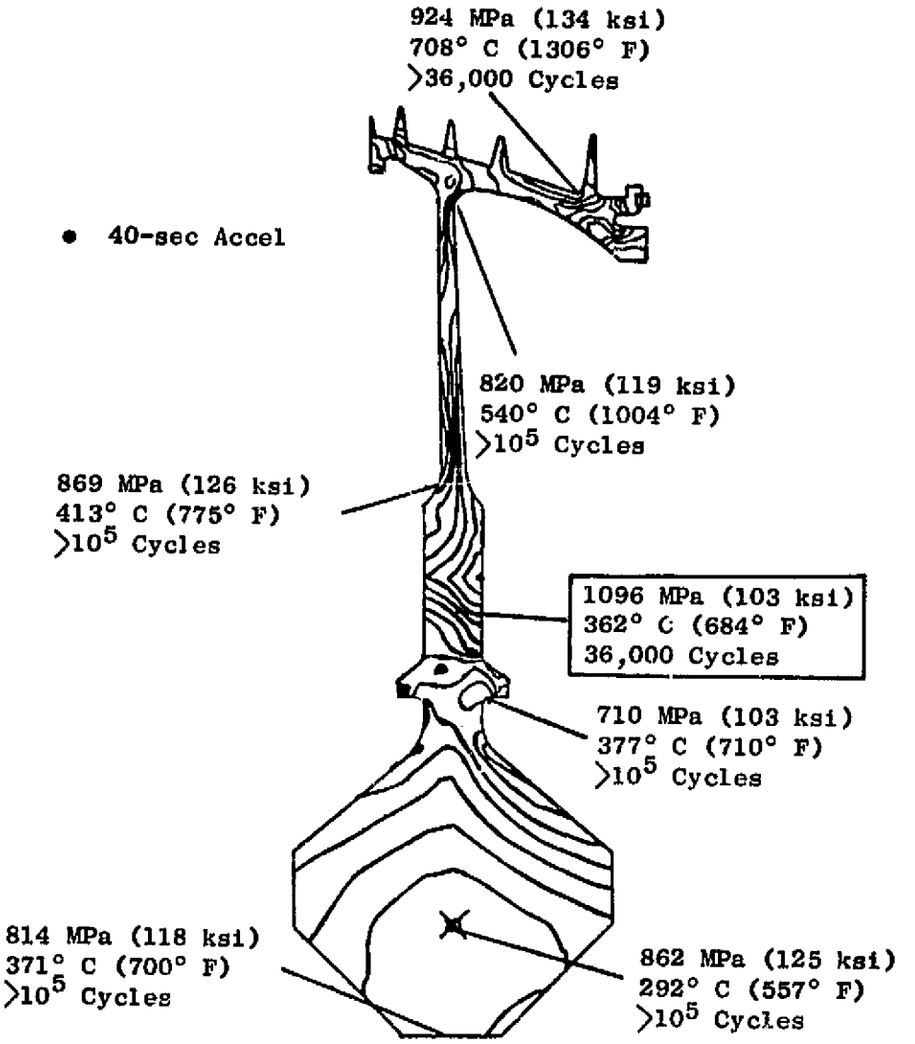

Figure 65. Interstage Seal Disk Finite Effective Stress Distribution, Temperature, and LCF Life.

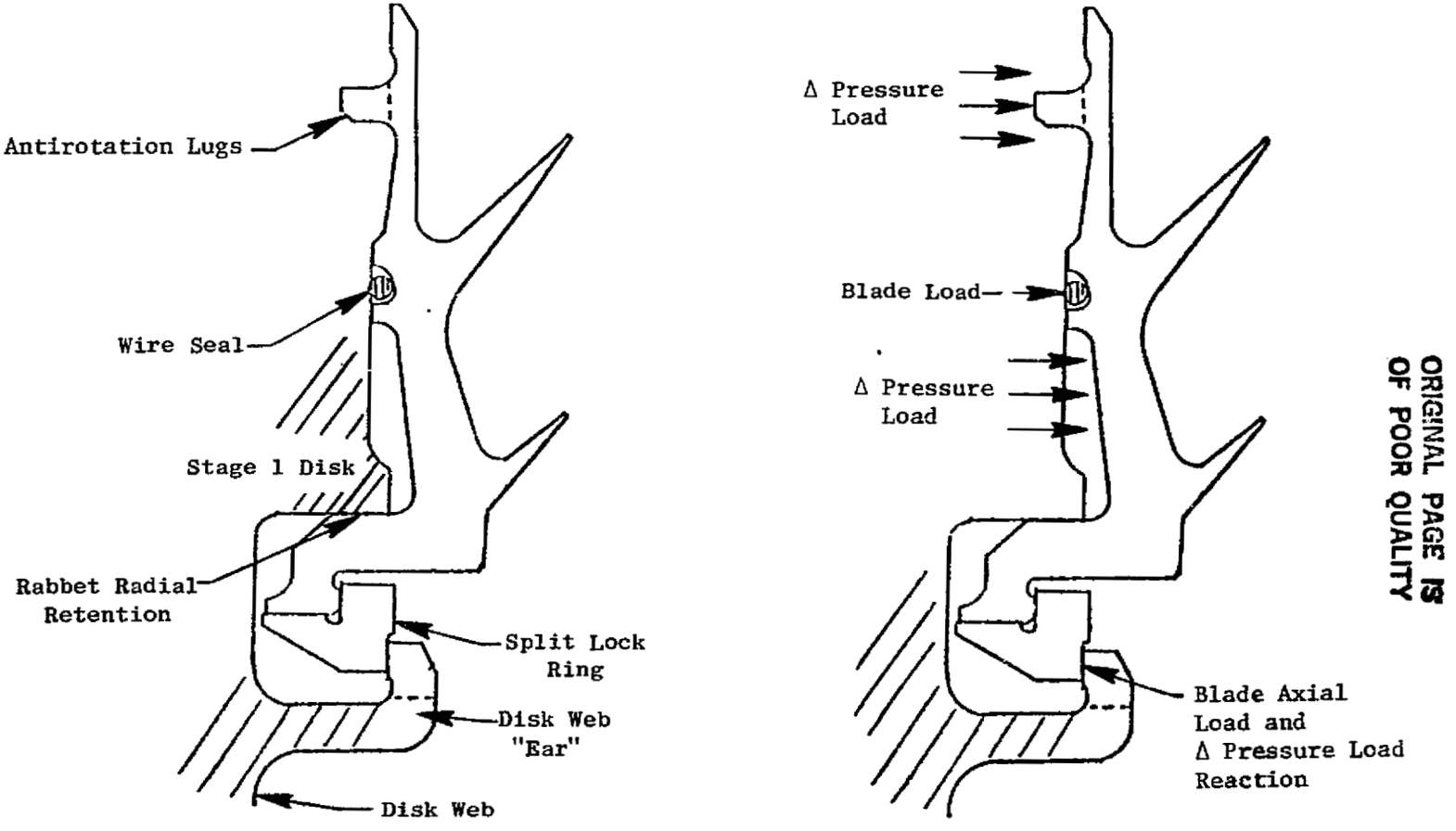

Figure 66. HP Turbine Boltless Retainer Design Features.

Both retainers were analyzed using FINITE elements. The boundary conditions and FINITE model were based on the CLASS/MASS analysis at the time 40 seconds into the takeoff. The resulting stresses and temperatures for this condition are shown in Figures 67 and 68 for the Stage 1 and 2 retainers, respectively.

5.2.1.7 Stage 2 Disk

The Stage 2 disk is manufactured from René 95. The stress and fatigue-life analysis for the Stage 2 disk, shown in Figure 69, is similar to the analysis of the Stage 1 disk. The disk post FINITE model and resulting stresses are shown in Figure 70. The stresses are based on maximum blade loads for the hot-day takeoff conditions.

The live disk portion was analyzed using the CYANIDE computer program. Locations on the disk where external loads are applied (boundary conditions) were taken from the CLASS-MASS analysis. The combined effects of temperature and loads at the 40-second case resulted in the stress distribution shown in Figure 71.

Stress-concentration factors were determined for 10 disk locations. Seven of the more critical locations are shown in Figure 69. A review of the figure indicates that the maximum combined stress at nearly all locations occurs 875 seconds after takeoff (this time element is at the maximum climb condition). Scallops have been added in the disk aft flange to reduce the effective stress concentration (hoop direction), thereby reducing the total stress. Calculated -3σ LCF life for all locations is greater than 36,000 cycles.

5.2.1.8 Aft Shaft/Seal Disk

The aft shaft was also analyzed using the FINITE computer program with boundary conditions taken from CLASS-MASS. Figure 72 shows the resulting shaft stresses for 40 seconds into the hot-day takeoff. The stress of 807 MPa (116 ksi) results in LCF life of 20,000 cycles using Inco 718 material (3σ properties). To achieve the life goal requirements for the FPS engine, an improved Inco 718 (Super Inco 718) would be required. The present Inco 718 material LCF life is limited to 20,000 cycles. Using Super Inco 718 for the flight propulsion system, the LCF life will exceed the objective of greater than 36,000 LCF cycles. For the ICLS and core engine, the material released to manufacturing is standard Inco 718.

5.2.1.9 Stage 1 Blade

The Stage 1 blade is an air-cooled design using cast, DS René 150 material. The major features and cooling circuits are shown in Figure 73. The blade rupture-life predictions are based on the 2-hour design mission shown in Table XIX.

In order to conduct a realistic mission-mix analysis, cycle data were utilized for various ambient conditions. Cycle data used were speed, coolant and gas temperatures, and gas loads. Analytical investigation to determine the blade rupture life indicated that three flight points in the mission,

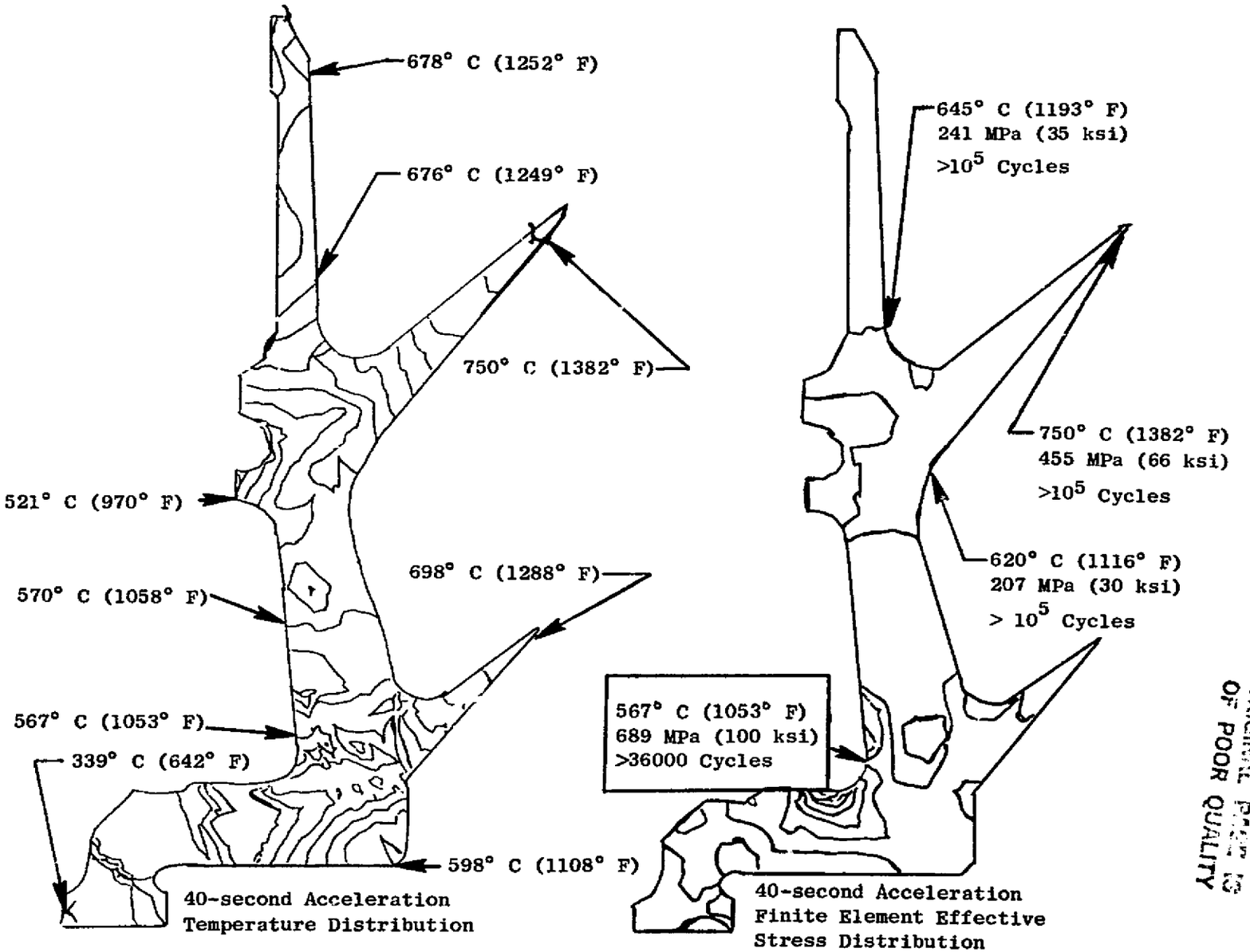

Figure 67. Stage 1 Aft Blade Retainer Temperature and Stress Profile.

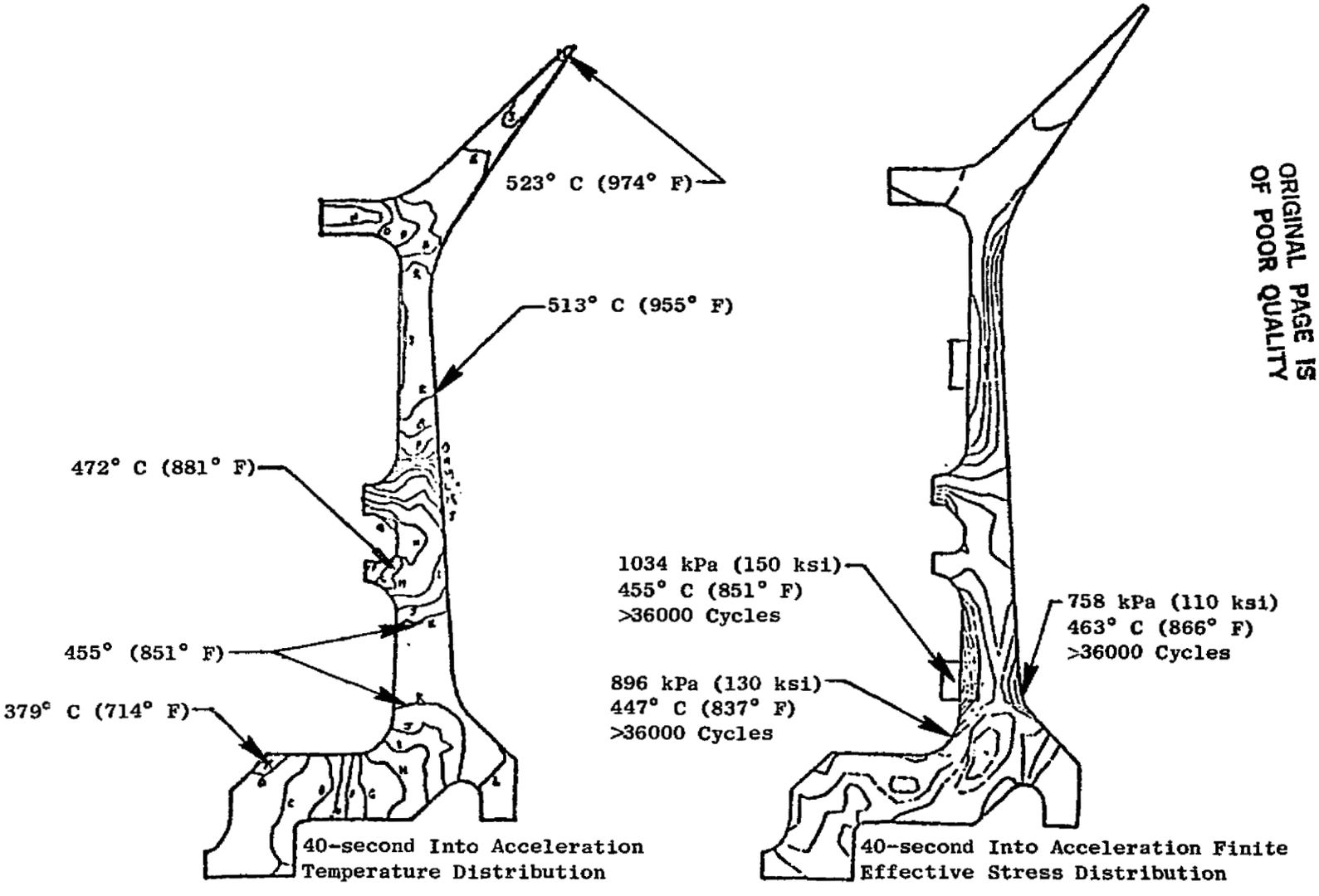

Figure 68. Stage 2 Aft Blade Retainer Temperature and Stress Profile.

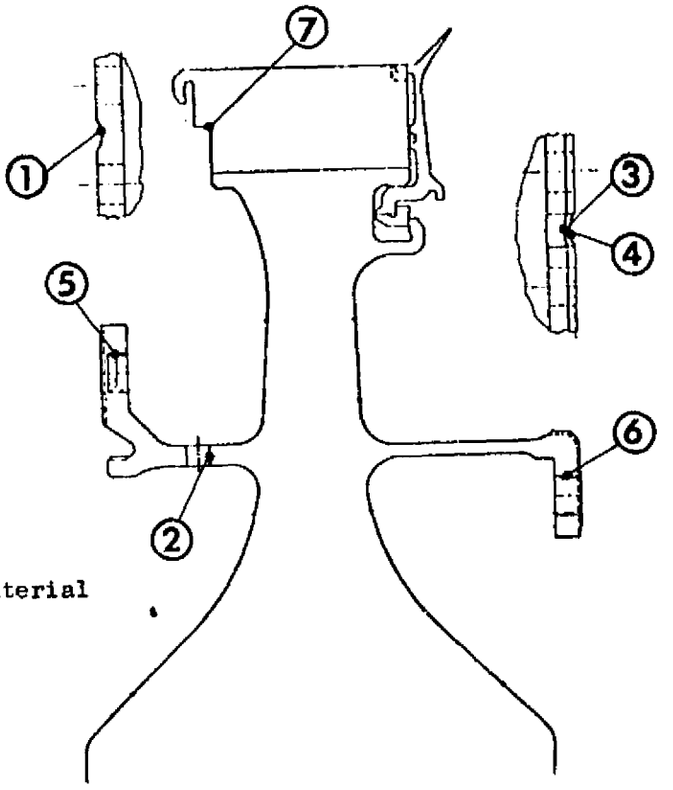

- René 95 Material

Location	Nominal Stress		$K_t\sigma$		Critical Time	Temperature		LCF Life
	MPa	ksi	MPa	ksi	sec	° C	° F	kilocycles
1. Forward Arm Flange Air-Passage Slot	407	59	476	69	875	552	1025	>100
2. Forward Arm Air Hole	427	62	1082	157	875	551	1023	45
3. Aft Arm Flange Double Slot	441	64	731	106	875	513	955	>100
4. Aft Arm Flange Air Slot	648	94	752	109	875	518	965	>100
5. Forward Arm Flange Bolt Hole	427	62	931	135	875	552	1025	>100
6. Aft Arm Flange Bolt Hole	455	66	993	144	875	517	963	>60
7. Disk Post Notch	234	34	703	102	40	338	640	>100

Figure 69. Stage 2 Disk Stress Concentration and LCF Life.

Lines of Constant Stress

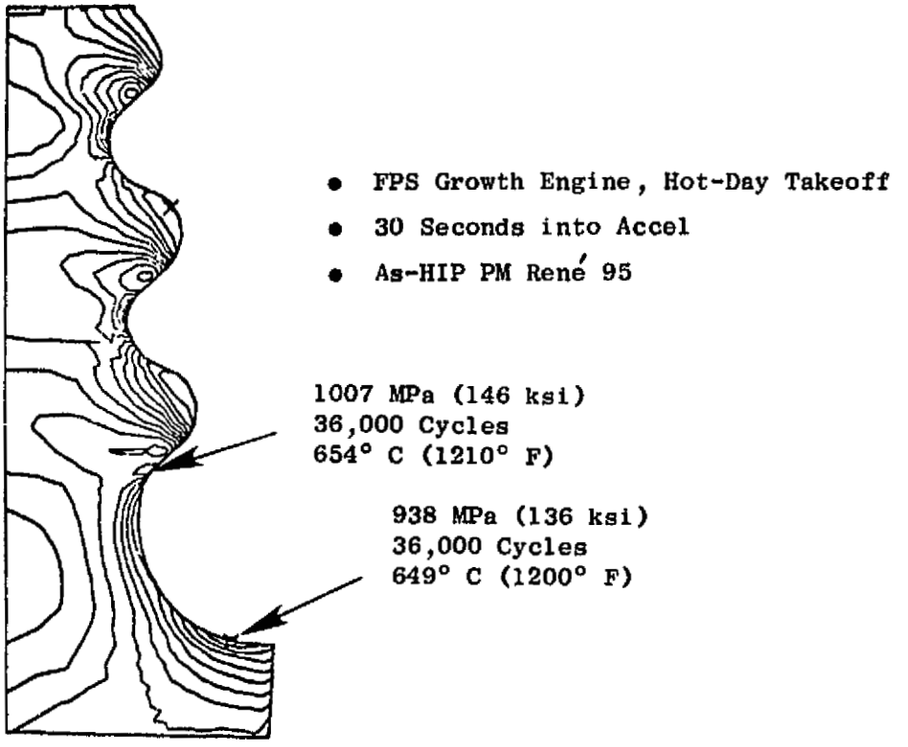

Figure 70. Stage 2 Disk Dovetail Elastic/Plastic (FINITE) Stress Analysis.

- 40 Seconds into Accel
- Hot-Day Takeoff

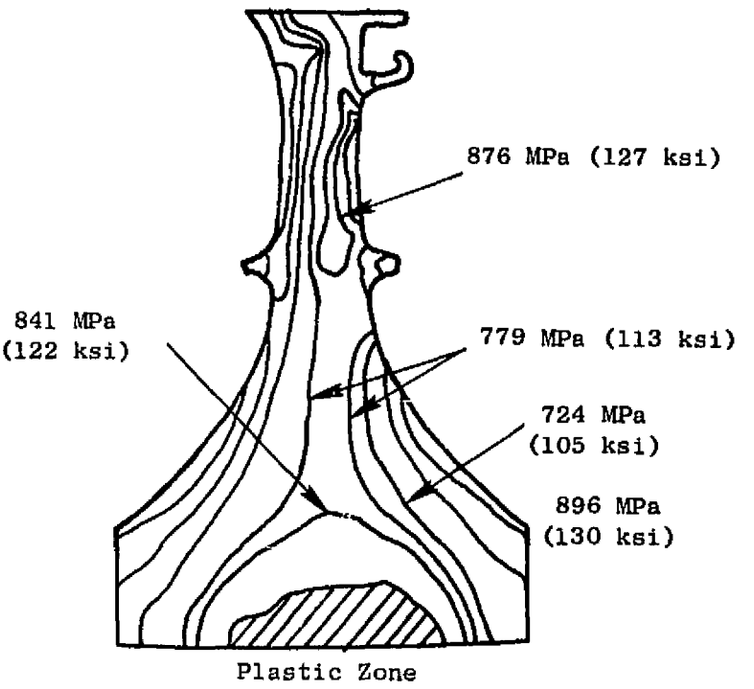

Figure 71. Elastic/Plastic Stress Analysis (CYANIDE).

- 40 Seconds into Accel, Hot-Day Takeoff

Effective Stresses: MPa (ksi)

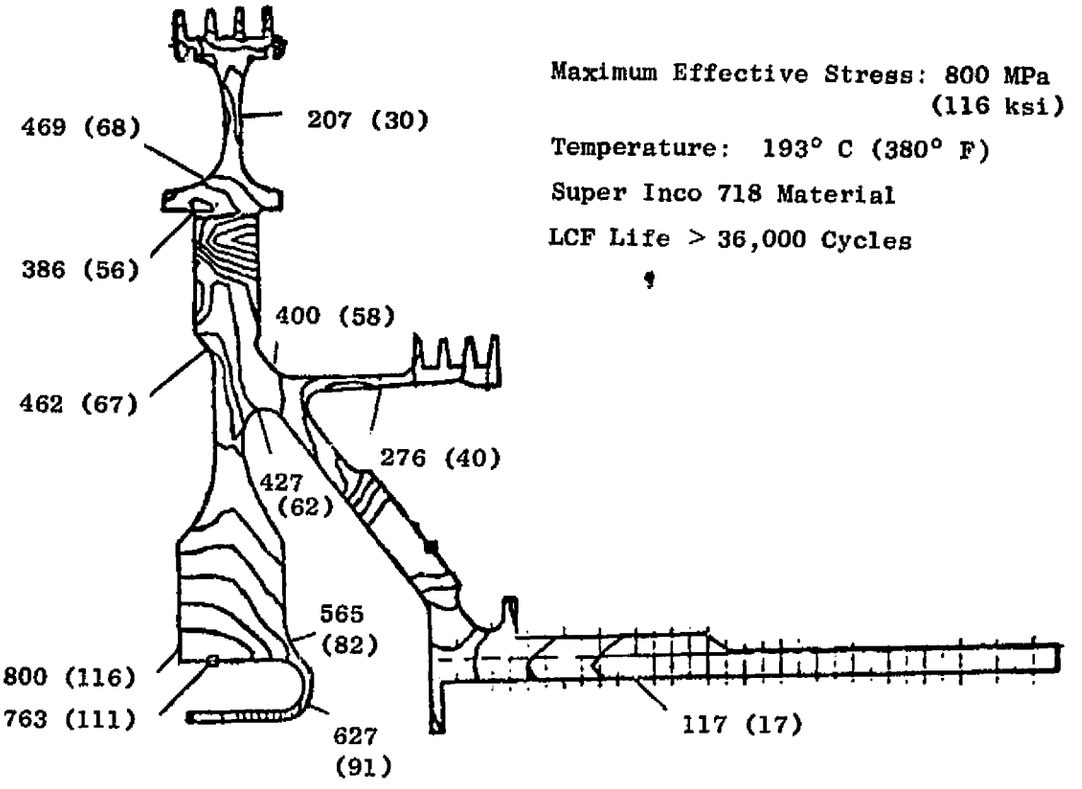

Figure 72. Aft Seal Disk (Growth Engine) Elastic (FINiTE) Stress Analysis.

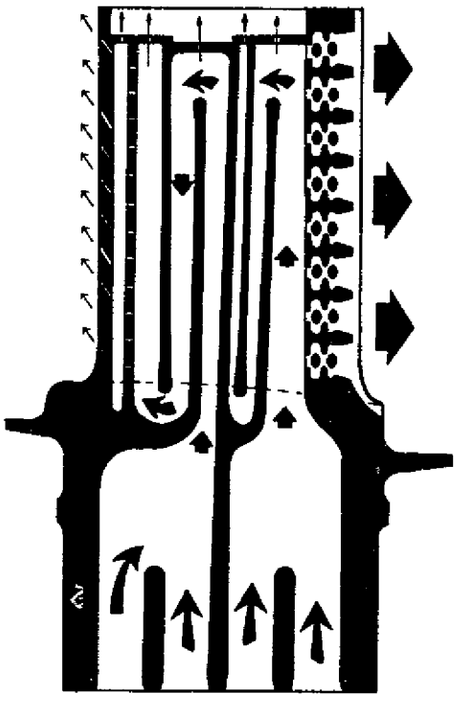

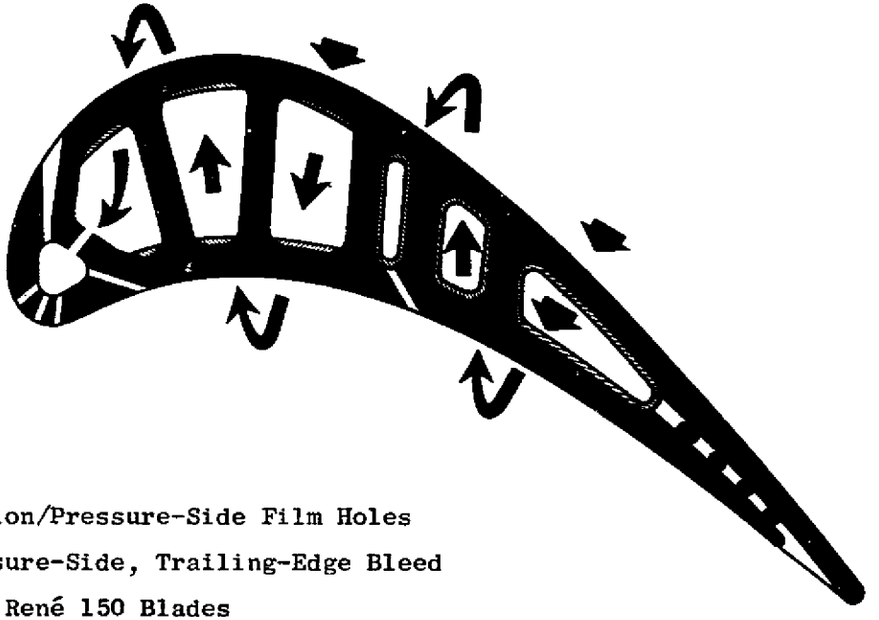

- Suction/Pressure-Side Film Holes
- Pressure-Side, Trailing-Edge Bleed
- Cast René 150 Blades
- PVD Coating
- Warm Air Impingement on Leading Edge
- Serpentine Convection Cooling
- Trailing-Edge Cold Bridge
- Turbulence Promoters on Ribs and Airfoil
- Impinged-Pin-Fin, Trailing-Edge Slot

Figure 73. Stage 1 Blade Design Features.

Table XIX. Design Mission Cycle.

Power Level Rating	Flight Conditions			Time	
	Altitude		Mach No.	Minutes	%
	km	ft			
Ground Idle/Taxi	0-1.83	0-6000	0-0.1	18.0	15.0
Takeoff (100%)	0-1.83	0-6000	0-0.3	2.0	1.7
Maximum Climb*	0-10.67	0-35,000	0.38-0.80	22.0	18.3
Cruise (90% - 70%)	4.57-12.19	15,000-40,000	0.60-0.85	48.0	40.0
Descent/Flight Idle	12.19-1.52	40,000-5,000	0.85-0.65	17.0	14.2
Loiter (60%)	1.52	5000	0.5	7.7	6.2
Approach (45%)				5.0	4.3
Reverse Thrust (90%)	1.83-0	6000-0	0.31-0.28	0.3	0.3
Total				120	100

*Calculated Airspeed: 128.6 - 164.6 m/sec (250 - 320 knots)

namely takeoff, maximum climb, and maximum cruise, were the primary critical flight conditons for determining rupture life.

Figure 74 shows the three main flight conditions. Each flight condition was divided into a percentage mission flight breakdown as a function of ambient temperature. Since the engine conditions vary as a function of ambient temperature, the percentage probability for varying ambient temperature adds a realistic approach to a mission mix as shown in the figure.

Detailed studies indicated the pitch section to be the rupture-life-limiting section (at hot-day conditions). Further studies involving a five-airfoil-section, rupture-life analysis also indicated that the pitch-line was rupture limited (without vibratory effects). The detailed, pitch-section, computer model for predicting the blade life is shown in Figure 75. The BUCKET CREEP III computer program was used to determine life-limiting location for the pitch section.

The pitch-section temperature distributions are calculated for each element in the model. Gas bending and centrifugal loads are applied to the blade section as external boundary conditions.

The objective of the blade design is to achieve a blade life of 18,000 mission mix hours and 18,000 LCF cycles. The rupture life used for the 18,000 mission mix hours at the three flight conditions is shown in Table XX. From these results, it can be seen that for only 300 hours at takeoff condition the blade uses 36% of the total life. This shows how takeoff conditions affect blade life due to the severe gas temperatures, speed, and gas loads.

Table XX. Stage 1 HPT Blade Mission Mix Summary.

Condition	Pitch Section, % Life Used	Total Time at Point, Hours
Takeoff	36	300
Maximum Climb	49	3,300
Maximum Cruise	15	7,200
Balance	<0.1	7,200
Total	100%	18,000

- 250 Hours at Maximum Takeoff Conditions = 18,000 Mission Hours
- Available Blade Life is 264 Hours
- 18,000 Total Calculated Hours

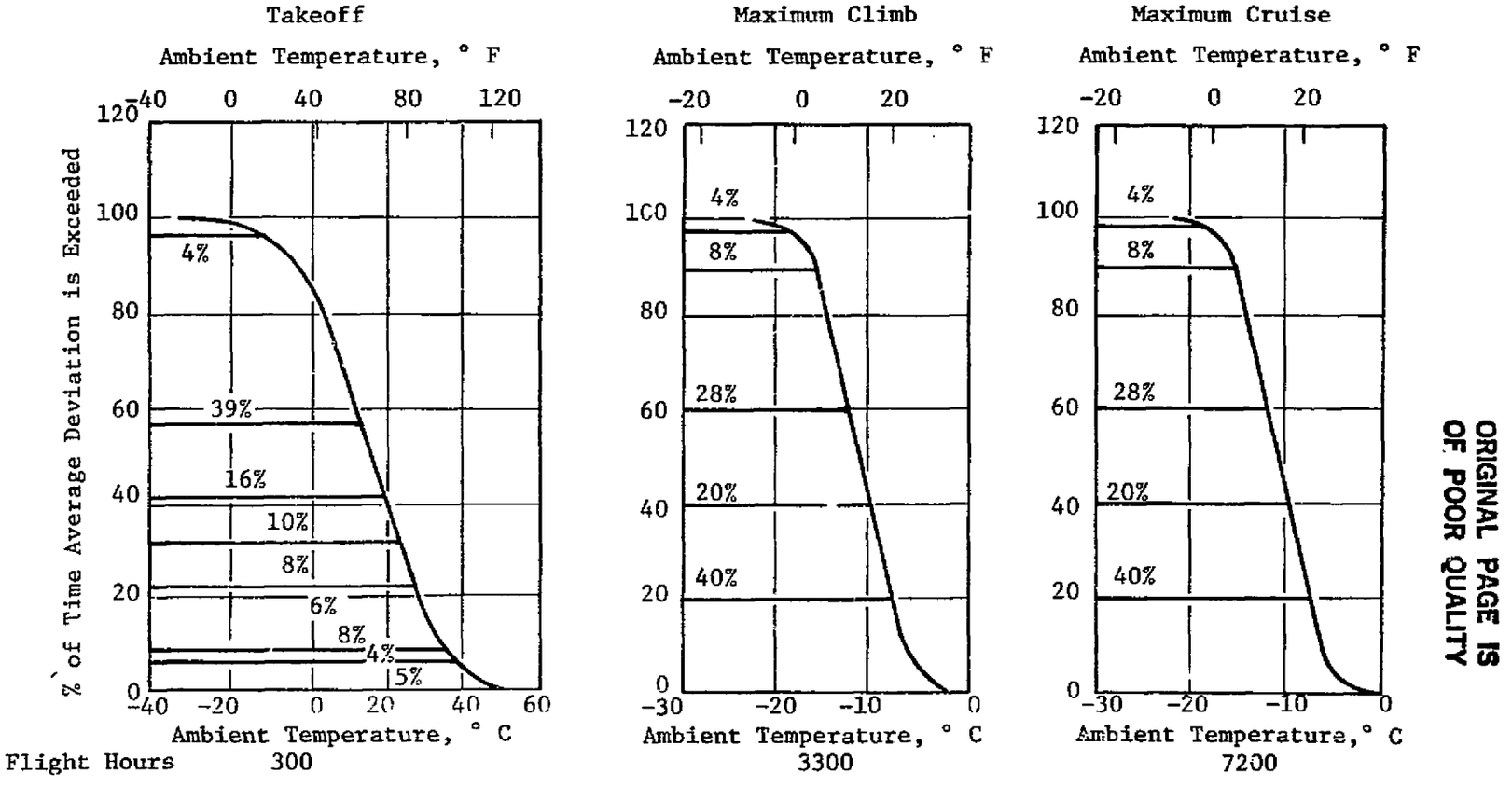

Figure 74. Mission-Mix Flight for Ambient Temperature Conditions.

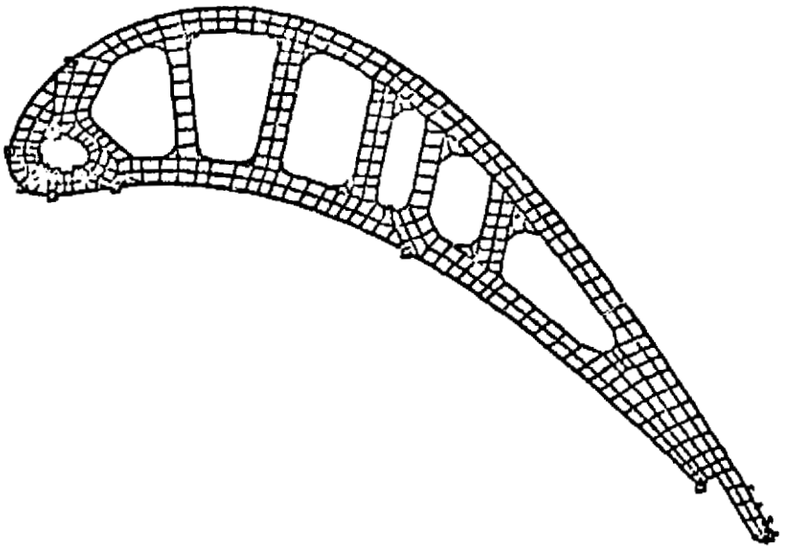

Figure 75. Stage 1 Blade, BUCKET-CREEP Program Model (Pitch Section).

The combined mechanical and thermal effects over 18,000 mission hours are equivalent to 250 hours at the severe maximum hot-day takeoff conditions. The blade rupture life meets this requirement.

A five-section airfoil model, shown in Figure 76, was generated to determine the change in blade tilt. During the 18,000 hours of blade life, this change can be induced by the creep and plasticity effects caused by the mechanical and thermal loads. Since blade tilt is incorporated in the blade casting to counteract the gas moment, any significant variation in tilt will result in changing the desired mechanically induced airfoil stresses. The change in blade tilt effects due to creep was found to be insignificant. Generating the five-section airfoil model also allowed evaluation of the rupture lives at various blade spans.

The rupture-life hours, when combined with the relative vibratory-stress levels between sections, are used to predict minimum life at the critical airfoil location and span section. The combined effects of mechanical stresses (thermal, gas bending, and centrifugal) and vibratory stresses indicate that the trailing edge at 25% span is the life-limiting blade location. This life analysis is based on first-flex vibratory mode. The allowable vibratory stress of 145 MPa (21 ksi), single amplitude, for the first-flex mode is more than adequate to meet the 18,000 hours blade life. Vibratory levels are expected to be well below these values.

The blade airfoil LCF life prediction is based on determining the total local strain experienced during transient accel and decel. Life prediction is determined by using the material-strength LCF data curve (at temperature) for the same blade strain levels.

The engine transient analysis consisted of determining the turbine blade environment due to engine speed and temperature from start to ground idle, accelerating to maximum takeoff for 2 minutes, and then decelerating to ground idle. These basic excursions and engine measured parameters are shown in Figure 77. The blade airfoil temperatures are defined using the engine parameters. The BUCKET CREEP III program was used to analyze the thermal and mechanical strains during the transient. The blade external conditions consisted of varying centrifugal load and gas bending moments as a function of flight condition.

The resulting stress characteristic for the leading-edge film hole (pitch section) versus time is shown in Figure 78. The leading-edge location was determined to result in the minimum LCF life. Starting from zero speed (zero stress), the leading edge is seen to slightly go into a tensile stress. This is the result of accelerating the engine using the engine starter. Fuel is introduced at around 22 seconds and is ignited. The effect is a faster temperature rise of the leading edge relative to the average for the whole airfoil section. The thermal stresses are compressive and higher than the tensile-stress effects of centrifugal, thereby driving the leading edge into a net compressive stress. As the difference between the bulk temperature of the section and the local temperature of the leading edge diminishes, the compressive thermal stresses diminish, thereby reducing the net compressive stresses (22 to 300 sec). The time between 22 and 300 seconds is considered combustor

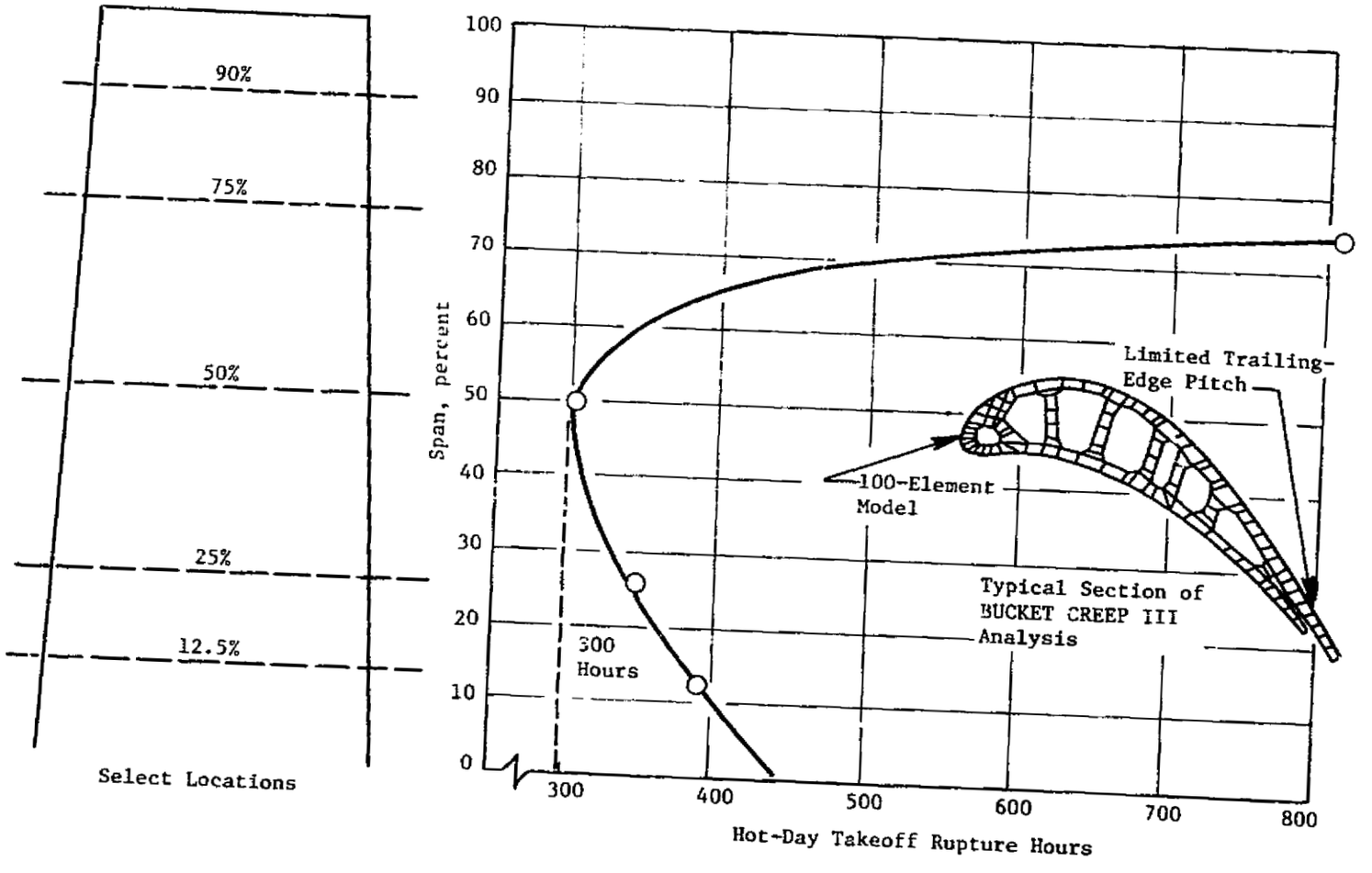

Figure 76. Stage 1 Blade-Five Section, Rupture Life Including Creep Effects on Reduction of Blade Tilt.

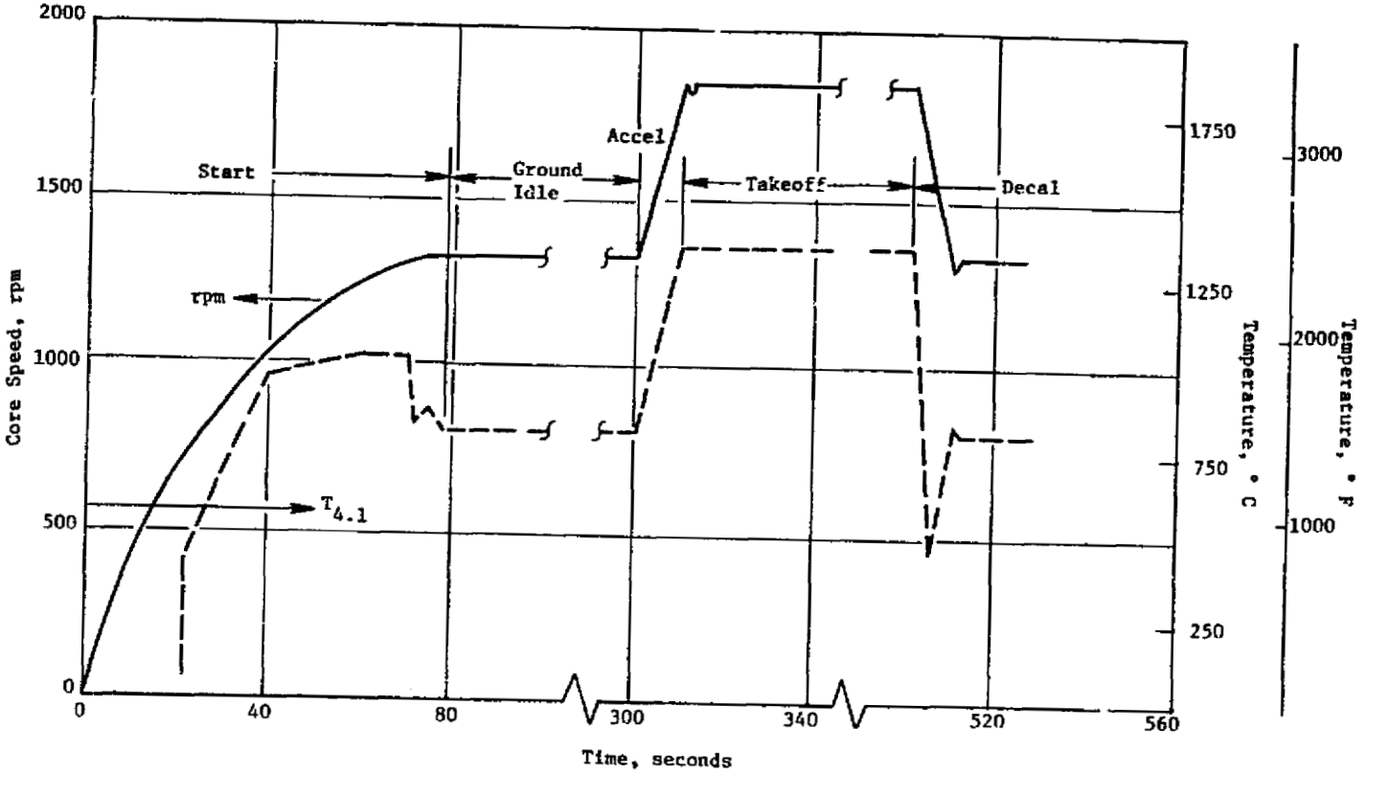

Figure 77. FPS Base Stages 1 and 2 Blade Transient Cycle.

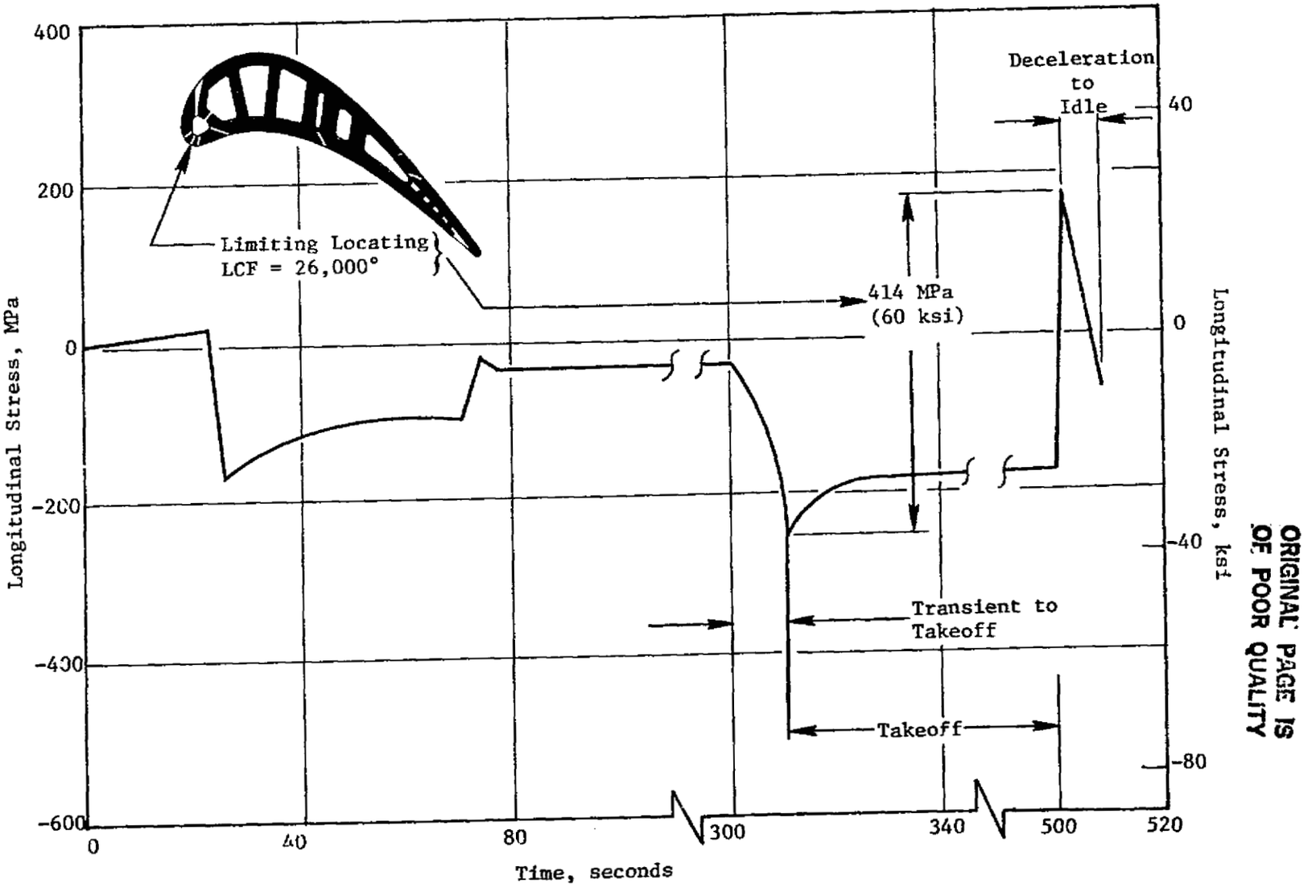

Figure 78. FPS Base Stage 1 Blade Transient Analysis (Pitch Section).

lightoff and idle conditions. Takeoff then takes place, and the leading edge is driven into further compression because high gas temperatures heat the leading edge to temperatures higher than 1038° C (1900° F). The engine is assumed to continue operation for 120 seconds and then initiate a climb mode. The analysis then assumes an engine chop to ground idle. This results in the leading-edge thermal stresses going into a lower level of thermal compressive stresses that, combined with the tensile centrifugal stresses, drives the leading edge into tension. LCF life is then based on the total stress hysteresis: 414 MPa (60 ksi) for the leading edge. Material strength data for René 150 at 414 MPa (60 ksi) and a leading-edge temperature is calculated to provide a life of 26,000 cycles.

Additional LCF life analysis was also conducted for the thrust-reverse condition in order to determine the deterioration life effects. Figure 79 shows the leading-edge (pitch-section) stress characteristics during the engine flight idle to thrust reverse condition. The total stress of 117 MPa (17 ksi) for the thrust reverse has shown this condition to result in minimal LCF life. This conclusion can be seen from using Miner's Rule as defined in the figure.

A blade frequency analysis was conducted to determine blade natural frequencies and to establish relative vibratory airfoil and shank stresses. The resulting Campbell diagram, shown in Figure 80, represents the basic, primary, blade natural-frequency vibratory modes. These are represented by the relative horizontal lines. The oblique lines represent engine passing frequencies caused by various static flowpath components. The intersection of the oblique lines with the blade natural frequencies are considered to be in resonance at the specific speeds. These are speeds that must, therefore, be avoided other than passing through to reach operating speeds.

The highest levels of vibratory blade excitation come from the Stage 1 nozzle. All the primary modes have speed margins in the proximity of the resonance speed.

Blade platform dampers have been included as part of the damping methods for reducing blade vibratory stresses. The damper is an Inco 625 sheet metal strip located on the underside of the blade platform and is in contact with each adjacent platform from the adjacent blade. At maximum takeoff speed the damper has an equivalent "g" load of 85.8 N (19.3 lbf). The effect of an 84.5 N (19 lbf) damping load is an estimated vibratory-stress level of approximately 21 MPa (3 ksi) for the first-flex vibratory mode.

The blade dovetail shown in Figure 81 consists of an axial, two-tang design. The blade neck and dovetail loads are based on the growth-engine takeoff conditions. The upper tang contains a generous fillet for lower stress concentration (K_t) in order to improve LCF capability. The upper-tang depth is also larger than that of the bottom tang due to the higher induced blade loads. The bottom-tang fillet uses compound radii to enhance the blade dovetail LCF life capabilities to meet the 18,000 cycles life objective.

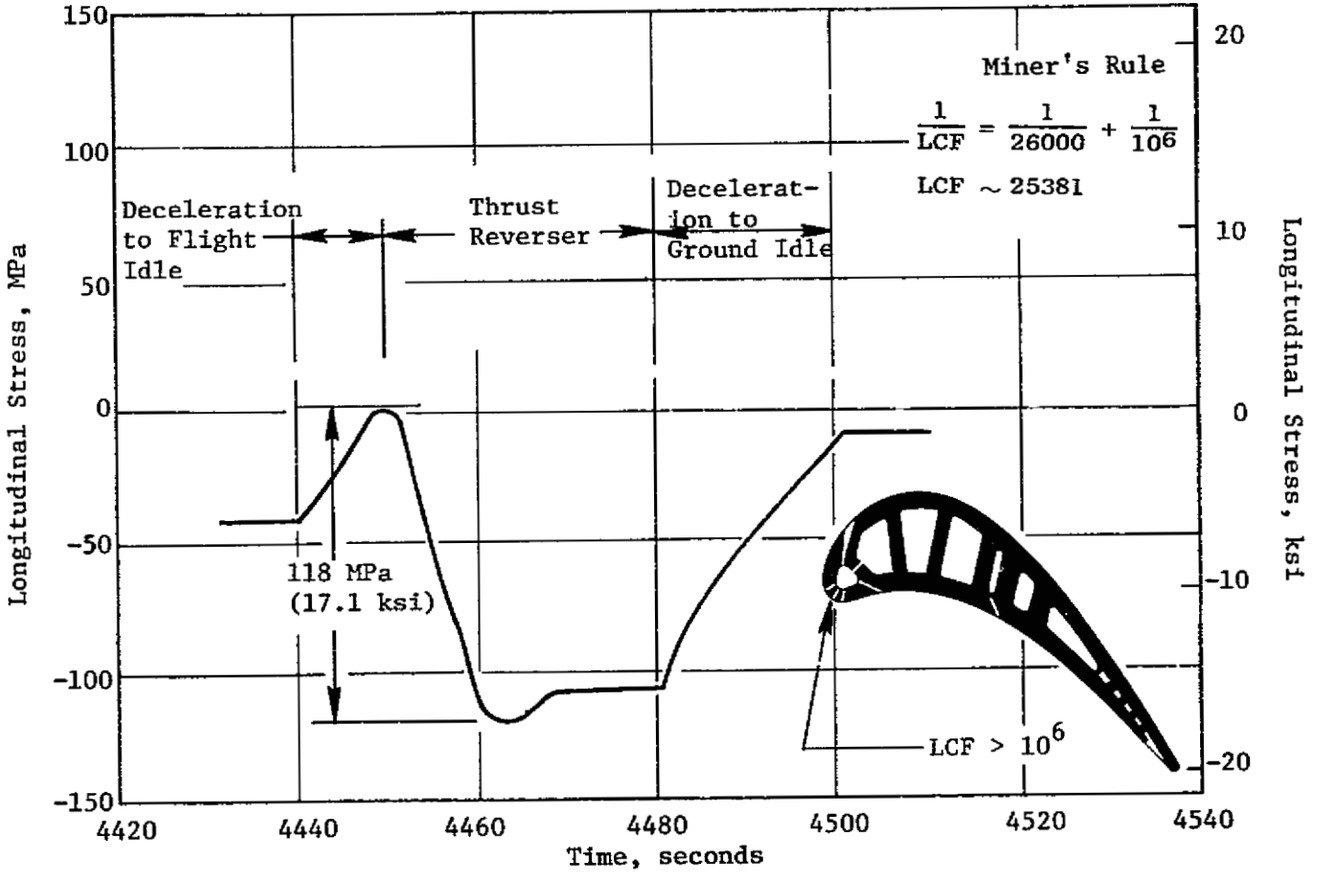

Figure 79. FPS Base Stage 1 Blade Thrust Reverse Transient Stress for Leading Edge at Pitch Section.

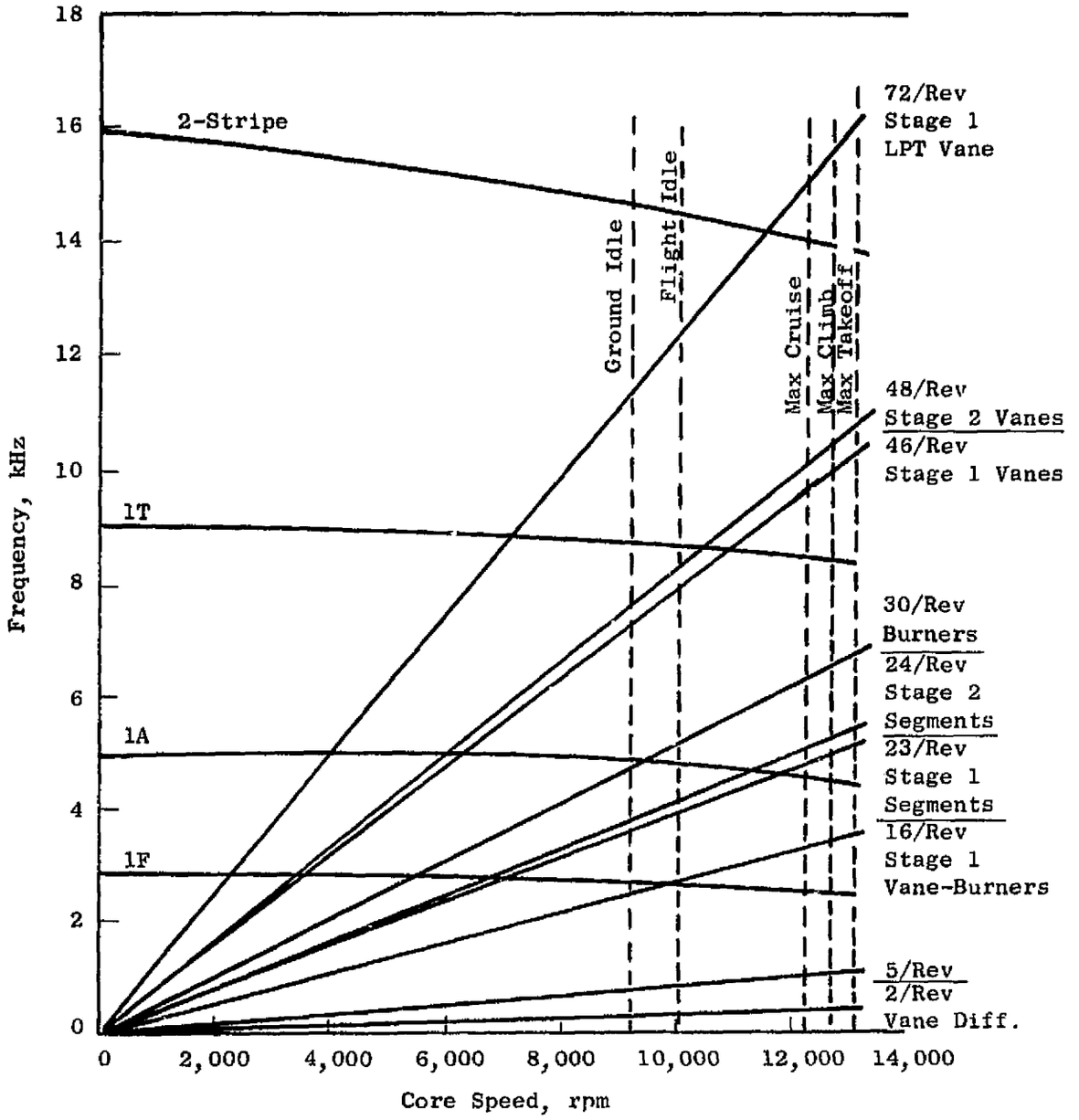

Figure 80. FPS Base Stage 1 Blade Campbell Diagram.

- Low Cycle Fatigue Life Exceeds 18,000 cycles

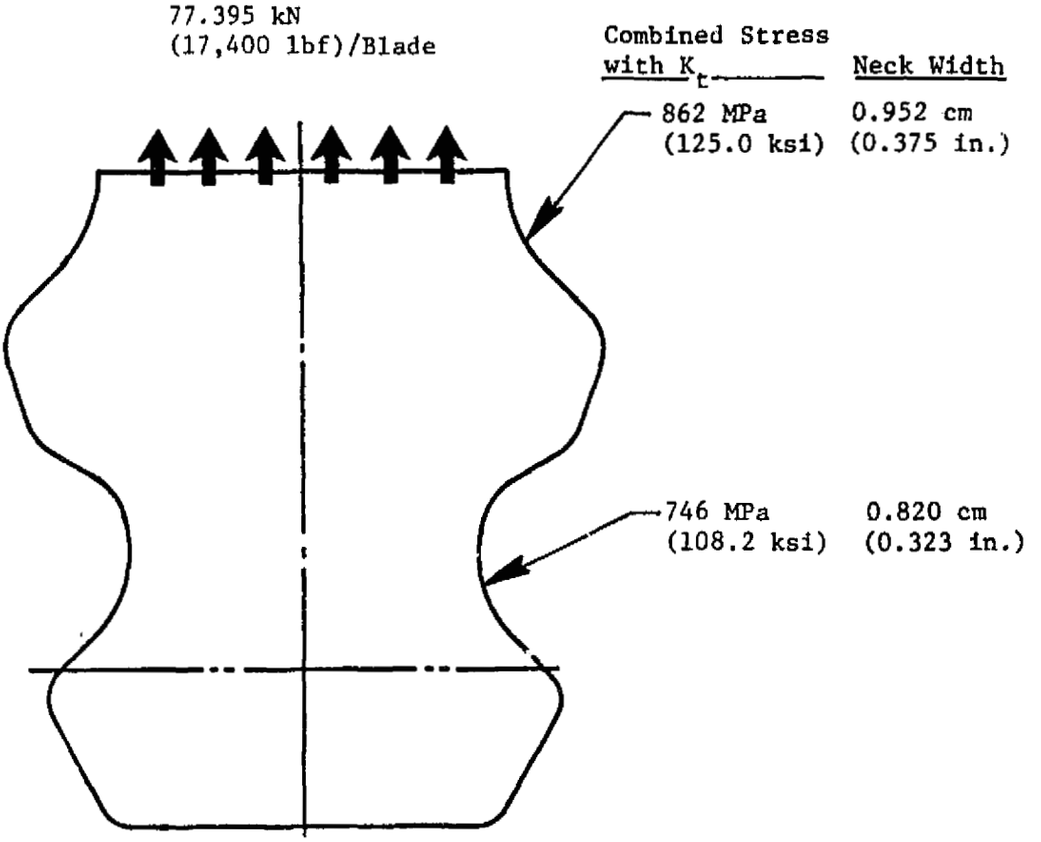

- Hot-Day Takeoff Conditions
- N = 13,948 rpm
- René 150, 3σ Properties
- Axial Chord = 3.45 cm (1.36 in.)

Figure 81. Stage 1 Blade Dovetail Stress.

The blade dovetail for Stages 1 and 2 was analyzed using the MULTI HOOK computer program. The input to the use of this program includes the centrifugal loads and net blade moments (Mx and Mg) existing at the blade dovetail mesh. These loads are used as the external boundary conditions in using the MULTI HOOK program. The program converts these loads into an equivalent load at the four corners of each tang and also at the center of the axial length. Stresses are also defined along the dovetail mesh radius at 15° intervals.

GE experience has shown that the calculated maximum stress levels using this program are higher relative to stresses obtained using FINITE. Field experience has also shown dovetail lives to be higher relative to calculated values. The latest test experience has been the CF6-50 Stage 1 blade, René 150 material, which was run for 1000 "C" cycles. No cracks have been observed in these blades. Additionally the E^3 blade calculated stress levels are lower than the CF6-50 (René 150 material) Stage 1 blade, while the Stage 2 blade stresses are very similar (three-tang design).

Although there is an axial compressive stress induced in the dovetail, it is felt that this is more than offset by the higher calculated stress values obtained by using MULTI HOOK computer program relative to a 3-D finite analysis.

The presence of the cooling hole may have some effect on the tangential vector load. Since these loads can be transmitted only across the ribs, a nonuniform distribution may also exist. Also the K_t effects may be slightly different.

In order to assess the level of stress distribution, a 3-D model of the dovetail is being made. The effects of the cooling hole slots, however, shall be treated as a 2-D.

5.2.1.10 Stage 2 Blade

The Stage 2 blade is an air-cooled design using cast, DS René 150 material. The design features and cooling geometry are shown in Figure 82. The blade rupture-life predictions are based on the 2-hour mission as defined for the Stage 1 blade.

The procedure defined to predict the rupture life was based on using the cycle data information of speed, coolant and gas temperatures, and gas loads. Detailed rupture analysis also indicated that the rupture life was influenced by three flight points in the mission: takeoff, maximum climb, and maximum cruise.

A mission-mix, rupture-life analysis similar to that described for the Stage 1 blade resulted in Table XXI.

A detailed blade pitch-section computer model for predicting the blade life was generated as shown in Figure 83. The BUCKET CREEP III computer program was used to determine the limiting life location for the pitch section.

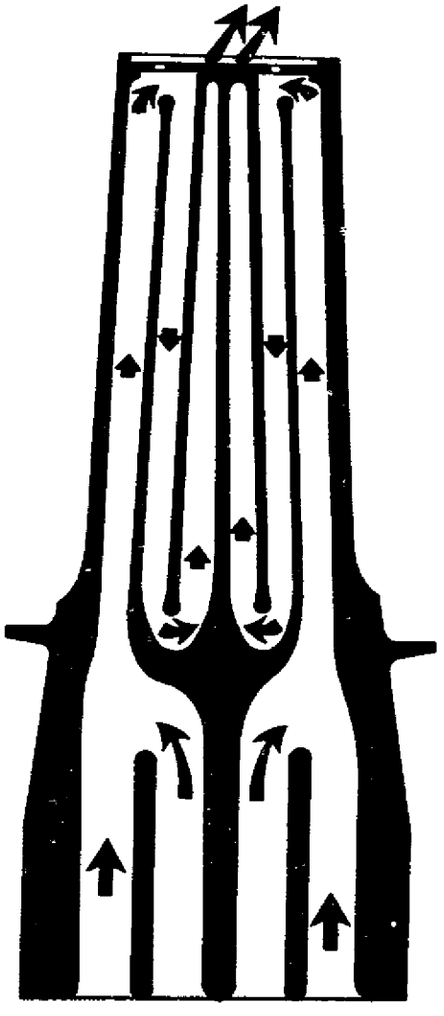

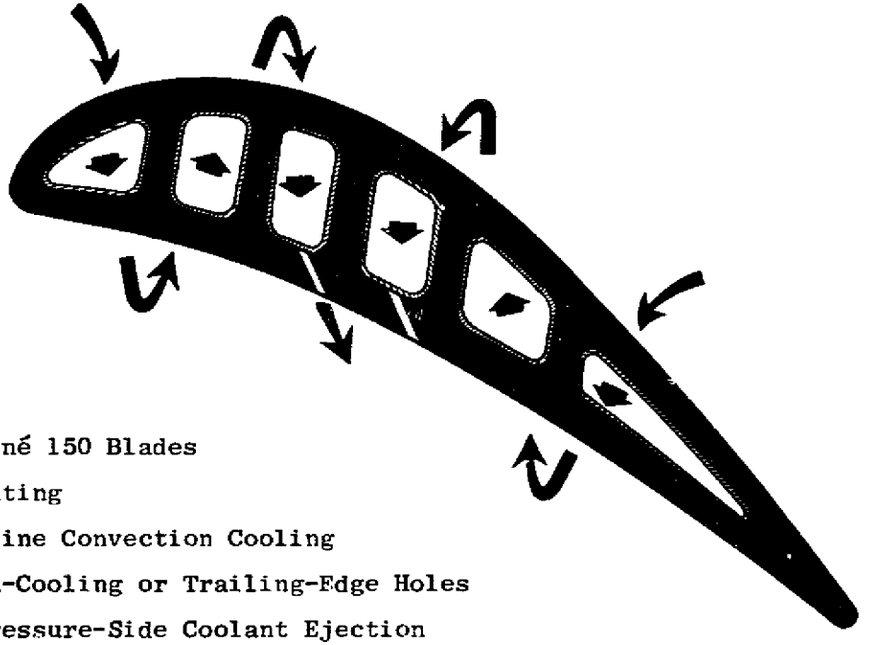

- Cast René 150 Blades
- PVD Coating
- Serpentine Convection Cooling
- No Film-Cooling or Trailing-Edge Holes
- Tip, Pressure-Side Coolant Ejection for Cooling Exit and Increasing Torque
- Turbulence Promoters on Ribs and Airfoil Walls

Figure 82. Stage 2 Blade Design Features.

The temperature distributions were calculated for each element in the model. The mechanical loads, centrifugal and gas bending, are applied as external boundary conditions.

Table XXI. Stage 2 HPT Blade Mission Mix Summary.

Condition	Pitch Section, % Life Used	Total Time at Point, Hours
Takeoff	33.5	300
Maximum Climb	48.2	3,300
Maximum Cruise	18.3	7,200
Balance	<0.1	7,200
Total	100	18,000

- 340 Hours at Maximum Takeoff = 18,000 Mission Hours
- Available Blade Life is 341 Hours
- 18,000 Total Calculated Hours

The combined mechanical and thermal stresses result in the rupture lives shown in Figure 84. As indicated in the figure, the blade life objective of 18,000 hours is achievable.

Blade LCF life-prediction analysis for the pitch section was based on determining the total strain occurring in the local surface of the airfoil. The analysis considered transient conditions from the initial combustor lightoff, through ground idle, into the takeoff, and back to ground idle. The analysis considered the combined effects of stress and temperature and indicated the trailing edge to be the limiting LCF location. Calculated LCF life is greater than 30,000 cycles.

A blade vibratory analysis was conducted to determine the natural frequencies. Figure 85 represents the Stage 2 blade Campbell diagram for the primary frequency modes.

The first-torsional, blade-frequency mode is in proximity to that of the 24/rev Stage 2 vane segments at the flight idle conditions. Due to the low speed and pressures, the level of excitation is considered to be low. Once the blade frequencies are determined from actual bench testing, a more detailed Campbell diagram can be established which will more accurately predict the resonance locations.

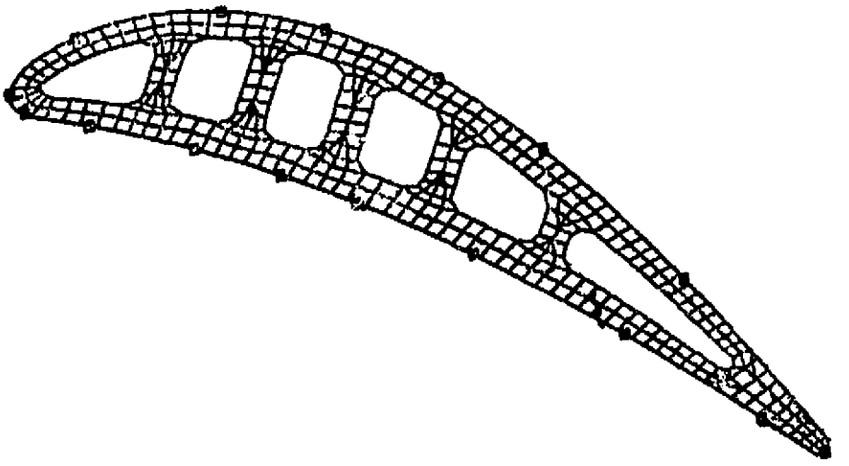

Figure 83. Stage 2 Blade BUCKET-CREEP Program Model.

- FPS Base, Hot-Day Takeoff (13,414 rpm)
- 340 Hours = 18,000 Hours Mission Mix (Blade Life Objective)

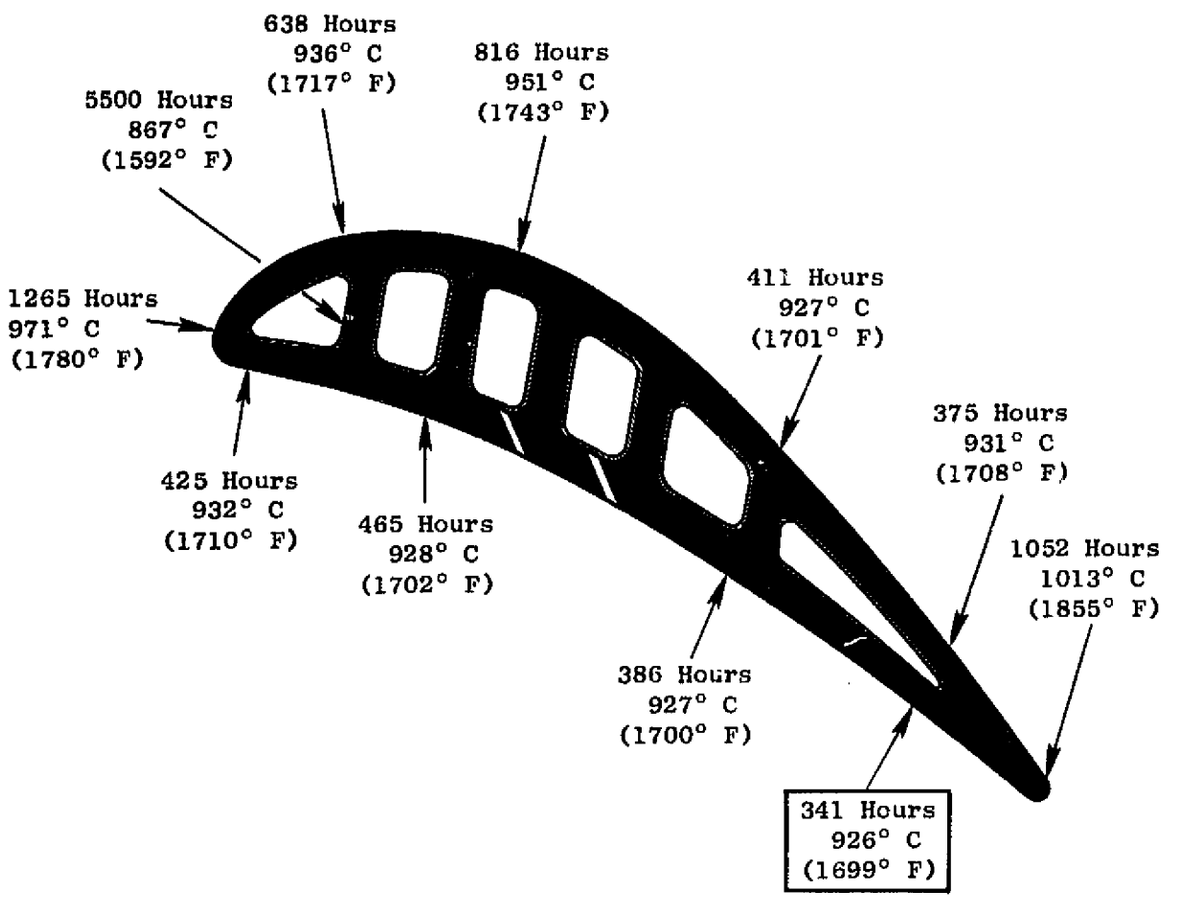

Figure 84. Stage 2 Blade Pitch-Section Rupture Life.

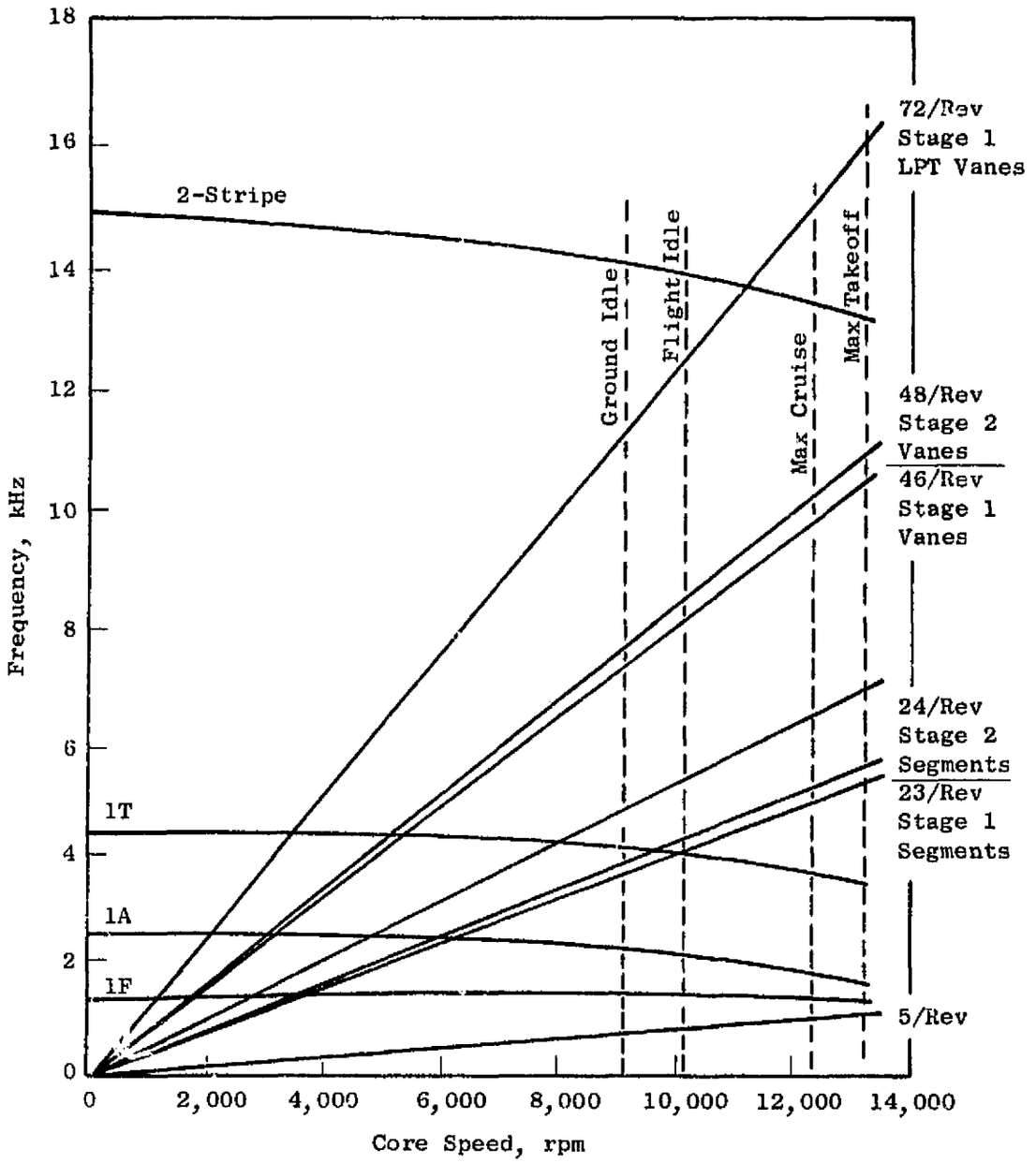

Figure 85. FPS Base Stage 2 Blade Campbell Diagram.

The Stage 2 blade includes geometry features that allow mounting of a damper assembly as shown in Figure 86. The forward angel wing acts as a windage cover, and its forward vertical surface closes the openings between adjacent blade shanks. There are 70 dampers used, each corresponding to 70 blades. The actual blade damping is carried out by the two lugs shown in the figure.

The lugs are radial, free floating, and can rotate a limited amount circumferentially. Each side of the top portion is in contact with an adjacent blade, thereby providing damping through its centrifugal induced load. The aft damper lug acts in the same way as the forward lug.

The blade dovetail, shown in Figure 87, is an axial, three-tang design. The blade neck loads are based on the growth-engine conditions. Dovetail geometry contours, consisting of radii and depth of tang, are well balanced between the upper and middle tang. The stress of the lower tang, which is higher than the other two, has LCF life capability exceeding 18,000 cycles.

5.2.1.11 Dynamic Analysis

A dynamic analysis for all the "flexible" members of the HPT rotor was completed to determine the speed conditions where mechanical resonance could occur. Resonance can occur if a component natural frequency is near the frequency of any external excitation within the engine operating speed. Resonance results in high vibratory stresses and deflections and can cause the component to fail in high cycle fatigue.

Frequency and mode shapes of a free vibration were determined for circumferential wave nodes (N) in the fundamental axial mode. The CLASS/MASS computer program was used to calculate the natural frequency at zero speed. These frequencies were then modified for a spectrum of engine speeds. From these modifications, frequencies of forward-traveling wave (f_F) and backward-traveling wave (f_B) are determined. Forward-traveling-wave frequency increases with engine speed; usually this wave mode does not produce any resonance. But the frequency of backward-traveling waves decreases with an increase in engine speed, and for a particular engine speed the frequency becomes zero. When the backward-traveling-wave frequency reaches zero, the corresponding engine speed is known as the critical engine speed. The zero natural frequency has the following significance: (1) the component has a stationary, backward-traveling wave (frequency = 0) and (2) under this situation the component can be excited by the presence of any static load (frequency = 0) of the same number of circumferential nodes. Since a zero frequency for backward-traveling wave can be excited by any static load, it is mandatory that the engine operating speed be below the critical value in order to avoid resonance.

Dynamic analyses were done for different values of N (number of circumferential nodes). The N which yielded lowest critical engine speed was considered to have the minimum safety margin. Safety margin is defined as:

S_M = (Critical Engine Speed - Maximum Engine Speed)/Maximum Engine Speed.

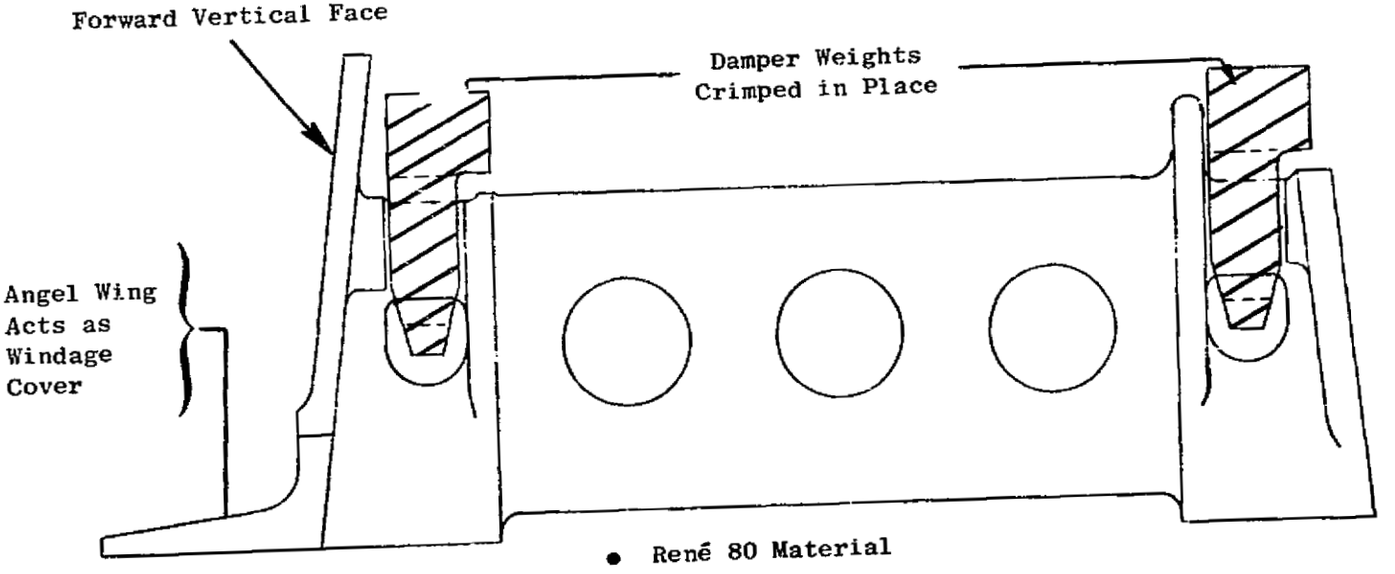

Figure 86. Stage 2 Blade Seal Damper.

- Low Cycle Fatigue Life Exceeds 18,000 Cycles

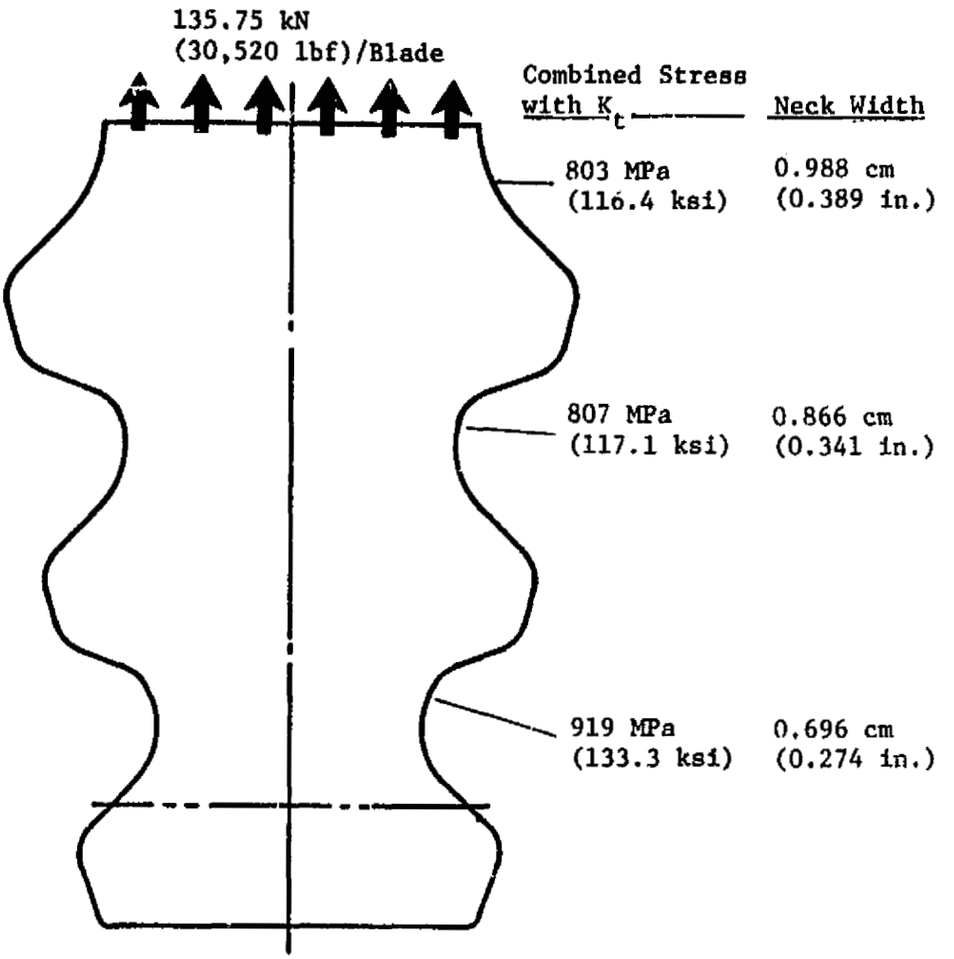

- Hot-Day Takeoff Conditions
- N = 13,948 rpm
- René 150, 3σ Properties
- Axial Chord = 4.83 cm (1.9 in.)

Figure 87. Stage 2 Blade Dovetail Stresses.

Table XXII summarizes the dynamic analysis of the flexible HPT rotor components.

Table XXII. Dynamic Analysis.

Component	Vibration Critical Nodes	Critical Engine Speed rps	Safety Margin
Forward Shaft	4	820	2.52
Inner Tube	3	610	1.62
Outer Liner	7	1030	3.42
Aft Seal Disk	5	610	1.61

The aft seal-disk vibration analysis, shown in Figure 88, considered the effect of the disk web unsupported length between the bolt circle and seal teeth. Flexibility in the web can cause excessive axial movement and give rise to pressure fluctuation in the adjoining air cavities; this may cause aerodynamic instability. The critical mode of vibration for the disk is for N = 5 with a safety margin of 1.61. The mode shape of vibration indicates the existence of axial movement. In order to avoid excessive axial motion, a damper was added to counteract any axial external excitation.

5.2.1.12 Bolt Design

There are three major HP rotor locations which require bolted joints, as shown in Figure 89. The bolts are designed to meet the following criteria:

- No Flange Separation - Flanges will not separate under any combined load and temperature condition.
- Torque Transmission - Torque load transfer will only occur through friction between mating flange surfaces, without any slippage of the mating surfaces.

Bolt loads were determined from the CLASS-MASS rotor analysis for hot-day takeoff conditions. Torque loads were determined from the maximum engine-required torque as defined in the FPS cycle.

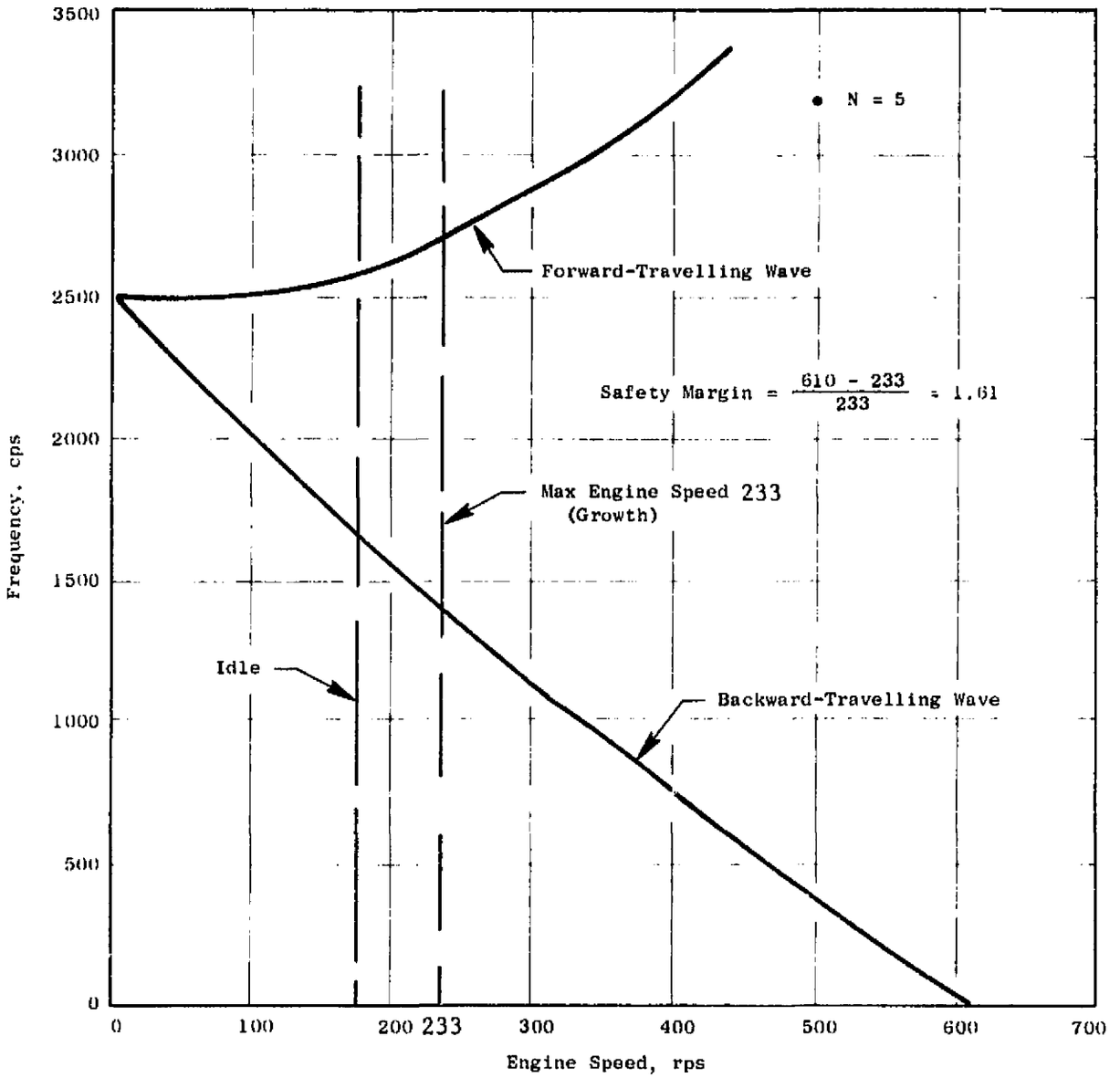

Figure 88. Aft-Seal Disk Frequency or Free Vibration.

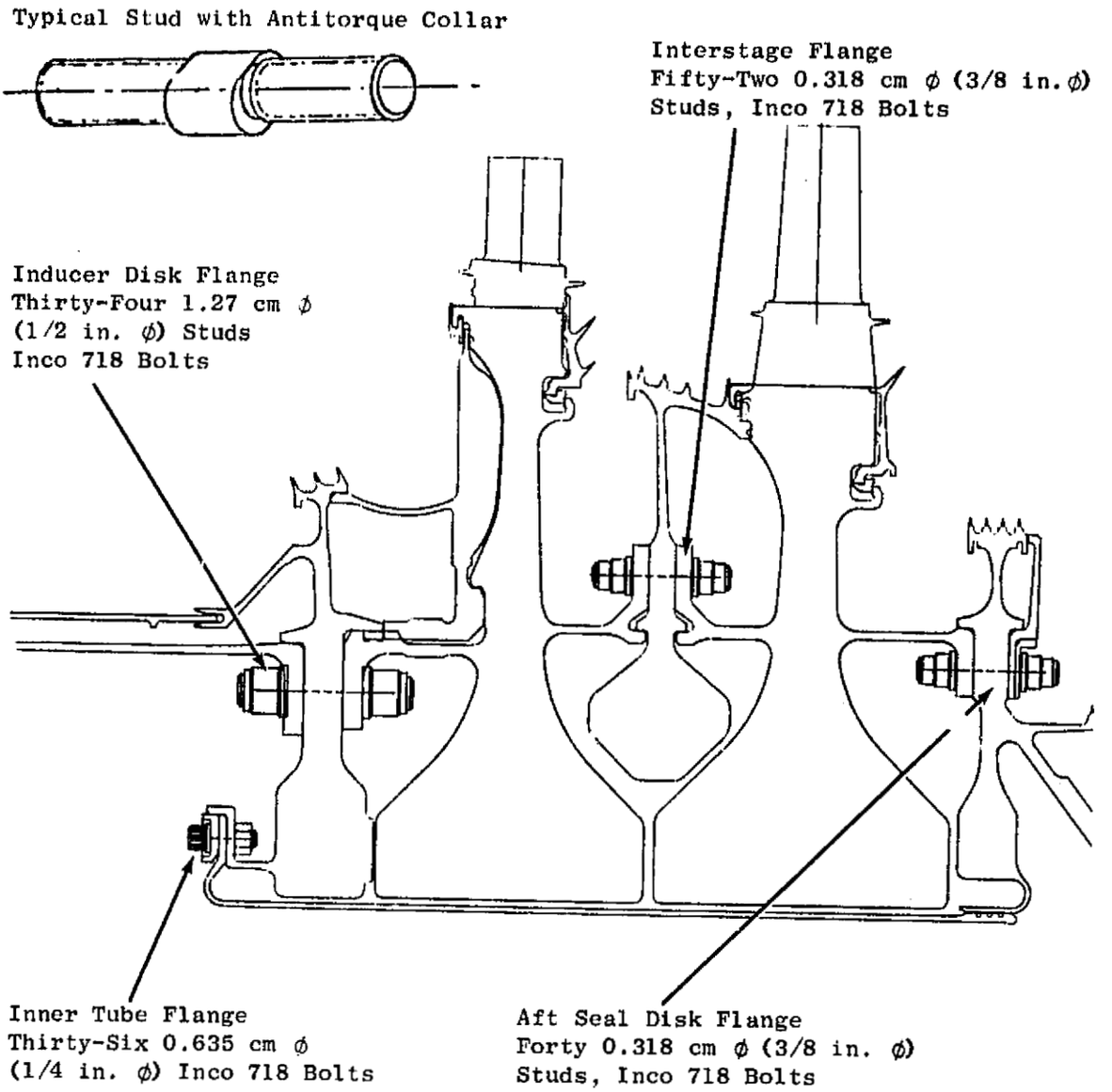

Figure 89. Rotor Bolt Flanges.

The CLASS-MASS rotor computer model includes the flanges at each fastening location. CLASS-MASS results include axial and moment load transferred between flanges through the bolts.

Life objective for all bolts is 9000 hours of mission-mix flight operation. The mission mix used for the analysis considered bolt temperature and loads at various flight conditions.

A bolt, when subjected to sustained loads at temperature, is susceptible to creep relaxation. Therefore, in determining the bolt size and number of bolts in a flange assembly, relaxation effects are included to ensure that the bolt can continue to transmit all loads after reduction in the bolt load has occurred.

The three main bolts analyzed were inducer-disk bolt, interstage-disk bolt, and aft-shaft bolt.

The GE Bolted Flange Analysis computer program (BOFLAN) was used to determine assembly torque requirements. Assembly torque was converted to an assembly cold-clamping load.

Figure 90 shows the analytical clamping results for the inducer-disk bolt. Evaluation of the bolt requirements shows that the necessary clamp loads were governed by the torque transmission. An 8% margin still exists after 9000 hours of maintaining the required clamp load to carry maximum engine torque.

Figure 91 shows the clamping load and relaxation characteristics for the interstage disk after 9000 hours of service flight operation. The bolt clamp-load requirements were established by the flange-separation loads.

The aft-shaft bolt analysis indicated that flange separation controlled the bolt size and number. The effect of the flange loads and temperatures resulted in minimal relaxation. Bolts at this location are more than adequate to meet the 9000 hours mission mix bolt life.

5.2.2 Static Components: Stress, Stress Concentration, LCF Life

The HPT static components and their assembly arrangement are shown in Figure 92. The forward and aft outer nozzle supports, or forward and aft HPT cases, constitute the primary elements of the HPT stator system. The casings are the engine structural link through the HPT and contain the internal (thermodynamic cycle) pressures of this section of the engine. Pressure loads, thrust loads, and related mechanical loads are carried by these casings.

The Stage 2 nozzle system is attached directly to internal flanges of the casings. Outer axial support of the Stage 1 nozzle is supplemented by the conical axial support; the nozzle outer axial load is transmitted to the casing inner flange by this conical axial support.

The Stage 1 shroud forward-support-ring assembly consists of structural, sealing, and airflow-metering components. The support ring is "saw cut" or

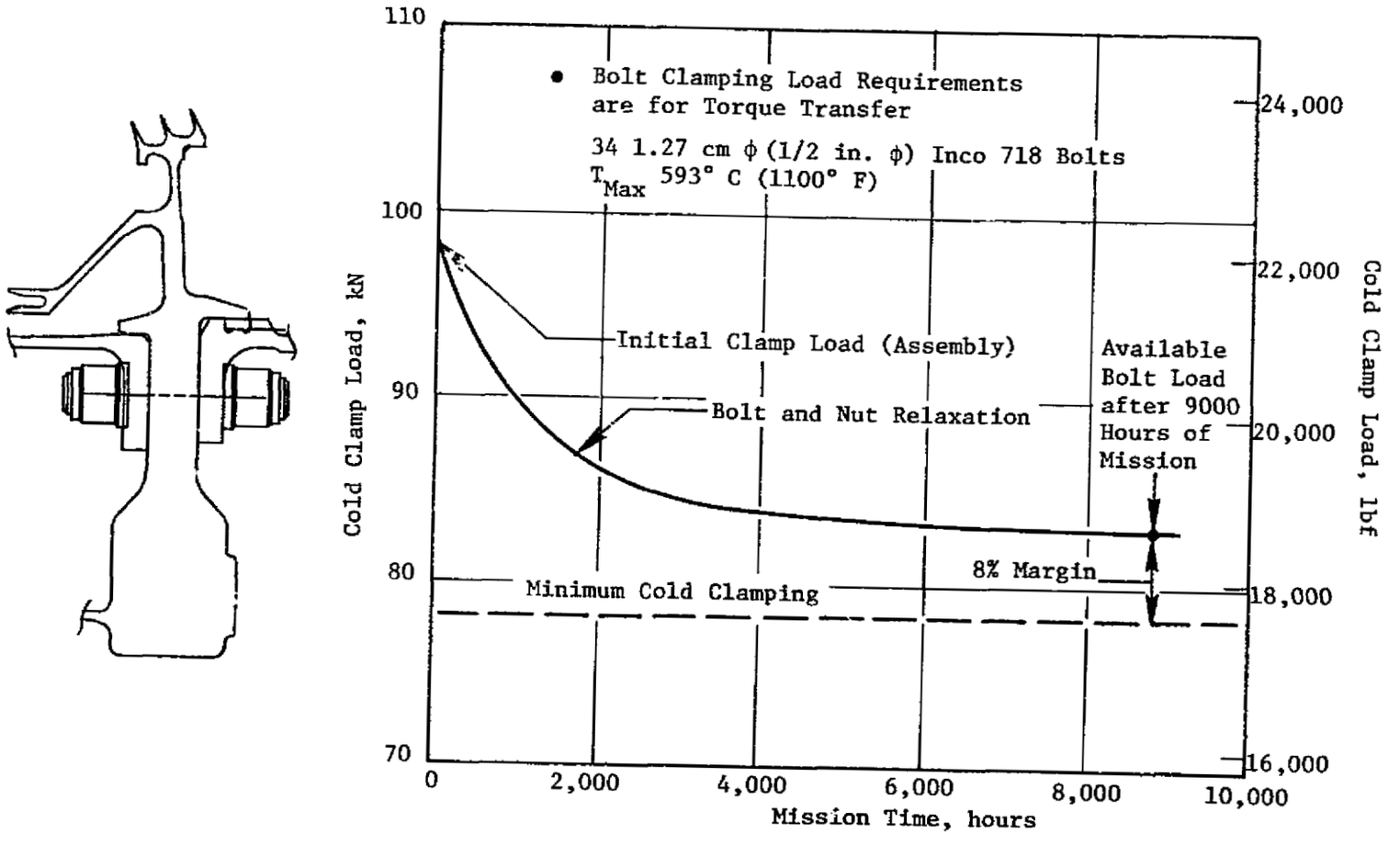

Figure 90. Inducer Disk Bolt Relaxation Analysis.

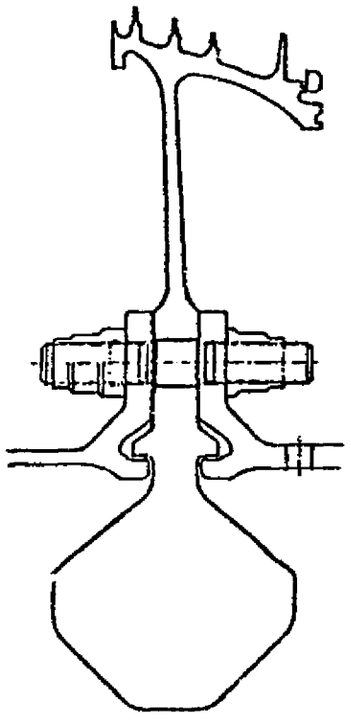

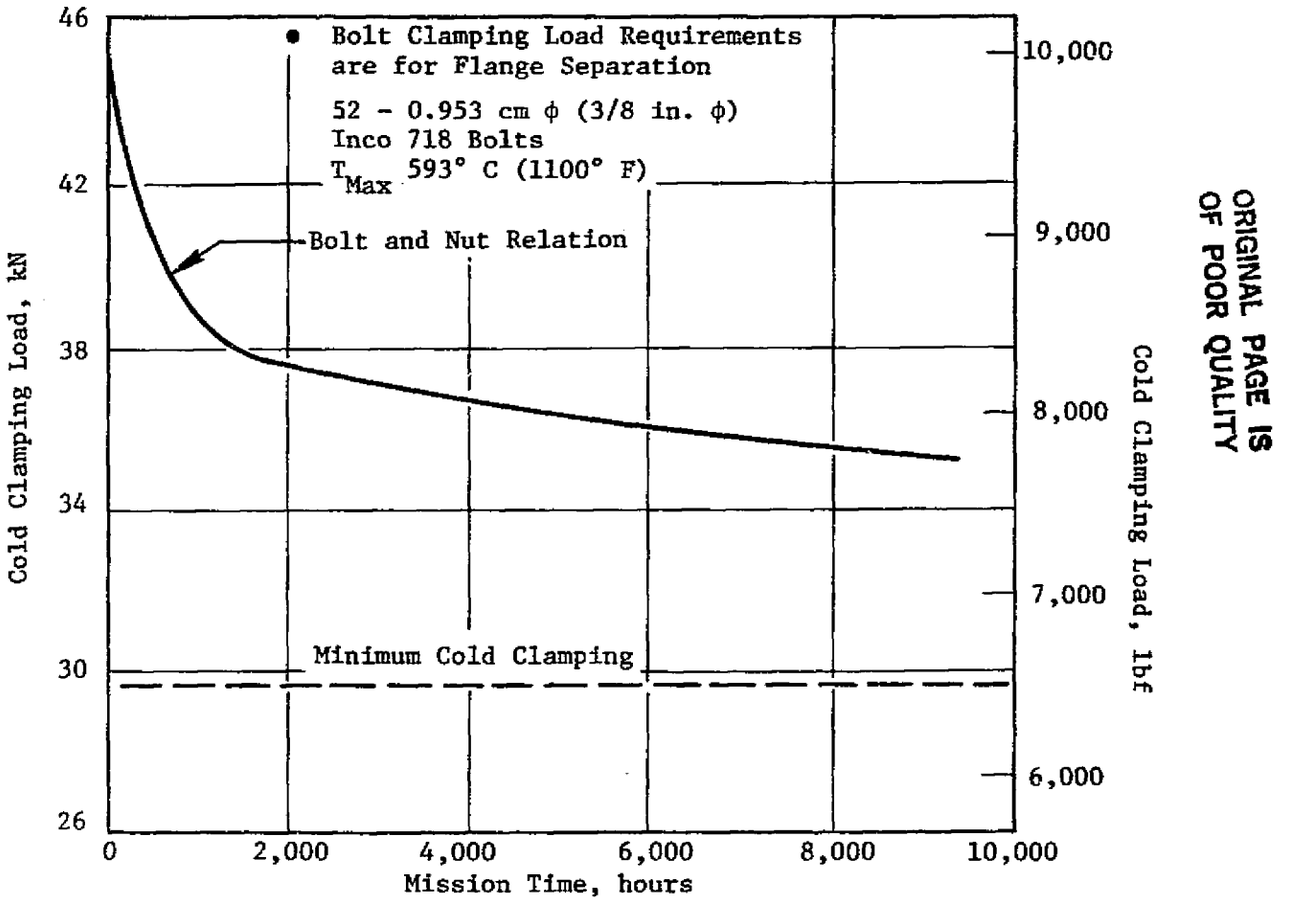

Figure 91. FPS Growth-Engine Interstage-Seal Disk Relaxation Analysis.

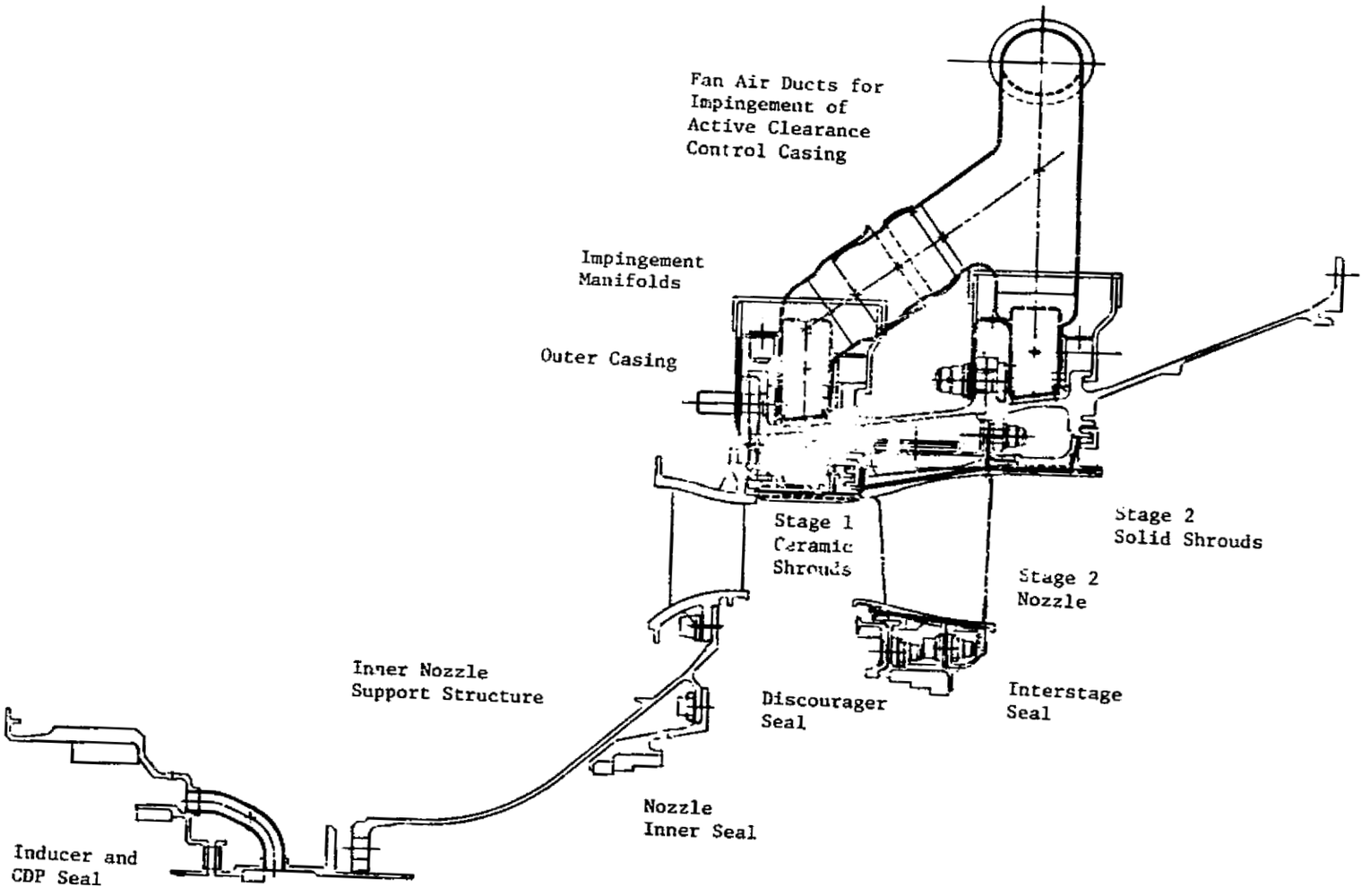

Figure 92. Static Components and Assembly Arrangement.

slotted from the inner edge and to relieve thermal stress and to reduce the effect of shroud growth. It is faced on forward and aft sides by trapped, 360° seal plates that are free to grow radially independent of the structural ring. Between these seal plates and moving with them are hollow rivet elements that meter the flow of compressor-discharge air used to cool the Stage 1 shrouds.

The predominant component of stress in the casings is thermally induced. The extremes of the stress range occur during takeoff transients and while the ACC system is in operation at maximum climb and maximum cruise conditions. Figure 93 shows various stresses and temperature with the corresponding LCF life at different locations.

5.2.2.1 Casings

The material selected for the HPT casings to meet the life requirement of 36,000 flight cycles in an FPS design is Direct Age Inco 718 (DA718). This is a newly developed material under evaluation of process capability and component performance; LCF is up to 10 times that of standard Inco 718. The factor of cyclic life advantage of DA718 over standard Inco 718 varies with temperature and stress level, but it is sufficient to provide greater than 50,000 cycles of LCF life at all potentially stress-limiting locations.

The outer axial support for the Stage 1 nozzle had adequate LCF life using standard Inco 718. The shroud support is made of René 41. René 41 provides an additional 111° C (200° F) margin over Inco 718 to the knee of its strength curve.

5.2.2.2 Stage 1 Nozzle Support

The Stage 1 inner nozzle support configuration is shown in Figure 94. The material is forged René 41, welded and machined to the desired contour. For the FPS base engine, the end flanges would be René 41 forgings; the remaining structure would be fabricated from René 41 sheet metal for reduced cost.

The nozzle-support reaction loads originate from the loads due to airfoil gas loading and from the inner seal. The Stage 1 nozzle segments are bolted to the aft flange for vane-structure support and for proper vane-flowpath location. The discourager seal and inner seal mounting systems are also supported from this component.

Load transfer to the compressor outlet guide vane (OGV) is provided by sixty-four 0.953 cm (3/8 in.) diameter bolts fastened to the forward flange and OGV flange.

The support structure was analyzed based on differential pressure across the wall, vane gas loads, and outer axial-support loads. An LCF life analysis based on the worst conditions, 40 seconds into hot-day takeoff, indicates the structure is capable of meeting the objective life of 36,000 cycles.

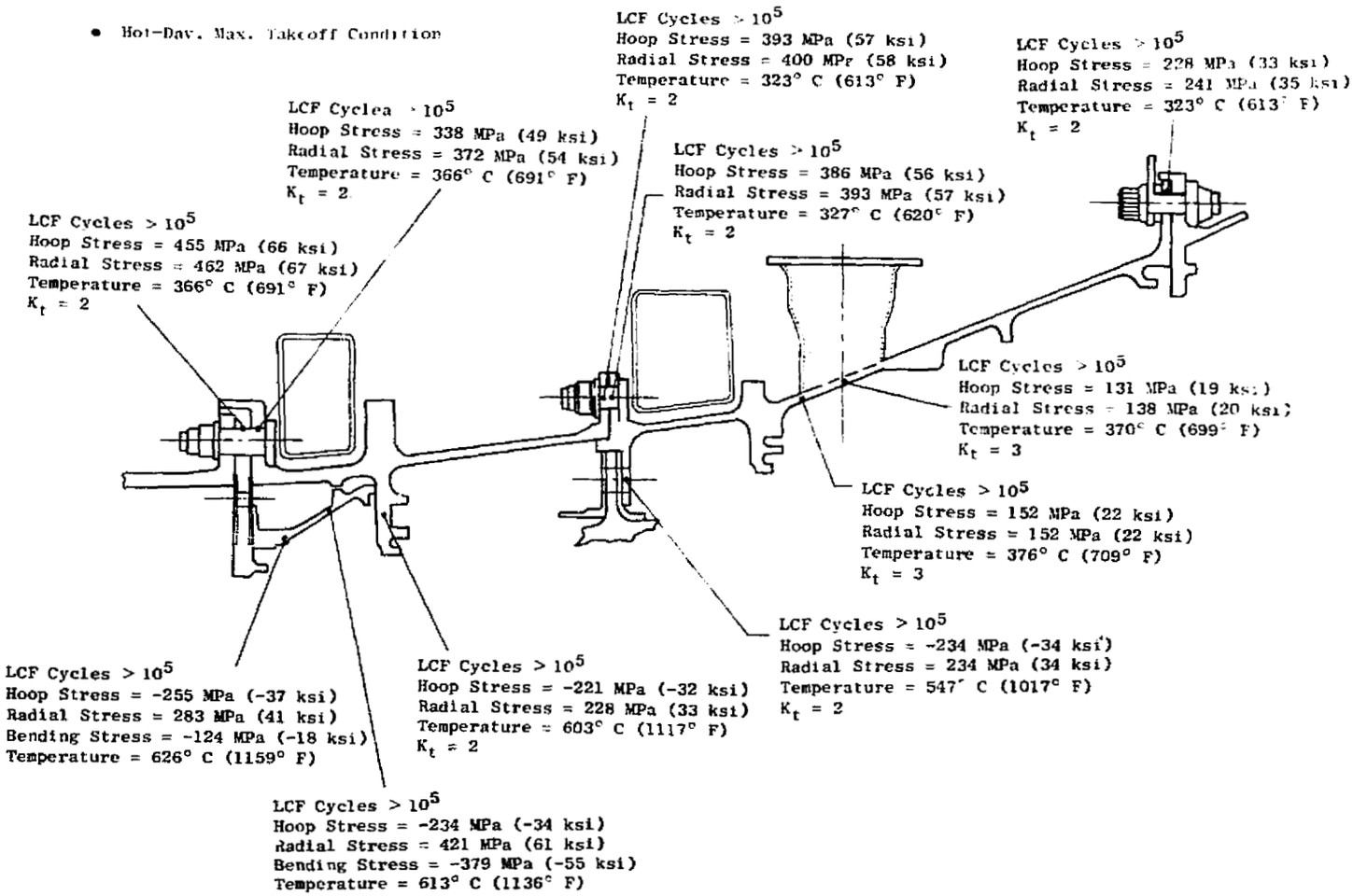

Figure 93. Casing LCF Life, Stress, and Temperature at Hot-Day Maximum Takeoff.

- 40 Seconds into Takeoff, +50° C (122° F) Hot Day
- René 41
- LCF Life ~36,000 Cycles

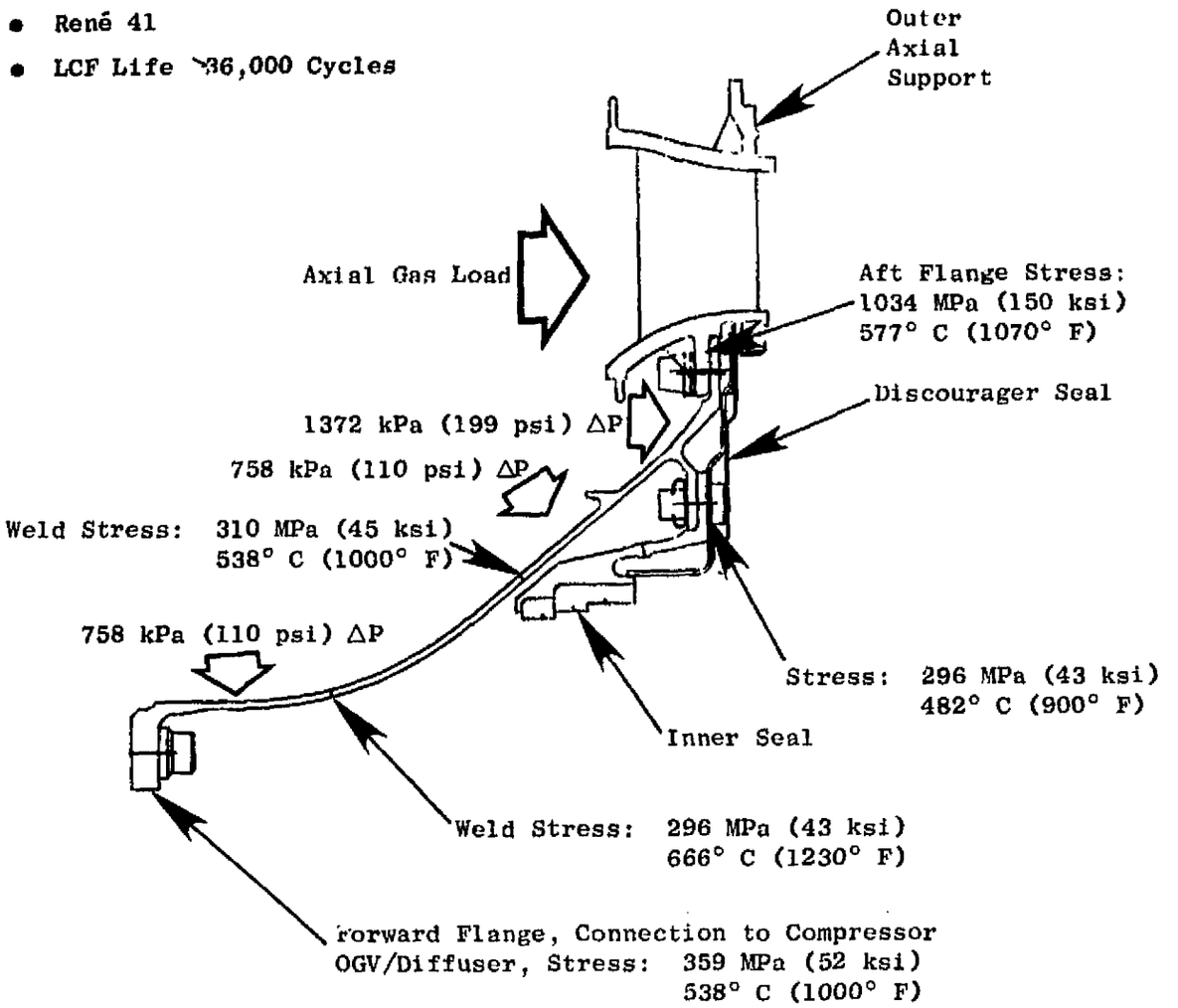

Figure 94. FPS Growth Engine Inner Nozzle Support.

The inducer and piston balance seal shown in Figure 95 serves the following functions:

- Contains the inducer/air-expander system that provides the air for cooling Blade 1 and Blade 2.
- Reduces CDP leakage through the forward-seal arrangement with the compressor balance piston seal disk (CDP leakage) bypass.
- Transports CDP leakage through bypass tubes. This air is then used for purging the cavity formed between Nozzle 1 and Blade 1 at the inner flowpath.
- Provides a bolt shield and reduces the bolt temperature caused by the CDP air leakage. The bolt therefore is exposed to lower temperatures, thereby requiring a smaller bolt size for the same load requirements, after relaxation effects are considered.

The inducer-structure stress analysis was performed for 40 seconds in the hot-day takeoff conditions. LCF life results are shown in Figure 96. Based on the material strength data for René 41 and Inco 903A, the LCF life objective of 36,000 cycles is reached.

5.2.2.3 Stage 1 Nozzle

The Stage 1 nozzle, shown as an exploded view in Figure 97, consists of a brazed airfoil-to-band assembly. The airfoil design consists of 46 individual aerodynamically shaped vanes manufactured from MA754 material. Two airfoils are brazed into each MAR-M-509 material band segment for a total of 23 segments. Additional features of the design can be seen in Figure 97 and include impingement inserts for improved airfoil cooling and inner- and outer-band impingement cooling. Flowpath seals are used between band segments to reduce cooling-air leakage along the length of the segments.

The Stage 1 nozzle design mechanical features are shown in Figure 98. The airfoil cooling is accomplished by forward and aft impingement inserts. The two cavities formed by the inserts are separated by a slanted rib. The forward insert is placed into the airfoil cavity from the inner flowpath and brazed to the airfoil at that end. The aft insert is placed into the aft cavity from the outer flowpath and brazed at the outer end of the airfoil.

The 23 segments are bolted to the inner nozzle support by a total of 46 bolts. (Each segment contains two bolts.) A pin is located on one end of the band flange and is used for radial and circumferential positioning of the segment to maintain the proper flowpath contour.

The inner and outer band segments are cast from MAR-M-509 material. The bands contain compartmentized cavities for improved impingement and film cooling. The inner and outer bands have integral gussets to improve the airfoil-to-flange load distribution.

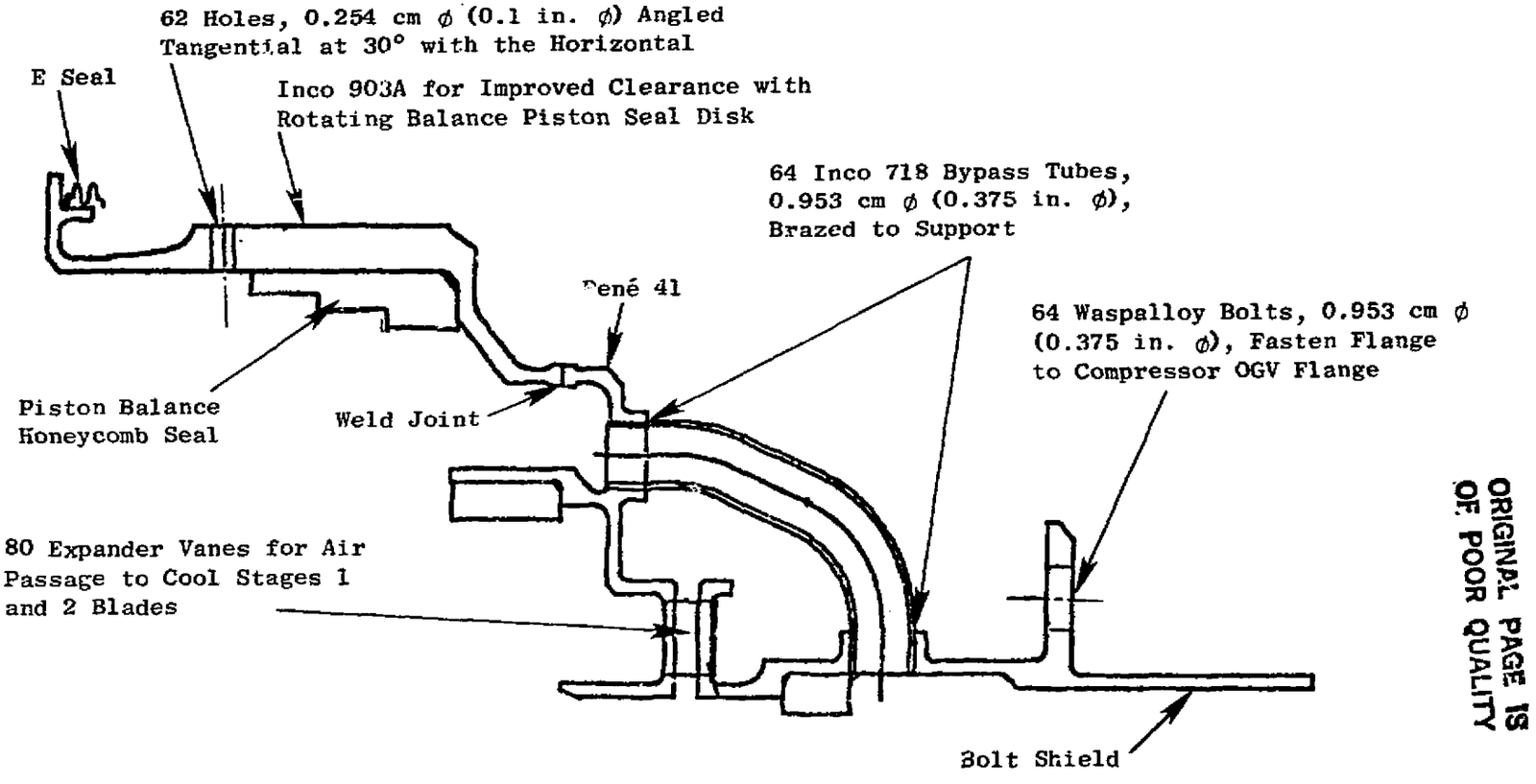

Figure 95. Inducer and Piston Balance Seal Configuration.

• 40 Seconds into Hot Day Takeoff

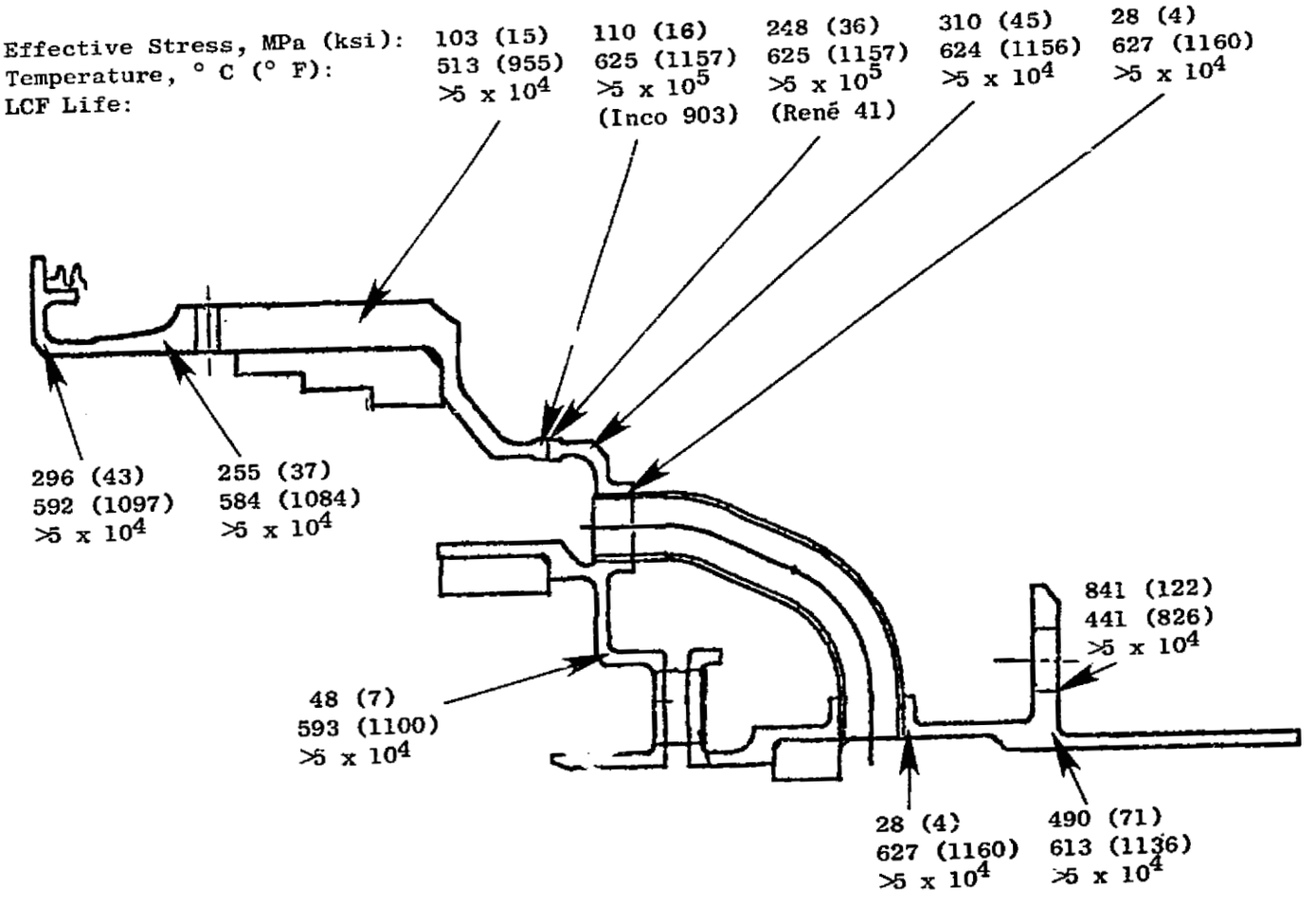

Figure 96. Inducer and Piston Balance Seal Stresses.

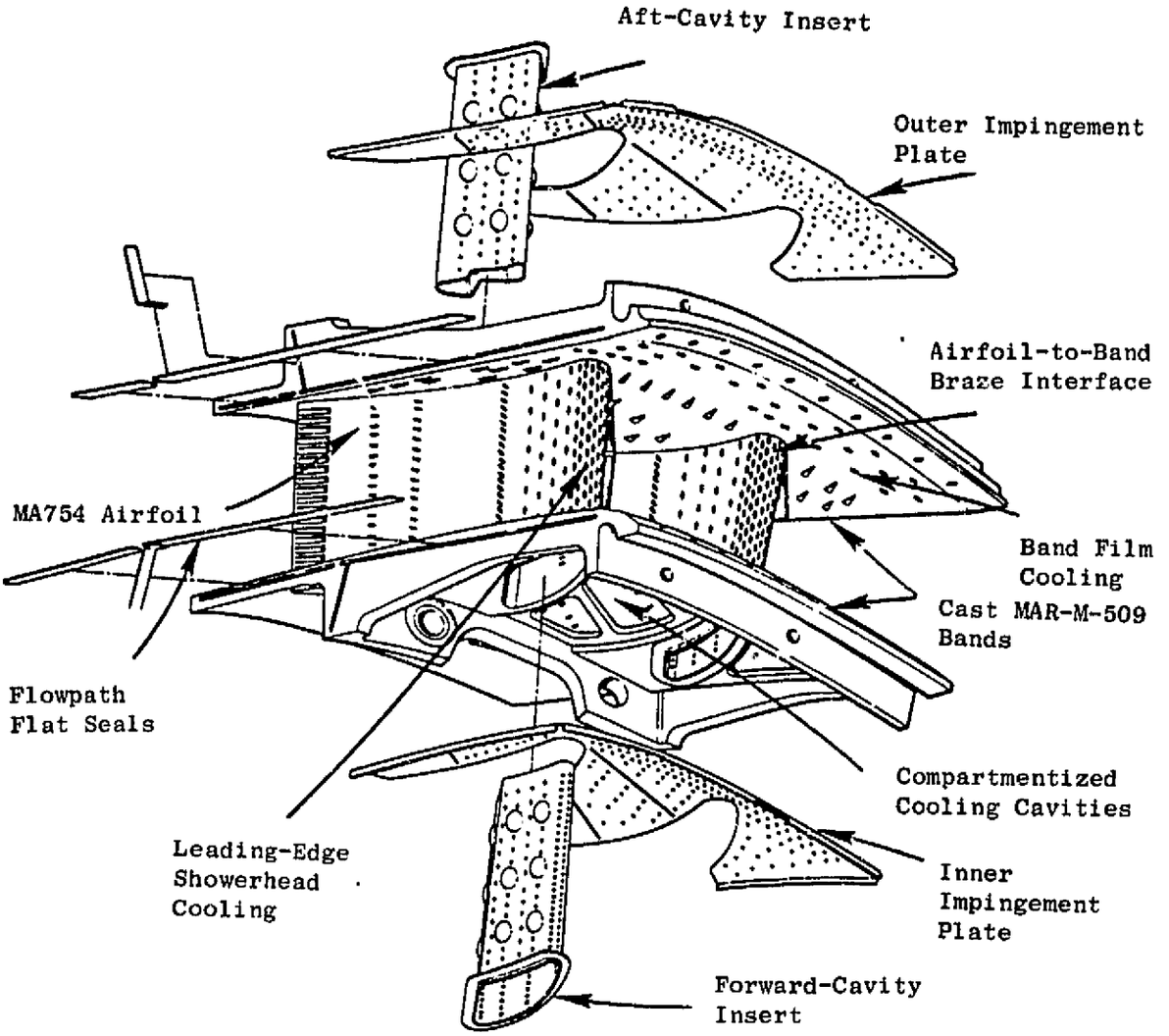

Figure 97. Stage 1 Vane Manufacturing.

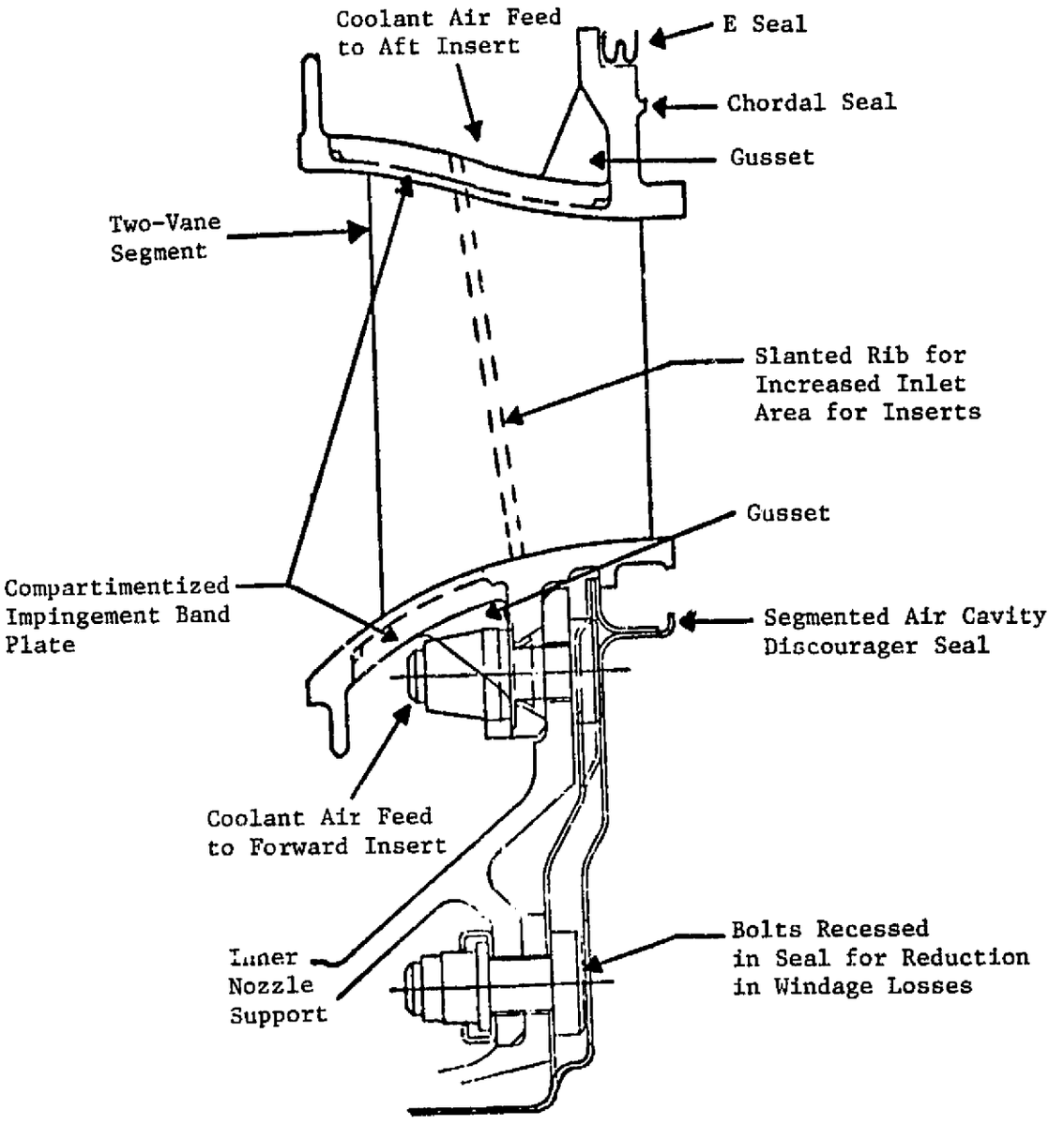

Figure 98. Stage 1 Nozzle Design Features.

The nozzle flange, located on the inner band, was analyzed based on the maximum induced moments due to gas load and also due to the inner and outer axial-support mismatch occurring during engine transient operation. Maximum flange stresses occur at 15 seconds after takeoff. The induced flange bending stress, as shown in Figure 99, is well below the 269 MPa (39 ksi) (3σ) 0.2% yield allowable stress for MAR-M-509.

The aft-cavity, suction-side wall is subjected to a high pressure differential that tends to induce bulging of the wall. This "ballooning" effect changes the aerodynamic contour and results in loss of turbine efficiency. The vane design therefore considers the positions of the rib (the rib also separates the forward and aft airfoil cavities) so that the panel stresses at temperature will be minimum. The MASS analysis was used to determine the panel stresses based on the orthotropic modulus properties of the MA754 airfoil alloy. The wall was geometrically modeled as panel sectors. The resulting calculated deflection based on hot-day takeoff operation is shown in Figure 100. As can be seen from the curve, the resulting bulge of only 0.05 mm (0.002 in.) for 600 hours of maximum engine takeoff conditions is more than adequate to meet engine part requirements.

The Stage 1 vane airfoil LCF life-limiting location was determined to be the 65% span. The LCF life is determined by analyzing the total local strain range occurring between maximum takeoff transient through a 2-minute takeoff and throttle chop to idle. The total local strain is therefore a function of the induced thermal stresses occurring during these two operating flight conditions, plus the mechanical stresses. The mechanical stresses are the result of gas loading and moment induced in the airfoil due to the axial thermal growth mismatch occurring between the inner and outer nozzle support. The mismatch induces an axial load at the outer support which results in a moment in the airfoil.

Figure 101 shows the calculated LCF life for the Stage 1 vane airfoil section at the limiting locations. The engine conditions used were based on a maximum gas peak temperature profile with full engine-deterioration parameters and at maximum hot-day takeoff conditions. The airfoil temperature assumptions are therefore based on maximum-severity engine conditions.

The maximum peak gas temperature of 1740° C (3163° F) is based on the average temperature gas profile plus the effects of the combustor pattern factor. Average gas profile temperature is a function of the cycle data. A temperature of 78° C (140° F) was added to the profile values for design considerations. This adder takes into account engine-to-engine variations, deteriorations, control tolerances, and other known parameters that can vary within each engine system.

5.2.2.4 Stage 2 Nozzle

The Stage 2 nozzle shown in Figure 102 consists of 48 René 150 airfoils brazed as pairs into 24 René 80 inner and outer bands. The selection of René 150 material for the airfoil provided increased LCF and rupture strength

- 15 Seconds into Accel
- MAR-M-509 Band Material

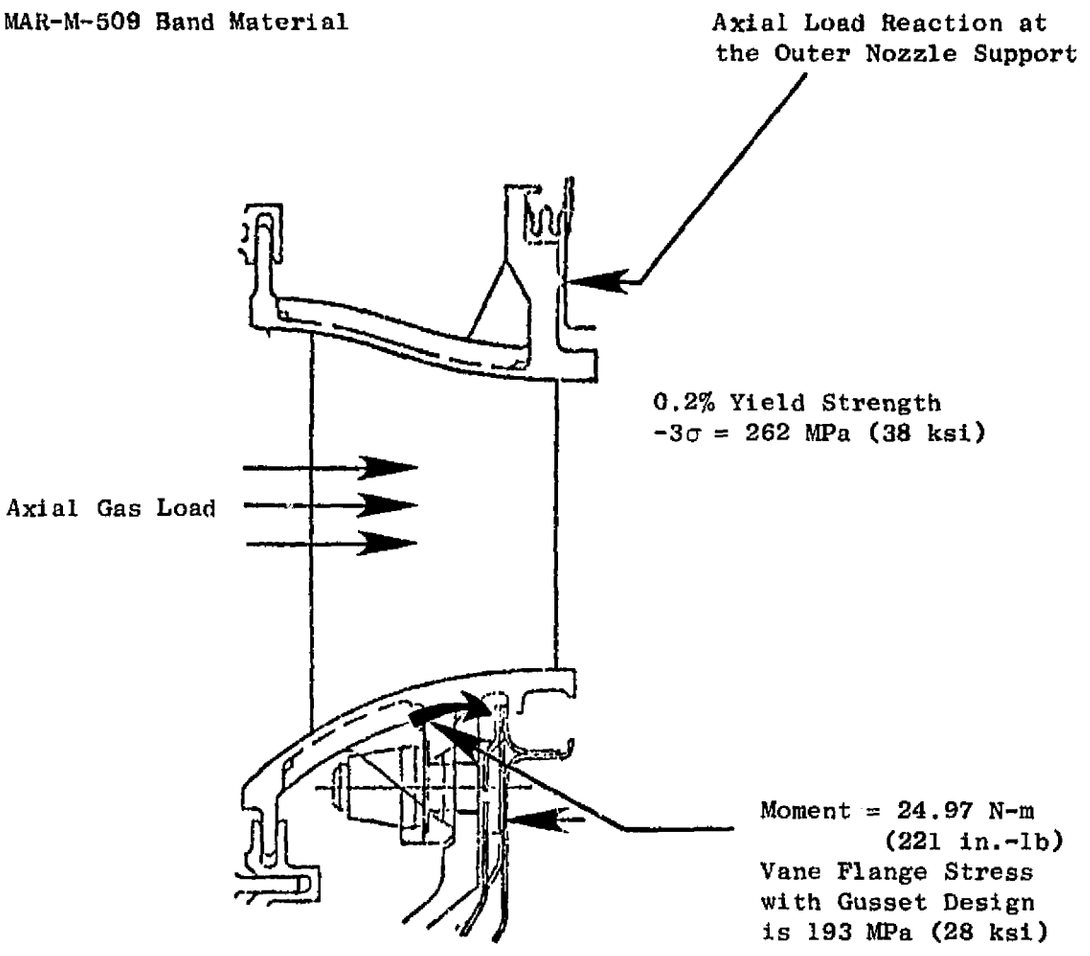

Figure 99. FPS Base Stage 1 Inner Nozzle Flange Stress.

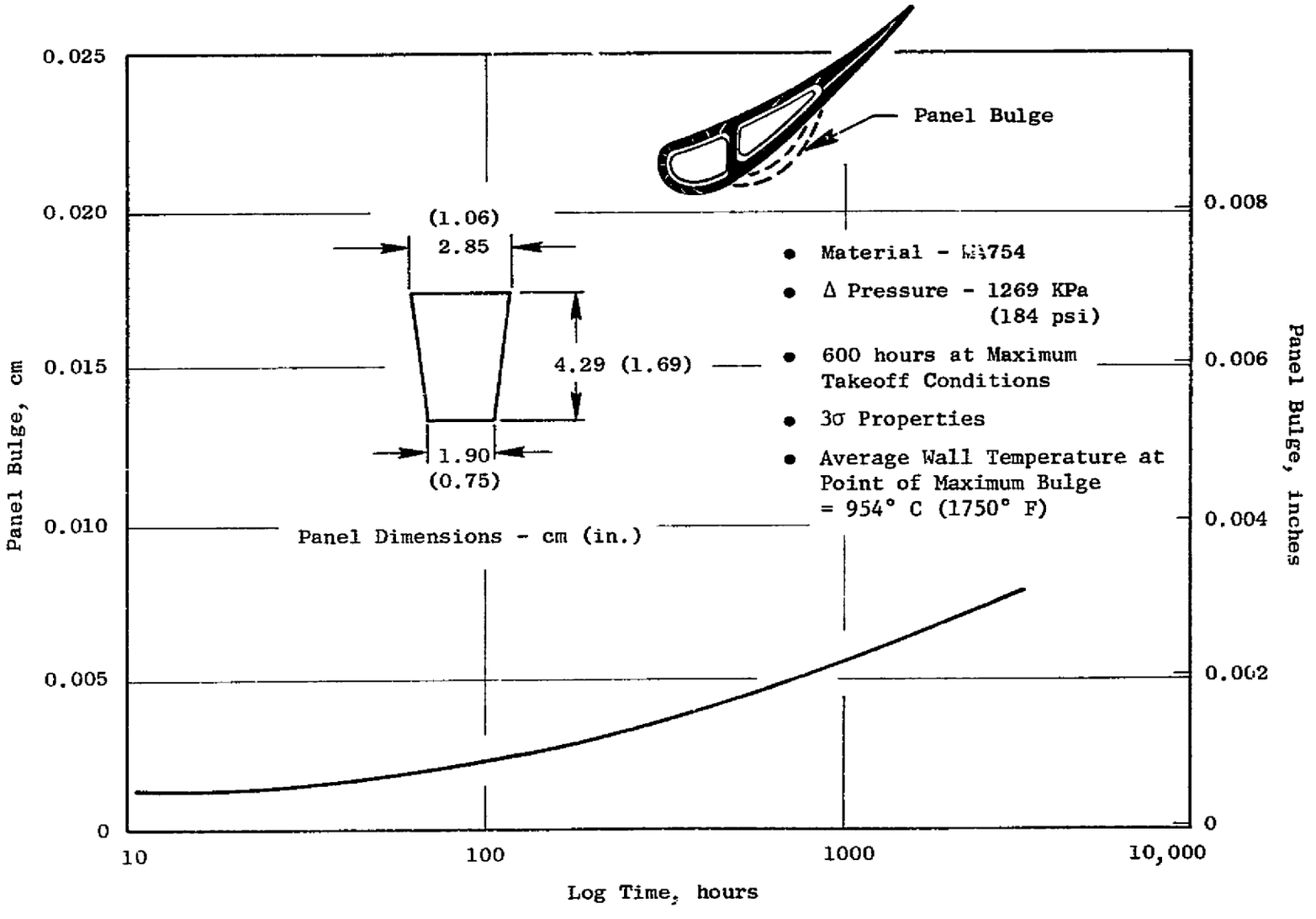

Figure 100. Stage 1 Vane Suction-Side Panel Creep Bulge Versus Time.

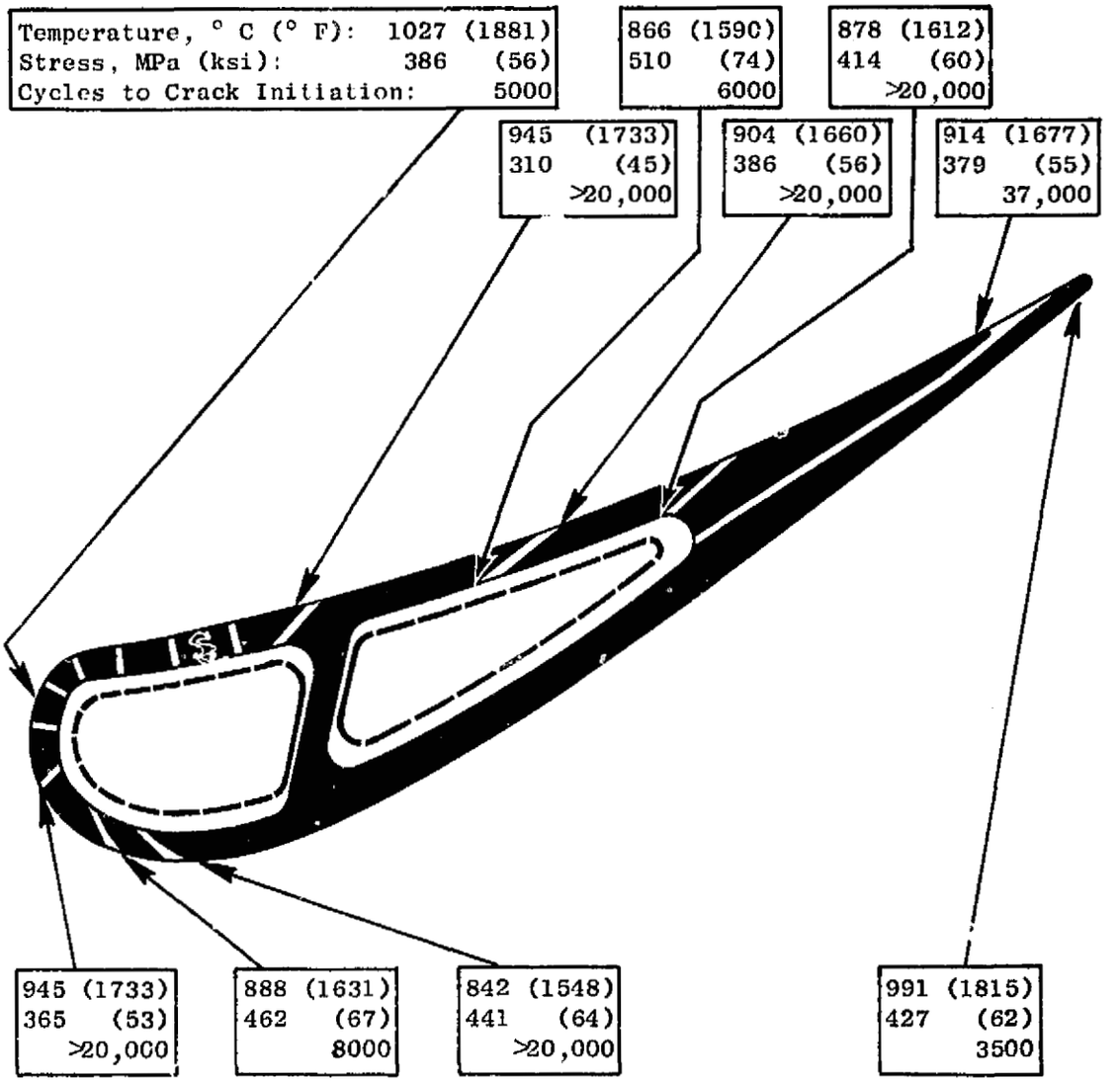

MA754 Material

Transient Conditions: Idle to Max. Takeoff and Back to Idle

Figure 101. Stage 1 Nozzle Airfoil LCF Life at 65% Span at Maximum Takeoff Condition (Table IX).

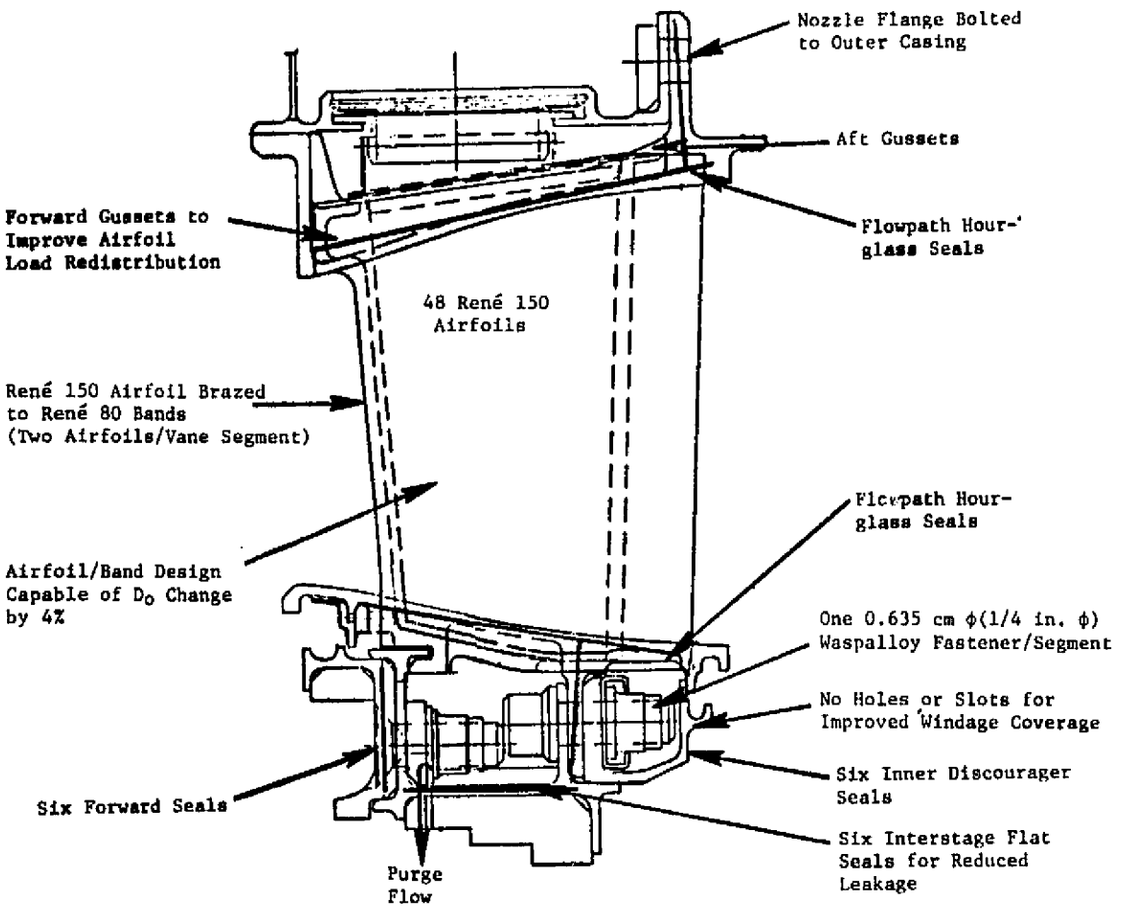

Figure 102. Stage 2 Nozzle Design Features.

capabilities relative to René 80 or René 125. This selection resulted in a reduction in cooling-air requirements while meeting the objective life of 18,000 LCF cycles.

There are 24 segments, composed of two vanes each, that make up the Stage 2 nozzle. The attachment hooks on the vane nozzle are standard GE design where the nozzle segments are bolted to a single outer-casing flange, simply supported at a forward hook, and bolted together at an integral manifold beneath the flowpath inner band. This joins the nozzle segments into an integral structure that forms and supports nozzle-cooling manifolds and an inner-stage seal. The cooling air supplied by the seventh-stage of the compressor is directed to a manifold designed for a low-pressure-drop system with a sealing spoolie arrangement feeding directly into the vane airfoil. The system provides cooling of the vane airfoil in the hot flowpath and purges the inter-stage seal cavity formed by the Stage 1 aft blade retainers and the Stage 2 blade damper.

The Stage 2 nozzle flowpath was determined by accounting for thermal deflections of the nozzle from the cold to hot position. The cold position (for manufacturing) is set to allow the nozzle to be at the prescribed design flowpath location during maximum climb operating conditions. Clearances and steps have been set to obtain correct relations with adjacent blades and shroud hardware.

The airfoil design features are shown in Figure 103. The airfoil contains one cavity with an impingement insert for optimum cooling. Local ribs are strategically located along the spanwise and chordwise directions for maintaining impingement distance between the insert and the inside wall. Additionally, the suction-side wall is thicker, with ribs extended as shown, for purposes of minimizing wall bulging or deflection.

Low cycle fatigue analyses for the 65% and 95% spans were determined based on maximum takeoff conditions. Figure 104 summarizes the LCF life results for these two sections. The limiting location was found to be at the trailing edge with an LCF life expectancy of 20,000 cycles. This exceeds the goal requirement of 18,000 cycles. Figure 105 shows the flange nozzle stresses based on maximum gas loads occurring during takeoff coditions. These stresses are well below the 0.2% yield stress for the René 80 material.

5.2.3 Ceramic Shrouds

5.2.3.1 General Description

One of the life-limiting elements of engine hot sections is that part of the flowpath wall opposite the HPT Stage 1 rotor blade tips. The components forming this section, the turbine shroud segments or hot-gas-path seal segments, operate in a harsh environment and can require a substantial amount of cooling air. They are exposed to combustor gas leaving the Stage 1 turbine nozzle at close to Mach 1. The turning and acceleration of the gases through the blade row results in complex flow patterns due to leakage over the blade tips. Collectively, the above phenomena produce high convection and high heat

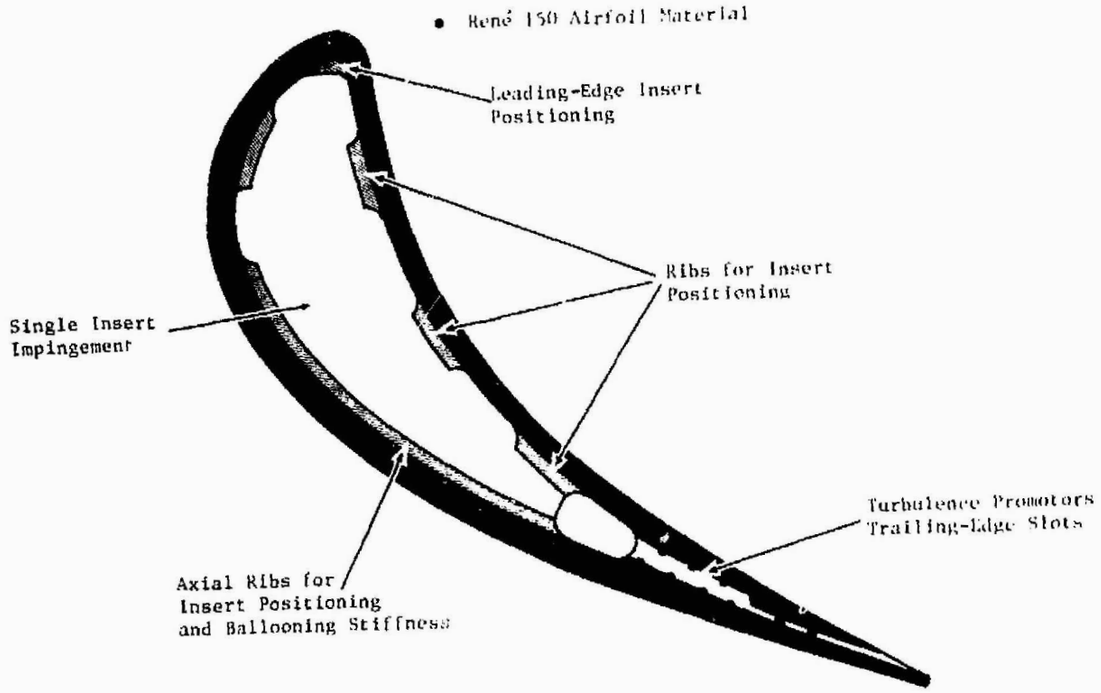

Figure 103. Stage 2 Nozzle Airfoil Design Features.

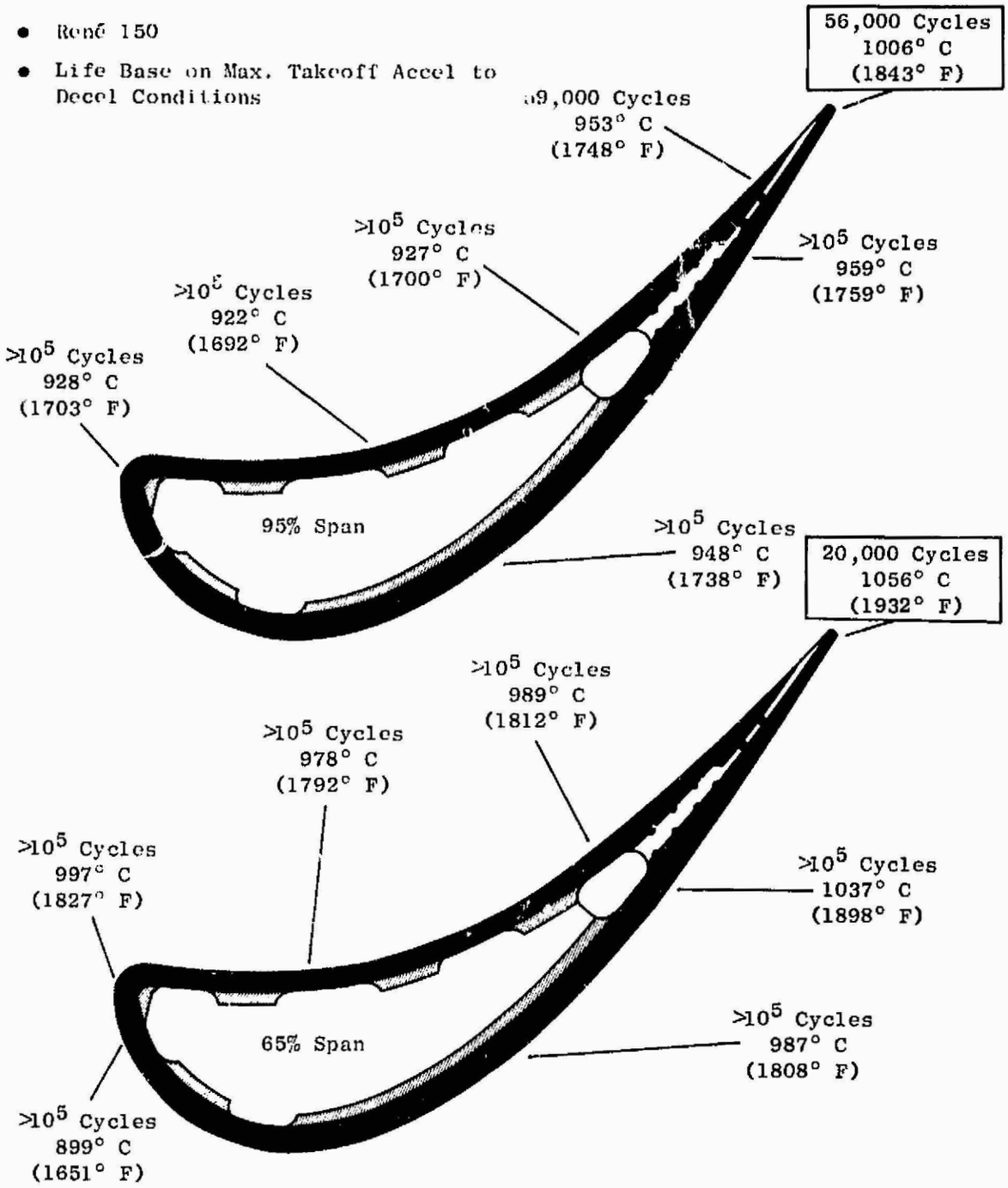

Figure 104. Stage 2 Airfoil LCF Life.

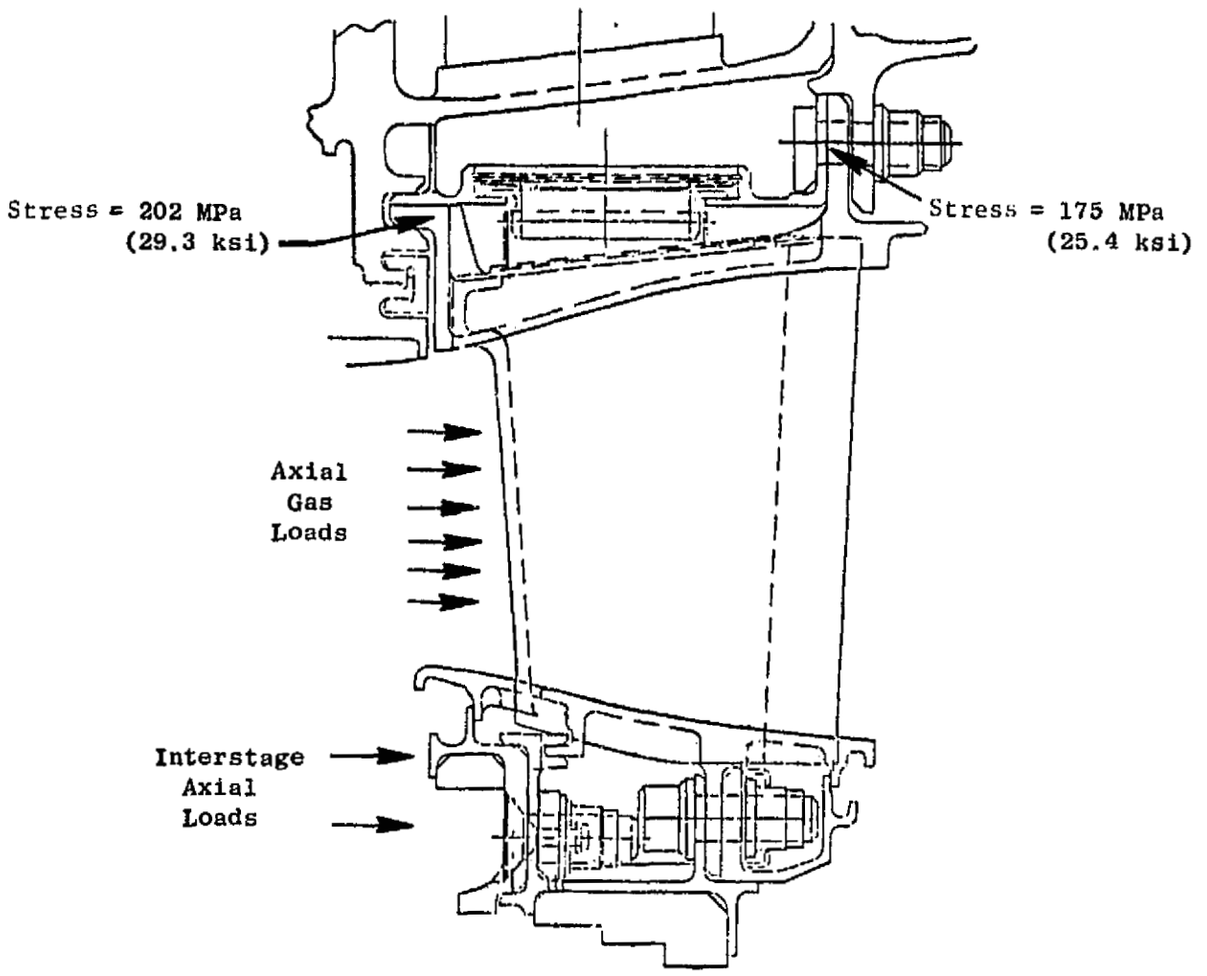

Figure 105. Stage 2 HP Nozzle Stresses Due to Gas Loads.

load over a relatively large surface area. The shrouds experience engine vibration and pressure fluctuation from passing blades. They undergo thermal cycling from start/stop and power-setting changes. In addition, unlike other cooled surfaces exposed to these severe conditions, the shroud surface must be able to survive blade rubs. This severly impacts cooling control; cooling control is affected by wall thickness and frequently depends on maintaining numerous small-diameter-film-hole patterns.

In the past, an effective way of coping with all of these conditions and requirements has been through the use of metal surfaces, either in a high-density cast or wrought form or in a lower density sintered or hot-pressed form. The high thermal conductivity of metal lends itself to maintaining acceptable surface temperatures, whether with film cooling or with only back-side impingement cooling. On the other hand, the lower density designs provide a degree of abradability that causes less blade-tip wear and helps to maintain better tip clearance. The lower density surface also provides a lower elastic modulus and, thus, contributes to lower thermal stress. However, regardless of the material choice, the surface will still reach high temperatures and will require metal alloys with good, high-temperature, oxidation resistance.

As turbine inlet temperatures increase cooling-air requirements increase, and it becomes increasingly difficult to maintain the low surface temperatures necessary in long-life applications. The alternative approach is a new concept in material for the surface exposed to the hot-gas stream. Ceramics provide this alternative. With stable-oxide ceramics, the oxidation resistance is unlimited for all practical purposes. In addition, appropriately selected ceramics have low thermal conductivity and serve to reduce the amount of cooling air required to keep the supporting materials at desired temperatures. Further, these ceramics have a low coefficient of thermal expansion which, at temperatures above 1204° C (2200° F), result in a thermal expansion determined to be close to the expansion of the metallic support. Plasma-sprayed zirconia has all of these characteristics.

5.2.3.2 Design and Analysis

The ceramic shroud design shown in Figure 106 consists of a plasma-sprayed, zirconia/Y_2O_3 ceramic, surface layer integrally bonded to an oxidation-resistant, cast, Rene 77 backing. This backing provides for attachment of the shroud to the support structure. The metal backing has a peg array interface to provide mechanical anchoring or interlocking to supplement the ceramic/metal-backing bond adherence. NiCrAlY is the bond coat, and a blend coat of bond coat and top coat provides a transition layer.

The effectiveness of zirconium oxide as a surface layer arises from very low thermal conductivity, chemical stability, and high melting point. For the NiCrAlY bond coat, long-term durability requires that temperature be limited to about 982° C (1800° F). This will prevent oxidation of the bond coat (with associated volume change) and will prevent its diffusion into the base metal. In this way, the integrity of the bond joint is maintained.

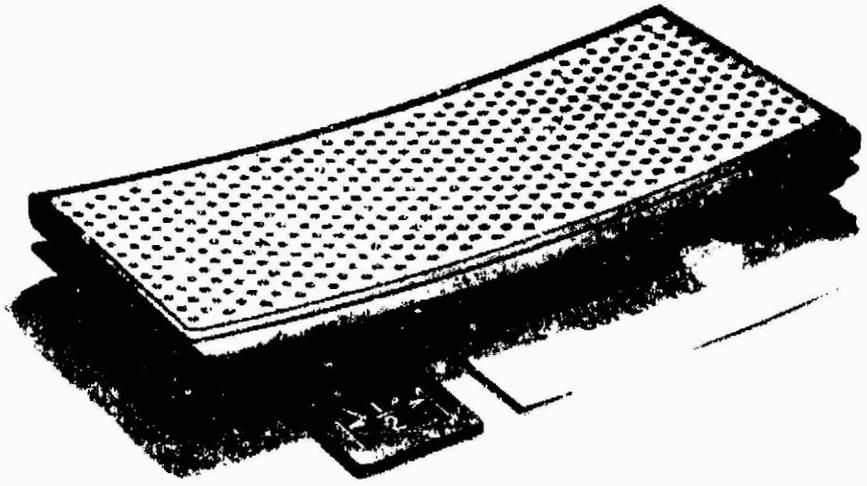

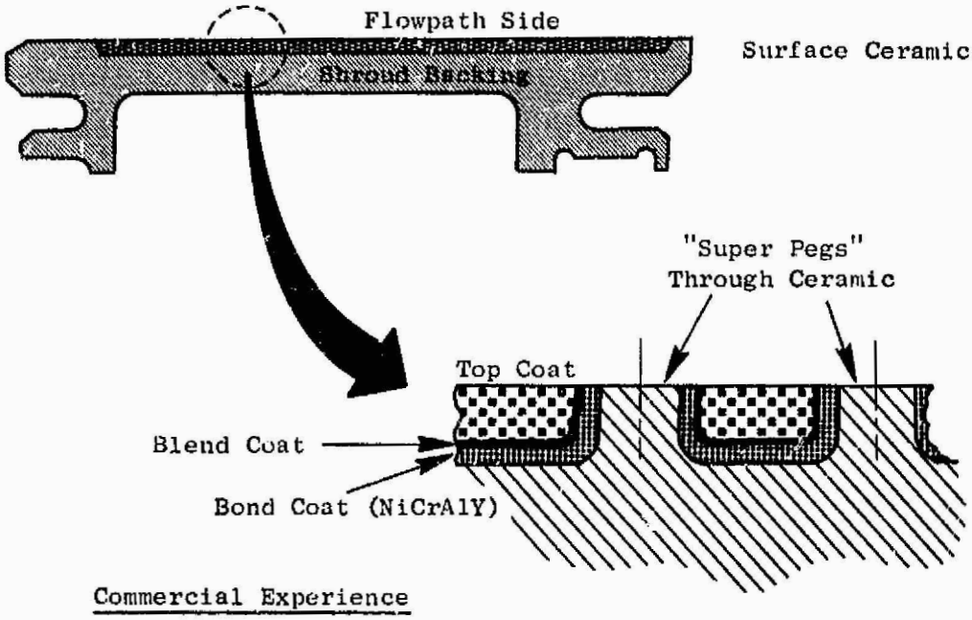

Commercial Experience

1980: 625 "C" Cycles, 166:46 Endurance Hours

1979: 65:22 Performance Testing Hours

Figure 106. Ceramic Shroud.

Temperature distribution in the shroud cross section as a function of ceramic thickness is shown in Figure 107. The bond-coat temperature remains below 982° C (1800° F) down to a ceramic thickness of about 0.051 cm (0.021 in.). At the same time the peg end remains at about 1038° C (1900° F) from about 0.051 cm (0.020 in.) ceramic thickness and up. The peg end operates well below the ceramic surface temperature because of the rapid drop in temperature below the ceramic surface and because of the high thermal conductivity of the metal peg. This effect is moderated somewnat as the slenderness ratio of the peg increases with ceramic thickness. This peak temperature of the peg end needs to be maintained for only 85 hours out of the 9000 hours in an overhaul period for a typical operating mission.

Radial and eccentric tolerance stackup can require variation in the ceramic-layer thickness over a range of 0.051 cm (0.020 in.). The loop of engine components contributing to this stackup is shown schematically in Figure 108.

The above constraints dictate that the ceramic layer have a thickness of at least 0.102 cm (0.040 in.) plus an allowance for blade rub. The 0.102 cm (0.040 in.) provides the 0.051 cm (0.020 in.) minimum for bond-coat thermal protection and 0.051 cm (0.020 in.) for stackup.

The temperature distribution through the shroud cross section, combined with the mounting constraint that maintains the curvature, give rise to the thermal stresses shown in Figure 109. These show adequate thermal cyclic life.

5.3 MAINTAINABILITY

Ease of maintenance was emphasized throughout the design of the high pressure turbine.

The turbine assembly consists of three basic modules

- Stage 1 nozzle/combustor/diffuser module
- Stage 2 nozzle and shroud support module
- Turbine rotor module.

The Stage 1 nozzle/combustor/diffuser module is shown in Figure 110. The assembly consists of arranging the 23 nozzle segments circumferentially and aligning the nozzles to fit in the inner nozzle support. This assembly is then mated to the combustor and diffuser which has also been built as a subassembly. Mating these two assemblies is completed by the inner flange bolt arrangement between the diffuser and inner nozzle support. All honeycomb seals are then ground relative to the diameter of the combustor casing forward flange. This procedure provides an improved static seal concentricity relative to engine centerline.

The Stage 2 nozzle and shroud support module is shown in Figure 111. At this level of assembly, all shrouds and seals are ground with respect to the

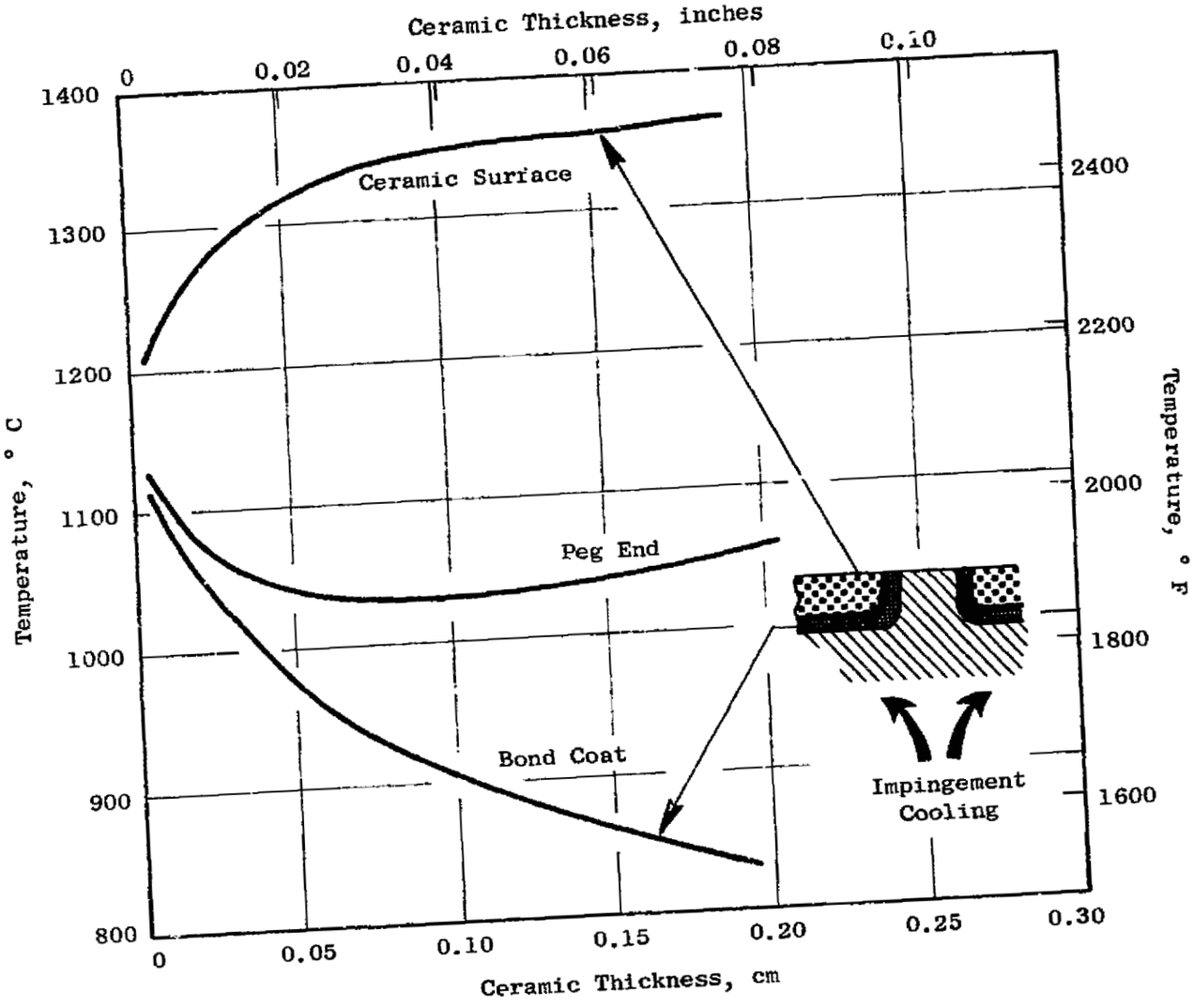

Figure 107. Stage 1 Shroud Temperature Versus Thickness of Ceramic Layer.

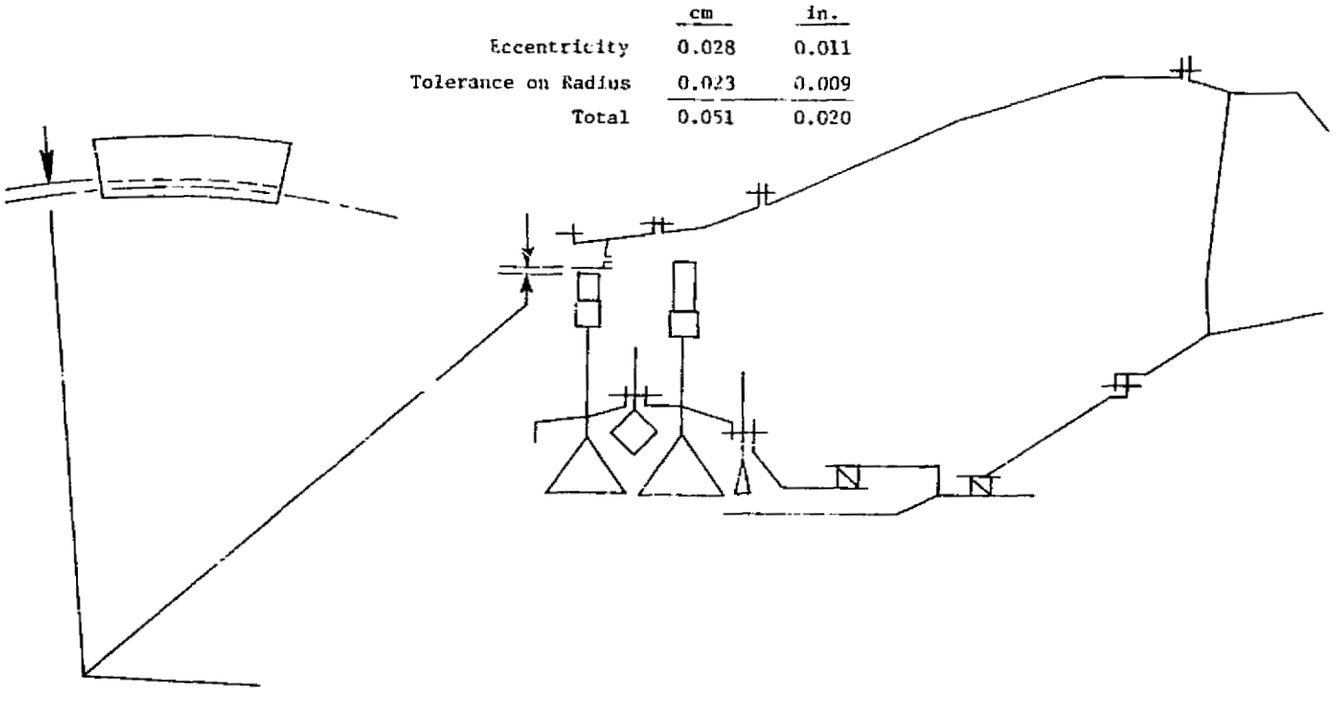

Figure 108. Ceramic Shroud Thickness Allowance for Engine Stackup.

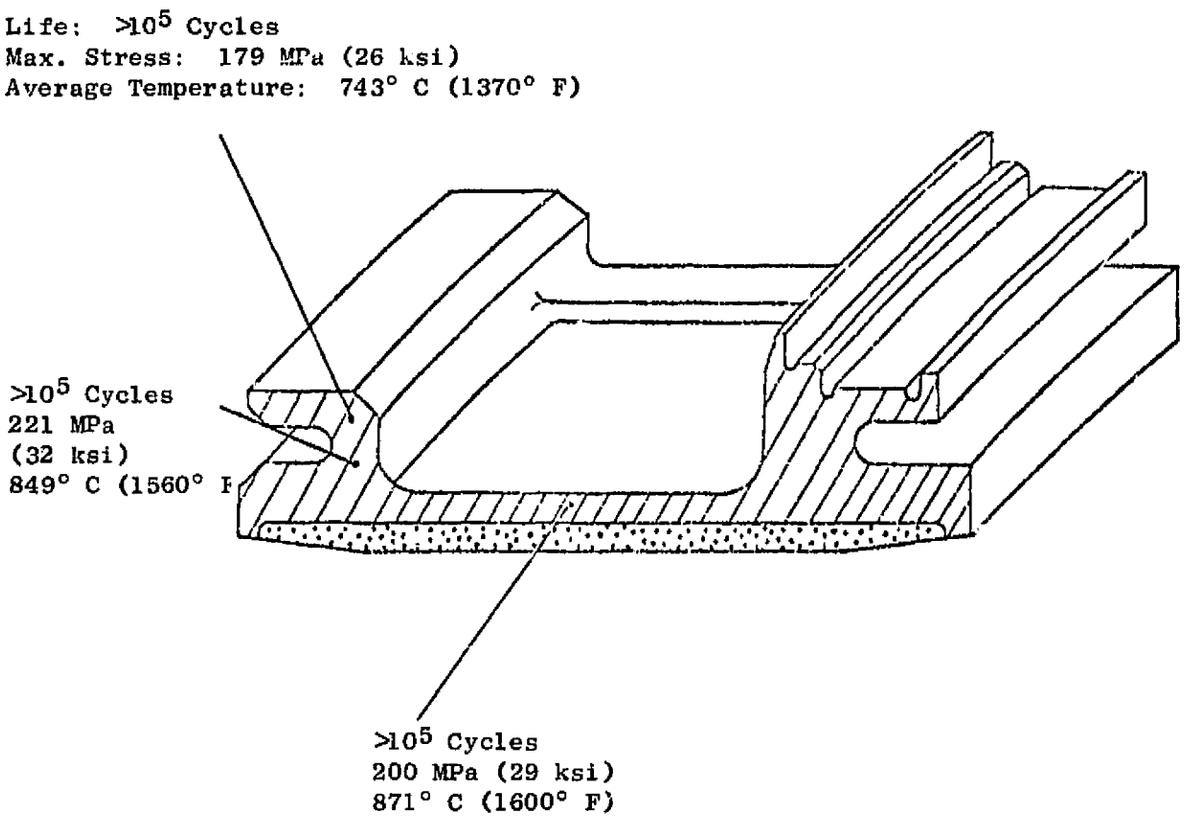

Figure 109. Ceramic Shroud Stress/Life.

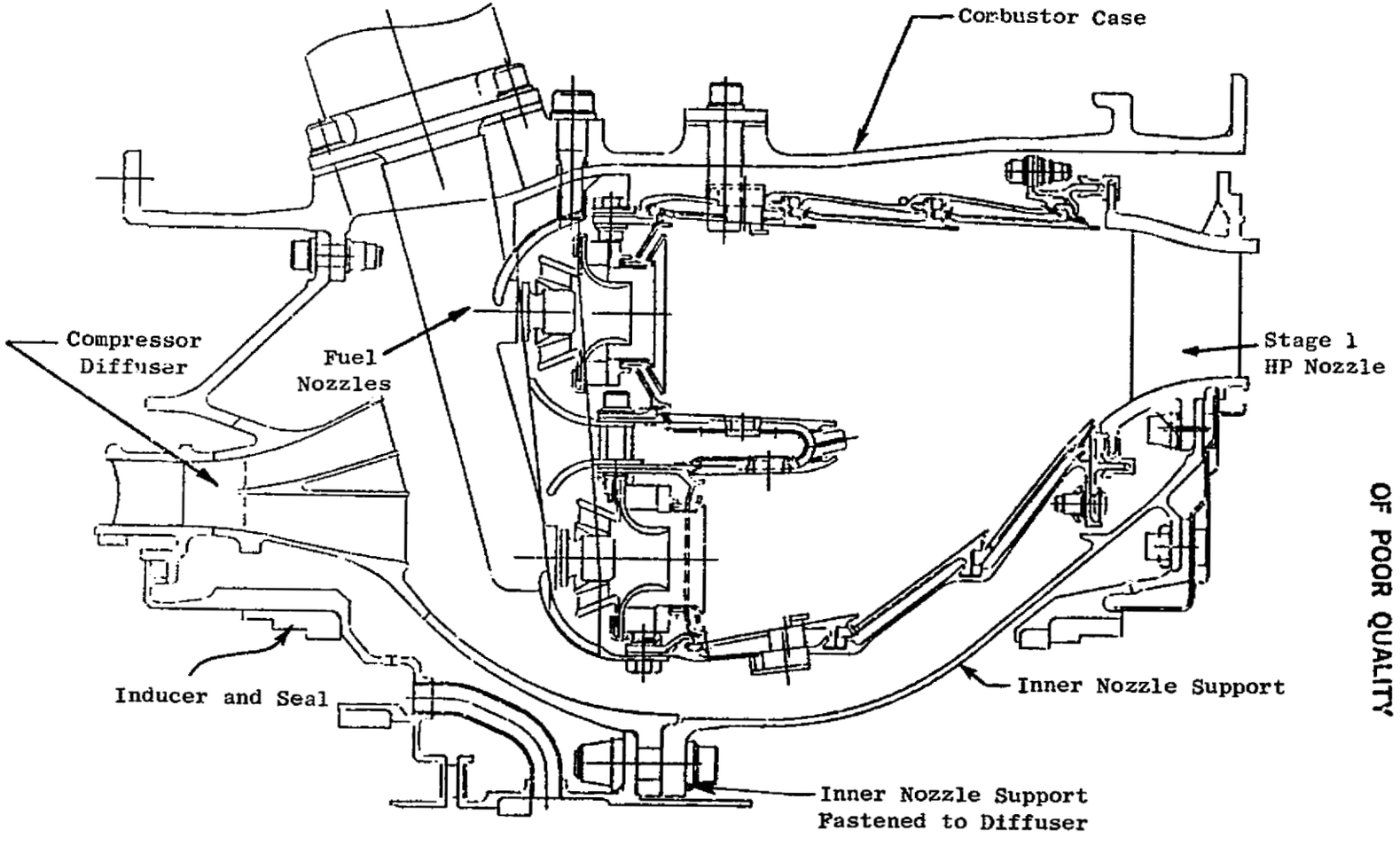

Figure 110. Stage 1 Nozzle/Combustor/Diffuser Module Assembly.

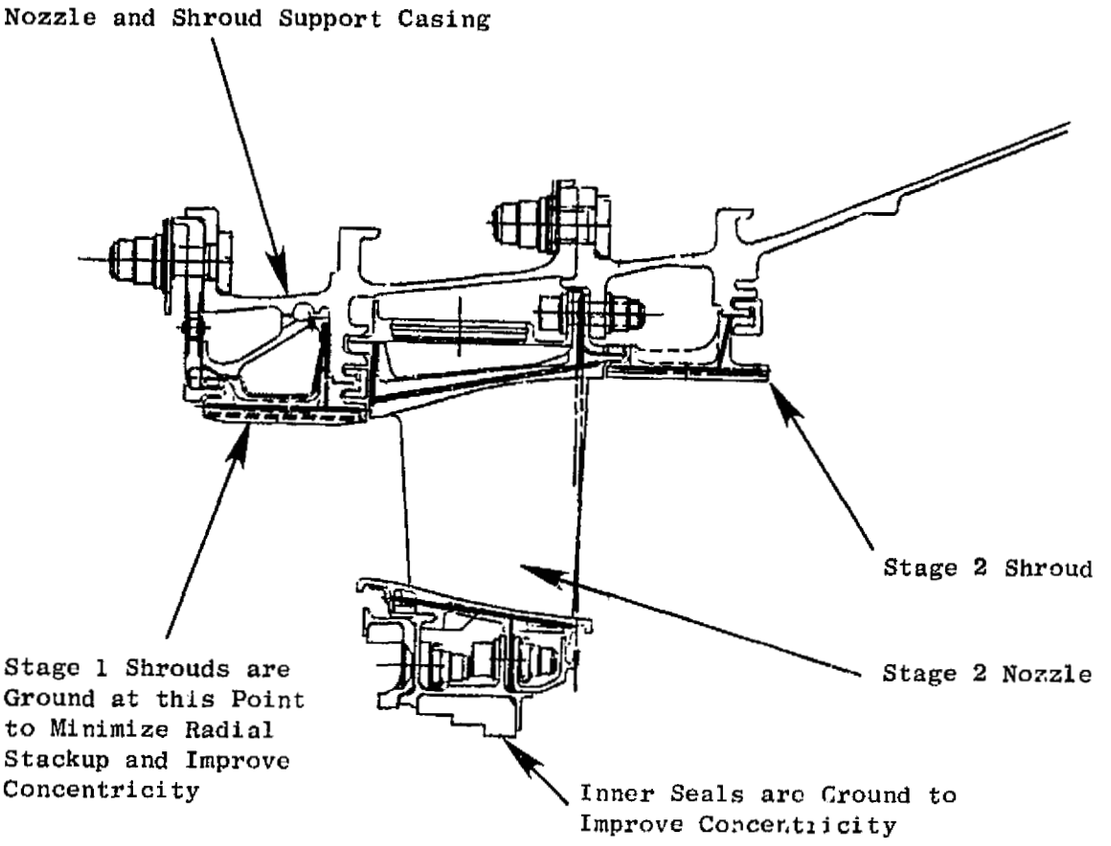

Figure 111. Stage 2 Nozzle and Shroud-Support Casing Module Assembly, Engine Level.

casing. This grinding operation results in reducing the radial stackup and thereby improving concentricity relative to the casing. Axial and radial inspections are determined at this assembly level. These inspections are used in determining relative clearances between the static and rotating components.

The turbine rotor module is shown in Figure 112. At this assembly level, the Stage 1 and 2 blades have already been tip ground while assembled in the Stage 1 and 2 disks. Balancing has also been completed. The rotor is balanced at the two planes as shown. The HP shaft and forward outer liner are balanced and installed as part of the compressor module.

Engine level assembly for the HP turbine is accomplished by installing the Stage 1/combustor/diffuser module into the compressor casing. The turbine rotor is then placed into the engine assembly. Fastening for the turbine rotor assembly is completed at the HP shaft aft flange bolt interface.

In order to install the Stage 2 nozzle and shroud module, the Stage 2 aft blade retainer, blades, and dampers are removed from the rotor assembly. These components are match-marked prior to removal for reassembly in their original balance position.

After Stage 2 nozzle module is assembled and fastened to the combustor aft flange, the Stage 2 blades, damper, and aft blade retainer are reassembled in their original position (orientation).

In summarizing, for ease of maintainability and disassembly two fastening joints will remove the whole turbine (except Stage 1 nozzle). If the Stage 1 nozzle needs to be removed, the inner nozzle support flange allows ease of disassembly.

5.4 FPS ASSEMBLY WEIGHT

A turbine weight summary for the FPS base engine is shown in Table XXIII.

Table XXIII. FPS Weight Data Base.

	kg	lbm
Total Turbine	414	913
HPT Stator	132	290
HPT Rotor	282	623

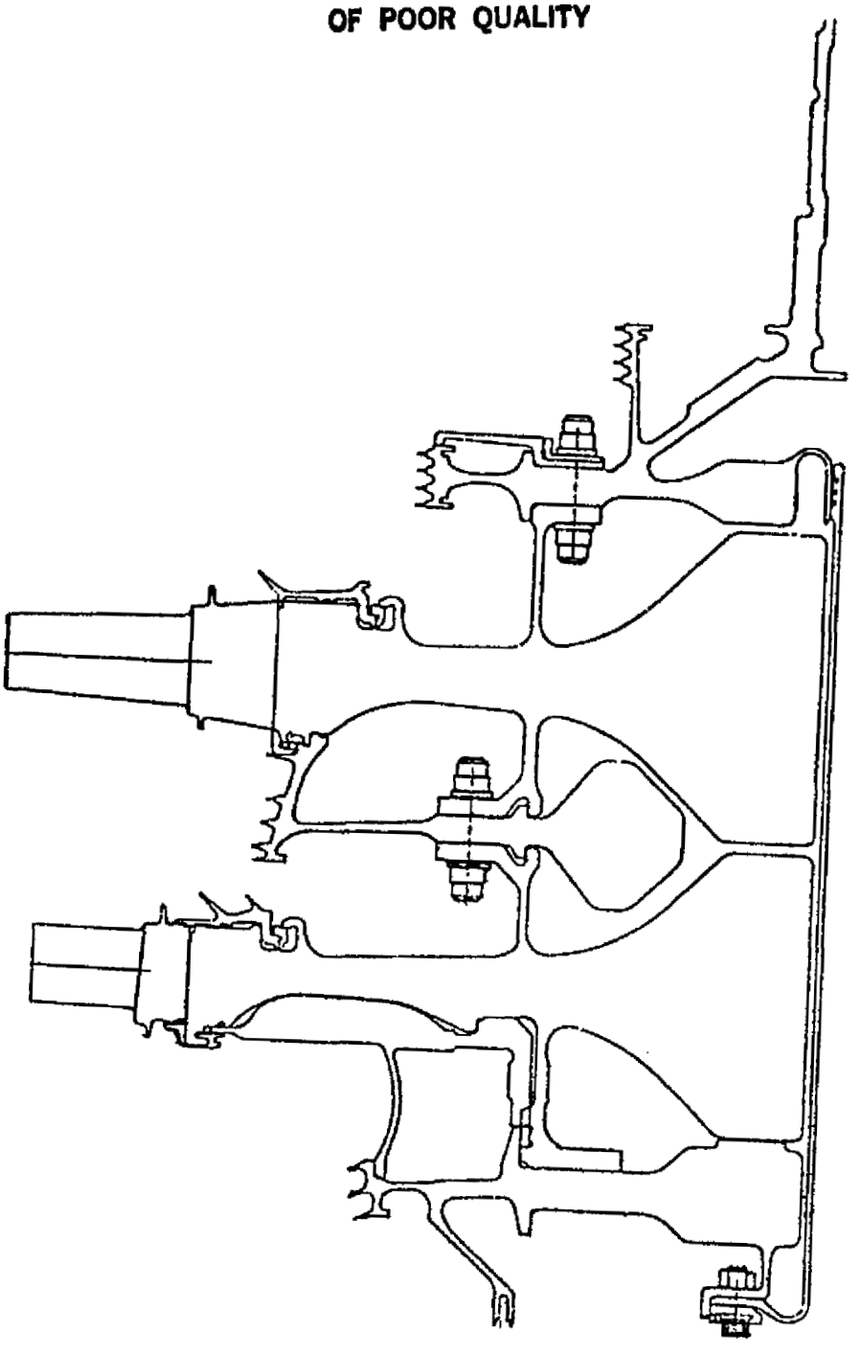

Figure 112. HP Turbine Rotor Module Assembly.

REFERENCES

1. Neitzel, R.E., Hirschkron, R., and Johnston, R.P., "Study of Turbofan Engines Designed for Low Energy Consumption," NASA-Lewis Research Center, CR-135053, 1976.

2. Neitzel, R.E., Hirschkron, R., and Johnston, R.P., "Study of Unconventional Aircraft Engines Designed for Low Energy Consumption," NASA-Lewis Research Center, CR-135136, 1976.

3. Steinberger, C.A., Stotler, C.L., and Neitzel, R.E., "Study of the Cost and Benefits of Composite Material in Advanced Turbofan Engines," NASA-Lewis Research Center, CR-134696, October 1974.

4. Ross, E.W., Johnston, R.P., and Neitzel, R.E., "Cost Benefit Study of Advanced Materials Technology for Aircraft Turbine Engines," NASA-Lewis Research Center, CR-134702.

5. Hillery, R.V. and Johnston, R.P., "Cost Benefit Study of Advanced Materials Technology for Aircraft Turbine Engines," NASA-Lewis Research Center, CR-135235.

6. Johnston, R.P., Hirschkron, R., Koch, C.C., and Neitzel, R.E., "Energy Efficient Engine - Preliminary Design and Integration Study," NASA-Lewis Research Center, CR-13544.

SYMBOLS AND TERMS

A	Area, vane flow area; m^2 (in^2)
ACC	Active Clearance Control
Accel	Acceleration
AR	Aspect Ratio = blade height (h)/blade Axial Width (AW)
AW	Airfoil Axial Width, cm (in)
BFM	Backflow Margin: Differential pressure between the spent impingement air pressure and the gas-side pressure, $[(P_{S_c} - P_{T_g})/P_{T_g}] \times 100\%$
bhp	Brake horsepower
C_0	Velocity available in isentropic expansion of turbine inlet flow across the group total-to-static pressure ratio, m/sec (ft/sec)
CDP	Compressor Discharge Plane, Compressor Discharge Pressure
CF6	General Electric commercial turbofan engine family
D	Diameter; m, cm (in)
d_o	Airfoil throat dimension, cm (in)
Decel	Deceleration
DS	Directionally Solidified, Directional Solidification
E^3	Energy Efficient Engine
F	Force, N (lbf)
f_B	Frequency of backward-traveling wave, Hz
f_F	Frequency of forward-traveling wave, Hz
FADEC	Full Authority Digital Electronic Control
FOD	Foreign Object Damage
FPS	Flight Propulsion System. Refers to the fully developed configuration of the Energy Efficient Engine which would be suitable for airframe installation.

h	Heat Transfer Coefficient ($W/m^2 \cdot C(^\circ F)$)
Δh	Energy extraction, kJ/kg (Btu/lbm)
HCF	High Cycle Fatigue
HIP	Hot Isostatic Pressing (Pressed)
HP	High Pressure
HPT	High Pressure Turbine
ICLS	Integrated Core/Low Spool. The complete turbofan test configuration of the E^3.
K_t	Stress Concentration Factor
ℓ	Length, blade tip shroud overhang length; cm (in.)
L	Length, length of airfoil; cm (in.)
LCF	Low Cycle Fatigue
LP	Low Pressure
LPT	Low Pressure Turbine
M	Mach number
MXCR	Maximum cruise operating point
N	Turbine speed, rpm
NDT	Nondestructive Testing
ODS	Oxide Dispersion Strengthened
OGV	Outlet Guide Vane (Compressor or Turbine)
P	Pressure, Pa (psi)
PM	Powder Metallurgy
PVD	Physical Vapor Deposition
P/A	Pressure/Area; Stress kPa/m^2 ($ksi/in.^2$)
R1	Rotor 1
R2	Rotor 2
sfc	Specific fuel consumption, $kg/N \cdot hr$ ($lbm/lbf \cdot hr$)
SLTO	Sea Level Takeoff
S1	Stator 1
S2	Stator 2
T	Total Temperature, Temperature; K (° R)

T_{tb}	Relative Blade Total Temperature
ΔTamb	Temperature above ambient at standard day conditions
U	Rotor tangential velocity at the mean radius, m/sec (ft/sec)
V	Velocity, m/sec (ft/sec)
W	Flow, kg/sec (lbm/sec)
z	Blade tip shroud interlock angle, degrees
$\Delta\beta s$	Airfoil unguided turning, defined from the point at which the throat orthogonal intersects the suction surface to the point at which the suction surface becomes tangent to the trailing-edge circle - degrees
Γ	Turbine exhaust swirl, degrees
η	Turbine efficiency based on shaft power and ideal power available in the expansion of W_{41} from P_4 to P_{42}
θ	Blade tip shroud angle denoting direction of shroud first-flex vibration mode, degrees
σ	Solidity
ϕ	Assembled p[illegible]ist rotation angle of blade tip shroud, degrees
ψz	Zweifel number

Subscripts

a	Air
amb	Ambient
	Coolant, compressor
CDT	Coolant Temperature Relative to the Dovetail
DT	Dovetail
g	Gas
h	Hub
P	Pitch
t	Tip
S,s	Static
SC	Static Coolant

T,t	Total
TB	Total Condition Relative to the Blade
25	Core compressor inlet plane (Engine Stations)
3	Compressor exit plane
40	Combustor exit plane
41	HPT Rotor 1 inlet plane
49	LPT Rotor 1 inlet plane

END

DATE

JAN 9, 1985